Amphiphilic Polymers: Crystallization-assisted Self-assembly and Applications in Pharmaceutical Formulation

A DISSERTATION
SUBMITTED TO THE FACULTY OF
UNIVERSITY OF MINNESOTA
BY

Ligeng Yin

IN PARTIAL FULFILLMENT OF THE REQUIREMENTS
FOR THE DEGREE OF
DOCTOR OF PHILOSOPHY

Marc A. Hillmyer, Advisor

April, 2013

Acknowledgements

First and foremost, I would like to thank my advisor Prof. Marc Hillmyer. His guidance and continuous support not only helped me improve scientific conduct, but also triggered me to be passionate about polymer science and further take full responsibility of research projects. Besides, Marc was always very open-minded, which granted me much freedom in exploring different areas and pursuing what I love.

I was greatly blessed to spend the last five years and a half in the Polymer Group at University of Minnesota. I have been continuously growing in the friendly and collaborative atmosphere. In particular, I would like to thank Prof. Tim Lodge for his help on small-angle neutron scattering including data acquisition, treatment, and interpretation. I thank Prof. Theresa Reineke for her valuable biological perspective on macromolecules in biological studies. I also thank many other members for the priceless daily interactions through whether training on instrument, sharing chemicals, or debating on specific questions: Dr. Sara Arvidson, Dr. Zhifeng Bai, Dr. Liang Chen, Dr. Soohyung Choi, Molly Dalsin, Dr. Gina Fiore, Dr. William Gramlich, Yuanyan Gu, Dr. Elizabeth Jackson, Dr. Justin Kennemur, Dr. Shingo Kobayashi, Dr. Hau-Nan Lee, Dr. Sangwoo Lee, Dr. Chun Liu, Dr. Ameara Mansour, Mark Martello, Dr. Henry Martinez, Maria Miranda, Dr. Adam Moughton, Dr. Tushar Navale, Matthew Petersen, Dr. Louis Pitet, Dr. Yang Qin, Ralm Ricarte, Dr. Megan Robertson, Dr. Myungeun Seo, Dr. Jihoon Shin, Joshua Speros, Swapnil Tale, Dr. Rajiv Taribagil, Grayce Theryo, Dr. Eric Todd, Dr. Athanasios Touris, Yaoying Wu, Dr. Jihua Zhang, and Can Zhou.

I thank Dr. Steve Guillaudeu, Dr. Bob Schmitt, and Dr. Trey Porter at The Dow Chemical Company, whose comments during monthly meetings and through daily emails helped me pick up the cellulosics project and further make progress. I also thank Dr. Antons Sizovs at Virginia Tech for providing a trimethylsilyl-protected glucose methacrylamide monomer with very high purity.

Much of the progress cannot be achieved without the staff's diligent work on maintaining the instrument and expert advice on learning a technique. I thank Dr. Letitia Yao, Dr. Wei Zhang, Dr. Bob Hafner, Chris Frethem, and David Giles at Minnesota, Dr. Yun Liu and Dr. Steve Kline at NIST, and Dr. Steve Weigand at Argonne National Laboratory.

Last but not least, I thank my wife, Dr. Meng Jing (in chemistry too!), my parents, and my parents-in-law for their love and continuous support. Meng is always there at my hardest times, encouraging me and offering advice. We do not talk about chemistry every day at home, but I did enjoy numerous scientific conversions that started on the sofa in our living room. Plus, I always love the food she created and have been well fed over the last several years. I am excited to continue sharing chemistry with Meng for the rest of my life.

Dedication

To Meng, Moms, and Dads.

Abstract

Amphiphilic polymers are macromolecules that simultaneously contain hydrophobic and hydrophilic components. These molecules not only attract much attention in academic research but also are important materials in industry. Application areas include detergency, oil field, paints, agriculture, food, cosmetics, and pharmaceutics. This dissertation highlights my efforts since the November of 2007 on three separate systems of amphiphilic polymers, which addresses both the fundamental self-assembly behavior in solution and applications in pharmaceutical formulation. Chapter 2 describes the self-assembled micelles in water that contain semicrystalline polyethylene (PE) as the core-forming material. Poly(*N*,*N*-dimethylacrylamide)–polyethylene (AE) diblock copolymers were chosen as the model system. An AE diblock copolymer with relatively low PE composition resulted in micelles with oblate ellipsoidal cores in water, in which crystalline PE existed as flat disks at the center and rubbery PE resided on both sides. In contrast, a control sample with a rubbery polyolefin as the hydrophobic component resulted in micelles with spherical cores in water. The morphology transition was ascribed to the crystallization of PE. The heat-assisted direct dissolution for sample preparation was identified as a stepwise "micellization–crystallization" procedure. In addition, the morphology of the aggregates exhibited much dependence on the composition of AE copolymers, and wormlike micelles and bilayered vesicles were obtained from samples with relatively high PE compositions. Chapter 3 demonstrates the precise synthesis of glucose-containing diblock terpolymers from a combination of anionic and reversible addition-fragmentation chain-transfer (RAFT)

polymerizations. The resulting micelles exhibited excellent stability in several biologically-relevant media under *in vitro* conditions, including 100% fetal bovine serum. These particles may find applications as serum-stable nanocarriers of hydrophobic drugs for intravenous administration. Chapter 4 presents the development of novel cellulose derivatives as matrices in amorphous solid dispersions for improving the bioavailability of poorly water-soluble drugs in oral administration. Hydroxypropyl methylcellulose (HPMC) was modified with monosubstituted succinic anhydrides using facile anhydride chemistry, and the resulting materials simultaneously contained hydrophobic, hydrophilic, and pH-responsive moieties. Several HPMC esters of substituted succinates exhibited more effective crystallization inhibition of phenytoin under *in vitro* conditions than a commercial hydroxypropyl methylcellulose acetate succinate (HPMCAS). (341 words)

Table of Contents

List of Tables

List of Figures

1 Background

1.1 Amphiphilic Molecules – Small and Large

Amphiphilic molecules are compounds that have covalently connected hydrophilic ("water-loving", polar) and hydrophobic ("water-hating", nonpolar) components. Common examples include surfactants (surface-active agents) and (polar) lipids such as phospholipids, the essential building materials of the bilayered cell membranes. These molecules often consist of a charged, hydrophilic head group attached to an aliphatic hydrocarbon chain. Surfactants and lipids have rather low molar masses on the order of 500 g mol^{-1}, and thus referred here as "small" molecules. Due to the affinity to multiple environments, amphiphilic molecules can spontaneously organize in solutions that preferentially solublize some but not all of the components of the molecules. For example, when dodecyl sulfate (a surfactant) is mixed with water, the hydrophobic aliphatic tails can associate into the inner nonpolar domain to minimize the expose to the aqueous medium, and the polar sulfate heads form the outer hydrophilic layer to provide the necessary stability (Figure 1.1). As other nonpolar molecules can be doped into the inner oily domain, such aggregates can greatly enhance the partition of hydrophobic substances in the aqueous environment. Besides, amphiphilic molecules can assemble at the interfaces between incompatible substances (e.g., oil and water), and thus are able to modify interfacial properties and increase compatibility. Amphiphilic molecules have found applications in many aspects of our life including detergency, agriculture, food, pharmaceutics, coatings, and oil field.[1, 2]

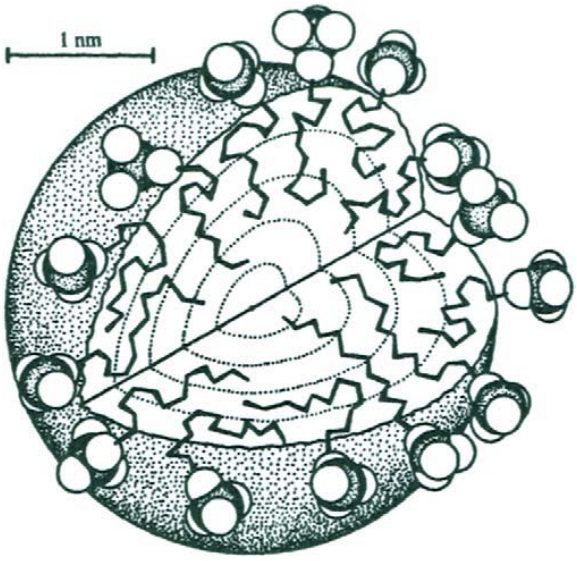

Figure 1.1 A spherical micelle from the association of dodecyl sulfate in water (adapted from Israelachvili J. *Intermolecular and Surface Forces*, Academic Press, London, 1985, p.215).

Similar to the conventional surfactants and lipids, amphiphilic polymers also simultaneously contain hydrophilic and hydrophobic components. Their molar masses are 10–1000 times larger than the "small" molecules and thus here referred to as "large" molecules. These macromolecules offer much larger design flexibility in the structures than the low molar-mass amphiphiles.[3] Controllable parameters include the number and chemical identity of components, molar mass, dispersity, composition, and architecture. As such, almost an infinite number of possible structures may be produced. Amphiphilic polymers with simply two components may have linear (statistical or block), branched (graft), and star (miktoarm star or star block) architectures (Figure 1.2). In addition, individual components may have unique structure-orienting features (e.g., crystallization, formation of helixes) and exhibit special responses to external stimuli (e.g., temperature,

pH, ionic strength). Such freedom in the structural design means a wide range of length scales, time scales, and levels of interactions in the resulting associated nanostructures. Many efforts are being taken to amphiphilic polymers including synthesis, self-assembly in solution, and potential applications in a wide variety of fields.[4, 5]

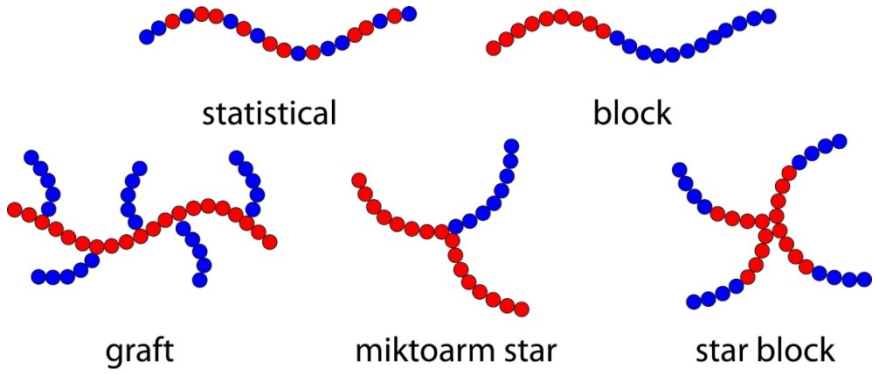

Figure 1.2 Structures of two-component amphiphilic polymers. The blue and red circles indicate hydrophilic and hydrophobic repeat units, respectively.

This thesis contains my work on three separate amphiphilic polymeric systems. Chapter 2 gives the advancement on understanding the self-assembly behavior of amphiphilic diblock copolymers with crystallizable polyethylene (PE) as the hydrophobic component in water. Chapter 3 describes the development of glucose-containing diblock terpolymers as serum-stable nanocarriers of low-solubility drugs during intravenous administration. Chapter 4 presents the development of novel cellulose ether esters with hydrophobic and hydrophilic substituents that are statistically distributed along the backbone and their formulations with low-solubility drugs for bioavailability enhancement during oral administration. The following introduction will describe the current theoretical understanding and experimental efforts of associated nanostructures

from amphiphilic molecules. This part is by far a comprehensive review and readers are directed to several books[1, 6] for detailed information. The micellization of amphiphilic polymers on one hand have much in common with that of surfactants and lipids in terms of thermodynamics, but on the other hand may be significantly affected by a variety of kinetic factors based on the processing pathways.

1.2 Self-assembly of Small Amphiphilic Molecules

1.2.1 Thermodynamics of Micellization

The organization of amphiphilic molecules into associated colloidal structures in a selective solvent can be represented by Equation 1.1 in analogy to a chemical reaction. *S* is an amphiphilic solute and S_n is a micelle with an aggregation number of *n*. Common *n* values for surfactants and lipids in aqueous solutions are 50–100.[7] The association process is thermodynamically driven, or in a thermodynamically favorable manner, and thus is spontaneous and often called self-assembly. At a given temperature (*T*) and pressure (*P*), micellization only happens above a threshold concentration value, or critical micelle concentration (CMC). Experimentally, the associated micelles start to form at CMC and the concentration of unassociated amphiphilic solutes in solution remains roughly constant above CMC.[7] Thermodynamic evaluation suggests that the change of Gibbs free energy during micellization, $\Delta G_{\text{mic}}^{\ 0}$, is related with CMC as shown in Equation 1.2, in which *R* is the gas constant, *T* is the absolute temperature, and CMC is in mole fraction units. Further, the Gibbs–Helmholtz equation gives the relation of the change of enthalpy during micellization, $\Delta H_{\text{mic}}^{\ 0}$, with the temperature dependence of CMC (Equation 1.3). Therefore, experimental determination of CMC in a range of temperatures provides $\Delta G_{\text{mic}}^{\ 0}$, $\Delta H_{\text{mic}}^{\ 0}$, and $\Delta S_{\text{mic}}^{\ 0}$ (the change of entropy during micellization). The values of some surfactants as determined by this method are listed in Table 1.1.

$$nS \leftrightarrow S_n \quad (1.1)$$

$$\Delta G_{\text{mic}}^{\ 0} \approx RT \ln \text{CMC} \quad (1.2)$$

$$\Delta H_{\mathrm{mic}}{}^{0} = \left(\frac{\partial(\Delta G_{\mathrm{mic}}{}^{0}/T)}{\partial(1/T)} \right)_{p} = -RT^{2} \left(\frac{\partial \ln \mathrm{CMC}}{\partial T} \right)_{p} \quad (1.3)$$

The $\Delta G_{\mathrm{mic}}{}^{0}$ values are negative, and thus consistent with the spontaneous nature of the micellization process. Further structural analysis of surfactants with linear alkyl chains as the hydrophobic component divides $\Delta G_{\mathrm{mic}}{}^{0}$ into the contribution from the terminal methyl group (ΔG_{CH3}), that from the methylene groups in the chain (ΔG_{CH2}), and that from the hydrophilic group ($\Delta G_{\mathrm{hydrophilic}}$) as shown in Equation 1.4. *m* is the number of the methylene groups in the hydrophobic tail. Experimental analysis of the dependence of CMC on *m* gave a ΔG_{CH2} of −1.72 kJ mol^{-1} at 25 °C.[7] In other words, the CMC value decreases by 50% as the number of methylene groups increases by 1. Therefore, the CMC value of an amphiphilic polymer with a rubbery hydrocarbon chain of 200 methylene units (corresponding to a molar mass of 2.8 kg mol^{-1}) is ca. 60 orders of magnitude smaller than that of a surfactant with a 12-carbon tail. For reference, the CMC value of sodium dodecyl sulfate is 8.1×10^{-3} M.[7] Therefore, there would be no experimentally detectable free chains in an aqueous dispersion of such polymers.

$$\Delta G_{\mathrm{mic}}{}^{0} = \Delta G_{\mathrm{CH3}} + m\Delta G_{\mathrm{CH2}} + \Delta G_{\mathrm{hydrophilic}} \quad (1.4)$$

Table 1.1 Thermodynamic properties of five surfactants during the micellization process at or near 25 °C.

Surfactant	ΔG_{mic}^0 (kJ mol^{-1})	ΔH_{mic}^0 (kJ mol^{-1})	ΔS_{mic}^0 (J K^{-1} mol^{-1})
Dodecyl pyridinium bromide	−21.0	−4.06	56.9
Sodium dodecyl sulfate	−21.9	2.51	81.9
N-Dodecyl-*N*,*N*-dimethyl glycine	−25.6	−5.86	64.9
Polyoxyethylene (6) decanol	−27.3	15.1	142.0
N,*N*-Dimethyl dodecyl amine oxide	−25.4	7.11	109.0

Reproduced from Paul C. Hiemenz and Raj Rajagopalan, *Principles of Colloid and Surface Chemistry*, 3rd ed.; CRC Press: Boca Raton, FL, 1997, page 374.

The $T\Delta S_{mic}^0$ values of the surfactants as shown in Table 1.1 are uniformly positive, and give remarkably larger contribution to ΔG_{mic}^0 than the ΔH_{mic}^0 values, which are both positive and negative. These results suggest that the micellization process is largely entropy-driven. It might be counterintuitive that the entropy increases as the amphiphilic solutes change from an individually solvated state to a collectively associated form. Instead, it is the solvent water (not explicitly shown in Equation 1.1) that gains much entropy in this process. In the bulk liquid, water molecules form loose, rather disordered networks due to hydrogen bonding. In comparison, water cannot form effective hydrogen bonding with the hydrophobic tails of surfactants and have to adopt special conformations around them, which corresponds to a more ordered state. The micellization process reduces the amount of possible solvated hydrophobic tails and thus lessens the disturbance of the disordered hydrogen-bonded network of water molecules.

Such entropy-driven association of amphiphilic molecules is commonly referred as the "hydrophobic effect". Therefore, it is more accurate to describe micellization as the entropic expulsion of the hydrophobic component from the solvent than to think about the dual affinity of amphiphilic molecules, which may imply the enthalpic contribution. The hydrophobic effect is also commonly observed in amphiphilic polymers and plays an important role in their micellization behavior. On the other hand, other forces (e.g., crystallization, formation of helixes) may also be present and significantly affect the final micelle structures.

1.2.2 Micellar Polymorphism of Surfactants and Lipids

Besides spherical micelles as shown in Figure 1.1, four other morphologies (shapes) of micelle aggregates are also commonly observed from surfactants and lipids (Figure 1.3). Studying polymorphism not only improves the fundamental understanding of the micelle structures, but also expands the application range of these materials. For example, cylindrical (or wormlike, threadlike) micelles can tremendously modify the viscoelastic properties of the aqueous solution and have found applications such as enhanced oil recovery[2] and drug delivery carriers with extended releasing profile.[8] Evaluating the structure of amphiphilic molecules themselves gives very useful guidance about possible morphologies of the resulting stable structures. The conformation of an individual surfactant molecule is dictated by the interplay of the hydrophobic attraction between neighboring molecules and the hydrophilic repulsion between the polar head groups. A key parameter is the packing parameter (p) as defined in Equation 1.5, in

which v_t is the volume of the hydrophobic tail, a_h is the optimal head group area, and $l_{c,t}$ is the critical chain length. Based on simple packing considerations, $p < 1/3$ corresponds to spherical micelles, $1/3 < p < ½$ corresponds to cylindrical micelles, and $1/2 < p < 1$ corresponds to bilayered vesicles.[7] Other factors that may affect the micelle morphologies including solvent and the external environment (e.g., pH, ionic strength, temperature, pressure, external shear forces, magnetic field).

$$p = \frac{v_t}{a_h l_{c,t}} \quad (1.5)$$

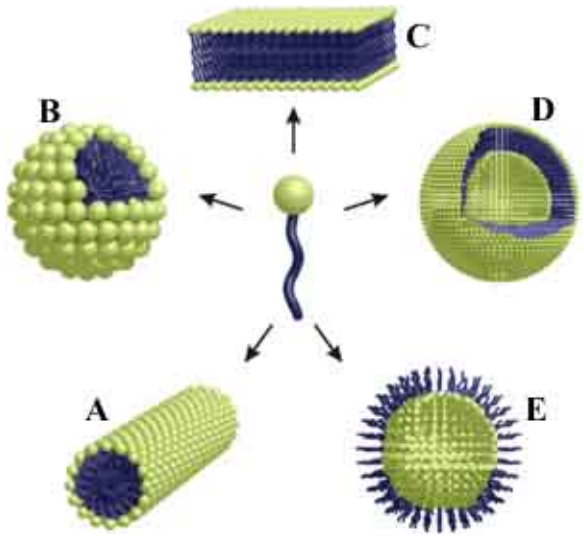

Figure 1.3 Micelles of five different morphologies commonly observed in small surfactants and lipids including (A) cylinders, (B) spheres, (C) planar bilayers, (D) flexible bilayers, or vesicles, and (E) inverted micelles. Reproduced from http://www.vcbio.science.ru.nl.

1.3 Self-assembly of Amphiphilic Diblock Copolymers

1.3.1 Theoretical Modeling

The self-assembly of amphiphilic block copolymers in selective solvents is conceptually analogous to that of surfactants and lipids. The connecting pattern, molar mass, and solubility of the component blocks dictate the morphology and size of the resulting aggregated structures. The simplest case is a nonionic *AB* diblock copolymer in a selective solvent *S*, in which *A* and *B* denote the lyophilic and lyophobic blocks with a degree of polymerization of N_A and N_B, respectively. Three morphologies–bilayered vesicles, cylinders, and spheres–are commonly considered, which are labeled with a geometric index *i* of 1, 2, and 3, respectively.[9] The inner micelle cores are made of insoluble *B* blocks, which are surrounded by the outer micelle coronae composed of swollen *A* blocks. The core–corona interface is small compared to the size of the core or corona domains.

Theoretical modeling can predict the thermodynamically stable morphology and packing characteristics (aggregation number *n*, size of the core *R*, thickness of the corona *H*) of polymeric micelles.[9, 10] For nonionic *AB* diblock copolymers, the free energy per chain, F_{chain}, is evaluated and the minimum among the three morphologies corresponds to the equilibrium state. F_{chain} comprises three contributions,

$$F_{\text{chain}} = F_{\text{interface}} + F_B + F_A \quad (1.6)$$

in which $F_{\text{interface}}$, F_{B}, and F_{A} are the free energies per chain of the interface, the micelle core, and the micelle corona, respectively. First, the interfacial free energy is given by

$$F_{\text{interface}} = \gamma s \quad (1.7)$$

in which γ is the surface tension per unit area and *s* is the interfacial area. γ is largely dictated by the interaction between the lyophobic *B* block and the solvent *S* (γ_{BS}). Next, the difference in the free energy of the core between different morphologies is the elastic energy, $F_{\mathrm{B,elastic}}$,

$$F_{B,\mathrm{elastic}} \approx b_i \frac{R^2}{a^2 N_B} \quad (1.8)$$

in which b_i is a numerical factor that depends on the geometry ($b_1 = \pi^2/8$, $b_2 = \pi^2/16$, and $b_3 = 3\pi^2/80$),[11] and *a* is the length of a monomer unit. The radius of the core, *R*, is equal to $iN_Ba^3/(\varphi_B s)$, in which φ_B is the volume fraction of the *B* block within the core (close or equal to 1, assuming minimal amount of solvent *S* within the core). Finally, F_{A} is the free energy of swollen *A* blocks in the solvent *S*. Besides early treatment using self-consistent field (SCF) methods,[12-18] polymers in dilute solutions are recently modeled based on the scaling theory.[19] The scaling model introduces the concept of correlation blobs to account for the polymer density correlations, and treats a polymer molecule in a semidilute solution as a Gaussian coil of interconnected correlation blobs. The size of a correlation blob (ξ) is chosen such that the interaction free energy per blob is $k_{\mathrm{B}}T$, in which k_{B} is the Boltzman constant. Since the core–corona interface is sharp, the swollen *A* blocks in solution can be viewed as chains tethered at the interface, or polymer brushes.[20, 21] The interface is concave in spherical and cylindrical micelles, and thus the blob size ξ is dependent on the distance from the center *r* (Figure 1.4 and Equation 1.9). The chain ends are assumed to be located in the outmost blob.

$$\xi(r) = \xi(R)\left(\frac{r}{R}\right)^{(i-1)/2} \approx \sqrt{s}\left(\frac{r}{R}\right)^{(i-1)/2} \quad (1.9)$$

The volume fraction of monomer *A* in solution, $\varphi_A(r)$, is related with the blob size as $\xi(r) \approx a\ \varphi_A(r)^{-\nu/(3\nu-1)}$, in which ν is the power-law exponent that reflects the solvent quality (ν = 1/2 for theta solvents, and $\nu \approx 3/5$ for good solvents). The thickness of the corona H_i can thus be obtained based on the conservation of mass,

$$\int_R^{H_i+R} \varphi_A(r)\left(\frac{r}{R}\right)^{i-1} \mathrm{d}r = \frac{N_A a^3}{s} \quad (1.10)$$

Therefore, F_A (the product of $k_B T$ and the number of blobs) is given as

$$F_A = k_B T \int_R^{H_i+R} \frac{\mathrm{d}r}{\xi(r)}$$

$$\approx \begin{cases} (R/\sqrt{s})\ln(1+H_3/R) & i=3 \\ 2(R/\sqrt{s})\left[(1+H_2/R)^{1/2}-1\right] & i=2 \\ H_1/\sqrt{s} & i=1 \end{cases} \quad (1.11)$$

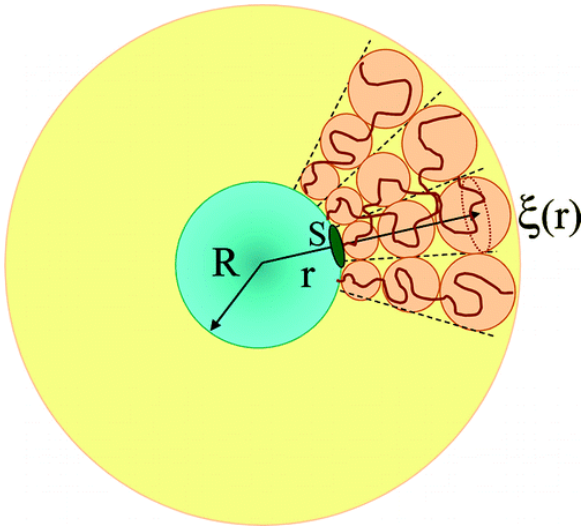

Figure 1.4 Scheme of a spherical micelle from nonionic block copolymers. One swollen *A* corona block is made of a string of correlation blobs, and each correlation blob has a free energy of $k_B T$. Reproduced with permission from Ref[10].

In the starlike regime ($H_i/R >> 1$), spherical micelles are thermodynamically more favorable than cylinders and bilayered vesicles. F_A of spherical micelles with highly curved interface is much smaller than that of the other two morphologies with less curved interface. This result can be rationalized by considering the strong steric repulsion of the rather long corona chains congested across the interface. The aggregation number n exhibits strong dependence on the degree of polymerization of the insoluble B block while rather weak dependence on that of the swollen A block (Equation 1.12).

$$n \approx N_B^{4/5} \left(\frac{a^2 \gamma_{BS}}{k_B T} \right)^{6/5} \quad (1.12)$$

In the crew-cut regime ($H_i/R >> 1$), the elastic stretching of the insoluble A blocks triggers the morphology transition from sphere to cylinder or from cylinder to bilayered vesicles, although F_B is still smaller than $F_{\text{interface}}$ or F_A.[9, 10] The aggregation number n exhibits much stronger dependence on the degree of polymerization of the swollen A block than that in the starlike regime (Equation 1.13).

$$n \approx N_B^{2} \left(\frac{a^2 \gamma_{BS}}{N_A k_B T} \right)^{6\nu/(2\nu+1)} \quad (1.13)$$

The theoretical calculations using scaling model exhibits reasonable agreement with the experimental results in systems such as polybutadiene–polystyrene (PB–PS)[22] and polyisoprene–polystyrene (PI–PS)[10] in *n*-heptane. On the other hand, significant deviations have also been reported about the power-law exponents of several strongly segregated systems such as poly(ethylene oxide)–poly(ethylene-*alt*-propylene) (PEO–PEP) in water in the starlike regime ($n \sim N_{\text{PEO}}^{-0.51}$),[23] poly(acrylic acid)–polystyrene (PAA–PS) in water in both starlike ($n \sim N_{\text{PS}}^{0.2} N_{\text{PAA}}^{-0.15}$)[24] and crew-cut regime ($n \sim$

$N_{PS}^{-0.6}N_{PAA}^{-0.15}$),[25] and polystyrene–poly(4-vinylpyridine) (PS–P4VP) in toluene in the starlike regime ($n \sim N_{P4VP}^{1.93}N_{PS}^{-0.79}$).[26] The deviation is largely ascribed to the non-equilibrium aggregates from amphiphilic polymers. In contrast to surfactants and lipids, amphiphilic polymers may have tremendous practical difficulty to form aggregates at the equilibrium state; the CMC is often not accessible and no exchange is observed between the individual chains and those in micelles. Nevertheless, the theoretical modeling deepens our understanding of the structure and thermodynamics of polymeric micelles, which further provides guidance towards designing the molecular structures of amphiphilic polymers.

1.3.2 Micellar Polymorphism – Experimental Results

Much experimental progress has been reported on controlling the morphology of micelles from amphiphilic *AB*-type diblock copolymers since the mid-1990s. The development is facilitated by the advancement of synthetic techniques (e.g., living anionic,[27] controlled radical,[28-30] and ring-opening polymerizations[31]), sample preparation methods (e.g., nanoprecipitation[32]), and characterization methods (e.g., cryogenic transmission electron microscopy[33] and small-angle X-ray or neutron scattering[34]). Common strategies of morphology control include changing the molecular characteristics of diblock copolymers and adjusting the external environmental stimuli such as solvent, pH, and temperature.

From the synthetic viewpoint, controlling the length of the lyophilic *A* and the lyophobic *B* blocks is a straightforward approach towards manipulating the morphology

of the resulting micelle aggregates. “Living” polymerizations provides convenient access to polymers with precisely-controlled degree of polymerization (N), narrow dispersity ($Đ$), and well-defined end groups. More importantly, the advancement of polymerization techniques with a variety of mechanisms gives much freedom in choosing the chemical identity of the component blocks. Successful examples include polyolefins,[27] polyethers,[27] polyacrylates,[27-30] polyamides,[28-30] and polyesters.[31] To date, systems that have been reported to show morphological dependence on the degree of polymerization of component blocks include PAA–PS,[32, 35] PEO–PS,[36] PAA–polybutadiene (PAA–PB),[37] PEO–PB,[38-40] PEO–poly(ethylethylene) (PEO–PEE),[38] and PEO–poly(γ-methyl-ε-caprolactone) (PEO–PMCL)[41] in water, PI–PS in *n*-heptane,[10] and PEO–PB[42] and PMMA–PS[43] in ionic liquids. In general, decreasing the composition of the lyophilic blocks triggered morphology transition from spheres with highly-curved interfaces to cylinders and further bilayered vesicles with relatively flat interfaces. For example, a phase diagram that illustrates the morphology of the micelles from PEO–PB diblock copolymers in water as a function of the degree of polymerization of the hydrophobic PB block (N_{PB}) and the weight fraction of the hydrophilic PEO block (w_{PEO}) is reproduced as Figure 1.5. At a constant length of the hydrophobic PB block (N_{PB} = 46 or 170), longer hydrophilic PEO blocks tend to require more curved interfaces to relieve the crowdedness between adjacent corona chains. As such, the elastic energy of the PEO chains (F_A) is lowered in spherical micelles, which contributes significantly to the total free energy (F_{chain}). Besides, the coexistence of micelles with different morphologies in the self-assembly of amphiphilic diblock copolymers was commonly observed.[35, 39, 42, 44] As

shown in Figure 1.5, large portions of the phase diagram contain coexisting bilayered vesicles and cylinders (B + C) or cylinders and spheres (C + S), and the window that corresponds to pure cylinders is very small. Possible reasons include (i) the inability of producing aggregates that reach global equilibrium, which is due to the high molar mass of polymers and the strong incompatibility between the lyophobic block and solvent;[40, 45] (ii) the small difference between the free energy of micelles with different morphologies;[46, 47] and (iii) the finite dispersity of the component blocks. In addition, the phase boundaries of morphologies in terms of copolymer compositions showed significant variations between different systems (lyophobic block, lyophilic block, and solvent). Although excellent agreement was achieved between the experimental results and theoretical calculations in the system of PI–PS in *n*-heptane,[10] the phase diagrams in most other systems were determined experimentally without explicit comparisons to the theoretical predictions.[35, 38]

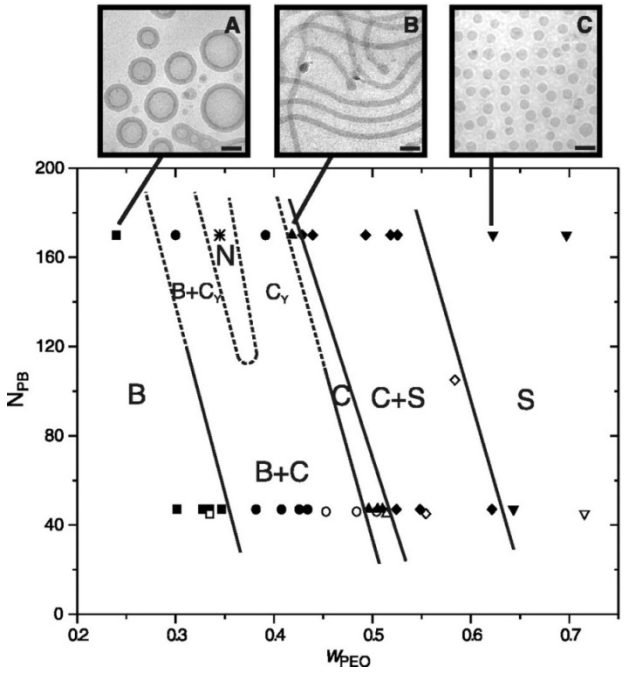

Figure 1.5 A phase diagram that illustrates the morphology of micelle aggregates from PEO–PB diblock copolymers in water as a function of N_{PB} and w_{PEO}. B: bilayered vesicles, C: cylinders, S: spheres, C_Y: brached cylinders, and N: network. Reproduced with permission from Ref[39].

Besides controlling molecular characteristics, adjusting external environmental parameters may also lead to effective morphology control of micelles from *AB*-type diblock copolymers. Bhargava et al. established the phase diagram of one PEO–PS(10–100) sample (the values in the parentheses denote the number-average molar masses of the component blocks in kg mol^{-1}) as a function of the concentration of the copolymer along with the composition of *N*,*N*-dimethylformamide (DMF)/water as the solvent (Figure 1.6).[47] While DMF is nonselective to both blocks, water is selective to the PEO block. At a fixed copolymer concentration, the micelle morphologies evolved from spheres to cylinders and finally vesicles as the water content increased in the solvent mixture. The transition was ascribed to the increased interfacial free energy ($F_{interface}$)

between the hydrophobic PS block and the mixed solvent, which led to an increased stretching of the PS blocks in the core and less curved interfaces with a smaller interfacial area. Similar morphological dependence on the solvent was also observed in PS–PI[48] and PS–poly(dimethylsiloxane) (PS–PDMS)[49] in dialkyl phthalates. Besides, adjusting the temperature may also lead to the effective morphology control. For example, Abbas et al. observed the transition from vesicles to cylinders and finally spheres of PS–PDMS(4–12) as the temperature was increased to trigger a decreased selectivity of the solvent, diethyl phthalate.[49] Interestingly, the observed micelles in these studies are believed to be in the equilibrium state as the morphology transition is reversible with the change of solvent composition or temperature.[47-49] In addition, micelles with ionizable hydrophilic blocks may undergo morphology changes at different pH, as demonstrated in the system of P4VP–PS in DMF/water mixtures by Shen et al.[50]

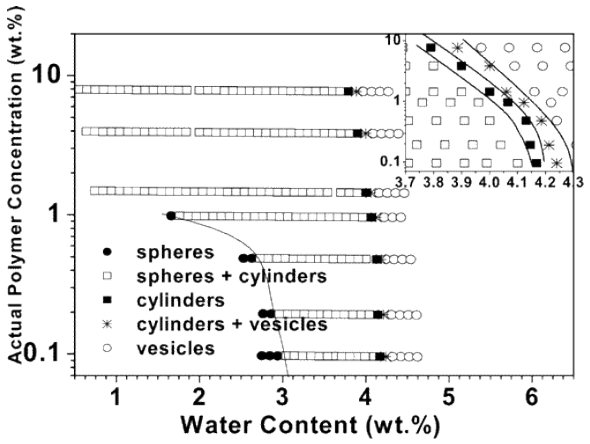

Figure 1.6 A phase diagram that illustrates the morphology of micelle aggregates from a PEO_{227}–PS_{962} diblock copolymer as a function of the concentration of the copolymer and the content of water in the DMF/water mixture. Reproduced with permission from Ref[47].

1.3.3 Preparation of Block Copolymer Micelles

In contrast to the aggregates from lipids and surfactants, few reported polymeric micelles are believed to be at the equilibrium state. The thermodynamic minimum may be revealed by reversible aggregate structures with the change of external stimuli[47-49] or chain exchange between individual micelles.[51-59] In fact, the structures of the self-assembled micelles from many amphiphilic polymers are highly dependent on the pathways through which the samples are prepared, or "it is all about the process".[60] This effect on one hand gives much practical difficulty in studying the equilibrium structures, but on the other hand provides abundant opportunities during processing to prepare a wide variety of stable, kinetically-trapped aggregates.

The simplest method is direct dissolution, in which neat amphiphilic polymers are directly dispersed within the solvent of choice at a desired concentration. The process may be assisted via prolonged stirring, thermal, or ultrasound treatment. Thin-film hydration, which is a slight modification of direct dissolution, includes first preparing a thin layer of the neat polymers and thus facilitates the following solvation in solution. In general, direct dissolution and thin-film hydration are effective at treating samples with low overall molar masses and small lyophobic compositions. Besides, the glass transition (T_g) and melting temperatures (T_m) of the lyophobic blocks should be lower than the processing conditions to ensure some molecular freedom for the core-forming material. Nevertheless, the unimer–aggregate equilibrium may still be difficult to reach within reasonable experimental time frame (several minutes to days), especially in systems with lyophobic components that are extremely incompatible with the solvent. In these cases,

the CMC values are extremely low and the stabilization may instead take micelle scission and fusion pathways.[61]

Nanoprecipitation involves solvents other than the target solvent and may be well suitable for samples with high molar masses, large lyophobic compositions, high T_g and T_m lyophobic components, and strong interfacial tension between lyophobic components and the target solvent.[35, 62] The sample is first dissolved in a common good solvent, then a selective solvent (which is also miscible with the starting solvent) is added to trigger the micellization, and finally any other solvent is removed (e.g., by evaporation) or replaced by the target solvent (e.g., by dialysis). The key points include using a good starting solvent to provide molecular freedom for all components and adding the second solvent slowly enough to ensure the stabilization of the copolymers at each specific solvent composition. Nanoprecipitation has been successfully used in research laboratories for a wide variety of amphiphilic polymers.[4, 5] However, the requirement of large quantities of (organic) solvents and the slow processing are detrimental to the potential in scaling-up.

Amphiphilic polymers can adopt microphase-separated structures in bulk[63, 64] and these pre-existing patterns may be well transferred to the micelle aggregates in solution. The following approach is similar to direct dissolution, but often requires careful annealing for the preparation of the desired microphase separation patterns in bulk and effective preservation of these patterns during subsequent solvation. Interesting structures include hexagonally-packed cylinders of lyophobic components in a matrix of lyophilic components, which may result in cylindrical micelles after solvating the lyophilic components. It has to be reminded that the cylinder window in the phase diagram of

diblock copolymer micelles may be extremely narrow through thin-film hydration (Figure 1.5) or nanoprecipitation (Figure 1.6). In contrast, the cylinder window in the molten diblock copolymers is rather large.[64, 65] Successful preservation during following solvation can be realized by either using high T_g or T_m materials as the core-forming components or introducing covalent cross-linking. Reported examples include Janus micelles,[66-69] core-shell nanofibers,[70] and multicompartment cylinders.[71]

Recent advances of the processing methods of amphiphilic polymers feature novel approaches of remodeling self-assembled nanostructures. For example, Chen et al. demonstrated that spherical PI–PS micelles in *n*-hexane/THF mixtures can be facilely transformed to cylindrical micelles by extrusion through nanoscale pores.[72] The solvent was chosen such that the lyophobic PS block was only slightly insoluble and thus the micelles were able to deform and reorganize rather easily. Besides, the diameter of the pores was smaller than that of the micelles. As a result, the spherical micelles were jammed inside the pores and pushed to fuse into cylindrical micelles. The resulting wormlike micelles may reverse to spheres at quiescent conditions, but the morphology was envisioned to be locked via post-processing steps such as covalent cross-linking. As such, extrusion holds great promise as a powerful and facile method of producing cylindrical micelles. In addition, cylindrical micelles can be obtained by tuning the complexation of amine additives and PAA corona,[73] the interfacial instability of emulsions during solvent evaporation,[74-76] and polymerization-induced self-assembly. [77]

1.4 References

1. Alexandridis, P.; Lindman, B., *Amphiphilic Block Copolymers: Self-Assembly and Applications*. 1st ed.; Elsevier: Amsterdam, 2000.

2. Zana, R.; Kaler, E. W., *Giant Micelles: Properties and Applications*. 1st ed.; CRC Press: Boca Raton, FL, 2007.

3. Lodge, T. P.; Bang, J. A.; Li, Z. B.; Hillmyer, M. A.; Talmon, Y. *Faraday Discuss.* **2005,** 128, 1-12.

4. Gohy, J. F. *Adv. Polym. Sci.* **2005,** 190, 65-136.

5. Riess, G. *Prog. Polym. Sci.* **2003,** 28, (7), 1107-1170.

6. Hamley, I. W., *Block Copolymers in Solution: Fundamentals and Applications*. John Wiley & Sons, Ltd.: New York, 2005.

7. Hiemenz, P. C.; Rajagopalan, R., *Principles of Colloid and Surface Chemistry*. 3rd ed.; CRC Press, Taylor & Francis Group, LLC: Boca Raton, FL, 1997.

8. Tan, J. P. K.; Kim, S. H.; Nederberg, F.; Appel, E. A.; Waymouth, R. M.; Zhang, Y.; Hedrick, J. L.; Yang, Y. Y. *Small* **2009,** 5, (13), 1504-1507.

9. Zhulina, E. B.; Adam, M.; LaRue, I.; Sheiko, S. S.; Rubinstein, M. *Macromolecules* **2005,** 38, (12), 5330-5351.

10. Zhulina, E. B.; Borisov, O. V. *Macromolecules* **2012,** 45, (11), 4429-4440.

11. Semenov, A. N. *Sov. Phys. JETP* **1985,** 61, 733.

12. Meier, D. J. *J. Polym. Sci., Part A: Polym. Symp.* **1969,** 26, (1), 81-98.

13. Helfand, E.; Wasserman, Z. R. *Macromolecules* **1976,** 9, (6), 879-888.

14. Helfand, E.; Wasserman, Z. R. *Macromolecules* **1978,** 11, (5), 960-966.

15. Helfand, E.; Wasserman, Z. R. *Macromolecules* **1980,** 13, (4), 994-998.

16. Leibler, L.; Orland, H.; Wheeler, J. C. *J. Chem. Phys.* **1983,** 79, (7), 3550-3557.

17. Leermakers, F. A. M.; Scheutjens, J. *J. Chem. Phys.* **1988,** 89, (5), 3264-3274.

18. Noolandi, J.; Hong, K. M. *Macromolecules* **1983,** 16, (9), 1443-1448.

19. de Gennes, P. G., *Scaling Concepts in Polymer Physics*. 1st ed.; Cornell University Press: Ithaca, NY, 1979.

20. Degennes, P. G. *Macromolecules* **1980,** 13, (5), 1069-1075.

21. Halperin, A.; Tirrell, M.; Lodge, T., Tethered chains in polymer microstructures. In *Macromolecules: Synthesis, Order and Advanced Properties*, Springer: Berlin / Heidelberg, 1992; pp 31-71.

22. Halperin, A. *Macromolecules* **1987,** 20, (11), 2943-2946.

23. Willner, L.; Poppe, A.; Allgaieri, J.; Monkenbusch, M.; Lindner, P.; Richter, D. *Europhys. Lett.* **2000,** 51, (6), 628-634.

24. Zhang, L.; Barlow, R. J.; Eisenberg, A. *Macromolecules* **1995,** 28, (18), 6055-6066.

25. Azzam, T.; Eisenberg, A. *Angew. Chem., Int. Ed.* **2006,** 45, (44), 7443-7447.

26. Forster, S.; Zisenis, M.; Wenz, E.; Antonietti, M. *J. Chem. Phys.* **1996,** 104, (24), 9956-9970.

27. Baskaran, D.; Mueller, A. H. E. *Prog. Polym. Sci.* **2007,** 32, (2), 173-219.

28. Matyjaszewski, K.; Xia, J. *Chem. Rev.* **2001,** 101, (9), 2921-2990.

29. Hawker, C. J.; Bosman, A. W.; Harth, E. *Chem. Rev.* **2001,** 101, (12), 3661-3688.

30. Moad, G.; Rizzardo, E.; Thang, S. H. *Aust. J. Chem.* **2005,** 58, (6), 379-410.

31. Dove, A. P. *Chem. Commun.* **2008**, (48), 6446-6470.

32. Zhang, L. F.; Eisenberg, A. *Science* **1995,** 268, (5218), 1728-1731.

33. Cui, H.; Hodgdon, T. K.; Kaler, E. W.; Abezgauz, L.; Danino, D.; Lubovsky, M.; Talmon, Y.; Pochan, D. J. *Soft Matter* **2007,** 3, (8), 945-955.

34. Roe, R.-J., *Methods of X-ray and neutron scattering in polymer science*. Oxford University Press: New York, NY, 2000.

35. Zhang, L. F.; Eisenberg, A. *J. Am. Chem. Soc.* **1996,** 118, (13), 3168-3181.

36. Yu, K.; Eisenberg, A. *Macromolecules* **1996,** 29, (19), 6359-6361.

37. Yu, Y.; Zhang, L.; Eisenberg, A. *Langmuir* **1997,** 13, (9), 2578-2581.

38. Won, Y.-Y.; Brannan, A. K.; Davis, H. T.; Bates, F. S. *J. Phys. Chem. B* **2002,** 106, (13), 3354-3364.

39. Jain, S.; Bates, F. S. *Science* **2003,** 300, 460-464.

40. Jain, S.; Bates, F. S. *Macromolecules* **2004,** 37, (4), 1511-1523.

41. Zupancich, J. A.; Bates, F. S.; Hillmyer, M. A. *Macromolecules* **2006,** 39, (13), 4286-4288.

42. He, Y. Y.; Li, Z. B.; Simone, P.; Lodge, T. P. *J. Am. Chem. Soc.* **2006,** 128, (8), 2745-2750.

43. Simone, P. M.; Lodge, T. P. *Macromol. Chem. Phys.* **2007,** 208, (4), 339-348.

44. Chen, L.; Shen, H.; Eisenberg, A. *J. Phys. Chem. B* **1999,** 103, (44), 9488-9497.

45. Won, Y.-Y.; Davis, H. T.; Bates, F. S. *Macromolecules* **2003,** 36, (3), 953-955.

46. Rajagopal, K.; Mahmud, A.; Christian, D. A.; Pajerowski, J. D.; Brown, A. E. X.; Loverde, S. M.; Discher, D. E. *Macromolecules* **2010,** 43, (23), 9736-9746.

47. Bhargava, P.; Zheng, J. X.; Li, P.; Quirk, R. P.; Harris, F. W.; Cheng, S. Z. D. *Macromolecules* **2006,** 39, (14), 4880-4888.

48. Bang, J.; Jain, S.; Li, Z.; Lodge, T. P.; Pedersen, J. S.; Kesselman, E.; Talmon, Y. *Macromolecules* **2006,** 39, (3), 1199-1208.

49. Abbas, S.; Li, Z.; Hassan; Lodge, T. P. *Macromolecules* **2007,** 40, (11), 4048-4052.

50. Shen, H.; Zhang, L.; Eisenberg, A. *J. Am. Chem. Soc.* **1999,** 121, (12), 2728-2740.

51. Lund, R.; Willner, L.; Richter, D.; Dormidontova, E. E. *Macromolecules* **2006,** 39, (13), 4566-4575.

52. Lund, R.; Willner, L.; Stellbrink, J.; Lindner, P.; Richter, D. *Phys. Rev. Lett.* **2006,** 96, (6).

53. Lund, R.; Willner, L.; Richter, D.; Iatrou, H.; Hadjichristidis, N.; Lindner, P. *J. Appl. Crystallogr.* **2007,** 40, S327-S331.

54. Lund, R.; Willner, L.; Pipich, V.; Grillo, I.; Lindner, P.; Colmenero, J.; Richter, D. *Macromolecules* **2011,** 44, (15), 6145-6154.

55. Zinn, T.; Willner, L.; Lund, R.; Pipich, V.; Richter, D. *Soft Matter* **2012,** 8, (3), 623-626.

56. Choi, S.-H.; Lodge, T. P.; Bates, F. S. *Phys. Rev. Lett.* **2010,** 104, (4), 047802.

57. Choi, S. H.; Bates, F. S.; Lodge, T. P. *Macromolecules* **2011,** 44, (9), 3594-3604.

58. Choi, S. H.; Lee, S.; Soto, H. E.; Lodge, T. P.; Bates, F. S. *J. Am. Chem. Soc.* **2011,** 133, (6), 1722-1725.

59. Lu, J.; Choi, S.; Bates, F. S.; Lodge, T. P. *ACS Macro Letters* **2012,** 1, (8), 982-985.

60. Hayward, R. C.; Pochan, D. J. *Macromolecules* **2010,** 43, (8), 3577-3584.

61. Meli, L.; Santiago, J. M.; Lodge, T. P. *Macromolecules* **2010,** 43, (4), 2018-2027.

62. Tuzar, Z.; Kratochvil, P. *Surf. Colloid Sci.* **1993,** 15, 1-83.

63. Bates, F. S.; Fredrickson, G. H. *Annu. Rev. Phys. Chem.* **1990,** 41, 525-557.

64. Bates, F. S.; Fredrickson, G. H. *Phys. Today* **1999,** 52, (2), 32-38.

65. Cochran, E. W.; Garcia-Cervera, C. J.; Fredrickson, G. H. *Macromolecules* **2006,** 39, (7), 2449-2451.

66. Erhardt, R.; Böker, A.; Zettl, H.; Kaya, H.; Pyckhout-Hintzen, W.; Krausch, G.; Abetz, V.; Müller, A. H. E. *Macromolecules* **2001,** 34, (4), 1069-1075.

67. Erhardt, R.; Zhang, M.; Boker, A.; Zettl, H.; Abetz, C.; Frederik, P.; Krausch, G.; Abetz, V.; Muller, A. H. E. *J. Am. Chem. Soc.* **2003,** 125, (11), 3260-3267.

68. Voets, I. K.; Keizer, A. d.; Waard, P. d.; Frederik, P. M.; Bomans, P. H. H.; Schmalz, H.; Walther, A.; King, S. M.; Leermakers, F. A. M.; Stuart, M. A. C. *Angew. Chem. Int. Ed.* **2006,** 45, (40), 6673-6676.

69. Walther, A.; André, X.; Drechsler, M.; Abetz, V.; Müller, A. H. E. *J. Am. Chem. Soc.* **2007,** 129, (19), 6187-6198.

70. Liu, G. *Adv. Mater.* **1997,** 9, (5), 437-439.

71. Walther, A.; Yuan, J.; Abetz, V.; Muller, A. H. E. *Nano Lett.* **2009,** 9, (5), 2026-2030.

72. Chen, Q.; Zhao, H.; Ming, T.; Wang, J.; Wu, C. *J. Am. Chem. Soc.* **2009,** 131, (46), 16650-16651.

73. Cui, H.; Chen, Z.; Zhong, S.; Wooley, K. L.; Pochan, D. J. *Science* **2007,** 317, (5838), 647-650.

74. Jintao, Z.; Ryan C., H. *Angew. Chem. Int. Ed.* **2008,** 47, (11), 2113-2116.

75. Zhu, J.; Hayward, R. C. *J. Am. Chem. Soc.* **2008,** 130, (23), 7496-7502.

76. Zhu, J.; Ferrer, N.; Hayward, R. C. *Soft Matter* **2009,** 5, (12), 2471-2478.

77. Blanazs, A.; Madsen, J.; Battaglia, G.; Ryan, A. J.; Armes, S. P. *J. Am. Chem. Soc.* **2011,** 133, (41), 16581-16587.

2 Self-assembled Polymeric Micelles with Polyethylene Cores in Water*

2.1 Introduction

Amphiphilic block copolymers are macromolecules that contain covalently-connected hydrophilic and hydrophobic polymeric components. The self-assembly of these molecules into discrete nanostructures in a selective solvent is not only of fundamental interest,[1] but can be exploited for a wide variety of applications that include oil modification,[2] nanomaterial synthesis,[3-5] and controlled drug delivery.[6, 7] Of the many advantages that block copolymers offer over surfactants and lipids with low molar mass, large design flexibility is particularly interesting as a polymer with any kind of thermal properties, either rubbery, glassy, or semicrystalline, can be incorporated as the core-forming material as long as it is not fully compatible with the employed solvent.[8] To date, most effort has focused on amphiphilic block copolymers with rubbery (e.g., polybutadiene[9-13]) or glassy (e.g., polystyrene[14-16]) lyophobic components. By contrast, while some theoretical work was pioneered 22 years ago,[17] there has been limited experimental development toward self-assembled nanostructures with crystalline hydrophobic interiors. Reported studies include poly(ethylene oxide) (PEO),[18-23]

* Reproduced in part with permission from Yin, L.; Hillmyer, M. A. *Macromolecules* **2011,** 44, (8), 3021-3028, and Yin, L.; Lodge, T. P.; Hillmyer, M. A. *Macromolecules* **2012,** 45, (23), 9460-9467. Copyright 2011 and 2012 American Chemical Society.

polyethylene (PE),[18, 24-26] syndiotactic polypropylene (PP),[27] poly(ferrocenylsilane) (PFS),[28-34] the stereocomplex between poly(L-lactide) (PLLA) and poly(D-lactide) (PDLA),[35, 36] polyacrylonitrile (PAN),[37, 38] and regioregular poly(3-hexylthiophene) (P3HT)[39, 40] as the lyophobic materials in organic media, and polycaprolactone (PCL)[41-46] and PLLA[47-52] as the hydrophobic components in water.

Using crystalline polymers as the lyophobic component provides opportunities toward nanostructures with additional structural features. In the simplest case, the aggregation of a coil–coil diblock copolymes is largely governed by the elastic energy of the corona and the interfacial energy between the core and the solvated corona, since the elastic energy of the core is relatively small.[1] However, in a coil–crystalline system, the immiscible core blocks can crystallize, and the "extra" crystallization energy may result in unique aggregation behavior of the copolymers.[17] Several early examples reported platelet structures consisting of thin crystalline lamellae sandwiched by swollen corona layers on both sides.[18-21, 24] For example, Richter et al. observed thin platelet structures from PEP–PE diblock copolymers (PEP: poly(ethylene-*alt*-propylene)) in decane, a selective solvent for PEP.[24] The self-assembly was driven by the crystallization of PE during cooling, which resulted in platelets with thicknesses of several nanometers and lateral diameters of a few micrometers. Similar platelet structures were also observed in micelles with PEO cores in nonpolar solvents.[18, 20] In some other systems, the crystallization-driven self-assembly led to cylindrical micelles in solution. For example, poly(dimethylsiloxane)–poly(ferrocenyldimethylsilane) (PDMS–PFDMS) diblock copolymers self-assembled into elongated fibrous micelles with crystalline PFDMS cores

upon cooling in PDMS-selective *n*-alkanes. The epitaxial growth of the crystallizable core blocks was suggested to be the driving force toward the elongated wormlike structures.[53] Other crystalline polymers that form the cores of cylindrical micelles through similar "crystallization-driven self-assembly" processes include syndiotactic PP,[27] PE,[25] PAN,[37, 38] PLLA,[48, 51] and regioregular P3HT.[39, 40]

Polyethylene is a material that can crystallize due to its structural regularity and offers outstanding mechanical and barrier properties.[54] In sharp contrast to some nonpolar organic solvents, which can solubilize PE at elevated temperatures (e.g., 70 °C in decane[24]), water is extremely incompatible with PE. For example, the solubility of water in PE was estimated to be ca. 0.8 wt % at 200 °C.[55] Similarly, common solvents that can solubilize PE (e.g., alkanes and chlorinated solvents) at elevated temperatures are also incompatible with water. Therefore, special methods must be taken to prepare PE-containing nanostructures that are colloidally stable in water. As a result, only a limited number of studies have been reported on such nanostructures in water with PE as the hydrophobic domain. Weber et al. first reported single lamella nanoparticles of high-density polyethylene by the in-situ polymerization of ethylene in water at 23 °C,[56] and further the crystallinity may be adjusted by using different catalysts.[57,58] Zhu and coworkers investigated diblock copolymers and triblock terpolymers that contained linear PE as the only hydrophobic component in the system, in which the molar masses of PE were between 0.75 and 2.0 kg mol^{-1}.[59-61] The authors prepared the micelle dispersions by either casting a toluene solution of the block copolymers onto the surface of water or dialyzing a solution of the terpolymers in dimethylformamide (DMF) against water.

These methods resulted in elliptical or spherical nanoparticles, and their crystallinity was revealed by calorimetry. In addition, Kryuchkov et al. also observed some anisotropic nanostructures with crystalline PE cores from a linear statistical copolymer of ethylene and acrylic acid.[62] The authors used a solvent exchange method, but the starting solvent, tetrahydrofuran (THF), can only solublize copolymers within a narrow composition window.

This chapter describes my efforts towards the self-assembled nanostructures with polyethylene as the core-forming block in water. Poly(*N*,*N*-dimethylacryl-amide)–polyethylene (PDMA–PE, or AE) diblock copolymers were chosen as the model system. To elucidate the effect of the semicrystalline PE block, a PDMA–PEP diblock copolymer (AP) was made as the control sample, whose hydrophobic block was a rubbery polyolefin. First, the self-assembly behavior of the molten AE diblock copolymers in bulk was studied to determine the segregation strength between PDMA and PE. Next, the micellization of AE and AP diblock copolymers in solution was comprehensively investigated to reveal the effect of crystallization on the micelle morphology. In addition, the dependence of the micelle morphology on the composition of AE diblock copolymers was also examined.

2.2 Results and Discussion

2.2.1 Synthesis and Molecular Characterization

AE diblock copolymers were synthesized using a combination of anionic and reversible addition-fragmentation chain transfer (RAFT) polymerizations. As illustrated in Scheme 2.1, butadiene was initialized by *sec*-butyllithium, anionically polymerized in nonpolar cyclohexane at 40 °C, and end-capped with ethylene oxide to afford a hydroxyl-terminated polybutadiene. As determined by ^{1}H NMR spectroscopy, the number-average molar mass (M_n) was 3.1 kg mol^{-1} (end-group analysis), and 91% of the butadiene was incorporated in the 1,4-configuration. The dispersity ($Đ$) was 1.06 by size exclusion chromatography relative to polystyrene standards (SEC, in chloroform at 35 °C). Hydrogenation using heterogeneous catalyst Pt/SiO_2[63] afforded an ω-hydroxyl-functionalized PE. Full saturation (over 99%) was achieved and there was no apparent loss of hydroxyls as determined by ^{1}H NMR spectroscopy (Figure 2.1). Correspondingly, the calculated M_n of the PE-OH was 3.3 kg mol^{-1}. The measured $Đ$ was 1.16 (by SEC, in 1,2,4-trichlorobenzene at 135 °C, relative to PS standards), and no apparent chain degradation or inter-chain cross-linking was detected. The PE homopolymer precursor was a linear low-density polyethylene (LLDPE). 26 ethyl braches per 1000 carbon atoms were statistically distributed along the backbone, and the density was 0.936 g cm^{-3} at 23 °C. In DSC, the PE exhibited a melting peak at 105 °C and the crystallinity was 33% (1st cooling scan, at a rate of 10 °C min^{-1}). A RAFT trithiocarbonate chain transfer agent (CTA)[64] was then attached to the ω-end of the PE-OH, which enabled the subsequent reversible addition-fragmentation chain-transfer (RAFT) polymerization of *N*,*N*-

dimethylacrylamide (DMA). PDMA is a thermoplastic polymer with $T_g \approx 110$ °C,[65] and fully soluble in water in the probed temperature range, 22–120 °C.[66] With the length of the PE block being held constant, that of the PDMA block was systematically changed and a series of AE diblock copolymers were synthesized with the composition of PDMA in the range of 18–87 wt %. The molecular characteristics of the AE diblock copolymers are summarized in Table 2.1.

Scheme 2.1 Synthesis of AE and AP diblock copolymer.

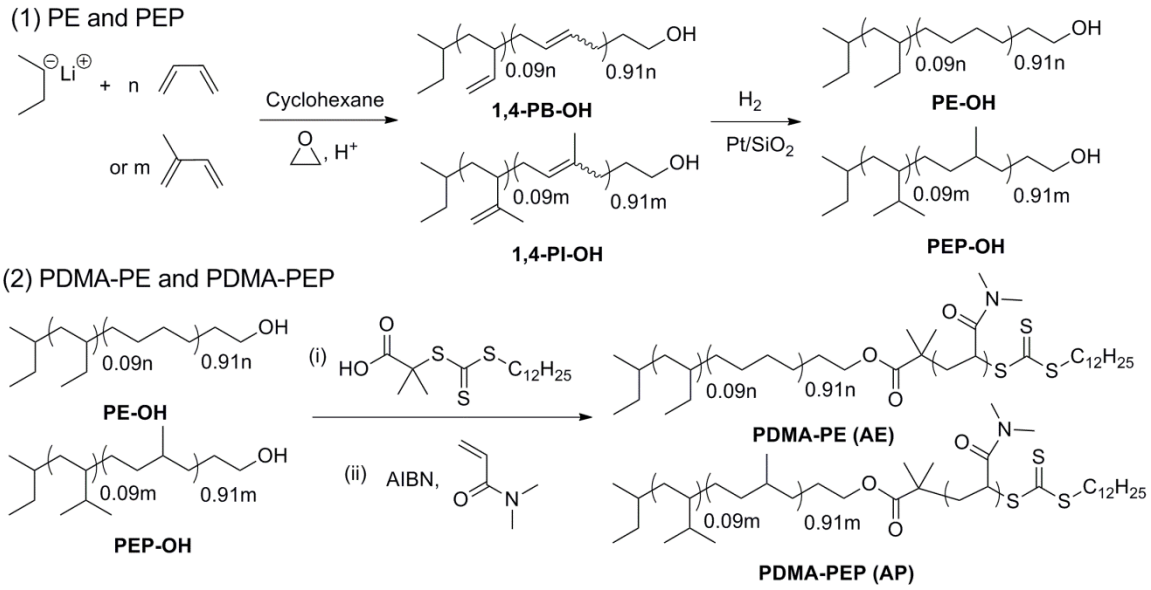

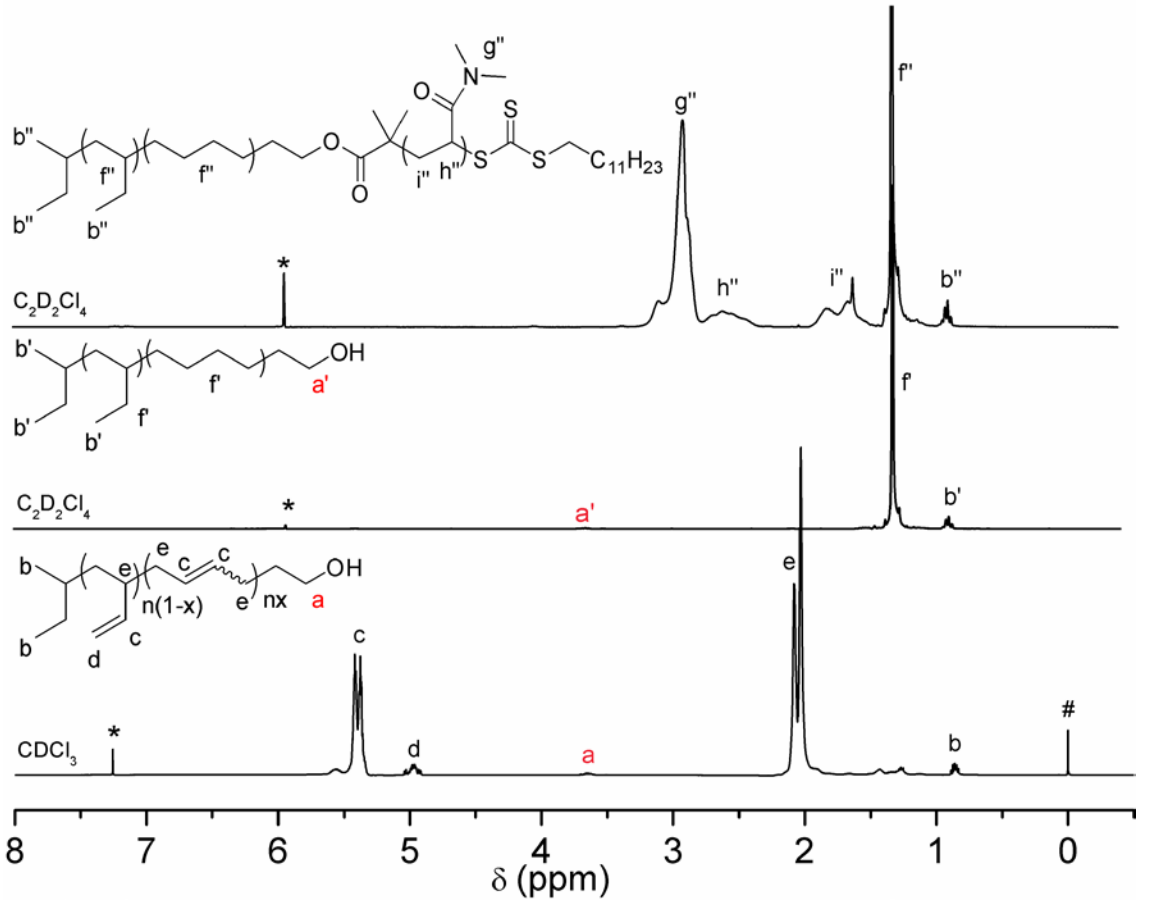

Figure 2.1 From bottom to the top: ^{1}H NMR spectra of 1,4-PB-OH (3.1 kg mol^{-1}), PE-OH (3.3 kg mol^{-1}), and AE(9–3) (12.6 kg mol^{-1}), respectively.

Table 2.1 Molecular characteristics of AE and AP diblock copolymers.

Sample[a]	$N_{PE\ or\ PEP}$[b]	N_{PDMA}[b]	M_n (kg/mol)[c]
AE(0.7–3)	57	7.1	4.0
AE(0.8–3)	57	8.0	4.1
AE(1.0–3)	57	9.8	4.3
AE(1.4–3)	57	14	4.7
AE(2.2–3)	57	22	5.5
AE(4.0–3)	57	41	7.3
AE(5.9–3)	57	59	9.2
AE(9.3–3)	57	94	12.6
AP(11–3)[d]	44	110	14.0

[a] The values in the parentheses are the number-average molar masses in kg mol^{-1} of PDMA followed by that of PE or PEP in the diblock copolymers as determined by ^1H NMR spectroscopy. [b] Number-average degree of polymerization. [c] Total number-average molar mass. [d] The dispersity ($Đ$) of AP(11-3) was 1.10 as determined by SEC relative to PS standards. SEC analysis of AE(9.3-3) was attempted using 1,2,4-trichlorobenzene as the eluent at 135 °C, but no detectable polymer eluted, which was possibly due to the adsorption of PDMA block to the columns.

Similar synthetic procedure was followed except that isoprene was substituted for butadiene to synthesize one PDMA–PEP diblock copolymer, AP(11–3), as shown in Scheme 2.1. The full saturation during hydrogenation, complete transformation of the end-group, and successful polymerization of the PDMA block were also supported by ^1H NMR spectroscopy (Figure 2.2). Besides, the blocking efficiency was monitored using SEC as shown in Figure 2.3. The elution curve of AP(11–3) shifted to a lower elution volume without a detectable residual PEP homopolymer signal. The molecular characteristics are also listed in Table 2.1. Similar to AE(9–3), AP(11–3) had a small

olefinic hydrophobic block of 3.1 kg mol^{-1}, and the mass fraction of the PEP block in the overall copolymer was 22 wt %. But in contrast to semicrystalline PE, the PEP block was rubbery with a T_g of −65 °C.

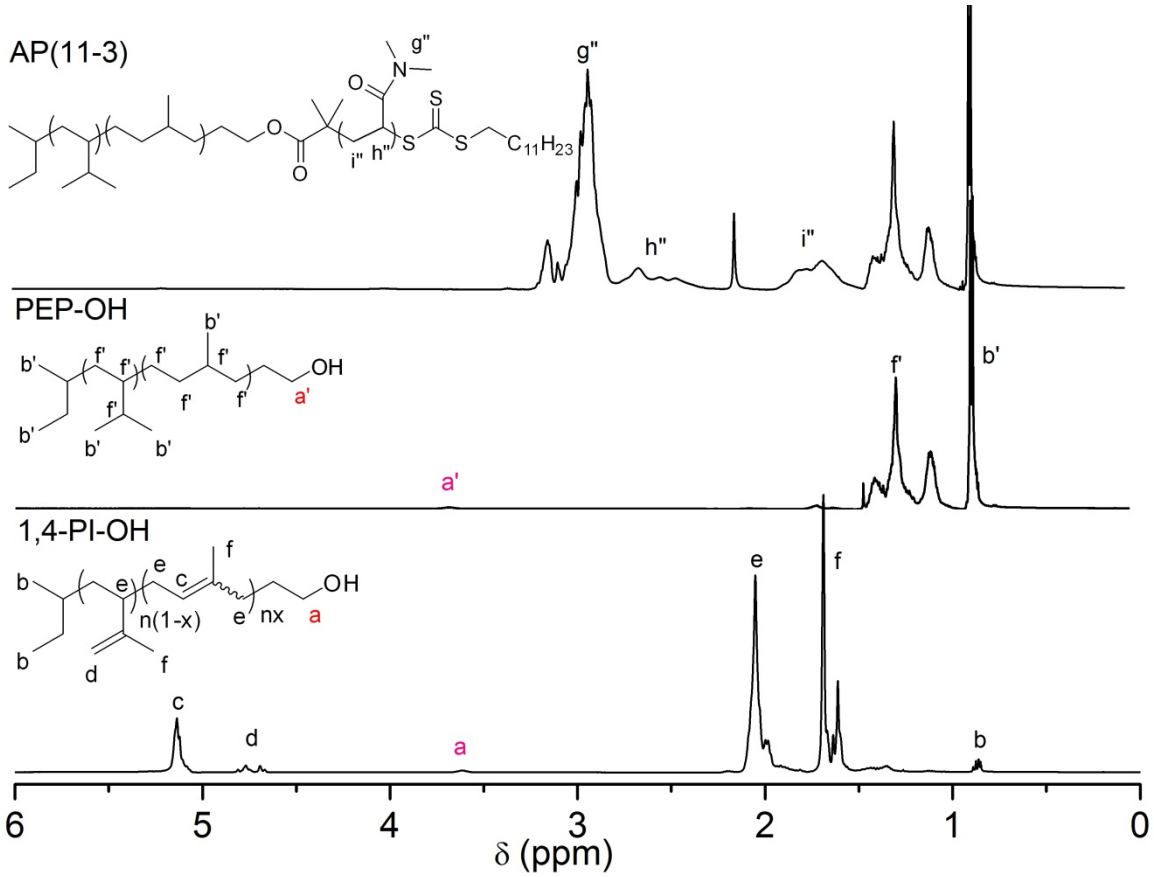

Figure 2.2 From bottom to the top: ^{1}H NMR spectra of 1,4-PI-OH (3.0 kg mol^{-1}), PEP-OH (3.1 kg mol^{-1}), and AP(11–3) (14.0 kg mol^{-1}).

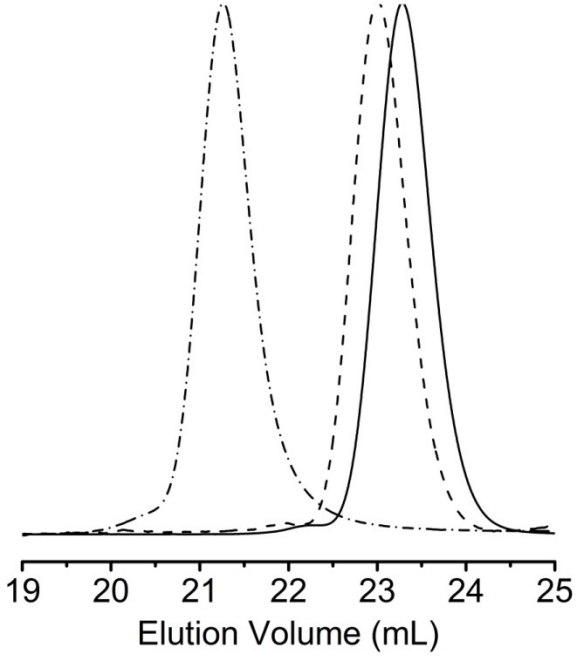

Figure 2.3 SEC traces of 1,4-PI-OH (3.0 kg mol^{-1}) (solid), PEP-OH (3.1 kg mol^{-1}) (dash), and AP(11–3) (dash dot). The mobile phase was $CHCl_3$ and the temperature was 35 °C. The *Đ* values relative to PS standards of 1,4-PI-OH, PEP-OH, and AP(11–3) were 1.06, 1.05, and 1.10, respectively.

2.2.2 Bulk Morphological Properties of AE Diblock Copolymers

Small-angle X-ray scattering (SAXS) was carried out to probe the microphase separation behavior of molten AE diblock copolymers in bulk. Despite the rather low overall molar masses (< 10 kg mol^{-1}), microphase separation between the two component blocks at 140 °C was supported by the sharp principal scattering peaks in all samples examined except AE(0.7–3), which had the shortest PDMA chains. As shown in Figure 2.4, several samples also exhibited higher-order scattering, which indicated the long-range order. The microphase morphologies were inferred by the relative positions of the secondary peaks. Identified morphologies included PE spheres (Bcc) and cylinders (Hex) in PDMA matrices, lamellae, and PDMA cylinders (Hex) in PE matrices. Interestingly,

PE cylinders in PDMA matrices were observed in AE(4.0–3) and AE(5.9–3), whose volume fractions of the PE blocks were 0.54 and 0.45, respectively. In general, polymers with a larger statistical segment length (a) exhibit stronger tendency to stretch in the molten state.[67] Since a_{PE} and a_{PDMA} were 8.2 and 5.8 Å, respectively, the PE chains were more easily stretched than the PDMA blocks.[68] Therefore, the interface tended to curve toward the PE blocks to allow the relaxation of PDMA chains at the expense of PE blocks. As a result, a lamellar phase tended to transform into a cylindrical phase with PE domains in a PDMA matrix, which was qualitatively consistent with the observations. Similarly, PEO−poly(1,2-octylene oxide) diblock copolymers with high conformational asymmetry were reported to form non-lamellar phases (cylinders and gyroid) near a f(PEO) of 0.5.[69] However, further quantitative analysis indicated that the conformational asymmetry alone failed to explain the shift of the phase boundary in the PDMA–PE system. According to Matsen and Bates, the mean-field phase boundary between Hex and Lam was at f(PE) ≈ 0.41 for samples with a conformational asymmetry factor, defined as $(a_{PE}-a_{PDMA})/(a_{PE}+a_{PDMA})$, of 0.17 and χN of 30.[67] At 140 °C, χN of AE(4.0–3) and AE(5.9–3) were 32 and 39, respectively. Therefore, both AE(4.0–3) and AE(5.9–3) should have formed lamellar phases. The reason for this discrepancy is not clear.

Table 2.2 Bulk morphological properties of AE diblock copolymers at 140 °C.

Sample	f_{PE}[a]	Bulk morphology[b]	d (nm)[c]
AE(0.7–3)	0.87	Dis	10.1[d]
AE(0.8–3)	0.86	Hex	10.5
AE(1.0–3)	0.83	Hex	10.9
AE(1.4–3)	0.77	Lam	13.8
AE(2.2–3)	0.68	Lam	16.0
AE(4.0–3)	0.54	Hex	21.6
AE(5.9–3)	0.45	Hex	25.2
AE(9.3–3)	0.34	Bcc	29.1

[a] Volume fraction of the hydrophobic PE blocks at 140 °C. Using literature density values: ρ(PE) = 0.785 g cm^{-3}. ρ(PMMA) of 1.13 g cm^{-3} was used as that of PDMA due to structural similarity.[68] [b] Morphologies of molten block copolymers as determined by SAXS: Lam = lamellae; Hex = hexagonally packed cylinders; Bcc = body-centered cubic spheres; Dis = disordered. [c] Domain spaces (d) as determined using the location of the primary scattering peaks (q^*) following $d = 2\pi/q^*$. [d] A broad peak at q = 0.0602 Å^{-1} with very low intensity was observed, and no other detectable secondary peaks (Figure 2.4).

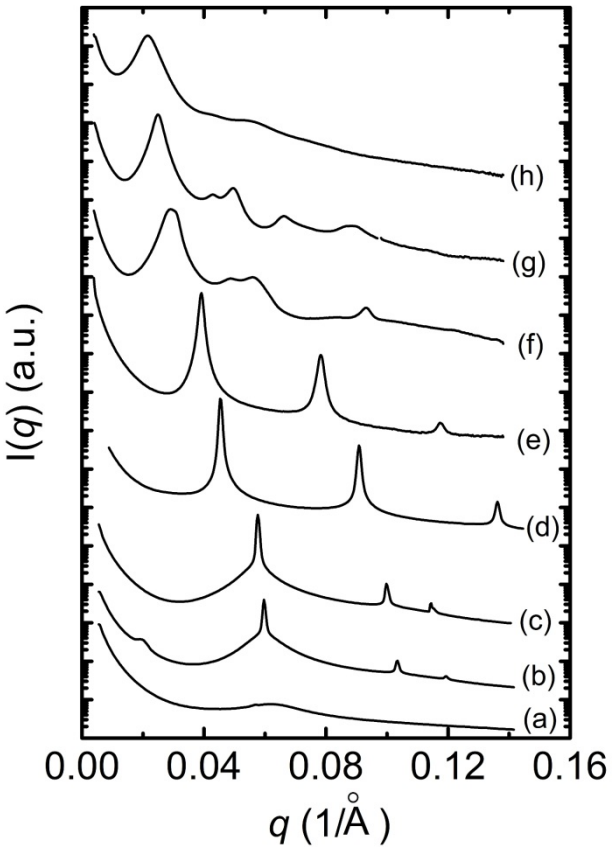

Figure 2.4 SAXS profile of molten AE diblock copolymers in bulk at 140 °C. From bottom to top: (a) AE(0.7–3), (b) AE(0.8–3), (c) AE(1.0–3), (d) AE(1.4–3), (e) AE(2.2–3), (f) AE(4.0–3), (g) AE(5.9–3), and (h) AE(9.3–3).

The Flory–Huggins interaction parameter χ between PE and PDMA blocks was estimated based on the temperature dependence of the domain spacing (D_{lam}) of a lamellae-forming sample, AE(2.2–3). D_{lam} is a function of the average statistical segment length of the two component blocks (a_{AE}), the total degree of polymerization (N), and χ. The prefactor was determined to be 1.40 by considering both volume fraction and conformational asymmetry.[67] The exact form is as shown in Equation 2.1.

$$D_{lam} = 1.40 a_{AE} N^{2/3} \chi^{1/6} \quad (2.1)$$

$$a_{AE} = \left(\frac{f_{PDMA}}{a_{PDMA}^{\ 2}} + \frac{f_{PE}}{a_{PE}^{\ 2}} \right)^{-1/2} \quad (2.2)$$

$$\chi(T) = \frac{221}{T} - 0.24 \quad (2.3)$$

The reference volume was 118 Å^3. An empirical temperature dependence of χ was extracted as Equation 2.3 (Figure 2.5). Correspondingly, χ between PE and PDMA was estimated to be 0.29 at 140 °C. These results led us to conclude that the synthesized PDMA–PE diblock copolymers fall into the intermediate-segregation regime. In addition, the obtained χ value between PE and PDMA was comparable to some other structurally similar systems such as LLDPE and PEO[70] or PLA,[71] whose χ were both estimated to be ~ 0.2 at 140 °C.

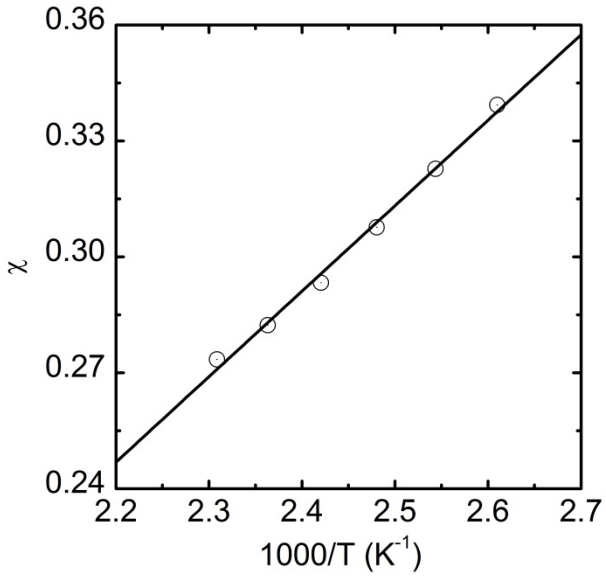

Figure 2.5 Temperature dependence of χ as determined through the change of the domain spacing (D_{lam}) of a lamellae-forming sample, AE(2.2–3), between 110 and 160 °C.

2.2.3 Oblate Ellipsoidal Micelles with Semicrystalline PE cores

Two samples with similar compositions and overall molar masses, AE(9–3) and AP(11–3), were initially used to study the effect of crystallization on the self-assembled micelles in water. The mass fractions of the hydrophilic PDMA blocks were rather large, and thus AP(11–3) was expected to form spherical micelles in water. Dry copolymer samples were directly mixed with desired amount of HPLC-grade water to target 0.5–3.0 wt % polymer in H_2O, and the aqueous dispersions were equilibrated at 120 °C in pressure vessels (i.e., above T_m of PE and T_g of PEP). The mixture became homogeneous (but not optically clear) after several hours, and was equilibrated at 120 °C for a total of 5–7 days. The aqueous dispersions were then cooled to 23 °C at a rate of 2 °C min^{-1}, and no apparent change was observed during this step. Such prepared samples exhibited slight blue tinge under day-light lamps and thus indicated nanosized scatterers.

During the course of the study some hydrolysis of the PDMA block was observed after prolonged heating at 120 °C. For example, ca. 40% of the amide groups were hydrolyzed in AP(11–3) after the aqueous dispersion was held at 120 °C for 7 days as determined by ^{1}H NMR spectroscopy. Hydrolysis was slowed by degassing the copolymer-water mixture prior to heating (for reasons that were unclear), although it could not be completely prevented. All samples described here were degassed and kept for 5–7 days at the same temperature (120 °C) to achieve a similar extent of hydrolysis. The ester bonds connecting the polyalkane and PDMA blocks were mostly intact after sample preparation (ca. 90% by end-group comparison in ^{1}H NMR spectra, and no separate homopolymer peaks in SEC for AP(11–3)). Since the micelle corona segments

were highly congested at the hydrophobic interface,[9] the chance of exposing these ester groups directly to the aqueous media was low.

Dynamic light scattering (DLS) provides information about the average size and size distribution of colloidal scatters suspended in a solvent. The second-order scattering intensity correlation functions, $g_2(t)$, were measured at five different angles between 60° and 120° at 25 °C, and converted to the first-order correlation functions, $g_1(t)$, using the Siegert relation $g_2(t) = 1 + |g_1(t)|^2$. The dispersity (defined as μ_2/Γ^2, in which μ_2 is the second cumulant and Γ is the average decay rate) of the suspended particles from the cumulant fitting of $g_1(t)$ were around 0.40 in both AE(9–3) and AP(11–3), which indicated the rather polydisperse nature of the micelles.[72] Besides, two separate decay modes were present in the distribution profile as generated with the REPES algorithm (Figure 2.6).[73] As such, the double-exponential expansion was used to fit the $g_1(t)$ data, and a linearity ($R^2 > 0.99$) between the translational diffusion coefficient (D) and squared scattering vector (q^2) was obtained for both modes. Through the Stokes–Einstein equation, two sizes of aggregates were obtained: R_h = 24, 92 nm in AE(9–3) and R_h = 25, 95 nm in AP(11–3). These values were quantitatively consistent with the REPES distribution profile, and thus corroborated a bimodal distribution of the micelles. On the other hand, quantitative analysis of the composition indicated that the copolymers mostly resided in the smaller micelles in both samples. Using Shibayama's bimodal analysis,[74] the mass fractions of the smaller and larger aggregates in the AE(9–3) dispersion were determined to be 88.6 wt % and 11.4 wt %, respectively. Similar results were obtained in the AP(11–3) dispersion, 89.0 wt % and 11.0 wt % for the smaller and larger aggregates,

respectively. If both the small and large aggregates were assumed to be spheres (mass ~ R^3), the number fractions of the smaller ones were estimated to be larger than 99.8% in both cases. Therefore, the smaller aggregates were greatly populated in the dispersions, and the probability of finding the larger ones was very low. These results were similar to the previous observations of our group.[75]

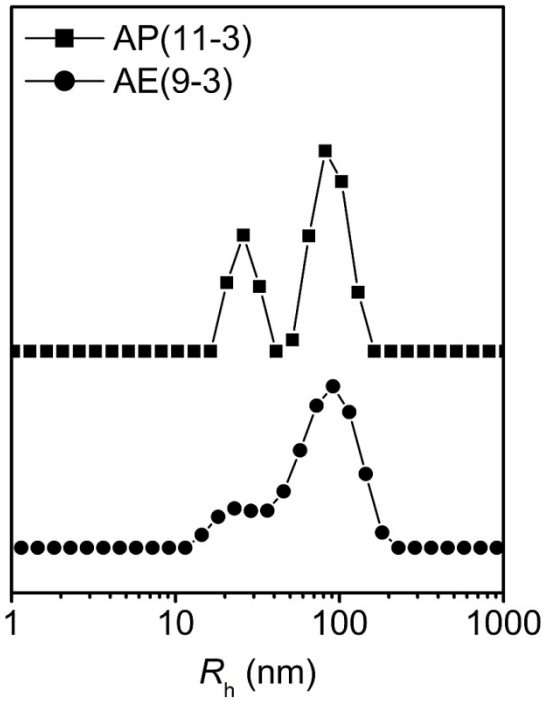

Figure 2.6 Apparent size distribution of the AE(9–3) and AP(11–3) micelles as generated from the REPES algorithm. The scattering angle was 90°.

Cryogenic transmission electron microscopy (cryo-TEM) directly visualizes micelles in vitrified ice and thus the results closely reflect the aggregate structures in their native aqueous environment. Spherical micelles were observed in AP(11–3) with rubbery hydrophobic component. The micelles showed uniformly circular cross-sections (Figure

2.7b), which corresponded to the micelle cores. The existence of the micelle corona was revealed by the open space between the micelle cores, and in some cases the diffuse layer of corona was discernible around the cores. The morphology was similar to previously reported micelles from amphiphilic diblock copolymers with rubbery hydrophobic components such as PEO–PB and PEO–PMCL.[10, 12, 76] By tracking the variation of optical density, the micelle core radius (R_c) was determined to be 9.2 ± 1.1 nm. Correspondingly, the average aggregation number (n) was 540 (using the melt density of PEP as 0.856 g cm^{-3} at 25 °C),[68] and the interfacial area per chain (a_0) was 2.0 nm^2. The degree of stretching of the hydrophobic chain (s) was 1.7, which was defined by $R_c/\langle h^2\rangle_0^{1/2}$ where $\langle h^2\rangle_0^{1/2}$ is the end-to-end distance of a polymer chain in the random-walk configuration. These values were similar to other highly segregated systems such as micelles from PEO–PB in water[10] and ionic liquids.[77] In addition, R_h of the spherical micelles was estimated to be 26 ± 1 nm by taking half of the distance between the centers of two adjacent micelles, which was consistent with the size of the small aggregates from the DLS analysis within experimental error. In addition, no large aggregates were observed in any of the grids (~ 3) prepared from the samples made in different trials.

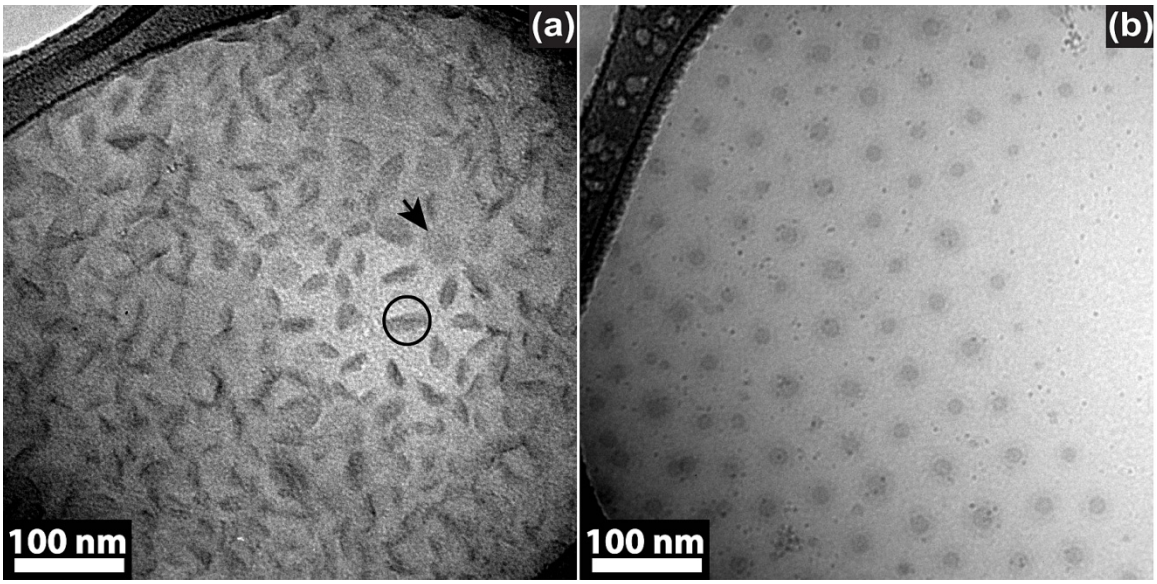

Figure 2.7 Representative cryo-TEM images from 0.5 wt % dispersions of (a) AE(9–3) and (b) AP(11–3), respectively.

In the 0.5 wt % AE(9–3) dispersion (Figure 2.7a), the majority of the aggregates also consist of small particles. Some micelles appeared rather dark and had rodlike cross-sections as one highlighted by a black circle, while others appeared rather light and had circular cross-sections as one indicated by a black arrow, and there were structures with intermediate contrast. The micelles prepared from several other AE diblock copolymers with different compositions exhibited similar morphologies, as exemplified by AE(3–1.4) in Figure 2.8a. Under the employed conditions, the crystalline PE within the cores was clearly visualized, while the amorphous PE was barely discernible; the electron densities (ρ_e) of crystalline PE, rubbery PE and amorphous ice were 337, 313, and 314 electrons nm^{-3}, respectively.[78] Aggregates with similar morphologies as revealed by cryo-TEM were obtained from PEO-modified lipids in water.[79, 80] The great similarity between these two systems led us to believe that the crystalline PE components within the micelle cores

were also likely to be disks. In other words, Figure 2.7a reveals the crystalline PE within the micelle cores viewed in different conformations relative to the electron beam—the dark rodlike particles were imaged edge-on, while those light, circular ones were imaged face-on. By tracking more than 100 particles, the lateral radius of the PE crystals was determined to be 15 ± 2 nm and the thicknesses was 5.5 ± 0.8 nm.

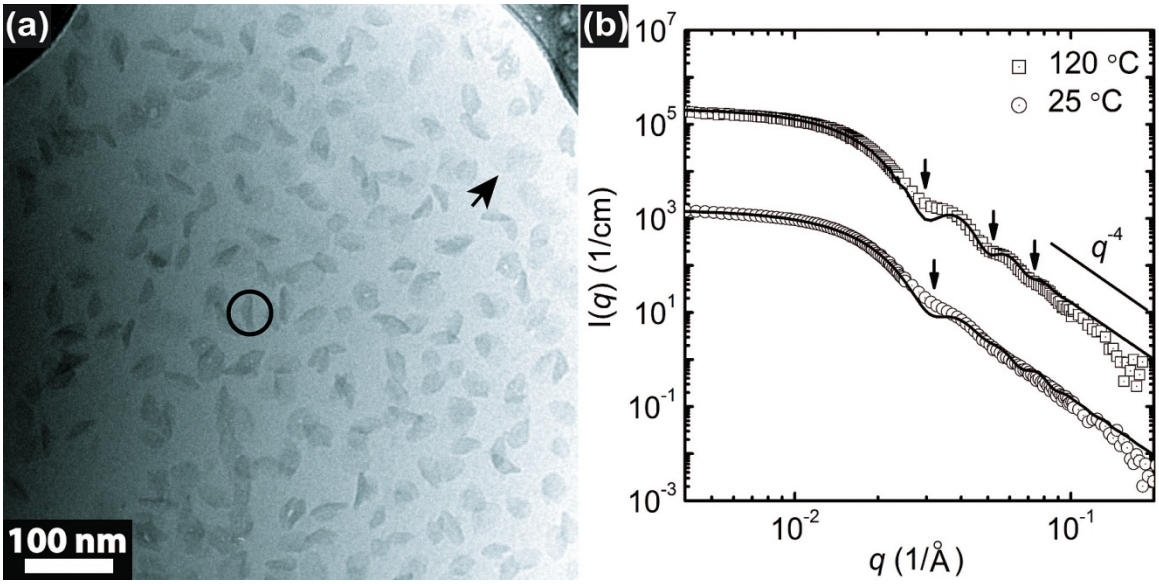

Figure 2.8 (a) A representative cryo-TEM image from a 0.5 wt % dispersion of AE(1.4–3) in water. (b) SANS profile of AE(1.4–3) micelles in D_2O at 25 °C (circles) and 120 °C (squares). The absolute intensity at 120 °C was shifted upward by a factor of 10^2 for clarity. The solid black curves represent the data modeling assuming an ensemble of non-interacting spheres at 120 °C and oblate ellipsoids at 25 °C, respectively.

Small-angle neutron scattering (SANS) was further carried out to elucidate the overall shape of the PE micelle cores that contained both crystalline and rubbery components. Instead of AE(9–3), AE(1.4–3) will be focused on in this section because AE(1.4–3) had the shortest PDMA chains among all of the disk-forming samples.

Therefore, the total scattering profile of AE(1.4–3) included rather insignificant contribution from PDMA, and the data can be conveniently treated without explicit consideration of the swollen PDMA corona. A 0.5 wt % dispersion of AE(1.4–3) in water also exhibited disklike micelles with both edge-on (as highlighted by a black circle, exhibiting a dark, rodlike cross-section) and face-on (as highlighted by a black arrow, exhibiting light, circular cross-sections) orientations as shown in cryo-TEM **(**Figure 2.8a). The mean lateral radius and thickness of the crystalline PE cores were 18 ± 3 nm and 4.3 ± 0.8 nm, respectively. For SANS measurement, a hydrogenous AE(1.4–3) in D_2O was prepared following the same heat-assisted direct-dissolution procedure. Under this condition, the neutron scattering length densities (SLD) of crystalline and amorphous PE were quite similar, and sharply different from the D_2O medium—at 25 °C, the SLD values of crystalline PE, amorphous PE, and D_2O were -0.35×10^{-6} Å^{-2}, -0.33×10^{-6} Å^{-2}, and 6.36×10^{-6} Å^{-2}, respectively. As such, we treated the micelle cores to be homogeneous using an average SLD of -0.33×10^{-6} Å^{-2}, and did not make any distinction between the crystalline and amorphous components. Besides, we only included the hydrophobic PE cores in the form factor of the micelles, since the contribution from the PDMA corona was rather insignificant (the details are shown in Figure 2.21 in the Experimental Section). The scattering profile of a 3.0 wt % AE(1.4–3) dispersion at 25 °C is shown in Figure 2.8b (circles). Using model-free treatment, the radius of gyration (R_g) of the micelle cores was determined to be 12.5 ± 0.4 nm, and the interfacial area per chain (a_0) was 1.03 nm^2. Furthermore, form factor modeling was carried out to elucidate the shape of the overall PE cores. As shown in Figure 2.8b, the scattering profile of

AE(1.4–3) was well represented with a model of oblate ellipsoids with a minor axis (R_a) of 11.4 ± 0.2 nm and a major axis (R_b) of 17.4 ± 0.1 nm (Equation 2.19). A better fit was achieved by assuming that R_b followed the Gaussian distribution with a standard deviation of 1.0 nm while R_a was monodisperse. On the other hand, fitting the data using the model of spheres with radii (R_c) following the Gaussian distribution gave R_c = 13.7 ± 0.1 nm and dispersity (σ/R_c) = 0.171 ± 0.001 (Equation 2.13). Fitting the data using the model of randomly orientated disks whose thicknesses (L) were monodisperse while the radii (R_c) followed the Schulz distribution gave R_c = 12.4 ± 0.1 nm, dispersity = 0.116 ± 0.002, and L = 27.8 ± 0.1 nm (Equation 2.16). The results from neither of these two fittings were consistent with cryo-TEM data (R_c = 18 ± 3 nm).

The combined results from cryo-TEM and SANS led us to conclude that the AE(1.4–3) micelles contained "multi-compartment" cores—disks of crystalline PE existed as flat disks at the center, which were sandwiched by amorphous PE on both sides, and the overall PE cores can be approximated as oblate ellipsoids. Similarly, the AE(9–3) micelle cores were inferred to be also "multi-compartment" in nature. Previously, Weber et al. used a "nanohamburger" model with amorphous sheets of 1.4 nm thick residing on the both sides of a single lamella of 6.3 nm thick to describe the lamellar nanoparticles made of 70% crystalline PE.[56] On the other hand, micelles with no crystallinity (e.g., those with rubbery PEP cores from AP(11–3)) are spherical at relatively high hydrophilic block compositions. As such, the oblate ellipsoidal micelles with LLDPE cores of ca. 30% crystallinity can be viewed as intermediate structures between spheres with zero crystallinity and disks of HDPE of 70% crystallinity.

To investigate the micelle structures prior to crystallization, SANS experiments were further carried out on the dispersions of AE(1.4–3) in D_2O at 120 °C. Due to the extreme hydrophobicity, molten PE was not soluble in water even at 120 °C, in sharp contrast from several reported systems of crystalline polymeric surfactants in organic media.[18, 24, 29] Instead, AE copolymers should also aggregate into micelles at 120 °C, but as the PE was molten and thus these micelles were similar the micelles with rubbery PEP cores at 25 °C. The azimuthally integrated absolute scattering intensity is shown in Figure 2.8b as squares (shift upward by a factor of 10^2 for clarity). The change in the scattering profile from 120 to 25 °C was not likely to come from the variation of particle size distribution. The inter-micelle chain exchange was essentially prohibited (as discussed in Section 2.2.4), and thus the overall dispersity of particle size was unchanged. From model-free treatment, R_g of AE(1.4–3) micelles at 120 °C was determined to be 11.9 nm, and the interfacial area per chain (a_0) was 1.12 nm^2. Furthermore, the scattering profile can be well reproduced using a model of non-interacting spheres with radii that followed the Gaussian distribution, which is shown as the black solid curve in Figure 2.8b. The average radius (R_c) of the spheres was 15.5 nm, and the dispersity (σ/R_c) was 0.09. These results are in excellent harmony with the size of oblate ellipsoidal cores of PE at 25 °C, indicating minimal change of the aggregation number of individual micelles during crystallization.

To probe the thermal behavior, the AE(9–3) micelle solution was encapsulated in a hermetically-sealed aluminum pan and analyzed by DSC. The temperature was ramped between 20 and 120 °C at a rate of 2 °C min^{-1}. As illustrated in Figure 2.9a, an

endothermic transition peak was observed at 98 °C during the 2nd heating scan that corresponded to the melting of PE, and an exothermic peak occurred at 65 °C during the 2nd cooling scan that indicated the crystallization of PE. Similar to the PE nanocrystals in organic media,[24] the observed undercooling (39.5 K) is significantly smaller than that of PE crystals with similar lamellae size from homopolymers in bulk by Thompson–Gibbs equation (140 K). By tracking the 2nd cooling scan, the crystallinity of the micelle cores was determined to be ca. 30%, close to that of the PE homopolymer precursor. Similar results were obtained with the AE(1.4–3) dispersion. In contrast, no detectable thermal transitions were observed in the AP(11–3) 3.0 wt % sample (Figure 2.9b), which was consistent with the rubbery nature of the PEP micelle cores.

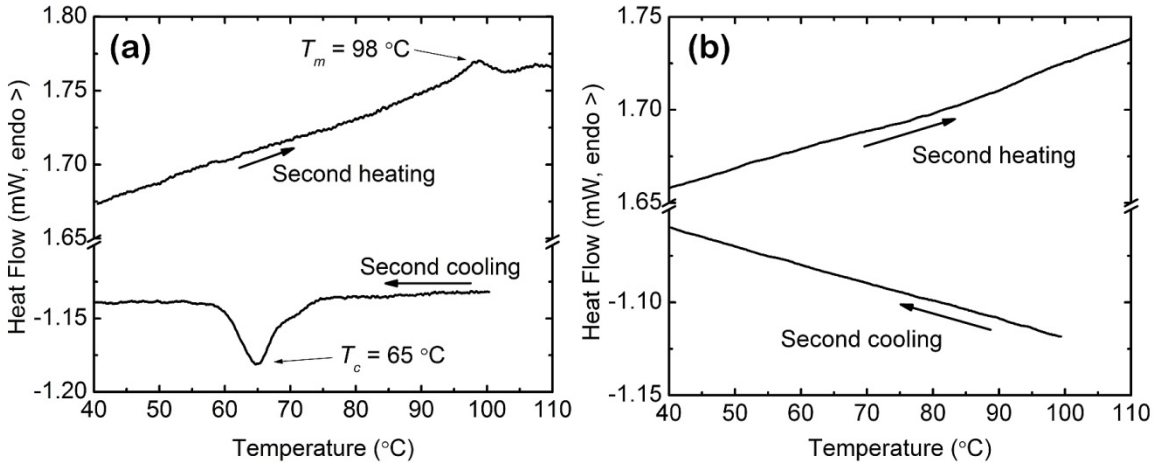

Figure 2.9 DSC profile of 3.0 wt % (a) AE(9–3) and (b) AP(11–3) micelle dispersions as the temperature was ramped at a rate of 2.0 °C min^{-1} between 20 and 120 °C.

Wide-angle X-ray scattering (WAXS) experiments were performed on the micelle dispersions to extract information about the crystal structure of PE in the confined nanosized cores. As shown in Figure 2.10a, two diffraction peaks were observed at 1.50

and 1.66 $Å^{-1}$, which corresponded to the (110) and (200) reflections of the orthorhombic crystal lattice of PE, respectively.[25, 81] This result indicated that the PE chains resided in the same form of crystal lattice as that most commonly observed in bulk.[54] The size of the nanocrystals was estimated to be ca. 25 nm from the full width at half-maximum of the (110) reflection using the Scherrer equation,[82] which was consistent with cryo-TEM data. Similar results were obtained with the AE(1.4–3) dispersion. However, the AP(11–3) sample showed no detectable diffraction in the same *q* range (Figure 2.10b), which was in line with the amorphous nature of the PEP cores.

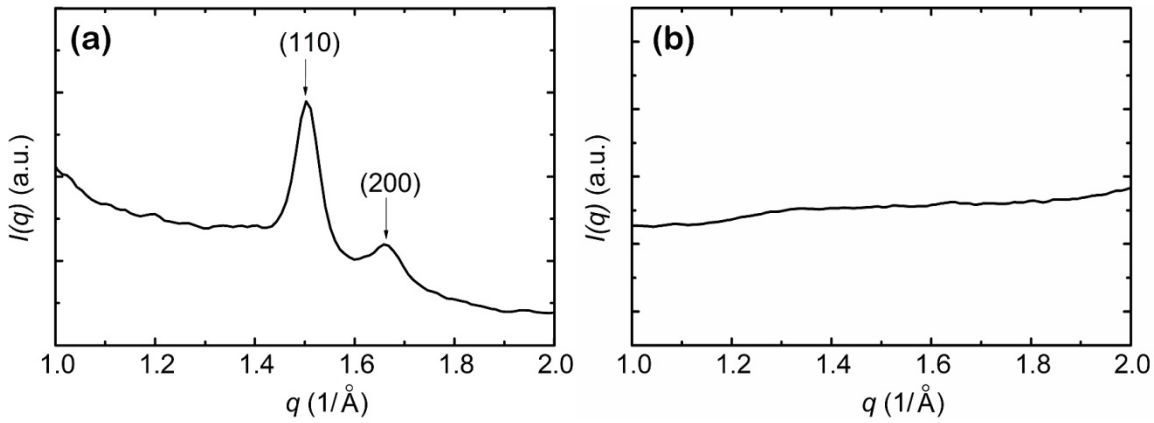

Figure 2.10 WAXS profile of 3.0 wt % (a) AE(9–3) and (b) AP(11–3) micelle dispersions at 23 °C.

2.2.4 "Frozen" Micelles

The interparticle chain exchange of the PE micelles was monitored following the pre-mixing and post-mixing protocol in SANS.[11, 83, 84] A*d*E(10–3) was synthesized from a partially deuterated PE (5.7 D per 8-H repeat unit), which had similar overall molar mass and composition to the hydrogenous AE(9–3). The solvent was a D_2O/H_2O mixture,

whose contrast closely matched that of the hydrogenous PDMA corona. Briefly, the premixed sample was prepared by mixing the A*d*E(10–3) and AE(9–3) neat polymers before being dispersed in solvents at 120 °C. The postmixed samples were prepared by mixing the premade AE(9–3) and A*d*E(10–3) micelle dispersions. The postmixed-unheated one was equilibrated at 23 °C, while the postmixed-heated sample was held at 120 °C for 7 days before the measurement at 23 °C. No inter-micelle chain exchange was expected between the semicrystalline PE cores at 23 °C, and thus the postmixed-unheated sample reflected the contrast condition at initial time (I_0). The premixed sample represented the intensity profile at infinitely long times (I_∞), if equilibration was achieved between cores with different isotopic distribution. If any chains exchanged between different micelles upon heating, the scattering profile of the postmixed-heated sample should deviate from the postmixed-unheated sample (I_0) and tend to resemble the premixed sample (I_∞). Nevertheless, the postmixed-heated sample showed a pattern that was virtually indistinguishable from the postmixed-unheated one after being kept at 120 °C for 7 days (Figure 2.11). Therefore, the micelles with PE cores were essentially “frozen” even at highest temperatures accessed, 120 °C.

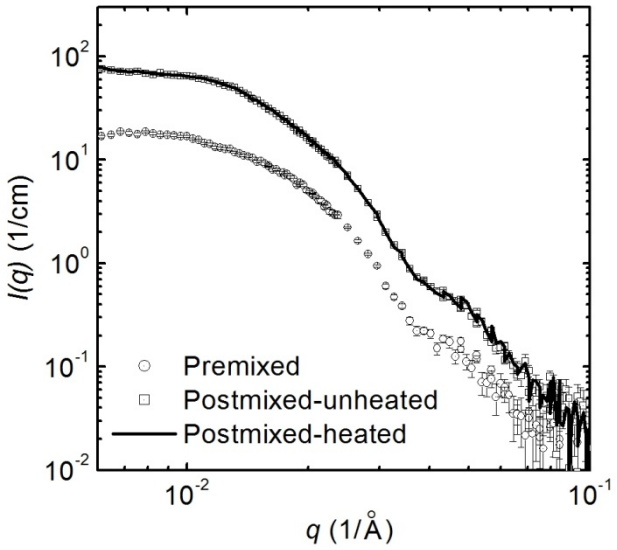

Figure 2.11 SANS scattering profiles of premixed (circles), postmixed-unheated (squares), and postmixed-heated (solid line) AE(9–3)/A*d*E(10–3) (1:1 by the volume of PE block) solutions in D_2O/H_2O mixture at 23 °C.

2.2.5 A Stepwise "Micellization–Crystallization" Process

In general, the morphology of diblock copolymer micelles can be rationalized by considering the free energy contributions from core chains, interface and corona chains. In the starlike regime of coil–coil diblock copolymers, spherical micelles with highly curved interfaces are commonly observed, which tend to relieve the crowding of corona chains. This effect is consistent with our observations in AP(11–3) micelles. On the other hand, oblate ellipsoidal micelles are anisotropic and additional factors can lead to their formation. There are three different mechanisms commonly encountered in the literature of disk micelles from diblock copolymers:

(i) *Extremely strong interfacial tension*. This effect was implicated for disks of ca. 100 nm diameter and 9 nm thickness from nearly symmetric polybutadiene–poly(hexafluoropropylene oxide) diblock copolymers. The disk morphology was ascribed

to the extremely strong interfacial tension between the fluoropolymer core and the hydrocarbon corona.[85]

(ii) *Rodlike corona or core blocks*. As exemplified by poly(*n*-hexyl isocyanate)–PEO diblock copolymers in toluene, the dominant nematic interaction between the rodlike corona blocks drove the extended, 2-dimensional packing along the interface.[86] While in the system of PEO–poly{(+)-2,5-bis[4'-((*S*)-2-methylbutoxy)-phenyl]styrene} (PMBPS) in water, the liquid crystalline PMBPS chains took parallel arrangements and led to the formation of disk cores.[87]

(iii) *Crystallization–induced morphologies*. Crystallizable lyophobic chains can fold and pack regularly, and thus drive the development of closely-packed lamellae. This mechanism has been shown in the large platelet micelles (lateral size on the order of several μm) from PEP–PE in decane[18, 24, 88] and PS–PEO in cyclopentane[18] because of the crystallizable PE and PEO blocks as well as small disks (~ 20 nm in diameter) in water from amphiphilic poly(2-hydroxyethyl vinyl ether)[89] and model collagen peptides[90] due to crystallizable C_{18} or C_{20} groups.

Since both PE and PEP are hydrocarbons, the incompatibility between PE and PDMA should be similar to that of PEP and PDMA in the AP(11–3) spherical micelles, and thus argues against the interfacial tension argument. There is also no reason to implicate rodlike corona blocks, as PDMA chains are known to be coils in water.[91] Besides, if there is any contribution from this argument, we would have observed the effect in the AP(11–3) micelles. In addition, neither PE nor PEP is rodlike, and thus argues against the possibility of rodlike core blocks. The combined cryo-TEM, SANS,

DSC and WAXS results on the AE(9–3) and AE(1.4–3) micelles corroborated the mechanism of crystallization-induced morphology transition (Figure 2.12). AE(1.4–3) aggregated into spherical micelles with rubbery PE cores in water at 120 °C. During cooling, PE crystallized between 75 and 55 °C and drove the micelle cores to be oblate ellipsoidal to accommodate the crystalline lamellae. Similar transitions were observed in poly(2-hydroxyethyl vinyl ether) (PHOVE) modified with hydrophobic octadecyl groups in water,[89] which melted at ca. 40 °C in bulk. As revealed by SAXS and SANS, the disklike micelles observed at room temperature reversibly changed to spherical micelles upon heating. Our work increased the carbon number by one order of magnitude (230 vs 18). As such, the aggregate morphology was also dictated by the thermal properties of the hydrophobic portion, but the transition occurred at higher temperatures.

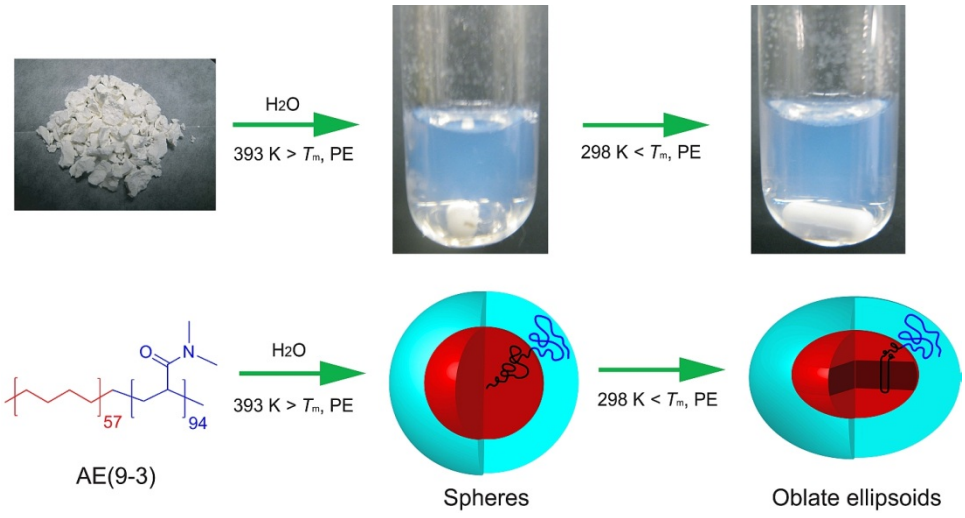

Figure 2.12 A stepwise "micellization−crystallization" procedure for the formation of oblate ellipsoidal micelles with semicrystalline PE cores in water.

Furthermore, the crystallization was restricted in each individual micelle cores of tens of nanometers. The size of the PE cores shown here was two orders of magnitude smaller than those prepared in organic media—the diameter of the oblate ellipsoidal structures was ca. 30 nm, while that of the platelet micelles from PEP–PE in decane was often several micrometers.[18, 24] The difference was due to the strong incompatibility between the aliphatic cores and water. As illustrated in Figure 2.12, instead of being molecularly dissolved in water, the AE diblock copolymers aggregated into spherical micelles at 120 °C prior to the crystallization of PE. In addition, the postmixed-heated sample showed virtually indistinguishable SANS profile from the postmixed-unheated sample after being held at 120 °C for 7 days, and thus the micelles at 120 °C were also "frozen" micelles. In other words, the intermicelle chain exchange was virtually prohibited.[11] Therefore, the crystallization upon cooling was confined within each micelle core and no change of the aggregation number can easily occur. The oblate ellipsoidal micelles from AE(9–3) can be viewed as the semicrystalline version of the spherical micelles with rubbery or glassy cores; if no crystallization happened, the morphology of AE(9-3) micelles at 25 °C closely resembled that of the spherical micelles from the noncrystalline AP(11–3), as shown in the AE(1.4–3) micelles at 120 °C. In contrast, the PEP–PE copolymers were fully dissolved in decane at the initial elevated temperatures (70 °C or above). Upon crystallization, each copolymer chain had sufficient molecular freedom and thus promoted the extended, sheetlike structures of several micrometers in diameter. In addition, the dimension of the PE lamellae within micelle cores was smaller than that of the crystallites from melts or solutions of PE homopolymers, whose thickness

follows in the range of 10–50 nm and the lateral dimension is on the order of several micrometers.

2.2.6 Wormlike Micelles and Bilayered Vesicles with PE Cores

Similar to AE(9–3) in the starlike regime, AE(1.4–3) with a shortened PDMA chain length also resulted in spherical micelles in water. Further decreasing the PDMA composition of AE diblock copolymers led to the formation of wormlike micelles and vesicles. When the PDMA composition was decreased to 20–23 wt %, wormlike micelle was the predominant morphology, as shown in Figure 2.13(a,b) for AE (1.0–3) and Figure 2.14 for AE(0.8–3). The radii of the worms were 13 ± 2 nm, and the contour lengths often exceeded 2 μm (corresponding to aspect ratios of more than ~10^2).

The existence of giant wormlike micelles was corroborated by SANS, and the scattering profile of a 1.0 wt % dispersion of AE(1.0–3) at 25 °C is shown in Figure 2.13c. The Guinier regime was not accessed in the lowest q range measured (ca. 10^{-3} $Å^{-1}$), and thus the average R_g of the worms were larger than 100 nm. Besides, we observed two characteristic minima in the medium q range, which reflected the cross-sections of the micelle cores (i.e., 0.01 $Å^{-1}$ < q < 0.2 $Å^{-1}$). The radii of the worm cores were determined to be 13.0 ± 0.7 nm. The decay power was −1.45 in the range of 1.0–8.0×10^{-3} $Å^{-1}$, which reflected the rigidity of the worms. For reference, the decay power of rigid rods is −1 in this range. The discrepancy indicated that the AE(1.0–3) wormlike micelles had some flexibility. Therefore, we fit the data using a model of non-interacting flexible cylinders,[101] and the result is shown as the solid black curve in Figure 2.13c. The

fitted cross-sectional radius (R_{cyl}) was 13.5 ± 0.1 nm, the persistence length (l_p) was 89 ± 2 nm, and the contour length (L) was 940 ± 60 nm. The dispersity of the radius (σ/R_{cyl}) was 0.22 assuming the Schulz distribution. The persistence length of these PE micelles was much smaller than that of wormlike micelles from PEO−PB[9] and PEO−PCL[43] diblock copolymers. The difference was likely to come from the semicrystalline PE cores, which formed many abrupt turning points along the contour (Figure 2.13b) as compared to those with rubbery PB or slightly crystalline PCL cores.

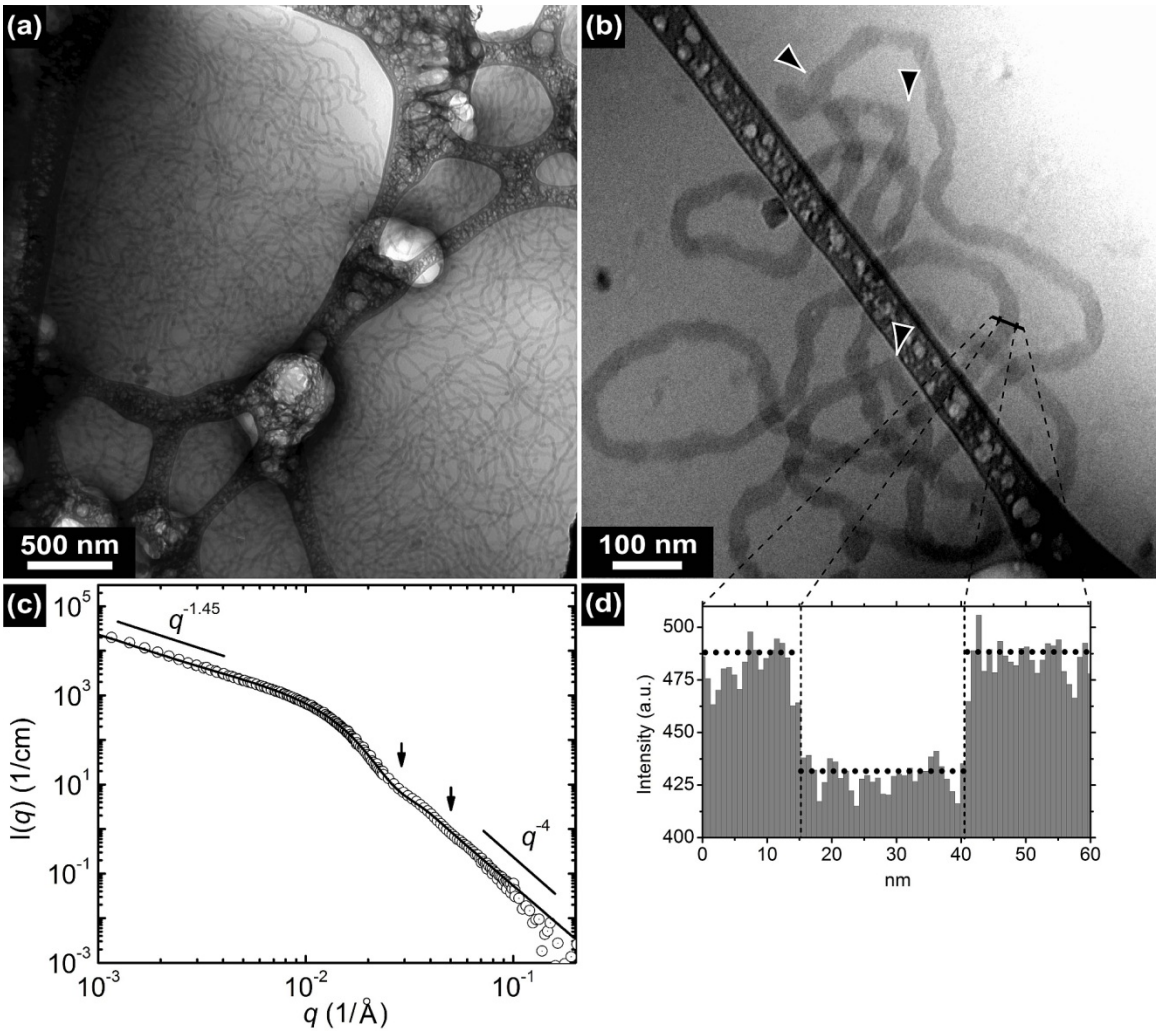

Figure 2.13 Cryo-TEM images taken from 0.5 wt % AE(1.0–3) in water at (a) low and (b) high magnifications. SANS profile (c) of AE(1.0–3) wormlike micelles dispersed in D_2O at a concentration of 1.0 wt % at 23 °C. The solid black curve represents the data modeling assuming an ensemble of non-interacting flexible cylinders with fixed lengths and radii that follow the Schulz distribution. The optical density profile across the core of one wormlike micelle is shown in (d) for the area that is highlighted by the solid black line in (b).

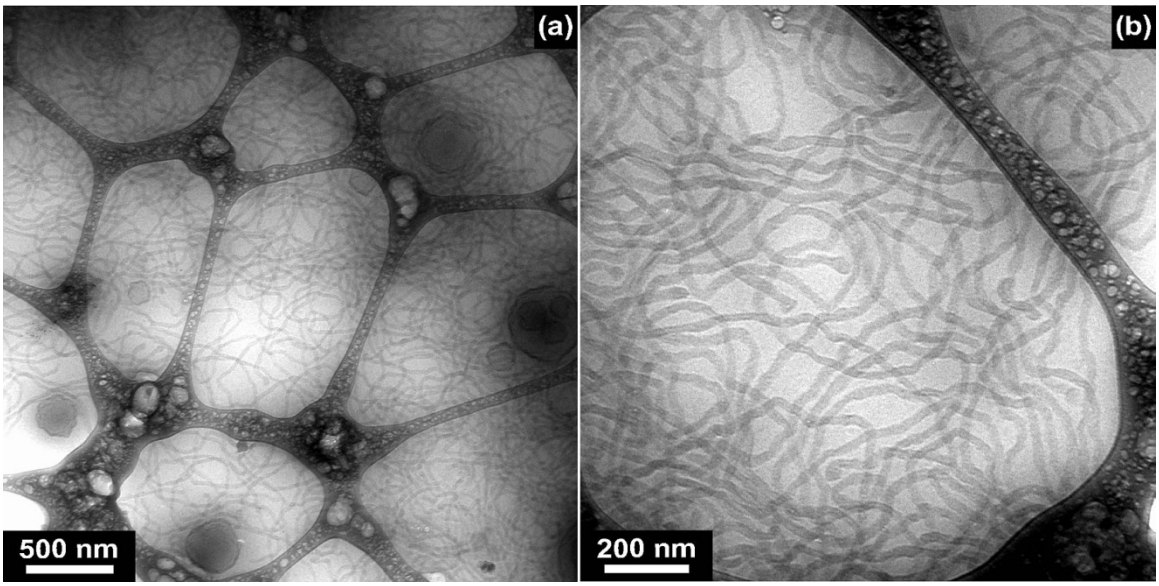

Figure 2.14 Cryo-TEM images taken from 0.5 wt % AE(0.8–3) in water at (a) low and (b) high magnifications.

Steady shear rheology revealed that the dilute dispersions of AE(1.4–3) oblate ellipsoids were Newtonian between 0.1 and 100 s^{-1}, i.e., viscosity was independent of shear rate. In contrast, a 2.0 wt % AE(1.0–3) dispersion exhibited shear-thinning behavior in the same range as shown in Figure 2.15, i.e., the viscosity decreased by increasing the shear rate. The decay power was –0.83. The shear-thinning behavior was consistent with the existence of highly anisotropic structures in the dispersion. On the other hand, the AE(1.0–3) dispersion was Newtonian at shear rates of larger than 100 s^{-1}. This result was consistent with the "frozen" nature of the micelles, i.e., no micellar scission/recombination as commonly observed in those from low-mass surfactants. Compared to previously reported PEO–PB wormlike micelles,[3] the AE(1.0–3) dispersion behaved more like a viscous liquid than an elastic solid, i.e., G' < G" in the frequency range of 0.1–100 rad s^{-1}. Besides, the zero shear viscosity of AE(1.0–3) was about 1

order of magnitude smaller than that of the best-performing PEO–PB worm dispersions at similar concentrations. This result was consistent with the relatively short contour length of the wormlike micelles, which was determined to be ~ 1 μm from SANS. In comparison, the contour length of the PEO–PB wormlike micelles was estimated to be ~9 μm.[9] The difference was tentatively ascribed to the larger dispersity of PDMA–PE than that of PEO–PB diblock copolymers—AE(1.0–3) has a short PDMA block of on average ~10 repeating units, which was made by RAFT polymerization, while those cylinder-forming PEO–PB samples had more than 50 EO repeating units, which were made by anionic polymerization. Therefore, AE(1.0–3) was likely to contain a rather large portion of copolymers with rather long hydrophilic chains, which formed "defect" spherical caps. As such, the average contour length was shorter than that of those PEO–PB worms. Correspondingly, AE(1.0–3) did not increase the elasticity of the aqueous dispersion as significantly as the best-performing PEO–PB diblock copolymers.

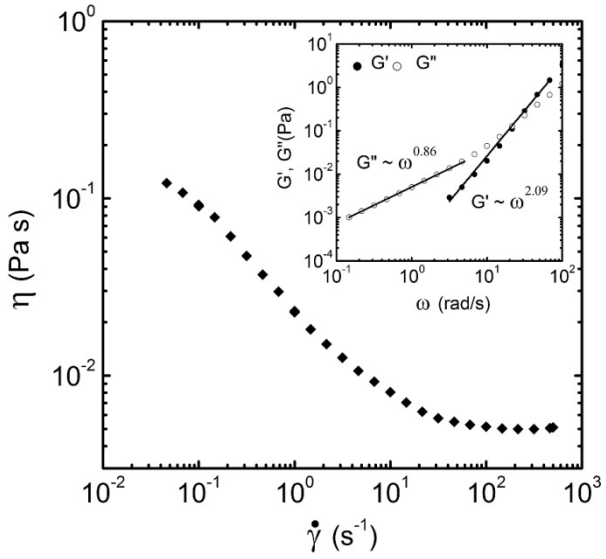

Figure 2.15 Steady and small-amplitude oscillatory (inset) shear measurement on a 2.0 wt % dispersion of AE(1.0–3) in water at 20 °C. The strain was held at 25% during the frequency sweep from 100 to 0.1 rad s^{-1}.

The semicrystalline nature of the wormlike micelles was supported by cryo-TEM. Figure 2.13b provides a close-up view of one single worm at high magnification. We observed several abrupt turning points as highlighted by black arrowheads. The surface energy at the core-corona interface would not be uniform along the contour of a worm. Instead, the crystallization of PE cores kinetically trapped this kind of feature. Similar morphology was not observed in the wormlike micelles with rubbery[9-13] or glassy cores,[14-16] whose contours were rather smooth and continuous. Besides, it was suggested that the crystalline PE cores might be similar to prisms with rectangular cross-sections rather than cylinders with circular cross sections, although the overall structure is wormlike.[17, 25] Indeed, the optical density across the hydrophobic domain was roughly constant and changed sharply at the interface in one selected area of the cryo-TEM image, as shown in Figure 2.13d. In comparison, cylindrical cores with uniform electron

densities would give projections in a continuous, parabolic manner (Figure 2.16). In addition, DSC (Figure 2.17) and WAXS (Figure 2.18) also confirmed the semicrystalline nature of the wormlike micelles.

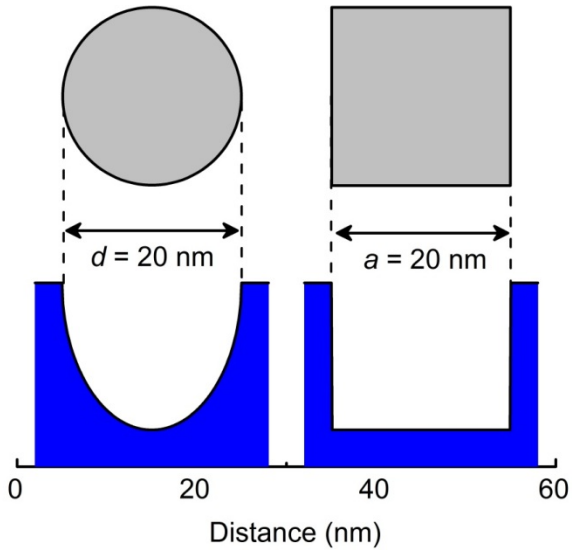

Figure 2.16 Simulation of the optical density profile across the core of a wormlike micelle with a circular (diameter = 20 nm) and square cross-section (side length = 20 nm).

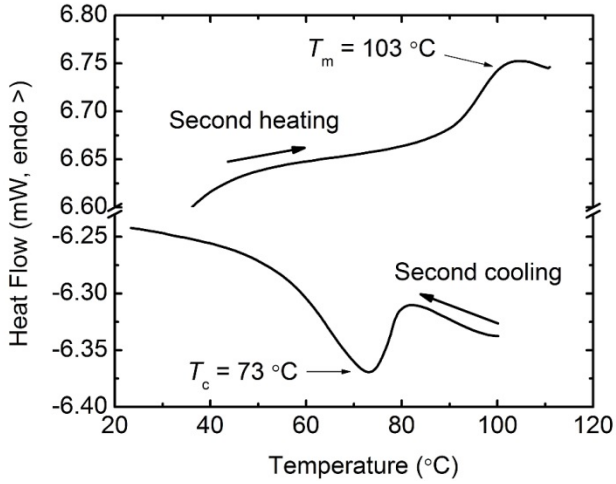

Figure 2.17 DSC curve of a 2.0 wt % wormlike micelle dispersion of AE(1.0-3) in water. The temperature was ramped at a rate of 2.0 °C min^{-1} between 20 and 120 °C.

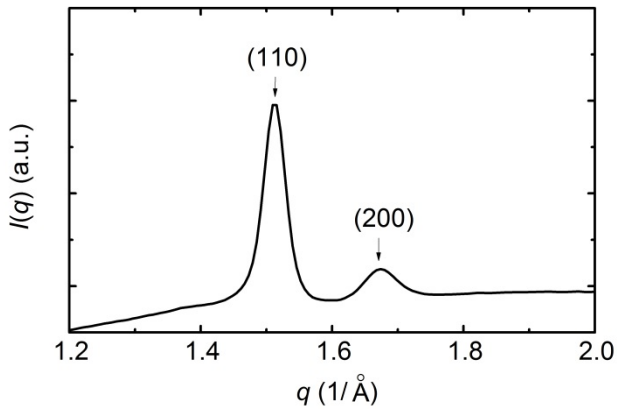

Figure 2.18 WAXS profile of a 2.0 wt % wormlike micelle dispersion of AE(1.0-3) in water at 23 °C.

Vesicles became the predominant morphology when the PDMA composition was further decreased to 18 wt %, as shown in Figure 2.19a for sample AE(0.7–3). The vesicles exhibited rough and irregular peripheries, in contrast to the smooth and round surfaces observed in systems with rubbery[9-13] or glassy[14-16] cores. Several sharp edges and vertices are highlighted by black arrowheads. Similar faceted vesicles were observed

from the self-assembly of phospholipids,[79] dendrimers,[92] and PCL-containing block copolymers.[44, 45] In cryo-TEM, the surface appeared to be not as rough in vesicles with PCL cores as those with PE cores, which was possibly due to the different degrees of crystallinity. As discussed by Olvera de la Cruz and coworkers, buckling occurs with additional curvature energy at deformed areas when a 2-D membrane made of a homogeneous and isotropic material wraps a closed object.[93] For membranes with two or more components, the morphology is dictated by the modulus and the volume fraction of each component. In our system, crystalline PE tends to be flat since it is harder than the amorphous PE. Indeed, we observed several cracked vesicles and one is highlighted by a white arrowhead in Figure 2.19a. Cracks and holes in the vesicle membrane may be beneficial in the triggered release of entrapped payloads that have limited permeability through the membrane.[43] If the crystalline component in the membrane increases (e.g., by using high-density polyethylene), a larger fraction of cracked vesicles is expected.

From the cryo-TEM images, the wall thickness of the PE vesicles was determined to be 18 ± 2 nm, and the overall diameter was mostly between 50 nm and 5 μm. The SANS profile of AE(0.7–3) vesicles in D_2O at 25 °C is shown in Figure 2.19b. The Guinier regime was accessed in the low q range of 1.0–3.0×10^{-3} $Å^{-1}$, and R_g was determined to be 71 ± 7 nm. The interfacial area per chain (a_0) was estimated to be 0.64 nm^2 using the Porod law in the high q region, which corresponded to a thickness of 17.6 nm under the assumption of locally planar structures. Therefore, the combination of cryo-TEM and SANS corroborated bilayered vesicles with a wall thickness of ca. 18 nm, and the average overall size of 10^2 nm. In addition, AE(0.6–3) was also prepared in which

PDMA was 16 wt %, and the sample underwent phase separation when being dispersed into water following the heat-assisted direct dissolution procedure.

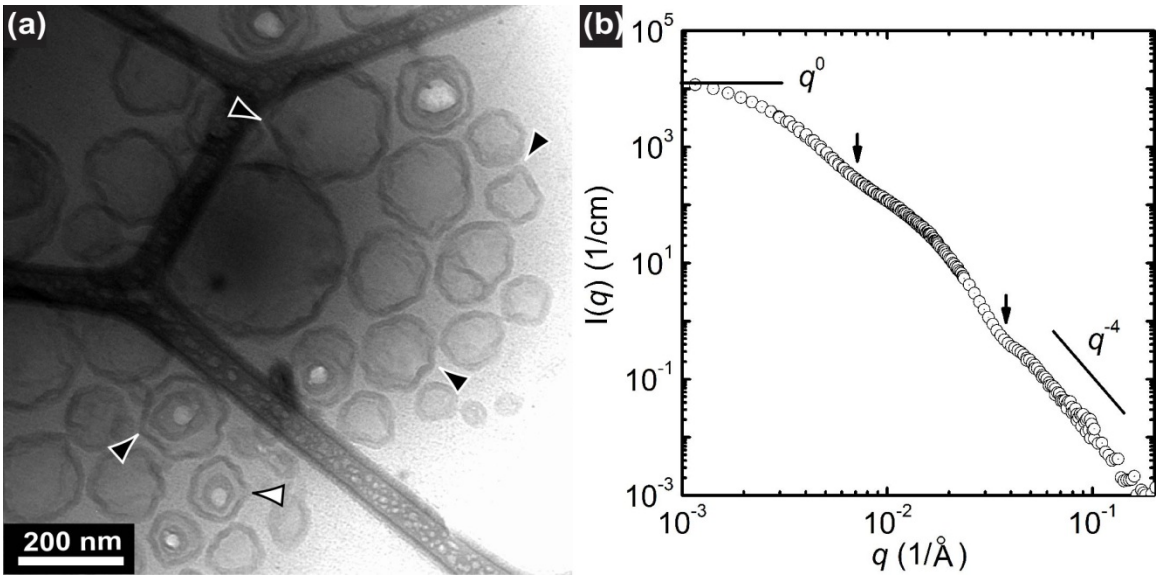

Figure 2.19 (a) A cryo-TEM image taken from a 0.5 wt % dispersion of AE(0.7–3) in water. Black arrowheads highlight abrupt turning points in the periphery of the bilayered vesicles. A white arrowhead points to a possible crack on the vesicle membrane. (b) SANS profile of AE(0.7–3) vesicles dispersed in D_2O at a concentration of 0.5 wt % at 25 °C.

The structural parameters of the PE micelles and vesicles as determined by cryo-TEM and SANS at 25 °C are summarized in Table 2.3. Decreasing the composition of the hydrophilic PDMA block from 30 to 18 wt % caused a morphological transition from spheres with highly-curved interfaces to wormlike micelles, and finally bilayered vesicles with relatively flat interfaces. Indeed, the interfacial area per chain followed the general trend: a_0 (oblate ellipsoids) > a_0 (wormlike micelles) > a_0 (vesicles). As the length of the hydrophobic PE block was held constant for the three PDMA–PE copolymers, the

interfacial curvature decreased for samples with shorter PDMA chains in response to the weaker requirement for releasing the crowding PDMA chains. Our results were consistent with previous observations of polymeric surfactants with rubbery[9-13] or glassy[14-16] hydrophobic components. Therefore, the semicrystalline version of the "universal" sequences of block copolymer micelle structures (oblate ellipsoidal micelles, wormlike micelles, and bilayered vesicles) was successfully prepared from PDMA–PE diblock copolymers in water by simply changing the composition of the copolymers. The overall structure of the aggregates was maintained after the crystallization of PE, while the local structures tended to be flat and anisotropic to accommodate the formation of lamellar crystals. The giant wormlike micelles and vesicles with PE cores hold great potential in applications that require enhanced mechanical integrity. For example, the wormlike micelles can be used as nanofibers with strong mechanical integrity for filtration applications. Noticeably, the diameter of the PE nanofibers was on the order of 20 nm, which is at least one order of magnitude smaller than those prepared from other methods such as electrospinning and melt blowing. Vesicles with PE peripheries are nanosized plastic bags, and would be useful as encapsulating vehicles that permit minimum leakage. In addition, the membrane permeability can be simply thermally controlled and the melting/crystallization temperature can be tuned by controlling the microstructure of the PE block (e.g., the content of 1,4-addition).

Table 2.3 Packing parameters of the micelle aggregates in the "crew-cut" regime.

Sample	SANS		cryo-TEM			
	R_g[a] (nm)	a_0[b] (nm^2)	Structures	D[c] (nm)	a_0[d] (nm^2)	p[e]
AE(0.7-3)	71	0.64	Vesicles	17.8	0.66	3.0
AE(1.0-3)	>100	0.86	Wormlike micelles	23.6	0.99	95
AE(1.4-3)	12.5	1.03	Oblate ellipsoids	35.2	*f*	*f*

[a] Radius of gyration as determined using the Guinier plot in the low q region. [b] Interfacial area per chain (a_0) calculated from the specific surface area (S_v) using the Porod plot in the high q region. One standard deviation was typically ± 10%. [c] The domain size of the hydrophobic cores: wall thickness for vesicles, side length for wormlike micelles assuming the cross-section was square, and lateral diameter for oblate ellipsoids. [d] Interfacial area per chain calculated based on the core domain size from cryo-TEM. [e] Aggregation number (p) calculated from the volume and bulk density of PE (ρ = 0.936 g/cm^3), corresponding to one oblate ellipsoidal particle, a unit length (1 nm) of wormlike micelles, or a unit area (1 nm^2) of vesicles. [f] Not determined due to the unknown shape and dimension of the micelle core in cryo-TEM. An average aggregation number of 2300 was obtained based on the particle volume (V_p) from extrapolated $I(q = 0)$ in SANS data.

2.3 Conclusions and Outlook

PDMA–PE diblock copolymers were used as a model coil–crystalline system to study the effect of crystallization on the self-assembly behavior in a strongly coil-selective solvent, water. A combination of anionic and RAFT polymerizations afforded PDMA–PE diblock copolymers with well-defined structures. The PE block was a hydrogenated 1,4-polybutadiene (a LLDPE) with a rather low M_n of 3.3 kg mol^{-1}, and the M_n of the PDMA block varied from 0.7 to 9.4 kg mol^{-1}. Molten PDMA–PE diblock copolymers were found to be in the intermediate-segregation regime, and χ was estimated to be 0.29 at 140 °C. Due to the extremely incompatibility between PE and water, a heat-assisted direct dissolution procedure was used to prepare the micelle dispersions. Dry AE samples were directly dispersed into water at a target concentration of 0.5–3.0 wt %, and then the mixtures were equilibrated at 120 °C for 5–7 days before they were cooled to 23 °C at a rate of 2.0 °C min^{-1}. In the "hairy" regime, where the composition of the hydrophilic PDMA block was rather high, the combination of DLS, cryo-TEM, and SANS results led us to believe that the micelles contained "multi-compartment" cores—crystalline PE formed rather flat disks at the center, which was embedded in rubbery PE, and the overall cores can be approximated as oblate ellipsoids. The thickness of the PE crystals at the center was 4−5 nm, and the lateral diameter was 30−35 nm. The crystallinity of the PE micelle cores were ca. 30%, similar to that of the PE homopolymer precursor. PE crystals resided in orthorhombic lattice, the most common form as observed in the crystallization of PE in bulk. In contrast, spherical micelles were obtained from a control sample with a rubbery PEP of 3.1 kg mol^{-1} as the hydrophobic block.

Therefore, the crystallization of PE induced the morphological transformation from symmetric spheres to anisotropic oblate ellipsoids. SANS results further suggested that instead of being molecularly dissolved, the AE copolymers aggregated into spherical micelles with molten PE cores in aqueous dispersions at 120 °C. In addition, the micelles were "frozen" in nature and no inter-micelle chain exchange was detected within 7 days at 120 °C. Therefore, the heat-assisted direct dissolution for sample preparation was a stepwise "micellization−crystallization" procedure, in which the AE diblock copolymers first formed micelles with rubbery PE cores at 120 °C and then the crystallization of PE at ca. 70 °C drove the formation of PE lamellae within individual micelles. This procedure was in sharp contrast with the "crystallization-driven" self-assembly as observed in numerous crystallizable samples in organic media. Lastly, the generality of this procedure was demonstrated as PE micelles with different morphologies, wormlike micelles and bilayered vesicles, were also prepared as revealed by cryo-TEM, SANS, and solution rheology. The morphology transformation was realized via manipulating the length of the hydrophilic PDMA block.

The crystallization-assisted micellization of block copolymers have started gaining attention[94] and there are many unanswered questions. In this PDMA–PE system, it is amazing that the PE chains crystallized to form one single disk at the center of each micelle. Is it possible to have multiple nuclei in this confined crystallization and under what circumstances will it happen? This question might be related with the size of the micelle cores, and multiple nuclei might occur in micelles with much larger cores, say 100 nm in diameter. Besides, the crystallizable components are uniformly distributed

within the spherical molten PE cores at 120 °C in these diblock copolymers; the short ethyl branches were randomly distributed along the backbone of the PE block, and the micelle cores made of one polymer are generally believed to be homogeneous. Therefore, it is interesting to see how crystallization occurs with heterogeneous cores. Possible structures include (mikto) arm star and linear *ABC* triblock terpolymers as shown in Figure 2.20, in which *A* is hydrophilic (e.g., PDMA), *B* is hydrophobic and crystallizable (e.g., PE), and *C* is hydrophobic and noncrystalline (e.g., PEP and poly(perfluoropropyleneoxide) (PFPO)). Both hydrophobic *B* and *C* blocks would reside in the micelle cores. If *B* and *C* are not compatible (e.g., PE and PFPO), the crystallization of *B* would occur from the small microdomains as defined by both the interface between core and corona and that between *B* and *C*. If *B* and *C* are compatible (e.g., PE and PEP), the crystallization of *B* would occur from disordered *BC* diblock melts. In one word, micelles with a hierarchy of delicate structures are expected.

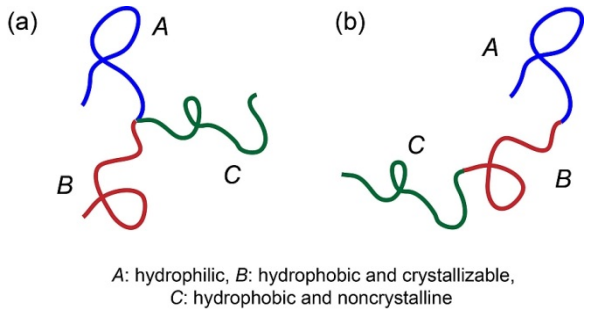

Figure 2.20 (a) (mikto) arm star and (b) linear *ABC* triblock terpolymers.

2.4 Experimental Section

Materials. All reagents were used as received unless otherwise noted. Butadiene sulfone-d_4 (98 atom % D, Aldrich), *sec*-butyllithium (1.4 M in cyclohexane, Aldrich), *n*-butyllithium (2.5 M in hexanes, Aldrich), *n*-butylmagnesium chloride (2.0 M in diethyl ether, Aldrich), oxalyl chloride (Aldrich, 99+%), chloroform-*d* (99.8 atom % D, Cambridge Isotope Laboratories), and 1,1,2,2-tetrachloroethan-d_2 (99.6 atom % D, Cambridge Isotope Laboratories) were used as received. 1,3-Butadiene (Aldrich, 99+%) and 1,3-isoprene (Aldrich, 99%) were purified with *n*-butyllithium multiple times, each for 1 h in salty ice water, degassed via three freeze-pump-thaw cycles, and stored in a burette immersed in a dry ice/acetone bath before use. 1,3-Butadiene-d_4 was prepared by the thermal decomposition of butadiene sulfone-d_4 following reported procedures.[95] The synthesized 1,3-butadiene-d_4 was purified in the same way as the hydrogenous counterpart before polymerization. Ethylene oxide (Aldrich, 99.5+%) was purified twice from *n*-butylmagnesium chloride, each for 4 h in salty ice water, degassed via three freeze-pump-thaw cycles, and stored in a burette immersed in a dry ice/acetone bath before use. 2,2′-Azobis(2-methylpropionitrile) (AIBN) was recrystallized from methanol twice and stored in a –30 °C refrigerator. A reversible addition-fragmentation transfer (RAFT) chain transfer agent (CTA) bearing carboxylic acid group, *S*-1-dodecyl-*S*'-(α,α'-dimethyl-α"-acetic acid)trithiocarbonate, was synthesized following reported procedure.[64] *N*,*N*-Dimethylacrylamide (DMA) (Aldrich, 99+%) was purified either via vacuum distillation or by passing through activated basic alumina to remove the inhibitor. Degassed cyclohexane used in anionic polymerization and toluene in RAFT

polymerization were purified by passing through columns packed with activated alumina and a supported copper catalyst.[96] Cyclohexane used during hydrogenation was purged with Argon for 30 min before use.

Synthetic Details. Hydroxyl-terminated 1,4-polybutadiene (1,4-PB-OH) was synthesized via anionic polymerization according to reported procedures.[95, 97] The polymerization of butadiene was allowed to proceed at 40 °C for 6 h. After a large excess (> 5-fold of stoichiometry) of ethylene oxide was added, the end-capping reaction was allowed to proceed at 23 °C for an additional 12 h. Methanol supplemented with HCl was degassed for quenching the reaction. The mixture of the reaction was first concentrated, and then dried in vacuum oven at 50 °C until constant mass was achieved. No additional steps were used to get rid of the residual lithium salts. Next, hydrogenation of 1,4-PB-OH to PE-OH was carried out under 500 Psig H_2 in a high-pressure reactor. The catalyst was Pt on silica from The Dow Chemical Company[63] and the solvent was cyclohexane. The crude product was first passed through a membrane with a pore size of 0.45 μm to remove the catalyst, and further purified by two precipitations into methnaol. The isolated product was further dried in vacuum oven at 50 °C until constant mass was achieved. The dry PE-OH was reacted with the carboxyl-terminated RAFT CTA with the aid of oxalyl chloride to give the ω-CTA-functionalized PE, or PE-CTA. The solvent was toluene, the temperature was 70 °C, and the reaction was allowed to proceed for 24 h. The product was purified by two precipitations from toluene at 70 °C into methaol at 23 °C followed by drying in a vacuum oven at 50 °C until constant mass was achieved. The synthesis of AE diblock copolymers with different target lengths of PDMA blocks was carried out

using similar procedures, as exemplified by the following synthesis of AE(9–3): a Shlenk flask was charged with PE-CTA (0.94 g, 2.7×10^{-4} mol), AIBN (8.3 mg, 5.1×10^{-5} mol), DMA (2.74 mL, 2.7×10^{-2} mol), toluene (25 mL, $[DMA]_0$ = 1.06 M) and a stir bar. The flask was degassed via three freeze-pump-thaw cycles and then charged with 3 psig of Argon. Next, the flask was isolated from the manifold, placed in a preheated oil bath at 75 °C, and the reaction was allowed to proceed for 3 h. The reaction was quenched by placing the mixture in ice water. The product was recovered by two precipitations from toluene at 75 °C into hexanes cooled by ice water. The conversion of the monomer was typically greater than 95% and overall recovered yield was more than 80%. The synthesis of 1,4-PI-OH, PEP-OH, PEP-CTA, and AP(11–3) were synthesized in a similar way as the those described above, except that 1,3-isoprene was substituted for 1,3-butadiene.

Molecular Characterizations. All ^{1}H NMR spectra were recorded on a Varian Inova 500 or a Varian Inova 300 spectrometer. Chloroform-*d* was used as the solvent except for those samples that contained PE, which were dissolved in 1,1,2,2-tetrachloroethane-d_2. The concentration was 20–30 mg mL^{-1}. For all spectra requiring quantitative analysis, a pulse delay of 30 s was employed to ensure complete relaxation. All room-temperature SEC data were obtained on a Hewlett-Packard 1100 series liquid chromatograph equipped with three Jordi polydivinylbenzene columns with pore sizes of 10000, 1000, and 500 Å, respectively. The eluents were monitored by a Hewlett-Packard 1047A refractive index detector. Chloroform was used as the mobile phase at 35 °C and the running rate was 1.0 mL min^{-1}. A 10-point calibration curve was made using PS standards purchased from Agilent Technologies. SEC data of PE and AE samples were

collected on a Polymer Laboratories 220 high-temperature liquid chromatograph, which was equipped with three 10-μm Mixed-B columns from Polymer Laboratories and a refractive index detector. 1,2,4-trichlorobenzene (TCB) at 135 °C was used as the mobile phase and the running rate was 1.0 mL min^{-1}. A 10-point calibration curve was made using PS standards purchased from Polymer Laboratories. Samples for density measurement were annealed at 140 °C for more than 4 h to remove cavities, slowly cooled to 23 °C, and placed in a home-built ethylene glycol–isopropanol mixture column[98] at 23 °C for 7 days before recording. The calibration was made using 15 glass beads with known densities, assuming a linear vertical density gradient.

Preparation of Micelle Dispersions. A pressure vessel was charged with dry AE diblock copolymers, HPLC-grade water, and a stir bar. The taregt concentration of polymers in solution was 0.5–3.0 wt %. The mixture was first degassed by Argon bubbling for 30 min and then the pressure vessel was placed in a preheated 120 °C oil bath. The temperature was held at 120 ± 1 °C for 5–7 days, and then the mixture was allowed to cool to 23 °C at a rate of ca. 2 °C min^{-1}.

Dynamic Light Scattering. All samples were passed through syringe filters with a pore size of 0.20 μm before being loaded into dust-free glass tubes. A decalin bath was used as the RI-matching matrix, and the temperature was controlled at 25.0 ± 0.3 °C. A Lexel model 75 Ar^+ laser with an operating wavelength of 488 nm was employed, and the scattering intensity was detected by a Brookhaven photomultiplier tube and processed using a digital correlator (BI-9000AT). The second-order scattering intensity correlation functions, $g_2(t)$, were measured at five different scattering angles between 60° and 120°,

and converted into the first-order correlation functions, $g_1(t)$, using the Siegert relation $g_2(t) = 1 + |g_1(t)|^2$. The $g_1(t)$ functions were fit by (i) the cumulant expansion as shown in Equation 2.4,

$$g_1(t) = A\exp(-\Gamma t)(1+\frac{\mu_2}{2!}t^2 - \frac{\mu_3}{3!}t^3) + \text{bkgd} \quad (2.4)$$

in which Γ is the average decay rate, and μ_2, μ_3 are the second and third cumulants, respectively. This expression describes an assembly of aggregates with a monomodal distribution and some finite dispersity ($\mu_2/\Gamma^2 < 0.3$);[72] and (ii) the double-exponential expansion, which assumes two distinct decay modes, each with zero dispersity as shown in Equation 2.5,

$$g_1(t) = A_1\exp(-\Gamma_1 t) + A_2\exp(-\Gamma_2 t) + \text{bkgd} \quad (2.5)$$

in which Γ_1 and Γ_2 are the decay rates of the fast and slow decay modes, respectively. A linear fitting through the origin was performed between Γ and q^2 to determine the translational diffusion coefficient (D), in which q is the amplitude of the scattering vector. The effective hydrodynamic radius, R_h, was calculated through the Stokes–Einstein relationship, $D = k_B T/(6\pi\eta R_h)$ (k_B: Boltzmann constant, T: absolute temperature, and η: viscosity of the medium).

Small-angle X-ray Scattering and Wide-angle X-ray Scattering. The SAXS and WAXS measurement were carried out at the 5-ID-D station of the Advanced Photon Source at Argonne National Laboratory. The energy of the synchrotron X-ray source was 17 keV, which corresponded to a wavelength of 0.729 Å. The sample-to-detector distance was 4000 mm (SAXS) and 236 mm (WAXS) to cover a q-range of 0.0065–0.17 $Å^{-1}$ and 0.62–4.6 $Å^{-1}$, respectively. The 2-D scattering images collected on the MAR (SAXS) and

Roper (WAXS) CCD detector were azimuthally integrated into 1-D profiles of I vs q using the data reduction software FIT-2D. Bulk samples for SAXS were melt pressed and encapsulated inside hermetically sealed aluminum pans, and the temperature was controlled within ± 0.2 °C with a Linkam DSC stage. The thicknesses of the samples were estimated to be 2.0 ± 0.1 mm. The background was not corrected for the SAXS profiles. Solution samples for WAXS were loaded into quartz capillary tubes (outer diameter: 2.0 mm, Charles Supper Co.), and the measurement was carried out at 23 °C. Scattering profiles from the capillary tube and solvent (HPLC-grade water) were also collected and used to normalize the WAXS profiles of micelle dispersions.

Cryogenic Transmission Electron Microscopy. Samples for cryo-TEM were prepared using a home-built controlled environment vitrification system (CEVS)[99] at 23 °C. An aliquot of the micelle solution (~ 8 μL) was loaded onto a lacey carbon support film that was held by a pair of tweezers in the CEVS filled with saturated water vapor. Excess solution was blotted away using a piece of filter paper to form thin films (with thicknesses of ca. 100–300 nm) spanning the holes of the lacey carbon. After a 15-s delay, the grid was quickly plunged into liquid ethane (at ~ 90 K) that was cooled by surrounding liquid nitrogen. The vitrified samples were stored in liquid nitrogen until they were transferred onto Gatan 626 cryogenic sample holder and examined in a JEOL 1210 TEM at ca. –177 °C. The accelerating voltage was 120 kV. Images were acquired using a Gatan 724 multiscan CCD camera and processed with Digital Micrographs version 3.3.1. The phase contrast was enhanced by imaging the samples at 8–20 μm underfocus.

Small-angle Neutron Scattering. SANS measurement was carried out on the NG-7 30-m beamline of the Cold Neutron Research Facility at the National Institute of Standards and Technology (NIST). Four setups, a wavelength of 8.0 Å with sample-to-detector distance of 15.3 m and a wavelength of 7.0 Å with sample-to-detector distances of 13.0 m, 3.0 m, and 1.0 m, were employed to cover a q range of 0.0009–0.38 $Å^{-1}$. Samples for measurement at 25 °C were loaded into NIST quartz cells with a thickness of 1.0 mm. Samples for measurement at 120 °C were held in NIST pressure cells with a thickness of 4.0 mm, inside which a quartz spacer that was ca. 1.5 mm thick was placed to form a solution with a thickness of ca. 2.5 mm in the beam path. The pressure cells were pressurized with 32 psig of N_2 to minimize the formation of air bubbles at 120 °C. The total counts of neutrons on one image were at least 10,000 to ensure sufficiently high signal-to-noise ratio. The raw data were corrected for blocked beam scattering, sample transmission, empty cell scattering, and detector efficiency, and then converted into absolute scale using direct beam flux method. Further, the scattering from solvent was subtracted to give the pure scattering from suspended particles. The SANS data was reduced and analyzed using the NIST software package version 7.04b in Igor Pro.[100]

The premixed sample was prepared by mixing dry AE(9–3) and A*d*E(10–3) samples in hot toluene (1:1 by the volume of PE block) followed by precipitating into room-temperature hexane twice. For all solution samples, a D_2O/H_2O mixture (76/24, v/v) was employed as the solvent to match the contrast of the corona PDMA block. In other words, the results should closely reflect the changes from the cores. Rather concentrated samples were prepared to increase the signal strength—the volume fraction

of PE micelle cores were ca. 1.0 %, which corresponded to ca. 4.0 wt % of the diblock copolymers in solution. The scattering profile of a 1.0 wt % A*d*E(10–3) sample was also collected and compared to that of the 4.0 wt % sample. Only minor discrepancy was observed in the range of $q < 0.006$ Å^{-1} after correcting the concentration, which was likely to result from some intermicelle interactions[9]. This difference should have little effect with the intra-micelle structure, and thus only the data with $q > 0.006$ Å^{-1} were shown.

Model-independent analysis. In the low q region ($9\times10^{-4} < q < 5\times10^{-3}$ Å^{-1}), the radius of gyration (R_g) of the suspended particles was calculated using the Guinier plot, which involves plotting $\ln[I(q)]$ vs q^2 following Equation 2.6.

$$\ln[I(q)] = \ln[I(q=0)] - \frac{q^2}{3} R_g^{\,2} \quad (2.6)$$

Further, the volume (V_p) of suspended particles was obtained using the extrapolated value of $\ln[I(q = 0)]$ following Equation 2.7.

$$\ln[I(q=0)] = \Phi(\Delta\rho)^2 V_p \quad (2.7)$$

in which Φ is the total volume fraction of the suspended particles in solution, and $\Delta\rho$ is the contrast between the suspended particles and the solvent. Φ was calculated from the scattering invariant, Q (as defined in Equation 2.8), using Equation 2.9. For the estimation of Q, the absolute scattering intensity was extrapolated to 10^{-5} Å^{-1} in the low q region using the Guinier plot, and 10 Å^{-1} in the high q region with the Porod plot (*vide infra*). The difference between the estimated Q over the range of 10^{-5}–10 Å^{-1} and the calculated Q over the measured q range (i.e., 0.0009–0.38 Å^{-1}) was less than 3%.

$$Q = \int_0^\infty q^2 I(q) \mathrm{d}q \quad (2.8)$$

$$Q = 2\pi^2 (\Delta\rho)^2 \Phi(1-\Phi) \quad (2.9)$$

In the high q region ($8\times10^{-2} < q < 3\times10^{-1}$ Å^{-1}), the scattering intensity decayed as q^{-4}, which indicated the sharp interfaces between the suspended particles and the solvent. From the Porod constant C_p as defined in Equation 2.10, the specific surface area (i.e., the surface area per unit volume of sample), S_v, was calculated following Equation 2.11.

$$C_p \equiv \lim_{q\to\infty} q^4 I(q) \quad (2.10)$$

$$C_p = 2\pi \cdot S_v (\Delta\rho)^2 \quad (2.11)$$

S_v is related with the average particle dimensions: $S_v = 6\Phi/D$ for spheres with a diameter of D, $S_v = 4\Phi/D$ for infinitely long cylinders with a diameter of the cross section of D, and $S_v = 2\Phi/D$ for vesicles with a wall thickness of D. In addition, the interfacial area per chain, a_0, of the micelles was calculated from S_v using Equation 2.12.

$$a_0 = \frac{S_v}{\Phi} \cdot \frac{M_n}{\rho \cdot N_A} \quad (2.12)$$

in which M_n is the number-average molar mass of the core-forming blocks (PE) of the micelles, ρ is the mass density, and N_A is Avogadro's number.

*Fitting the form factor with models***.** The scattering profiles of AE(1.4-3) micelles in D_2O at 25 and 120 °C were also fitted with the form factors of particles with different shapes to get quantitative information about their packing characteristics. The models included (1) spheres with radii of the Gaussian distribution, (2) randomly orientated disks with thicknesses that are monodisperse and radii that follow the Schulz distribution, and

(3) randomly orientated oblate ellipsoids with minor radii (R_a) that are monodisperse and major radii (R_b) that follow the Gaussian distribution. The smearing of form factors due to limited instrument resolution was also included using the NIST software package version 7.04b.[100]

The absolute scattering intensity of spheres with radii of Gaussian distribution is shown as Equation 2.13.

$$I(q) = N_0(\Delta\rho)^2 \int_0^\infty f(R_c) \cdot V_{sph}{}^2 \cdot F^2(qR_c) dR_c \quad (2.13)$$

in which N_0 is the total number of particles per unit volume, $f(R_c)$ is the normalized Gaussian distribution as described in Equation 2.14, V_{sph} is the volume of a sphere with a radius of R_c ($4/3\ \pi R_c^3$), and $F(qR_c)$ is the scattering amplitude of a sphere as described in Equation 2.15. σ and R_{avg} in Equation 2.14 were standard deviation and the average radius of the spheres, respectively.

$$f(R_c) = \frac{1}{\sigma\sqrt{2\pi}} \exp\left[-\frac{1}{2\sigma^2}\left(R_c - R_{avg}\right)^2 \right] \quad (2.14)$$

$$F(qR_c) = \frac{\sin(qR_c) - (qR_c)\cos(qR_c)}{(qR_c)^3} \quad (2.15)$$

The absolute scattering intensity of an ensemble of randomly orientated disks (or cylinders) with thicknesses (L) that are monodisperse and radii (R_c) that follow the Schulz distribution is shown as Equation 2.16.

$$I(q) = N_0(\Delta\rho)^2 \left(\frac{z+1}{z+2}\right) \int_0^x f_z(R_c) \cdot dR_c \int_0^{\pi/2} F_{cyl}{}^2(q,\alpha) \sin\alpha d\alpha \quad (2.16)$$

in which $f_z(R_c)$ is the normalized Schulz distribution of the radii as shown in Equation 2.17.

$$f_z(R_c) = (z+1)^{z+1} x^z \frac{\exp[-(z+1)x]}{R_{avg}\Gamma(z+1)} \quad (2.17)$$

R_{avg} is the mean radius and x is defined as R_c/R_{avg}. z is related to the dispersity by $z = (R_{avg}/\sigma)^2 - 1$, in which σ^2 is the variance of the distribution. $F(q,\alpha)$ is the amplitude for an ensemble of orientationally averaged rigid disks (or cylinders) as described in Equation 2.18, and α is defined as the angle between the cylinder axis and the scattering vector, q.

$$F_{cyl}(q,\alpha) = 2V_{cyl} \cdot j_0(qL\cos\alpha)\frac{J_1(qR_c\sin\alpha)}{qR_c\sin\alpha} \quad (2.18)$$

in which V_{cyl} is the volume of a cylinder with a radius of R_c and a length of L, $j_0(x)$ is defined as $\sin x/x$, and $J_1(x)$ is the first-order Bessel function.

The absolute scattering intensity of randomly orientated oblate ellipsoids with the minor radius (R_a) that is monodisperse and the major radius (R_b) that follows the Gaussian distribution is shown as Equation 2.19.

$$I(q) = N_0(\Delta\rho)^2 \int_0^\infty f(R_b) \cdot V_{ell}{}^2 dR_b \int_0^{\pi/2} F^2(qR_{orn})\sin\alpha d\alpha \quad (2.19)$$

in which V_{ell} is the volume (i.e., $4/3\ \pi R_a R_b{}^2$), R_{orn} is the orientation-dependent radius as described in Equation 2.20, and α is defined as the angle between the rotation axis and the scattering vector, q.

$$R_{orn} = R_b\sqrt{(\sin\alpha)^2 + (\cos\alpha)^2\left(R_a/R_b\right)^2} \quad (2.20)$$

The scattering profiles of AE(1.0–3) micelles in D_2O at 25 °C were fitted with a model of non-interacting flexible cylinders, whose cross-sectional radii follow the Schulz distribution as described by Pedersen et al.[101] and Chen et al.[102]

In the data fitting, only the contribution from the micelle cores of PE was considered and that from the coronae of PDMA was not included. To validate the assumption that the scattering of PDMA was insignificant in the total scattering, the calculated scattering profile of AE(1.4-3) spheres at 120 °C with considering PDMA was compared to that without PDMA (Figure 2.21). We followed the model of spherical micelles from diblock copolymers that was developed by Pedersen et al.[103, 104] Besides the self-correlation of the core, three terms were also included in the form factor: the self-correlation of the corona chains, the cross term between the core and the corona chains, and the cross term between different corona chains. Individual swollen PDMA molecules were assumed to be Gaussian chains, and the radial density distribution function of the PDMA corona followed a linear combination of two cubic *b* spline functions. In the calculation, the width of the corona profile (corresponding to the difference between the radius of the overall micelle and that of the micelle core) was chosen to be twice as much as that of the R_g of PDMA, and the fitting parameter of the two spline functions was 1.[105] The two calculated curves well overlapped in the low *q* region, which reflected the overall size and shape of the micelle cores, and became slightly different in the mid-to-high *q* region, which revealed the local structures at the core–corona interface. This plot suggested the contribution of the swollen PDMA corona chains was rather insignificant in the AE(1.4-3) spheres, which has the largest PDMA composition among the three

samples quantitatively investigated by SANS. Therefore, it is reasonable to treat the SANS data without explicitly considering the contribution from PDMA coronae.

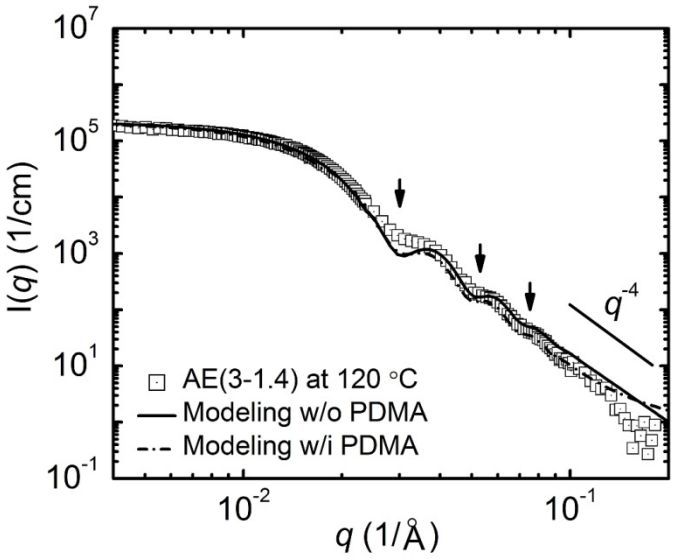

Figure 2.21 SANS profile of AE(1.4-3) spheres dispersed in D_2O at 120 °C (open squares), data modeling assuming an ensemble of non-interacting simple spheres without the contribution of PDMA corona (solid line), and data modeling assuming an ensemble of non-interacting core-shell spherical particles with the contribution of PDMA (dash dot line).

Shear rheometry. Steady and small-amplitude oscillatory shear measurements were performed on a AR-G2 rheometer (TA Instruments). A standard Couette cell was used—the length was 42 mm, and the gap was 1 mm between the inner cylinder (with a radius of 14 mm) and outer cylinder (with a radius of 15 mm). About 12 mL of the aqueous dispersions were loaded into the cup to fill the gap. The temperature was controlled at 20.0 ± 0.1 °C. The assembly was covered with water-soaked foams to minimize the evaporation of water. The frequency dependence of storage and loss moduli

(G' and G") was measured by linear dynamic (i.e., oscillatory) frequency sweeps from 100 to 0.01 rad s^{-1} at strains (e.g., 25%) that are located in the linear regime, which are determined by dynamic strain sweep experiments. The oscillatory torque of the data shown was at least 3 times as large as the limit of the rheometer (0.003 μN m). Steady shear measurements were carried out with the shear rate increasing from 0.01 to 500 s^{-1}. To minimize the transient effects, pre-shearing of 180 s, 60 s, and 30 s was employed before data collection for shear rates in the ranges of 0.01–0.1, 0.1–1.0, and 1.0–500 s^{-1}, respectively. The steady shear torque of the data shown was at least 10 times as large as the limit of the rheometer (0.01 μN m).

2.5 References

1. Zhulina, E. B.; Adam, M.; LaRue, I.; Sheiko, S. S.; Rubinstein, M. *Macromolecules* **2005,** 38, (12), 5330-5351.

2. Schwahn, D.; Richter, D.; Wright, P. J.; Symon, C.; Fetters, L. J.; Lin, M. *Macromolecules* **2002,** 35, (3), 861-870.

3. Won, Y.-Y.; Davis, H. T.; Bates, F. S. *Science* **1999,** 283, (5404), 960-963.

4. Wang, X. S.; Liu, K.; Arsenault, A. C.; Rider, D. A.; Ozin, G. A.; Winnik, M. A.; Manners, I. *J. Am. Chem. Soc.* **2007,** 129, (17), 5630-5639.

5. Walther, A.; Yuan, J.; Abetz, V.; Muller, A. H. E. *Nano Lett.* **2009,** 9, (5), 2026-2030.

6. Gaucher, G.; Dufresne, M. H.; Sant, V. P.; Kang, N.; Maysinger, D.; Leroux, J. C. *J. Controlled Release* **2005,** 109, (1-3), 169-188.

7. Kelkar, S. S.; Reineke, T. M. *Bioconjugate Chem.* **2011,** 22, (10), 1879-1903.

8. Lodge, T. P.; Bang, J. A.; Li, Z. B.; Hillmyer, M. A.; Talmon, Y. *Faraday Discuss.* **2005,** 128, 1-12.

9. Won, Y.-Y.; Davis, H. T.; Bates, F. S.; Agamalian, M.; Wignall, G. D. *J. Phys. Chem. B* **2000,** 104, (30), 7134-7143.

10. Won, Y.-Y.; Brannan, A. K.; Davis, H. T.; Bates, F. S. *J. Phys. Chem. B* **2002,** 106, (13), 3354-3364.

11. Won, Y.-Y.; Davis, H. T.; Bates, F. S. *Macromolecules* **2003,** 36, (3), 953-955.

12. Jain, S.; Bates, F. S. *Science* **2003,** 300, 460-464.

13. Jain, S.; Bates, F. S. *Macromolecules* **2004,** 37, (4), 1511-1523.

14. Zhang, L. F.; Eisenberg, A. *Science* **1995,** 268, (5218), 1728-1731.

15. Zhang, L. F.; Eisenberg, A. *J. Am. Chem. Soc.* **1996,** 118, (13), 3168-3181.

16. Bhargava, P.; Zheng, J. X.; Li, P.; Quirk, R. P.; Harris, F. W.; Cheng, S. Z. D. *Macromolecules* **2006,** 39, (14), 4880-4888.

17. Vilgis, T.; Halperin, A. *Macromolecules* **1991,** 24, (8), 2090-2095.

18. Lin, E. K.; Gast, A. P. *Macromolecules* **1996,** 29, (12), 4432-4441.

19. Xu, J. T.; Fairclough, J. P. A.; Mai, S. M.; Ryan, A. J. *J. Mater. Chem.* **2003,** 13, (11), 2740-2748.

20. Chen, W. Y.; Li, C. Y.; Zheng, J. X.; Huang, P.; Zhu, L.; Ge, Q.; Quirk, R. P.; Lotz, B.; Deng, L. F.; Wu, C.; Thomas, E. L.; Cheng, S. Z. D. *Macromolecules* **2004,** 37, (14), 5292-5299.

21. Zheng, J. X.; Xiong, H. M.; Chen, W. Y.; Lee, K. M.; Van Horn, R. M.; Quirk, R. P.; Lotz, B.; Thomas, E. L.; Shi, A. C.; Cheng, S. Z. D. *Macromolecules* **2006,** 39, (2), 641-650.

22. Mihut, A. M.; Chiche, A.; Drechsler, M.; Schmalz, H.; Di Cola, E.; Krausch, G.; Ballauff, M. *Soft Matter* **2009,** 5, (1), 208-213.

23. Mihut, A. M.; Crassous, J. J.; Schmalz, H.; Drechsler, M.; Ballauff, M. *Soft Matter* **2012,** 8, (11), 3163-3173.

24. Richter, D.; Schneiders, D.; Monkenbusch, M.; Willner, L.; Fetters, L. J.; Huang, J. S.; Lin, M.; Mortensen, K.; Farago, B. *Macromolecules* **1997,** 30, (4), 1053-1068.

25. Schmalz, H.; Schmelz, J.; Drechsler, M.; Yuan, J.; Walther, A.; Schweimer, K.; Mihut, A. M. *Macromolecules* **2008,** 41, (9), 3235-3242.

26. Schmelz, J.; Karg, M.; Hellweg, T.; Schmalz, H. *ACS Nano* **2011,** 5, (12), 9523-9534.

27. Radulescu, A.; Mathers, R. T.; Coates, G. W.; Richter, D.; Fetters, L. J. *Macromolecules* **2004,** 37, (18), 6962-6971.

28. Massey, J. A.; Temple, K.; Cao, L.; Rharbi, Y.; Raez, J.; Winnik, M. A.; Manners, I. *J. Am. Chem. Soc.* **2000,** 122, (47), 11577-11584.

29. Wang, X.; Guerin, G.; Wang, H.; Wang, Y.; Manners, I.; Winnik, M. A. *Science* **2007,** 317, (5838), 644-647.

30. Shen, L.; Wang, H.; Guerin, G.; Wu, C.; Manners, I.; Winnik, M. A. *Macromolecules* **2008,** 41, (12), 4380-4389.

31. Gadt, T.; Ieong, N. S.; Cambridge, G.; Winnik, M. A.; Manners, I. *Nat Mater* **2009,** 8, (2), 144-150.

32. Soto, A. P.; Gilroy, J. B.; Winnik, M. A.; Manners, I. *Angew. Chem., Int. Ed.* **2010,** 49, (44), 8220-8223.

33. Qi, F.; Guerin, G.; Cambridge, G.; Xu, W. G.; Manners, I.; Winnik, M. A. *Macromolecules* **2011,** 44, (15), 6136-6144.

34. Korczagin, I.; Hempenius, M. A.; Fokkink, R. G.; Stuart, M. A. C.; Al-Hussein, M.; Bomans, P. H. H.; Frederik, P. M.; Vancso, G. J. *Macromolecules* **2006,** 39, (6), 2306-2315.

35. Portinha, D.; Belleney, J.; Bouteiller, L.; Pensec, S.; Spassky, N.; Chassenieux, C. *Macromolecules* **2002,** 35, (5), 1484-1486.

36. Portinha, D.; Boue, F.; Bouteiller, L.; Carrot, G.; Chassenieux, C.; Pensec, S.; Reiter, G. *Macromolecules* **2007,** 40, (11), 4037-4042.

37. Lazzari, M.; Scalarone, D.; Hoppe, C. E.; Vazquez-Vazquez, C.; Lopez-Quintela, M. A. *Chem. Mater.* **2007,** 19, (24), 5818-5820.

38. Lazzari, M.; Scalarone, D.; Vazquez-Vazquez, C.; Lopez-Quintela, M. A. *Macromol. Rapid Commun.* **2008,** 29, (4), 352-357.

39. Patra, S. K.; Ahmed, R.; Whittell, G. R.; Lunn, D. J.; Dunphy, E. L.; Winnik, M. A.; Manners, I. *J. Am. Chem. Soc.* **2011,** 133, (23), 8842-8845.

40. Gilroy, J. B.; Lunn, D. J.; Patra, S. K.; Whittell, G. R.; Winnik, M. A.; Manners, I. *Macromolecules* **2012,** 45, (14), 5806-5815.

41. Du, Z. X.; Xu, J. T.; Fan, Z. Q. *Macromolecules* **2007,** 40, (21), 7633-7637.

42. Du, Z.-X.; Xu, J.-T.; Fan, Z.-Q. *Macromol. Rapid Commun.* **2008,** 29, (6), 467-471.

43. Rajagopal, K.; Mahmud, A.; Christian, D. A.; Pajerowski, J. D.; Brown, A. E. X.; Loverde, S. M.; Discher, D. E. *Macromolecules* **2010,** 43, (23), 9736-9746.

44. Ghoroghchian, P. P.; Li, G. Z.; Levine, D. H.; Davis, K. P.; Bates, F. S.; Hammer, D. A.; Therien, M. J. *Macromolecules* **2006,** 39, (5), 1673-1675.

45. Ahmed, F.; Discher, D. E. *J. Controlled Release* **2004,** 96, (1), 37-53.

46. He, W. N.; Xu, J. T.; Du, B. Y.; Fan, Z. Q.; Sun, F. L. *Macromol. Chem. Phys.* **2012,** 213, (9), 952-964.

47. Fu, J.; Luan, B.; Yu, X.; Cong, Y.; Li, J.; Pan, C. Y.; Han, Y. C.; Yang, Y. M.; Li, B. Y. *Macromolecules* **2004,** 37, (3), 976-986.

48. Zhang, J.; Wang, L. Q.; Wang, H. J.; Tu, K. H. *Biomacromolecules* **2006,** 7, (9), 2492-2500.

49. Agrawal, S. K.; Sanabria-DeLong, N.; Tew, G. N.; Bhatia, S. R. *Macromolecules* **2008,** 41, (5), 1774-1784.

50. Chen, C. K.; Lin, S. C.; Ho, R. M.; Chiang, Y. W.; Lotz, B. *Macromolecules* **2010,** 43, (18), 7752-7758.

51. Petzetakis, N.; Dove, A. P.; O'Reilly, R. K. *Chem. Sci.* **2011,** 2, (5), 955-960.

52. Petzetakis, N.; Walker, D.; Dove, A. P.; O'Reilly, R. K. *Soft Matter* **2012,** 8, (28), 3408-3414.

53. Lazzari, M.; Lopez-Quintela, M. A. *Macromol. Rapid Commun.* **2009,** 30, (21), 1785-1791.

54. Peacock, A. J. *Handbook of Polyethylene: Structures: Properties, and Applications*. Marcel Dekker: New York, 2000.

55. Heidman, J. L.; Tsonopoulos, C.; Brady, C. J.; Wilson, G. M. *AICHE Journal* **1985,** 31, (3), 376-384.

56. Weber, C. H. M.; Chiche, A.; Krausch, G.; Rosenfeldt, S.; Ballauff, M.; Harnau, L.; Goettker-Schnetmann, I.; Tong, Q.; Mecking, S. *Nano Lett.* **2007,** 7, (7), 2024-2029.

57. Tong, Q.; Krumova, M.; Gottker-Schnetmann, I.; Mecking, S. *Langmuir* **2008,** 24, (6), 2341-2347.

58. Yu, S. M.; Mecking, S. *Macromolecules* **2009,** 42, (11), 3669-3673.

59. Li, T.; Wang, W. J.; Liu, R.; Liang, W. H.; Zhao, G. F.; Li, Z.; Wu, Q.; Zhu, F. M. *Macromolecules* **2009,** 42, (11), 3804-3810.

60. Wang, W. J.; Liu, R.; Li, Z. Y.; Meng, C. F.; Wu, Q.; Zhu, F. M. *Macromol. Chem. Phys.* **2010,** 211, (13), 1452-1459.

61. Zhao, Y.; Shi, X. B.; Gao, H. Y.; Zhang, L.; Zhu, F. M.; Wu, Q. *J. Mater. Chem.* **2012,** 22, (12), 5737-5745.

62. Kryuchkov, V. A.; Daigle, J. C.; Skupov, K. M.; Claverie, J. P.; Winnik, F. M. *J. Am. Chem. Soc.* **2010,** 132, (44), 15573-15579.

63. Hucul, D. A.; Hahn, S. F. *Adv. Mater.* **2000,** 12, (23), 1855-1858.

64. Lai, J. T.; Filla, D.; Shea, R. *Macromolecules* **2002,** 35, (18), 6754-6756.

65. Krause, S.; Gormley, J. J.; Roman, N.; Shetter, J. A.; Watanabe, W. H. *J. Polym. Sci., Part A: General Papers* **1965,** 3, (10), 3573-3586.

66. Liu, H. Y.; Zhu, X. X. *Polymer* **1999,** 40, (25), 6985-6990.

67. Matsen, M. W.; Bates, F. S. *J. Polym. Sci., Part B: Polym. Phys.* **1997,** 35, (6), 945-952.

68. Fetters, L. J.; Lohse, D. J.; Richter, D.; Witten, T. A.; Zirkel, A. *Macromolecules* **1994,** 27, (17), 4639-4647.

69. Hamley, I. W.; O'Driscoll, B. M. D.; Lotze, G.; Moulton, C.; Allgaier, J.; Frielinghaus, H. *Macromol. Rapid Commun.* **2009,** 30, (24), 2141-2146.

70. Castillo, R. V.; Arnal, M. L.; Muller, A. J.; Hamley, I. W.; Castelletto, V.; Schmalz, H.; Abetz, V. *Macromolecules* **2008,** 41, (3), 879-889.

71. Anderson, K. S.; Lim, S. H.; Hillmyer, M. A. *J. Appl. Polym. Sci.* **2003,** 89, (14), 3757-3768.

72. Chu, B., *Laser Light Scattering: Basic Principles and Practice*. 2nd ed.; Academic Press: Boston, 1991.

73. Jakes, J. *Collect. Czech. Chem. Commun.* **1995,** 60, (11), 1781-1797.

74. Shibayama, M.; Karino, T.; Okabe, S. *Polymer* **2006,** 47, (18), 6446-6456.

75. Saito, N.; Liu, C.; Lodge, T. P.; Hillmyer, M. A. *Macromolecules* **2008,** 41, (22), 8815-8822.

76. Zupancich, J. A.; Bates, F. S.; Hillmyer, M. A. *Macromolecules* **2006,** 39, (13), 4286-4288.

77. He, Y. Y.; Li, Z. B.; Simone, P.; Lodge, T. P. *J. Am. Chem. Soc.* **2006,** 128, (8), 2745-2750.

78. Using the densities from literature: 0.98 g cm^{-3} (crystalline PE), 0.91 g cm^{-3} (amorphous PE), and 0.94 g cm^{-3} (low density amorphous ice).

79. Johnsson, M.; Edwards, K. *Biophys. J.* **2003,** 85, (6), 3839-3847.

80. Sandström, M. C.; Johansson, E.; Edwards, K. *Biophys. Chem.* **2008,** 132, (2-3), 97-103.

81. Weimann, P. A.; Hajduk, D. A.; Chu, C.; Chaffin, K. A.; Brodil, J. C.; Bates, F. S. *J. Polym. Sci., Part B: Polym. Phys.* **1999,** 37, (16), 2053-2068.

82. Ha, J. M.; Hamilton, B. D.; Hillmyer, M. A.; Ward, M. D. *Cryst. Growth Des.* **2009,** 9, (11), 4766-4777.

83. Meli, L.; Santiago, J. M.; Lodge, T. P. *Macromolecules* **2010,** 43, (4), 2018-2027.

84. Choi, S.-H.; Lodge, T. P.; Bates, F. S. *Phys. Rev. Lett.* **2010,** 104, (4), 047802.

85. Edmonds, W. F.; Li, Z.; Hillmyer, M. A.; Lodge, T. P. *Macromolecules* **2006,** 39, (13), 4526-4530.

86. Wu, J.; Pearce, E. M.; Kwei, T. K.; Lefebvre, A. A.; Balsara, N. P. *Macromolecules* **2002,** 35, (5), 1791-1796.

87. Zhang, H.; Lin, W. R.; Liu, A. H.; Yu, Z. N.; Wan, X. H.; Liang, D. H.; Zhou, Q. F. *Langmuir* **2008,** 24, (8), 3780-3786.

88. Leube, W.; Monkenbusch, M.; Schneiders, D.; Richter, D.; Adamson, D.; Fetters, L.; Dounis, P.; Lovegrove, R. *Energy & Fuels* **2000,** 14, (2), 419-430.

89. Nakano, M.; Matsumoto, K.; Matsuoka, H.; Yamaoka, H. *Macromolecules* **1999,** 32, (12), 4023-4029.

90. Gore, T.; Dori, Y.; Talmon, Y.; Tirrell, M.; Bianco-Peled, H. *Langmuir* **2001,** 17, (17), 5352-5360.

91. Trossarelli, L.; Meirone, M. *J. Polym. Sci.* **1962,** 57, 445-52.

92. Percec, V.; Wilson, D. A.; Leowanawat, P.; Wilson, C. J.; Hughes, A. D.; Kaucher, M. S.; Hammer, D. A.; Levine, D. H.; Kim, A. J.; Bates, F. S.; Davis, K. P.; Lodge, T. P.; Klein, M. L.; De Vane, R. H.; Aqad, E.; Rosen, B. M.; Argintaru, A. O.; Sienkowska, M. J.; Rissanen, K.; Nummelin, S.; Ropponen, J. *Science* **2010,** 328, (5981), 1009-1014.

93. Vernizzi, G.; Sknepnek, R.; de la Cruz, M. O. *PNAS* **2011,** 108, (11), 4292-4296.

94. He, W. N.; Xu, J. T. *Prog. Polym. Sci.* **2012,** 37, (10), 1350-1400.

95. Hillmyer, M. A.; Bates, F. S. *Macromolecules* **1996,** 29, (22), 6994-7002.

96. Pangborn, A. B.; Giardello, M. A.; Grubbs, R. H.; Rosen, R. K.; Timmers, F. J. *Organometallics* **1996,** 15, (5), 1518-20.

97. Wang, Y.; Hillmyer, M. A. *Macromolecules* **2000,** 33, (20), 7395-7403.

98. Gehlsen, M. D. Catalytic Hydrogenation of Polymer: Synthesis and Characterization of Model Polyolefins. Ph.D. Thesis, University of Minnesota, 1993.

99. Bellare, J. R.; Davis, H. T.; Scriven, L. E.; Talmon, Y. *J. Electron Micr. Tech.* **1988,** 10, (1), 87-111.

100. Kline, S. R. *J. Appl. Crystallogr.* **2006,** 39, 895-900.

101. Pedersen, J. S.; Schurtenberger, P. *Macromolecules* **1996,** 29, (23), 7602-7612.

102. Chen, W. R.; Butler, P. D.; Magid, L. J. *Langmuir* **2006,** 22, (15), 6539-6548.

103. Pedersen, J. S.; Svaneborg, C.; Almdal, K.; Hamley, I. W.; Young, R. N. *Macromolecules* **2003,** 36, (2), 416-433.

104. Choi, S.-H.; Bates, F. S.; Lodge, T. P. *J. Phys. Chem. B* **2009,** 113, (42), 13840-13848.

105. Bang, J.; Jain, S.; Li, Z.; Lodge, T. P.; Pedersen, J. S.; Kesselman, E.; Talmon, Y. *Macromolecules* **2006,** 39, (3), 1199-1208.

3 Glucose-functionalized, Serum-stable Polymeric Micelles from the Combination of Anionic and RAFT Polymerizations[†]

3.1 Introduction

Polymeric micelles, which can physically encapsulate or chemically conjugate molecules of interest in their hydrophobic cores, hold great potential for the controlled release of drugs through intravenous administration. The advantages of these nanoscopic carriers include improved loadings of hydrophobic drugs over the drugs themselves in aqueous biological media, prolonged circulation time, and passive targeting of malignant tissues based on the enhanced permeation and retention (EPR) effect.[1-4] Micelles are formed by the spontaneous aggregation of amphiphilic molecules in water, in which the hydrophobic components form the dense cores and the hydrophilic parts reside in the micelle coronae. Ideal hydrophilic polymeric coronae should (i) shield and solublize the hydrophobic cores and the payloads to increase the dose and bioavailability of poorly- or non-soluble drugs, (ii) exhibit minimal nonspecific interactions with blood components to avoid opsonization and minimize uptake by the mononuclear phagocyte system,[5] and (iii) target malignant cells via both passive (via particle size) and active targeting methods

[†] Reproduced in part with permission from Yin, L.; Dalsin, M. C.; Sizovs, A.; Reineke, T. M.; Hillmyer, M. A. *Macromolecules* **2012,** 45, (10), 4322-4332. Copyright 2012 American Chemical Society.

with high specificity (e.g., through site-specific ligands) while producing minimal side effects on healthy cells.[6] To date, poly(ethylene oxide) (PEO) has been the most widely used hydrophilic polymer in polymeric micelles due to minimal interactions with blood proteins, diminished enzymatic degradation, solubility in both organic solvents and water, and ready commercial availability.[7] However, PEO is not ideal and several disadvantages in practice have been gaining attention including thermal instability, hypersensitivity after intravenous and oral administrations,[7] and accelerated blood clearance due to the production of anti-PEO antibodies.[8] Moreover, functionalizing PEO is limited since there is often only one reactive site at the end of a PEO chain.[9, 10] Therefore, there is much need to explore PEO alternatives with enhanced functionality.[11]

Glycopolymers are synthetic macromolecules with carbohydrate moieties in the backbone or as pendant groups.[12-15] Natural carbohydrate-based materials have been widely used in food, pharmaceutical, and medical applications due to their excellent biocompatibility. Moreover, some carbohydrates exhibit specific interactions with proteins and other biological entities at cell surface (e.g., cells, pathogens), and thus are important in numerous cellular recognition processes including cell adhesion, cellular trafficking, cancer cell metastasis, and immune response.[16] Glycopolymers offer numerous advantages over PEO as the hydrophilic layer of micelle carriers including tunable hydrophilicity and more hydroxyls for further functionalization. Besides, the chemical structures and dispersity of synthetic carbohydrates can be precisely controlled to systematically understand the structure–property relationship.[17] Therefore,

incorporating carbohydrate moieties into polymeric micelles holds great potential for drug carriers with improved functionality and thus targeting efficiency and specificity.

To date, many synthetic efforts on glycopolymers have been undertaken. For example, carbohydrate monomers with olefinic groups have been synthesized including (meth)acrylamides,[18-20] (meth)acrylates,[21-29] vinyl triazole,[30] styrene derivatives,[31] vinyl ethers,[32] and norbornene derivatives.[33] Monosaccharides such as glucose,[18-20, 25-28, 32, 33] galactose,[21, 29] and mannose,[22, 30] along with disaccharides such as lactose[23, 24, 31] have been incorporated. Glycopolymers with controlled architecture and molar mass are prepared by numerous controlled polymerization techniques such as controlled radical[18-32] and ring-opening metathesis[33] polymerizations as well as post-polymerization modifications.[34, 35] Reversible addition-fragmentation chain transfer (RAFT) polymerization is particularly versatile due to the good control of monomers including (meth)acrylamides, fast kinetics, vast tolerance of solvents, and absence of metal catalysts.[18-20, 22, 27, 30, 32] Furthermore, thiocarbonate moieties not only can be quantitatively removed via facile aminolysis[36] to eliminate the potential biological implications of the chain-transfer agent fragments, but also provide unique chemical handles for functionalization with targeting moieties or imaging agents.

A small number of studies have been published on glycopolymers in polymeric micelles, though studies on sugar-based surfactants abound in literature.[37] In the simplest case, a hydrophobic polymer is covalently connected to a glycopolymer to form an *AB*-type amphiphilic diblock copolymer, in which *A* and *B* denote the hydrophobic and hydrophilic component, respectively. For example, Stenzel and coworkers developed a

hydrophilic, glucose-functionalized monomer, 2-methacrylamido glucopyranose (MAG), and copolymerized it using RAFT polymerization with a moderately hydrophobic uridine-functionalized monomer, 5'-*O*-methacryloyl uridine (MAU), to afford amphiphilic PMAU–PMAG diblock copolymers.[19] The resulting diblock copolymers self-assembled into micelles with glucose-functionalized coronae, and spherical and rodlike micelles in a dry, collapsed state were observed using transmission electron microscopy (TEM). Similarly, thermo-responsive or pH-responsive micelles with glucose or mannose included in the coronae were obtained from covalently-connected glycopolymers and polymers that exhibit LCST behavior in water such as poly(*N*-isopropyl acrylamide)[30] and poly (di(ethylene glycol) methyl ether methacrylate),[34] or pH-sensitive polymers such as poly(2-(diethylamino)ethyl methacrylate).[27] Micelles with glycoshells can also be obtained from more structurally-complicated ABA,[23, 24] BAB,[25] star-shaped $(BA)_4$,[26] and mikto-arm A_3B block copolymers.[29] Besides PMAU[19] and poly(acrylate)s[28, 35] that are slightly hydrophobic, more nonpolar polymers such as polystyrene[21] and poly(ε-caprolactone)[25, 26, 29] have also been used, which are desirable for solubilizing strongly lipophilic drugs.[38] In these cases, the carbohydrate monomers are usually first protected with nonpolar groups (e.g., acetyl[21] and isopropylidene[29]) to allow a homogeneous mixture during synthesis, since glycopolymers are generally only soluble in very polar solvents such as water and water/alcohol mixtures.

This chapter describes my efforts on glucose-functionalized diblock terpolymers that consist of aliphatic poly(ethylene-*alt*-propylene) (PEP) as the hydrophobic component and a glucose-functionalized[19] block as the hydrophilic component. Results

include synthesis, self-assembly in water, and *in vitro* stability in biologically-relevant media. PEP is a macromolecular saturated hydrocarbon with a low glass transition temperature (T_g) (ca. –65 °C), and is designed to eventually encapsulate drugs with very low aqueous solubility (e.g., ellipticine[39]). A trimethylsilyl-protected glucose-containing monomer, α-2-deoxy-2-methacrylamido 1,3,4,6-tetra-(*O*-trimethylsilyl) D-glucopyranose (TMS-MAG),[40] was used to prepare model synthetic carbohydrates that contain glucose moieties. Synthetic routes towards diblock terpolymers with precisely defined structures are demonstrated. Besides, the effects of glucose content on the physical properties of the diblock terpolymers (T_g and solubility), sample preparation, and the resulting micelle aggregates are comprehensively examined. In addition, the ability of these glucose-containing hydrophilic polymers as PEO alternatives to mediate micelle aggregation in the presence of physiological salts and serum are presented.

3.2 Results and Discussion

3.2.1 Synthesis and Molecular Characterization

The synthesis of α-2-deoxy-2-methacrylamido 1,3,4,6-tetra-(*O*-trimethylsilyl) D-glucopyranose (TMS-MAG) was carried out by Antons Sizovs and the details are described in our report.[40] Initially I attempted to synthesize a homopolymer of TMS-MAG using free-radical polymerization. As shown in Scheme 3.1, three polymerizations were carried out with high loadings of initiators, i.e., $[Initiator]_0$:$[TMS\text{-}MAG]_0$ = 1:10. At such chosen temperatures, the initiators all had a half-life of ca. 10 h. However, the conversions of TMS-MAG were less than 10% in all three cases after ca. 20 h as determined by ^{1}H NMR spectroscopy. Besides, only oligomers were obtained as revealed by SEC as shown in Figure 3.1. We hypothesize that the propagation of TMS-MAG, not the initiation, was extremely slow under those conditions. The results were rather surprising, since successful polymerizations of the unprotected counterpart, α-2-deoxy-2-methacrylamido D-glucopyranose (MAG), have been reported by different groups.[19, 20] As the TMS-MAG monomer only contained the α-anomer, the bulky *O*-trimethylsilyl on *C*1 were likely to exert too much steric hindrance on the neighboring methacrylamido reactive sites.

Scheme 3.1 Free-radical polymerizations of TMS-MAG.

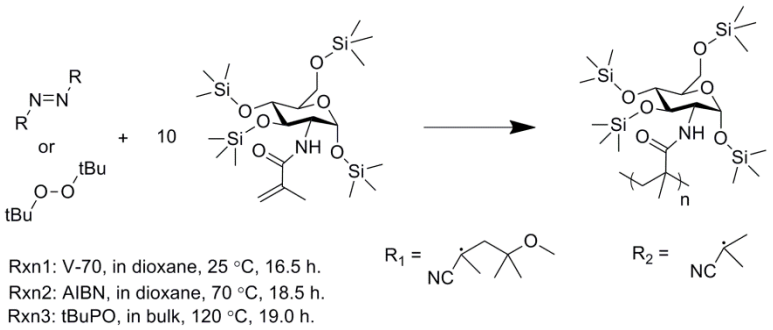

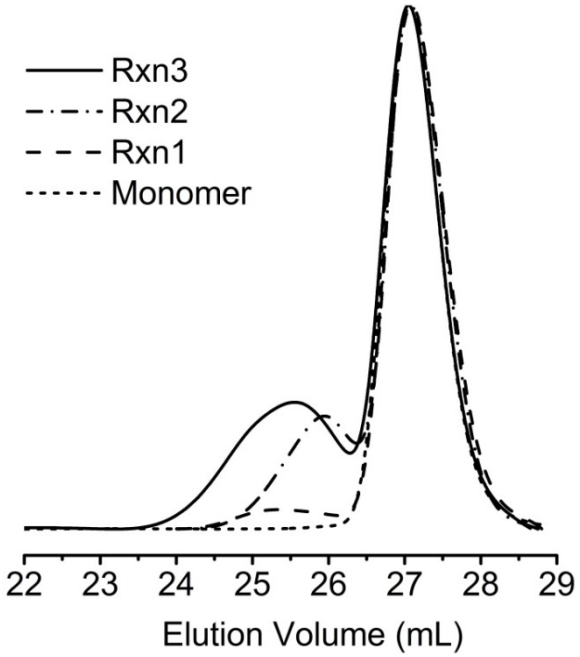

Figure 3.1 SEC traces of TMS-MAG and the reaction products (as reacted, without purification) from free-radical polymerizations as illustrated in Scheme 3.1.

The copolymerization of TMS-MAG with *N*,*N*-dimethyl-acrylamide (DMA) was then attempted to test whether copolymers that contain TMS-MAG can be made under similar conditioins. DMA is an acrylamide with much less bulky side groups than TMS-MAG. The copolymerization was mediated by a trithiocarbonate RAFT chain-transfer

agent (CTA)[41] in 1,4-dioxane (Scheme 3.2). The mole ratio of the reagents in the feed, $[AIBN]_0$:$[CTA]_0$:$[DMA]_0$:$[TMS\text{-}MAG]_0$, was 0.05:1.0:91.8:10.2, and the total concentration of the monomers was 2.0 M. After 3.0 h, the conversion of DMA and TMS-MAG were 81% and 64%, respectively, as determined by ^{1}H NMR spectroscopy. The product exhibited a monomodal distribution of molar masses as revealed by SEC and the dispersity (*Đ*) was 1.15 relative to PS standards (Figure 3.2). These results suggest glucose-containing copolymers with well-defined structures can be facilely synthesized by copolymerizing TMS-MAG with a reactive (meth)acrylamide with small steric hindrance from the side groups such as DMA .

Scheme 3.2 RAFT copolymerization of DMA (**1**) and TMS-MAG (**2**).

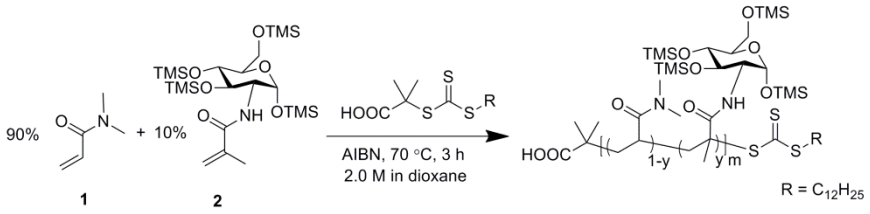

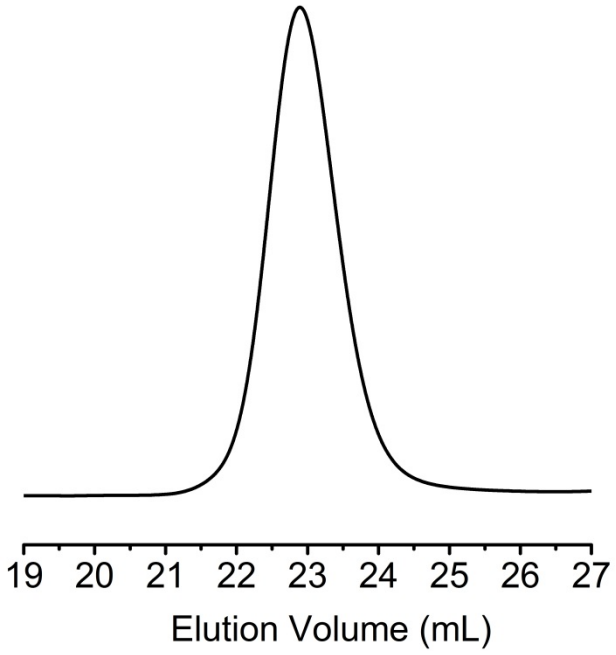

Figure 3.2 SEC chromatogram of the reaction product (as reacted, without purification) from the RAFT copolymerization of DMA and TMS-MAG as illustrated in Scheme 3.2.

Based on the success on copolymerization, I synthesized the glucose-containing poly(ethylene-*alt*-propylene)–poly(DMA-*grad*-MAG) (PG) diblock terpolymers using a combination of anionic and reversible addition-fragmentation chain transfer (RAFT) polymerizations as shown in Scheme 3.3. A hydroxyl-terminated PEP (as described in Chapter 2) was made by sequential anionic polymerization of isoprene in cyclohexane, end-capping with ethylene oxide at the ω-termini, quenching with acidic methanol, and hydrogenation using Pt/SiO_2 as the heterogeneous catalyst. The M_n (^{1}H NMR, end-group analysis) was 3.1 kg mol^{-1}, and $Đ$ (SEC, relative to PS standards) was 1.05. The polyisoprene precursor contained 91% 4,1-addition, and full saturation (> 99%, ^{1}H NMR) after hydrogenation was supported by ^{1}H NMR spectroscopy. The T_g of PEP-OH was

−65 °C as determined by DSC in the 2nd heating scan at a rate of 10 °C min^{-1}. Next, PEP-OH was esterified with a trithiocarbonate CTA[41] to afford the macromolecular CTA, PEP-CTA (**3**). DMA and TMS-MAG were copolymerized in the presence of PEP-CTA to afford the glucose-functionalized diblock terpolymers, as shown in Scheme 3.3. $[DMA]_0$:$[TMS\text{-}MAG]_0$ in the feed was adjusted from 1:1 to 22:1 (Table 3.1) to afford samples with varying glucose content. The molecular characteristics of the prepared diblock terpolymers are summarized in Table 3.2. The values in the parentheses of the sample IDs indicate the M_n of the two blocks in kg mol^{-1} followed by the mole fractions of TMS-MAG in the hydrophilic blocks as determined by ^1H NMR spectroscopy (Figure 3.3). In all cases, the conversions of DMA were larger than those of TMS-MAG. The reactivity ratios of DMA (**1**, as monomer 1) and TMS-MAG (**2**, as monomer 2) were determined to be $r_1 = 1.86$ and $r_2 = 0.16$ in free-radical polymerizations at 70 °C (*vide infra*). As such, we infer that the poly(meth)acrylamide copolymer blocks were gradient in nature.[42] SEC characterization of selected TMS-protected PG samples indicated that they were monomodal with apparent $Đ$ values in the range of 1.18–1.31 (Table 3.2 and Figure 3.4).

Scheme 3.3 Synthesis of PEP–poly(DMA-*grad*-MAG) diblock terpolymers.

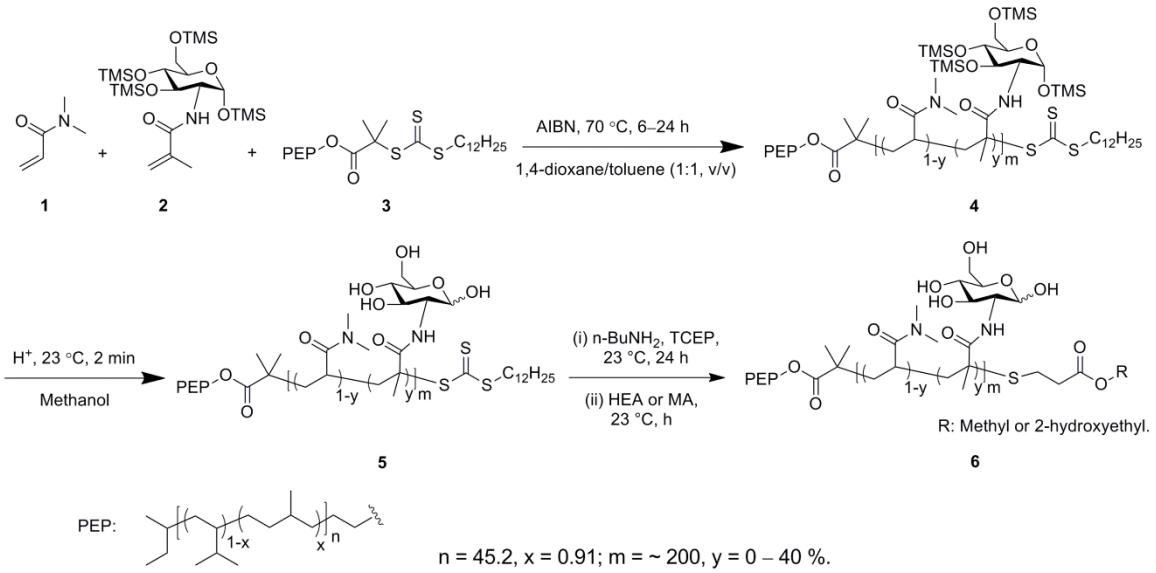

The TMS groups were removed through acid-catalyzed deprotection with methanol. The deprotection was quantitative and nearly instantaneous; 2 min of reaction at 25 °C led to >99% removal of TMS as determined by ^{1}H NMR spectroscopy (Figure 3.3). RAFT copolymerizations and hydrolyses can be done in a one-pot manner, which only required a solvent exchange from the mixture of toluene and 1,4-dioxane into that of THF and methanol. All of the seven reactions listed in Table 3.1 were carried out in this one-pot manner without isolating the protected PEP–poly(DMA-*grad*-TMS-MAG) terpolymers except PG(3-19-0.08). In the last step, the trithiocarbonate CTA fragment was removed through mild aminolysis with *n*-butyl amine followed by a thiol-ene reaction with an acrylate (i.e., methyl acrylate or 2-hydroxyethyl acrylate).[36] Quantitative removal was supported by the disappearance of the characteristic absorbance peak of the trithiocarbonyl moieties at 309 nm in UV-vis spectroscopy (Figure 3.5). This step

eliminated not only the possibility of aggregation due to the relatively long, hydrophobic C_{12} groups during micellization,[43] but also any potential toxicity from the trithiocarbonyl CTA fragments.[44]

Table 3.1 RAFT copolymerization of DMA (**1**, as monomer 1) and TMS-MAG (**2**, as monomer 2) using PEP-CTA as the macromolecular CTA to afford PEP–poly(DMA-*grad*-MAG) (PG) diblock terpolymers.

Sample[a]	$[AIBN]_0$:$[PEP\text{-}CTA]_0$: $[DMA]_0$:$[TMS\text{-}MAG]_0$[b]	$[M]_0$[c]	Time (h)	Conv. of DMA[d]	Conv. of TMS-MAG[d]
PG(3-26-0.39)	0.10 : 1 : 105.5 : 102.8	1.12	24	0.953	0.627
PG(3-24-0.21)	0.05 : 1 : 175 : 57	0.76	22	0.901	0.590
PG(3-39-0.21)	0.09 : 1 : 240.4 : 78.2	1.44	22	0.966	0.803
PG(3-24-0.16)	0.05 : 1 : 176.6 : 43.4	1.40	18	0.919	0.694
PG(3-19-0.08)	0.05 : 1 : 179.3 : 19.8	1.57	7	0.903	0.694
PG(3-20-0.04)	0.05 : 1 : 191.5 : 8.5	2.43	6	0.947	0.775

[a] The first two values in the parentheses are M_n in kg mol^{-1} of the component blocks, and the third values are the mole percentage of MAG repeating units in the hydrophilic block, all of which were determined by ^1H NMR spectroscopy. [b] The ratio of the concentrations of the initiator, macromolecular chain-transfer agent (PEP-CTA, **3**), and the two monomers in the feed. [c] The total concentration of the DMA and TMS-MAG monomers in the feed. [d] Conversion as determined by ^1H NMR spectroscopy.

Table 3.2 Molecular characteristics of amphiphilic diblock copolymers and terpolymers.

Sample[a]	N_{EP}[b]	N_{amide} or N_{EO}[b]	MAG mol %[c]	PEP wt %[d]	M_n (kg mol^{-1})[e]	$Đ$[f]
PG(3-26-0.39)	45	165	39	11	29	1.31
PG(3-24-0.21)	45	181	21	12	27	[g]
PG(3-24-0.16)	45	192	16	12	27	1.29
PG(3-19-0.08)	45	176	7.8	14	23	1.18
PA(3-21)	45	208	0	13	24	1.15
PO(3-25)[h]	45	565	0	11	28	1.02

[a] PG: PEP–poly(DMA-*grad*-MAG), PA: PEP–PDMA, and PO: PEP–PEO. [b] Degree of polymerization. [c] Mole fraction of MAG in the hydrophilic block. [d] Mass fraction of the hydrophobic PEP block. [e] Total M_n of the diblock copolymers and terpolymers. [f] All samples were measured on a SEC using $CHCl_3$ as the eluent at 35 °C relative to polystyrene standards, except PO(3-25), which was measured on a SEC with THF/*N*,*N*,*N*',*N*'-tetramethylethylenediamine as the eluent at 25 °C and equipped with a light scattering detector. The values of the PG diblock terpolymers before hydrolysis are reported, which are likely to be overestimates of the true values (the details are shown in Figure 3.4). [g] SEC analysis of this sample was not performed prior to deprotection. The RAFT polymerization of TMS-MAG and DMA mediated by PEP-CTA and the subsequent hydrolysis was carried out by Molly C. Dalsin. [h] Data reproduced from Ref[43].

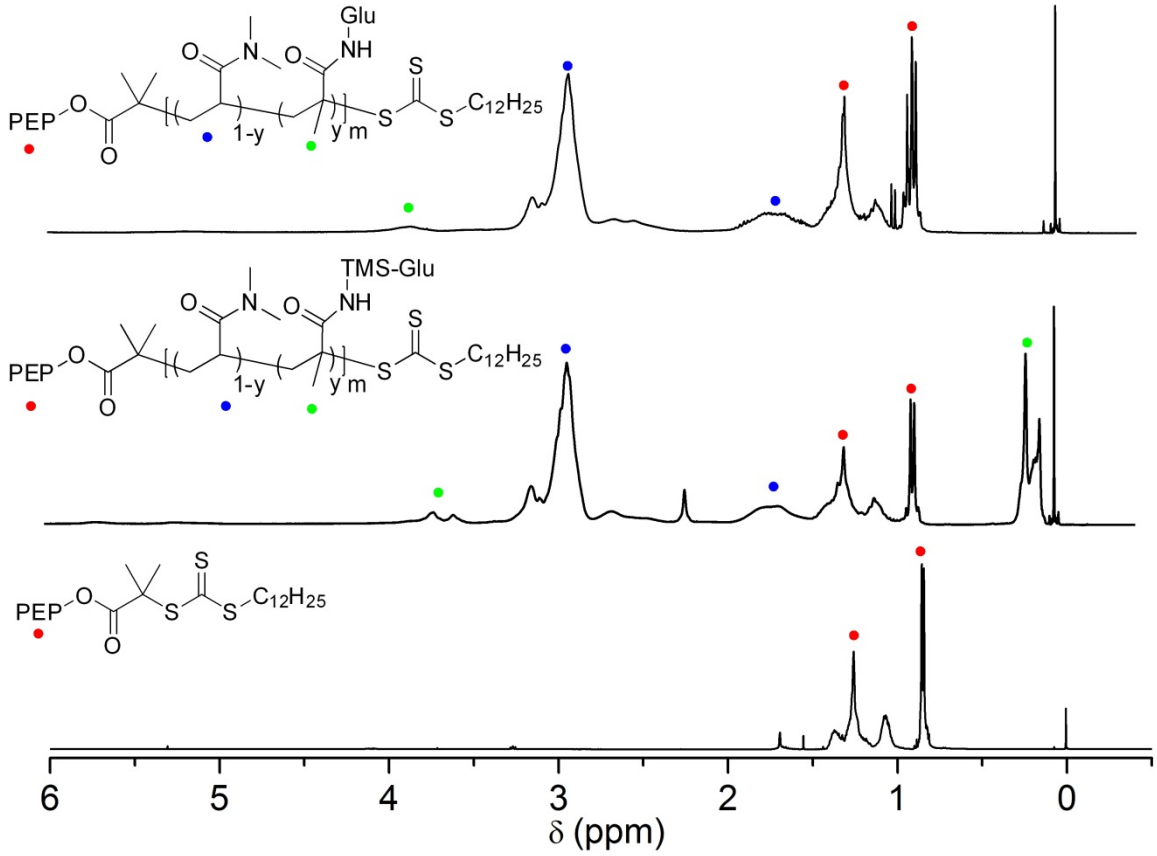

Figure 3.3 (From bottom to top) ^{1}H NMR spectra of macromolecular chain-transfer agent PEP-CTA (**3**), PG(3-19-0.08) before hydrolysis (isolated product), and PG(3-19-0.08) (isolated product) after hydrolysis.

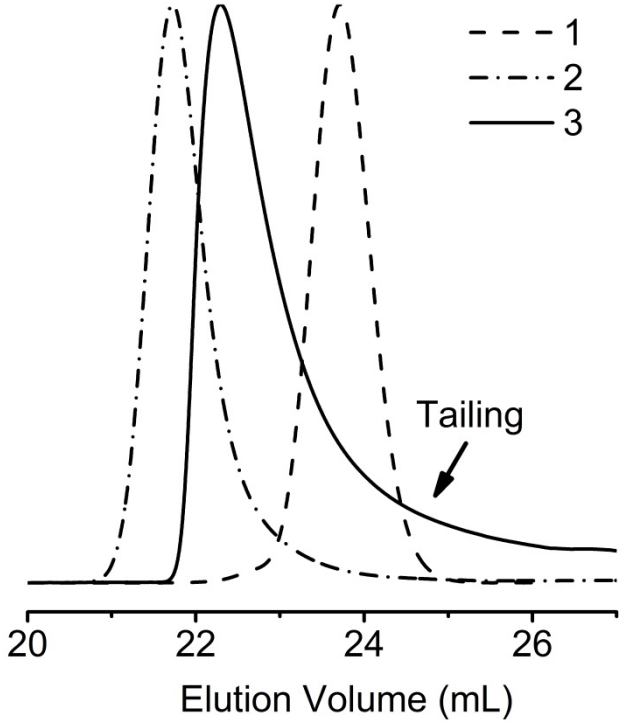

Figure 3.4 SEC traces of PEP-CTA (1), PG(3-19-0.08) before hydrolysis (isolated product, 2), and PG(3-19-0.08) after hydrolysis (isolated product, 3). The *Đ* values were 1.08, 1.18, and 1.60 for PEP-CTA, PG(3-19-0.08) before hydrolysis, and PG(3-19-0.08) after hydrolysis, respectively.

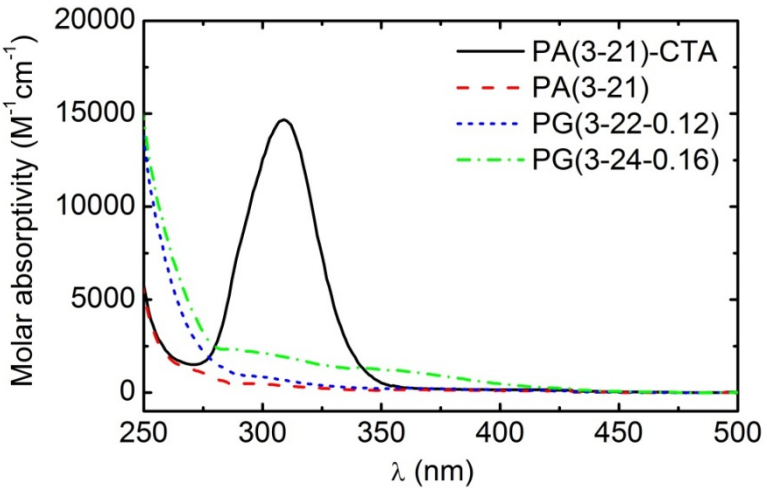

Figure 3.5 UV-vis spectra of PA(3-21)-CTA (before removing CTA, black solid line), PA(3-21) (after removing CTA, red dash line), PG(3-22-0.12) (after removing CTA, blue dot line), and PG(3-24-0.16) (after removing CTA, green dash dot line).

Two samples, PA(3-21) and PO(3-25) with similar compositions to the PG diblock copolymers but did not contain glucose in the hydrophilic blocks were also prepared. PA(3–21) was made by the RAFT polymerization of DMA in toluene at 70 °C, followed by removing the trithiocarbonate groups as described above. PO(3–25)[43] was prepared by the anionic polymerization of ethylene oxide in THF at 40 °C. The molecular characteristics of these two diblock copolymers are also listed in Table 3.2.

The reactivity ratios of DMA (**1**, as monomer 1) and TMS-MAG (**2**, as monomer 2) in free-radical polymerizations at 70 °C were further determined as shown in Scheme 3.4. The solvent was a 1:1 (v/v) mixture of toluene and 1,4-dioxane, same as that in the RAFT synthesis of the PG diblock terpolymers. Thirteen experimental runs were carried out with the monomer fractions of DMA in the feed (f_1) in the range of 0.10–0.90. The conversion of each monomer was kept at < 15.0% by adjusting the ratio of the monomers to initiator in the feed and the reaction time. f_1 and the conversion of two monomers were

determined by ^{1}H NMR spectroscopy, based on which the mole fractions of DMA in the copolymer (F_1) were calculated (Table 3.3). For Run 1 (f_1 = 0.905), the composition of the isolated copolymer product was also determined by ^{1}H NMR spectroscopy, and the obtained results (F_1 = 0.946) were consistent with the calculation based on f_1 and conversion (F_1 = 0.939).

Scheme 3.4 Copolymerization of DMA (**1**, as monomer 1) and TMS-MAG (**2**, as monomer 2) towards the reactivity ratios of DMA and TMS-MAG in free-radical polymerizations.

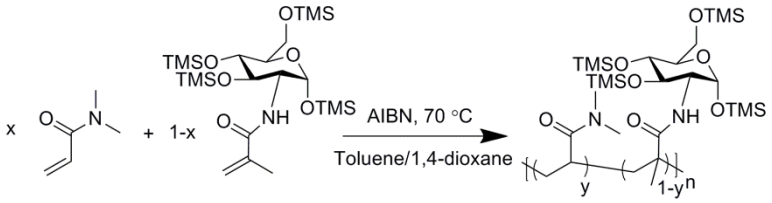

$[I]_0$:$[M]_0$= 1:400–1:5000, time = 10–15 min, conv. < 15.0 mol%.

Table 3.3 Experimental runs towards determining the reactivity ratios of DMA (**1**, as monomer 1) and TMS-MAG (**2**, as monomer 2) in free-radical polymerizations in a mixture of toluene and 1,4-dioxane (1:1, v/v) at 70 °C.

Run	f_1[a]	Conv. of DMA[b]	Conv. of TMS-MAG[b]	F_1[c]
1	0.905	13.0	8.02	0.939
2	0.796	8.32	4.11	0.888
3	0.699	8.19	3.88	0.830
4	0.595	10.7	4.59	0.773
5	0.502	14.9	6.48	0.698
6	0.502	9.79	3.62	0.731
7	0.481	11.8	4.74	0.698
8	0.465	7.42	2.71	0.704
9	0.465	11.3	4.34	0.694
10	0.390	8.36	3.27	0.621
11	0.333	8.90	3.08	0.591
12	0.250	8.21	2.68	0.504
13	0.101	12.4	2.68	0.342

[a] Mole fraction of monomer 1 (DMA) in the feed as determined by ^{1}H NMR spectroscopy. [b] The conversion of monomers as determined by ^{1}H NMR spectroscopy. [c] Mole fraction of monomer 1 (DMA) in the polymer as calculated by f_1 and conversion. The experimental errors in f_1 and F_1 were estimated to be less than 5 %.

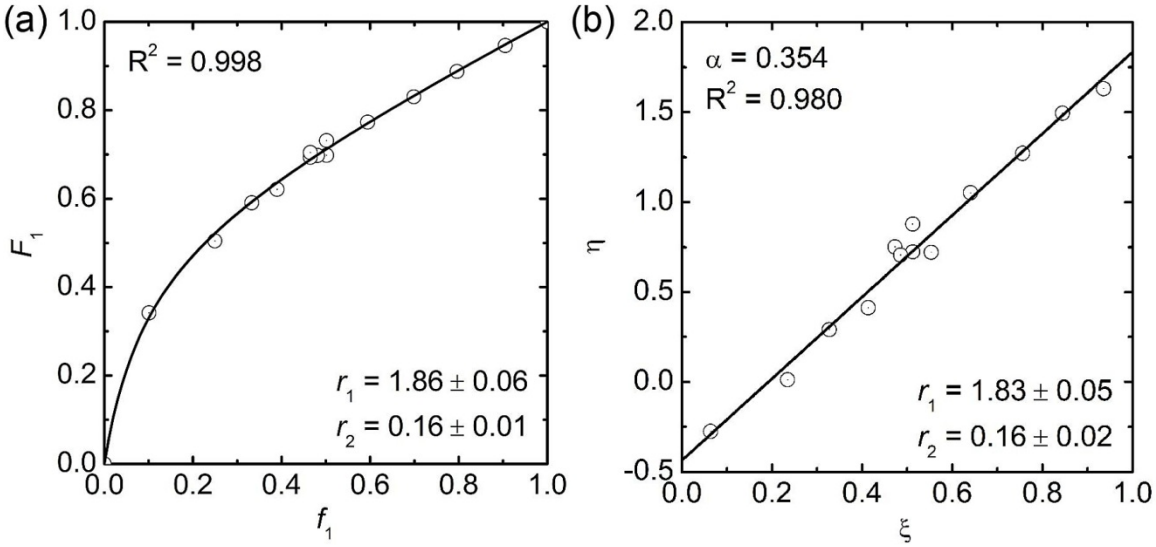

Figure 3.6 (a) Nonlinear fit following $F_1 = (r_1f_1^2 + f_1f_2)/(r_1f_1^2 + 2f_1f_2 + r_2f_2^2)$, and (b) linear fit using the Kelen-Tudos method towards determining the reactivity ratios of DMA (**1**, as monomer 1) and TMS-MAG (**2**, as monomer 2) in free-radical polymerizations at 70 °C.

The composition data were fit using the nonlinear method[45] following $F_1 = (r_1f_1^2 + f_1f_2)/(r_1f_1^2 + 2f_1f_2 + r_2f_2^2)$ and gave: $r_1 = 1.86 \pm 0.07$, $r_2 = 0.16 \pm 0.01$, as shown in Figure 3.6a. Data treatment with the linear Kelen-Tudos method[46] gave similar results: $r_1 = 1.83 \pm 0.05$, $r_2 = 0.16 \pm 0.02$. r_2 was much smaller than r_1 ($r_2/r_1 < 0.1$), which was consistent with the slow homopolymerization of TMS-MAG as described above. Methacrylamides often exhibit higher reactivity than acrylamides, and we ascribe the difference in our results to the great steric hindrance from TMS-protected glucosamine in TMS-MAG (α-anomer as well as large TMS groups). These results suggested that the self-propagation of the terminal TMS-MAG radials was ca. 6 times slower than their cross-propagation toward DMA, which had much smaller side groups than TMS-MAG monomers. On the other hand, propagating chains with terminal DMA radicals have only

ca. 2-fold preference over self-propagation. Since $r_1.r_2$ is 0.30 (< 1), TMS-MAG can be effectively copolymerized with DMA. The copolymerization strategy has also been employed in the nitroxide-mediated polymerization (NMP) of styrene and a methacryloyl galactose monomer, although no explicit determination of the reactivity ratios were reported.[21] As the monomer feed drifted with conversion (no azeotropic copolymerizations), we inferred that the poly(meth)acrylamide blocks were gradient copolymers. DMA was likely to be rich near the ester linkages between the PEP and poly(meth)acrylamide blocks, and MAG gradually increased along the backbone toward the ω-termini.

3.2.2 Self-assembly of PG Diblock Terpolymers in Water

The samples examined in this chapter all had very low hydrophobic content (PEP wt % < 15 %), and T_g of the PEP block (−65 °C) was well below room temperature. Therefore, there were no complications in micellization due to the high hydrophobic content[47] and "frozen" glassy or semicrystalline cores,[48] similar to previously studied poly(*n*-butyl acrylate)–PDMA diblock copolymers.[49] Nevertheless, kinetically-trapped aggregates may still be obtained due to the strongly hydrophobic PEP cores.[50, 51] For all samples except PG(3-26-0.39), the micelle dispersions in water were prepared by nanoprecipitation followed by dialysis. THF can solubilize PO(3-25), PA(3-21), and PG terpolymers with a relatively small content of MAG (e.g., PG(3-19-0.08)). On the other hand, more polar solvents (e.g., methanol) were required to supplement THF to fully solubilize the terpolymers with rather high MAG content. For example, a 15:2 (v/v)

mixture of THF/methanol was found to molecularly dissolve PG(3-24-0.16) as revealed by DLS. However, due to the vast polarity difference between PEP and PMAG (see Figure 3.7 for details), I was unable to find a solvent mixture that could well dissolve PG(3-26-0.39), which had the highest MAG content among all of the PG diblock terpolymers synthesized. Binary mixtures of THF with methanol, DMF, DMSO, and 2,2,2-trifluoroethanol with a variety of compositions were tried at 23 °C, which were also supplemented with a small amount of acetic acid, but none of them was found to able to fully dissolve PG(3-26-0.39). As such, the micelle dispersion of PG(3-26-0.39) was prepared by directly dispersing the neat sample in water at 60 °C for 2 weeks.

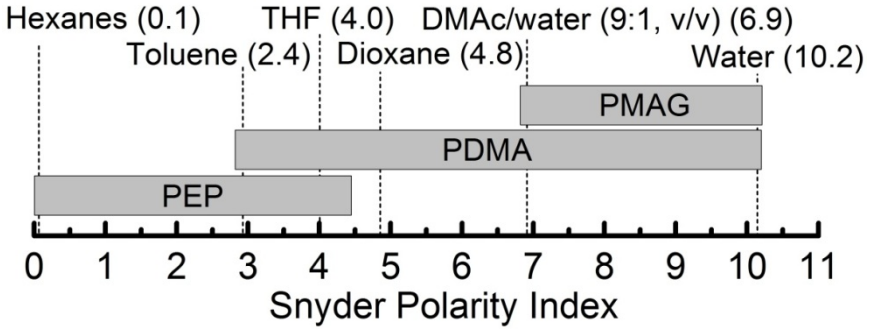

Figure 3.7 Experimental solubility diagrams of PEP, PDMA, and PMAG in terms of Snyder's polarity index[52] at 23 °C.

As shown in Figure 3.8, all micelle dispersions were clear with slight bluish tinge except the 1.0 wt % dispersion of PG(3-26-0.39) prepared through direct dissolution, which appeared white and cloudy and thus implied large aggregates. The DLS results of the micelle dispersions are summarized in Table 3.4 and Figure 3.9. Micelles with hydrodynamic radii of ca. 15 nm and narrow dispersity were obtained in the aqueous

dispersions of PO(3-25), PA(3-21), and PG(3-24-0.16). A small fraction of large aggregates existed in PG(3-24-0.21) by REPES analysis, and the peak positions (12, 84 nm) were consistent with the results from fitting the first-order correlation function ($g_1(t)$) using the double-exponential expansion (R_h = 12, 63 nm as shown in Figure 3.10). In the 1.0 wt % dispersion of PG(3-26-0.39) prepared by direct dispersion, the average R_h was 89 nm with a dispersity of 0.64 (at 90°) by cumulant analysis. Besides, the $\Gamma \cdot q^{-2}$ value showed strong angular dependence (Figure 3.11). These results collectively indicated rather broad size distributions of the suspended particles within the PG(3-26-0.39) dispersion. Fitting $g_1(t)$ using the double-exponential expansion gave R_h = 16, 144 nm. The larger particles corresponded to intermicelle aggregates, which will be discussed later in combination with cryo-TEM results.

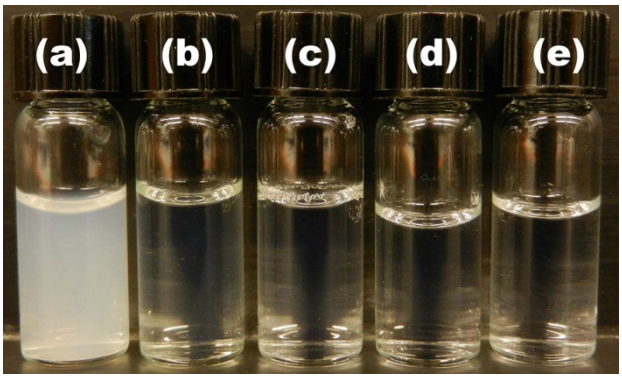

Figure 3.8 Pictures of ca. 1 wt % dispersions in water of (a) PG(3-26-0.39), (b) PG(3-24-0.21), (c) PG(3-24-0.16), (d) PA(3-21), and (e) PO(3-25). The illuminating source was a daylight lamp, and the outer diameter of the vials was 12 mm.

Table 3.4 DLS results of the aggregates from the self-assembly of amphiphilic diblock PA and PO copolymers and PG terpolymers in water

Sample	R_h (nm)[a]	μ_2/Γ^{-2} [b]	R_h (nm)[c]	Conc (wt %)[d]	Method[e]
PG(3-26-0.39)	89 ± 5	0.64	16, 144 ± 7[f]	1.0	DD
PG(3-24-0.21)	17.7 ± 0.2	0.23	12.2 ± 0.2, 63 ± 5	0.75	NP
PG(3-24-0.16)	16.0 ± 0.1	0.17		0.75	NP
PA(3-21)	14.1 ± 0.1	0.13		0.75	NP
PO(3-25)	18.9 ± 0.2	0.11		0.75	NP

[a] Hydrodynamic radii determined by fitting the first-order correlation functions ($g_1(t)$) using the cumulant expansion. Linear regression of Γ vs q^2 was enforced over 5–7 angles between 30° and 120°. [b] Dispersity at a scattering angle of 90°. [c] Hydrodynamic radii as determined by fitting $g_1(t)$ using the double-exponential expansion. Linear regressions of Γ vs q^2 of the two separate decay modes were performed over 5–7 angles between 30° and 120°. [d] Weight fractions of polymers in the aqueous dispersions. [e] Method of sample preparation: DD, direct dissolution; NP: nanoprecipitation followed by dialysis. [f] R_h corresponding to the fast decay mode was fixed at 16 nm when the first-order correlation functions were fit using the double-exponential expansion, and linear fitting of Γ vs q^2 was applied to the slow decay mode over 7 different scattering angles between 45° and 135°.

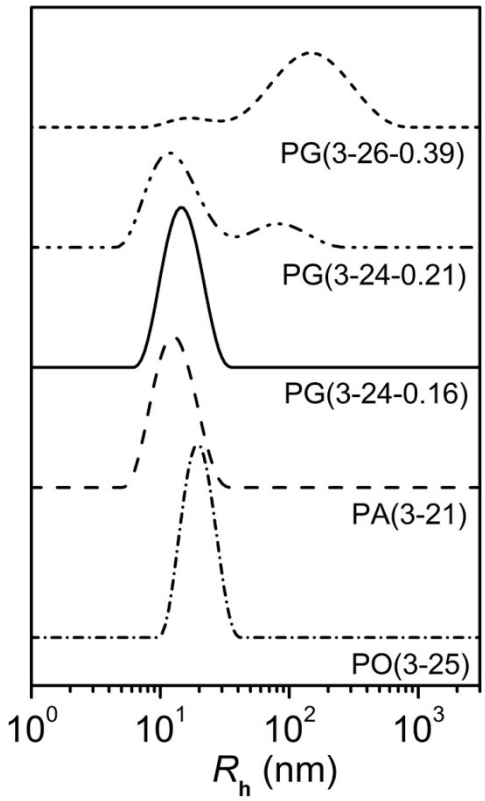

Figure 3.9 Apparent micelle size distribution of ca. 1 wt % dispersions in water of PO(3-25), PA(3-21), and three PG diblock terpolymers with different MAG compositions as listed in Table 2. The scattering angle is 90°. Peak values: 19 nm in PO(3-25), 13 nm in PA(3-21), 15 nm in PG(3-24-0.16), 12, 84 nm in PG(3-24-0.21), and 16, 150 nm in PG(3-26-0.39).

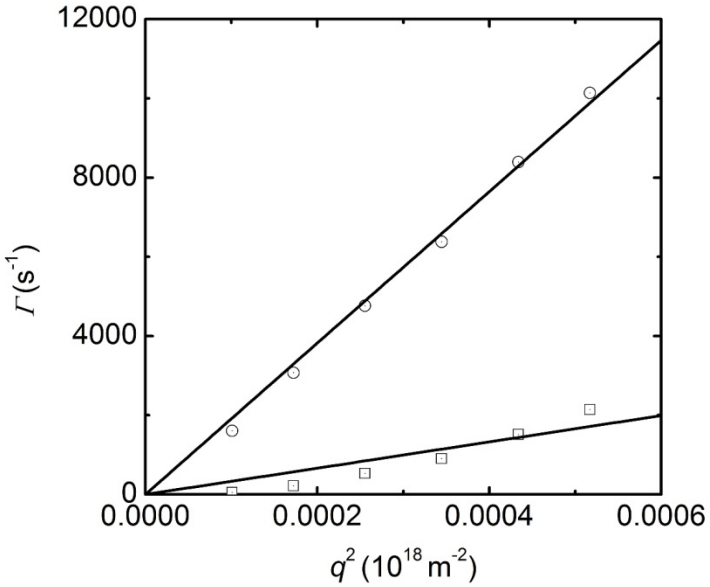

Figure 3.10 Linear fitting of Γ vs q^2 of the two decaying modes in the 0.75 wt % dispersion of PG(3-24-0.21) in water over 7 different scattering angles in the range of 45–135°. g_1(t) was fitted using the double-exponential expansion and shown as solid black curves.

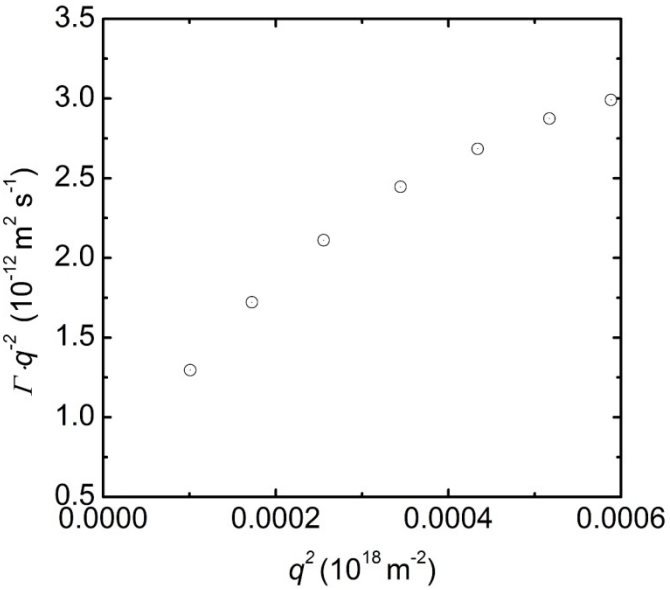

Figure 3.11 Angular dependence of $\Gamma \cdot q^{-2}$ in the 0.75 wt % dispersion of PG(3-26-0.39) in water over 7 scattering angles in the range of 45–135°. The decay rates at different angles, Γ, were extracted by fitting g_1(t) using the cumulant expansion.

The micelle dispersions were imaged by cryo-TEM, which provides direct visualization of micelles in their native aqueous environment. All of the images, including Figure 3.12 Figure 3.13, and Figure 3.14, clearly showed that spherical micelles with narrow dispersity were the predominant morphology in the PG and PA micelles investigated. The radii of the micelle cores (R_c) were 7 ± 1 nm in all of the samples examined. Correspondingly, the aggregation number (n) of the spherical micelles was 240 ± 120, the interfacial area per chain (a_0) was 2.6 ± 0.4 nm^2, and the degree of stretching of the PEP block was 1.3 ± 0.2 (s is defined as $R_c/\langle h^2\rangle_0^{1/2}$ and $\langle h^2\rangle_0^{1/2}$ is the root-mean-square end-to-end distance of unperturbed PEP chains, which is 5.4 nm at 25 °C). R_c of PA(3-21) in this report was slightly smaller than that made from PA(3-11) by direct dissolution at 120 °C in Chapter 2, which was 9 ± 1 nm. We believe there are two reasons: (i) a longer hydrophilic PDMA block in PA(3-21) than PA(3-11)—similar dependence of R_c on the degree of polymerization of the hydrophilic block was also observed in other amphiphilic polymeric systems with rather strong polarity difference, e.g., PS–PAA[47] and PB–PEO[53] in water; (ii) a different micellization method—as the selectivity of the solvents was changed in a very slow manner in nanoprecipitation, the interfacial energy between PEP and the outer solvents at the onset of micellization in nanoprecipitation was smaller than that in direct dissolution, which resulted in a lower aggregation number and thus smaller R_c in micelles prepared by nanoprecipitation than those via direct dissolution.[43]

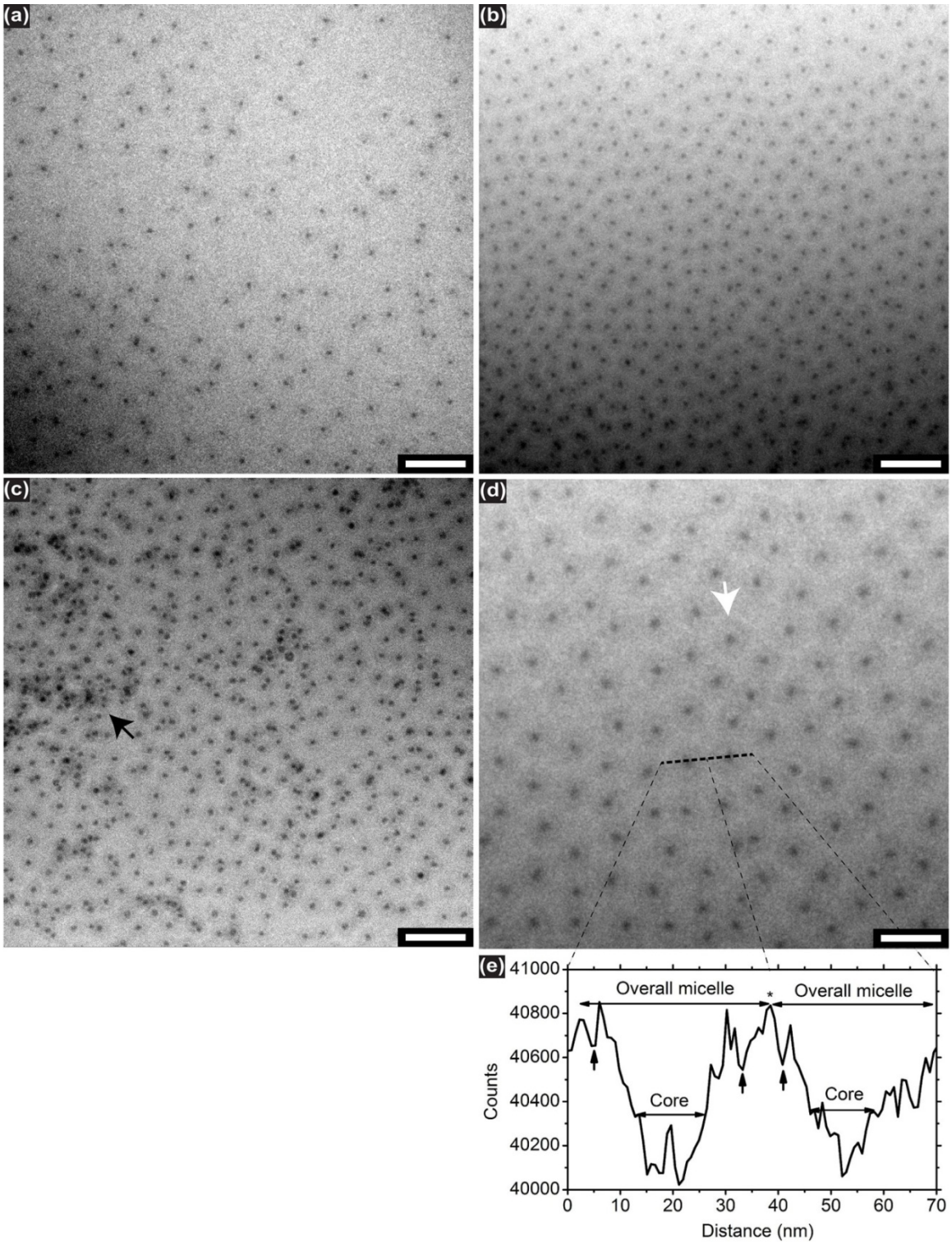

Figure 3.12 Representative cryo-TEM images of ca. 1 wt % dispersions in water of (a) PG(3-24-0.16), (b, d) PG(3-24-0.21) at low and high magnifications, respectively, and (c)

PG(3-26-0.39). The black arrow in (c) highlights an example of micelle aggregates resulting from sample preparation by direct dissolution. The white arrow in (d) highlights the gray halo around one micelle core. (e) Line profile of counts of electrons vs distance over two adjacent micelles as highlighted in (d). The width of the line is 0.76 nm. Black arrows highlight areas corresponding to the halos outside the micelle cores. The "*" sign highlights the area corresponding to the ice matrix between the two micelles. Scale bars indicate 100 nm in (a-c), and 50 nm in (d).

Interestingly, the coronae of the glucose-functionalized micelles were clearly observed as gray halos around the micelle cores in the cryo-TEM images as shown in Figure 3.12 and Figure 3.14. In comparison, the coronae were far less evident in PA(3-21) as shown in Figure 3.13, whose hydrophilic blocks were composed of PDMA only. All of the images were taken at similar underfocus levels, 8–12 μm, and no staining was applied during sample preparation. Previously, the existence of the swollen, diffuse micelle coronae of nonionic polymers (e.g., PEO) were often inferred from the space between adjacent dense micelle cores in cryo-TEM images.[54] Salts or acids of heavy elements can be applied to increase the contrast of micelle coronae made of ionic blocks (e.g., poly(methacrylic acid)).[55] However, these additives may change the native chain conformation in the dispersion.[56] Here the electron-dense glucose moieties in the PG diblock terpolymers greatly enhanced the native contrast of the micelle coronae; the electron density of the hydrophilic blocks in PG(3-24-0.21) was estimated to be 421 e^- nm^{-3}, compared to 397, 369, and 314 e^- nm^{-3} of PDMA, PEO, and amorphous ice respectively. Literature values of the densities at 25 °C were used during the calculation: glucose, 1.54 g cm^{-3}; PDMA, 1.21 g cm^{-3}; PEO, 1.13 g cm^{-3}, and amorphous ice, 0.94 g cm^{-3}. The electron density of the poly(DMA-*grad*-MAG) block was estimated by using a

blend of glucose and PDMA with the same composition and assuming the volume was additive. The contrast improvement would benefit studies on the conformations of polymer brushes in the swollen, diffuse state by imaging. From the line profile across two adjacent micelles (Figure 3.12e), the counts of electrons gradually decreased from the interface between cores and coronae to the outer periphery of the micelles, qualitatively consistent with the decreasing segment densities as reported in scattering measurements.[57] Besides, three local minima were observed as highlighted by the black arrows, which corresponded to the grey halos around the micelle cores. These halos indicated that MAG was not evenly distributed in the radial direction of the corona; in other words, MAG was more populated at the outer periphery of the corona than areas neighboring the core–corona interface. As such, the glucose moieties are readily exposed to the outer aqueous medium, which may benefit the potential functionalization off the hydroxyls and thus result in enhanced bioactivity.

The structure of the large aggregates in the 1.0 wt % dispersion of PG(3-26-0.39) was also revealed in cryo-TEM as shown in Figure 3.12c. Besides individual spherical micelles with core radii of 7 ± 1 nm, which were similar to those in the dispersions of PG(3-24-0.16) and PG(3-24-0.21), clusters of individual spherical micelles were also observed as highlighted by a black arrow in Figure 3.12c. Interestingly, the clusters appeared to be connected via micelle coronae, as individual micelle cores were unambiguously distinguished from each other. Therefore, the large particles in PG(3-26-0.39) were inter-micelle aggregates, rather than micelles with different structures (e.g., individual micelles with large n). As such, R_h corresponding to the fast decay mode was

fixed at 16 nm when $g_1(t)$ was fitted using the double-exponential expansion in DLS studies, and R_h = 144 ± 7 nm was obtained for the slow decay mode. Using Shibayama's bimodal scattering analysis,[58] the weight fractions of the fast and slow decay modes were determined to be 94.6 and 5.4 wt %, respectively. Therefore, individual micelles were much more populated than micelle clusters in the dispersion of PG(3-26-0.39), which was qualitatively consistent with our observation in cryo-TEM (Figure 3.14). In addition, the size and weight fractions of the micelle clusters decreased after the micelle dispersion was sonicated, but the clusters were not completely eliminated. For example, the 1.0 wt % micelle dispersion of PG(3-26-0.39) in water appeared to be almost clear with slight bluish tinge after 8 h of sonication. In DLS, the R_h corresponding to the slow decay mode decreased to 74 ± 2 nm using double-exponential expansion while the R_h corresponding to the fast decay mode was fixed at 16 nm. The weight fractions of the suspended particles corresponding to the fast and slow decay modes were 98.3% and 1.7%, respectively.[58] The R_h of the sample after sonication by cumulant analysis were 47.1 ± 0.8 nm (over 9 angles between 30° and 150°), and the dispersity was 0.397 (at 90°).

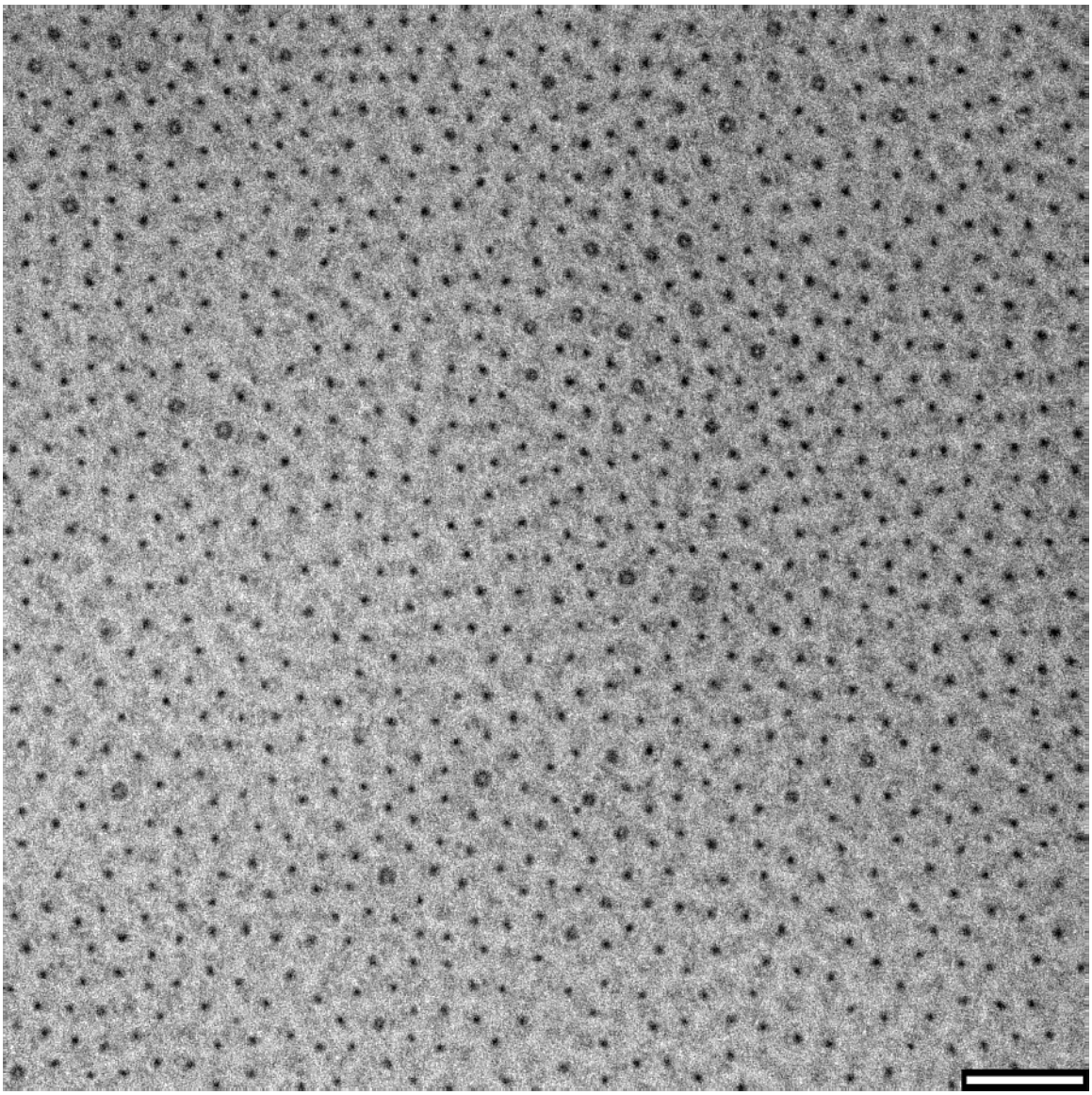

Figure 3.13 A cryo-TEM image of a 0.75 wt % dispersion of PA(3-21) in water. Spherical micelles with radii of 7 ± 1 nm were the predominant morphology. Some (ca. 2 % in number density) larger particles were also observed, which were possibly due to the excessive exposure of the electron beam. The scale bar indicates 100 nm.

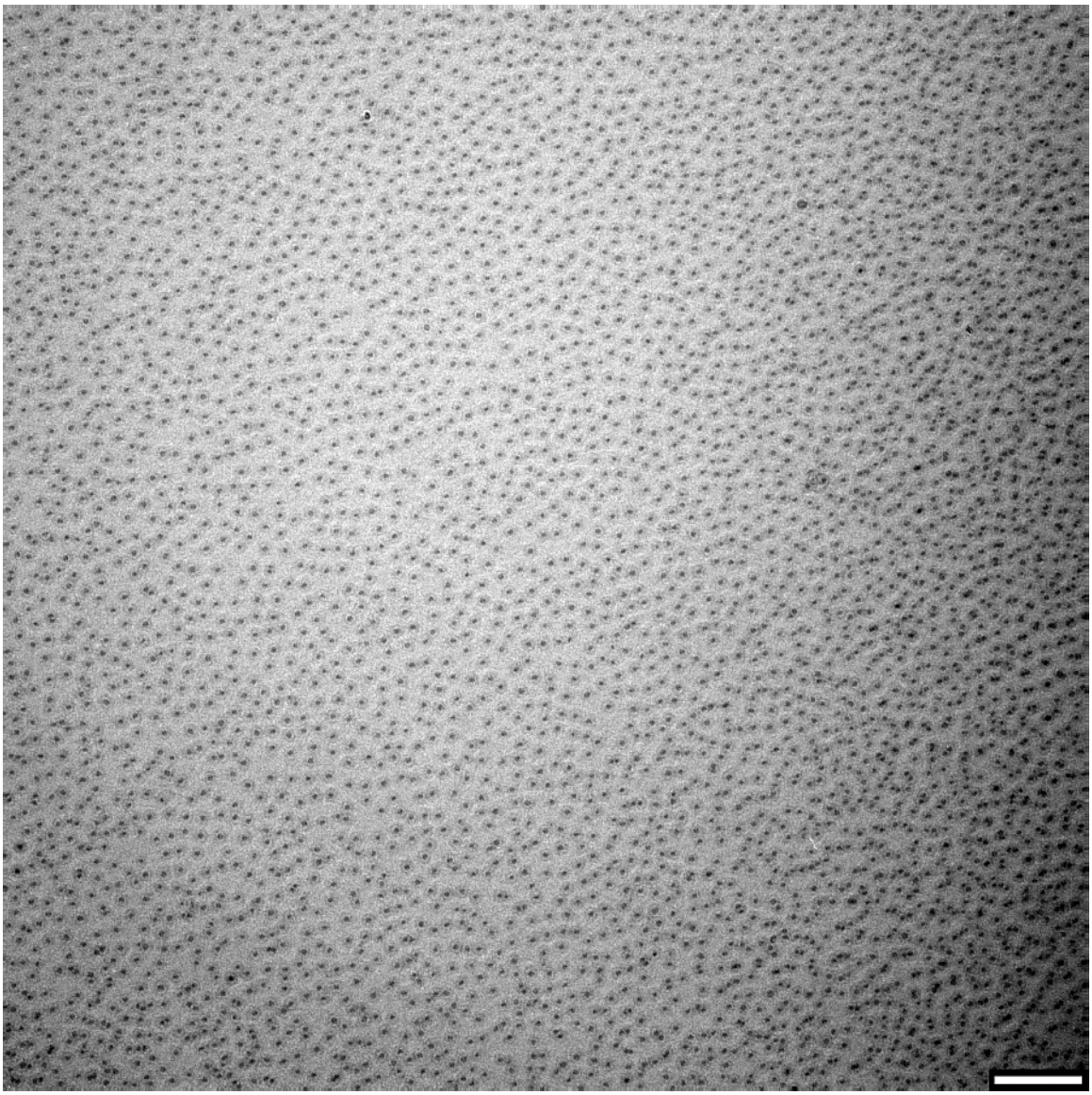

Figure 3.14 A cryo-TEM image of a 1.0 wt % dispersion of PG(3-26-0.39) in water. The scale bar indicates 200 nm.

We hypothesize that the PG micelle clusters were caused by the relatively high T_g of the hydrophilic blocks. For example, T_g of the hydrophilic blocks were determined be 147 and 177 °C in PG(3-24-0.16) and PG(3-39-0.21), respectively (Figure 3.15). The preparation of PG(3-19-0.08) and PA(3-21) dispersions via direct dissolution was also

attempted, and similar large aggregates were observed in DLS as those found in the 1.0 wt % dispersion of PG(3-26-0.39). In contrast, no micelle aggregates was observed in the aqueous dispersions of PO(3-25) via direct dissolution, whose hydrophilic PEO block had a T_m of ca. 55 °C. Since all of these samples contained PEP as the hydrophobic block and the overall molar masses and compositions were similar, these results indicated that the thermal properties of the nonionic, hydrophilic blocks are important in the micelle structures prepared via direct dissolution. As T_g were much higher than processing temperature (23 °C), the slow mobility of poly(DMA-*grad*-MAG) chains may also result in kinetically-trapped structures such as micelle aggregates. Possibly due to this reason, glycopolymer-containing amphiphiles have been mostly prepared by nanoprecipitation coupled with dialysis in literature.[18-29] However, direct dissolution is technically attractive because of simplicity, exclusion of organic volatiles, and possible high drug loading of hydrophobic drugs. Therefore, glycopolymers with T_g near or below ambient temperature are particularly interesting. For example, copolymerizing MAG with monomers whose polymers have low T_g (e.g., poly(hydroxyethyl acrylate), PHEA) may afford glycopolymers with moderate T_g (i.e., close to or below RT), and thus facilitate sample preparation through direct dissolution.

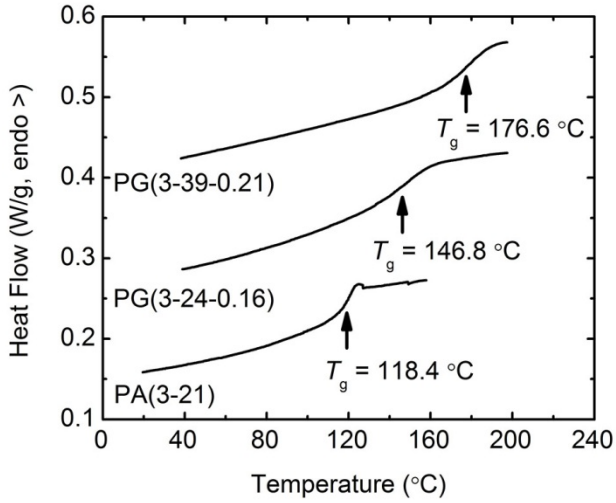

Figure 3.15 DSC results of PA(3-21), PG(3-24-0.16), and PG(3-39-0.21) neat samples between 20 and 200 °C at a rate of 10.0 °C min^{-1}. Shown are the 2nd heating scans.

3.2.3 Serum-stability of Glucose-functionalized Polymeric Micelles

The stability of the drug delivery vehicles after intravenous injection is critical in the circulation and payload-release performance. Specifically, the interaction between micelles and serum proteins must be minimal, because the adsorbed proteins may cause rapid clearance of the micelles (opsonization)[5, 59] or induce the release of payloads prior to reaching target sites.[38] The micelles from PG(3-24-0.16) were examined in four different media: PBS (containing physiological salts), Opti-MEM (containing physiological salts and small molecule nutrients), DMEM supplemented with 10% FBS (partial serum), and 100% FBS (full serum). The micelle size after a 1:5 (v/v) dilution in the four aqueous buffers was first measured by DLS. Next, the scattering intensity of the micelles diluted with 100% FBS was continuously monitored for 14 h to examine their long-term stability. Lastly, the stability of PG(3-24-0.16) micelles in 100% FBS was

examined by cryo-TEM and DLS. The controls are the micelle dispersions from PA(3-21) and PO(3-25).

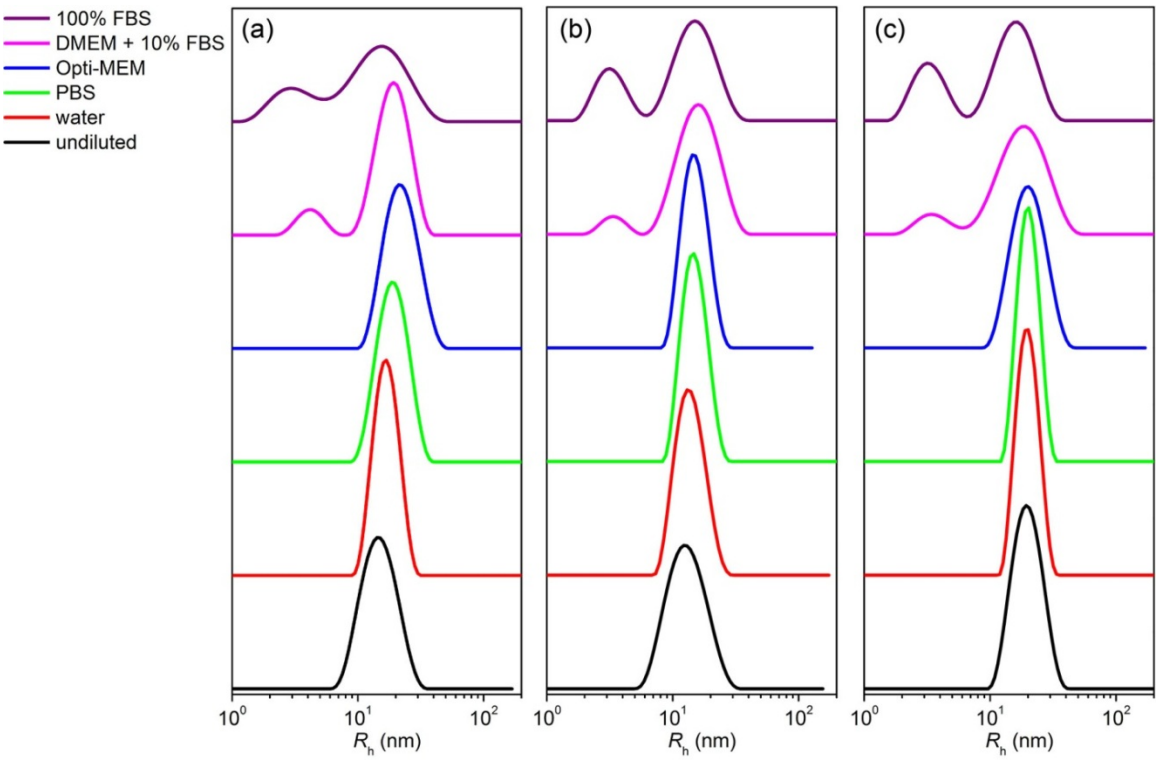

Figure 3.16 Apparent micelle size distributions of 0.75 wt % dispersions in water of (a) PG(3-24-0.16), (b) PA(3-21), and (c) PO(3-25) after 1:5 (v/v) dilutions with 5 different biologically-relevant media (from top to bottom: 100% FBS, DMEM supplemented with 10% FBS, Opti-MEM, PBS, and water. The undiluted samples in water are listed at the bottom for reference). The scattering angle is 90°.

Figure 3.16 shows the REPES size distribution of 0.75 wt % PG(3-24-0.16), PA(3-21), and PO(3-25) after a 1:5 (v/v) dilution with four different biologically-relevant media as well as DI water. Literature values of refractive index and viscosity of the buffers were applied during data treatment, which are listed in Table 3.5. All three micelle dispersions remained monomodal with narrow dispersity after being diluted with

PBS or Opti-MEM, although R_h was slightly larger than those being diluted with DI water. Quantitative analysis using cumulant expansion over 5–7 angles indicated that the difference of R_h in PBS, Opti-MEM from that in water was less than 10% (Table 3.6). Bimodal size distributions were observed in the micelle dispersions diluted with DMEM supplemented with 10% FBS and 100% FBS. It should be noted that the DMEM supplemented with 10% FBS and 100% FBS media themselves also exhibited bimodal distributions in DLS as shown in Table 3.6. The large particles with a R_h of 18 nm in 100% FBS from double-exponential analysis overlapped with the polymeric micelles, such as those from PG(3-24-0.16) after a 1:5 (v/v) dilution into DI water with a R_h of 19.1 nm. Therefore, data treatment of $g_1(t)$ using the double-exponential expansion cannot completely deconvolute the micelles from the serum proteins. Instead, the static scattering intensity (I_s) was used as the key parameter to monitor the micelle-protein interactions, since I_s is proportional to the mass-average molar mass (M_m) of the suspended particles ($I_s \sim KcM_m$, in which K is the prefactor depending on the setup of optics and c is the mass concentration in g L^{-1}). If any association of micelles happened (without considering sedimentation), I_s would increase in proportion to M_m. 5% decrease of I_s were observed in the three micelle dispersions diluted with 100% FBS over 14 h (Figure 3.18). This decrease was likely to come from the 100% FBS medium itself, whose intensity also decreased ca. 5% over 14 h (Figure 3.18). Moreover, no apparent change was observed in the REPES distribution profile of the three micelle dispersions in 100% FBS as well as the 100% FBS itself between t = 1 h and 14 h, as shown in Figure 3.19. These results indicated that the adsorption of serum proteins onto the glucose-

functionalized micelles, along with micelles with just PDMA or PEO corona, was insignificant over the course of 14 h.

Table 3.5 Literature values of refractive index (*n*) and viscosity (η) of water and four biologically-relevant media at 25 °C.

Media	**Water**[60]	**PBS**[60]	**Opti-MEM**[61, 62]	**DMEM + 10% FBS**[63, 64]	**100% FBS**[a]
n	1.332	1.334	1.333	1.3356	n.f.
η (cP)	0.890	0.911	0.935	0.940	n.f.

[a] The literature values of refractive index (*n*) and viscosity (η) of 100% FBS at 25 °C were not found (n.f.). The values of DMEM + 10 % FBS were used to approximate those of 100% FBS.

Table 3.6 DLS results of the aggregates from PA(3-21) and PO(3-25) diblock copolymers and PG(3-24-0.16) terpolymer in water after 1:5 (v/v) dilutions with five different media.

Sample[a]	DI water[b]	PBS[b]	Opti-MEM[b]	DMEM + 10% FBS[c]	100% FBS[c]
PG(3-24-0.16)	19.1 (0.082)	21.3 (0.069)	21.3 (0.072)	23.4 (0.687) 5.55 (0.132)	20.8 (0.476) 3.80 (0.243)
PA(3-21)	15.9 (0.073)	17.6 (0.074)	18.0 (0.067)	20.7 (0.690) 5.68 (0.133)	19.5 (0.487) 3.72 (0.234)
PO(3-25)	22.8 (0.030)	23.2 (0.045)	22.1 (0.168)	22.9 (0.635) 4.49 (0.145)	19.0 (0.485) 3.73 (0.251)
Buffers only	N.A.	N.A.	N.A.	15.0 (0.531) 3.68 (0.297)	18.0 (0.495) 3.53 (0.234)

[a] 0.75 wt % dispersions of PG(3-24-0.16), PA(3-21), and PO(3-25) in water prepared by nanoprecipitation. All R_h values were calculated using the literature values of viscosity and refractive index of the medium utilized as listed in Table 3.5. [b] R_h and μ_2/Γ^2 from fitting $g_1(t)$ using the cumulant expansion, the latter of which are enclosed in parentheses. R_h were determined by linear regressions of Γ vs q^2 over 5–7 angles in the range of 30–120°. The μ_2/Γ^2 values are obtained at 90°. [c] R_h and the scattering amplitudes from fitting $g_1(t)$ using the double-exponential expansion, the latter of which are enclosed in parentheses. R_h are determined by linear regressions of Γ vs q^2 over 5–7 angles in the range of 30–120°. The reported scattering amplitude values are at 90°.

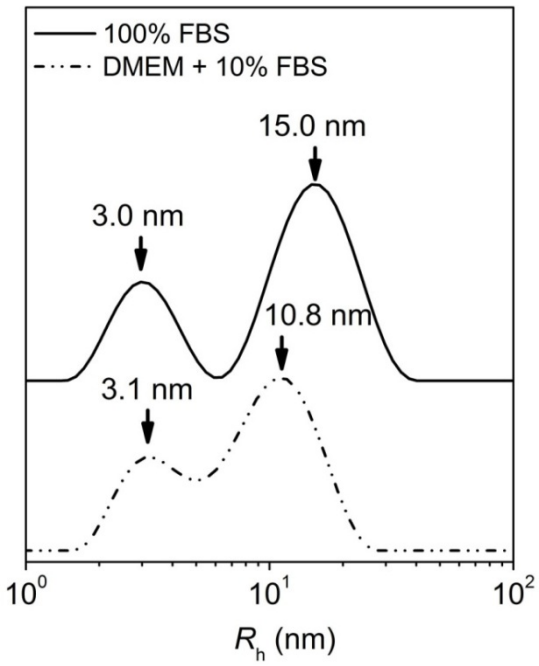

Figure 3.17 Apparent micelle size distributions of DMEM + 10% FBS and 100% FBS (buffers only) at 25 °C. The scattering angle is 90°.

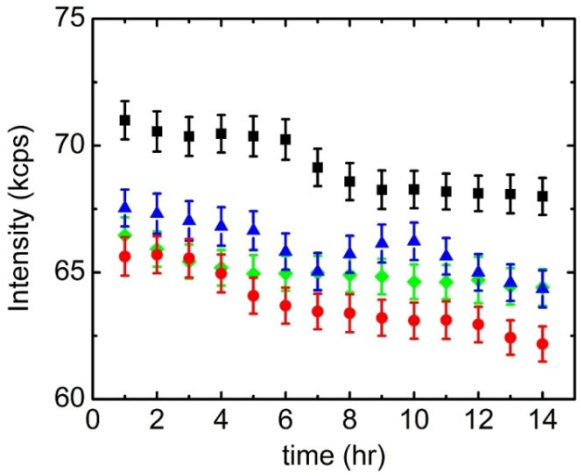

Figure 3.18 The static scattering intensity of 100% FBS (black squares), and 1:5 (v/v) dilutions with 100% FBS of 0.75 wt % dispersions in water of PG(3-24-0.16) (green diamonds), PA(3-21) (blue triangles), and PO(3-25) (red circles) over 14 h at 25 °C. The scattering angle is 90°.

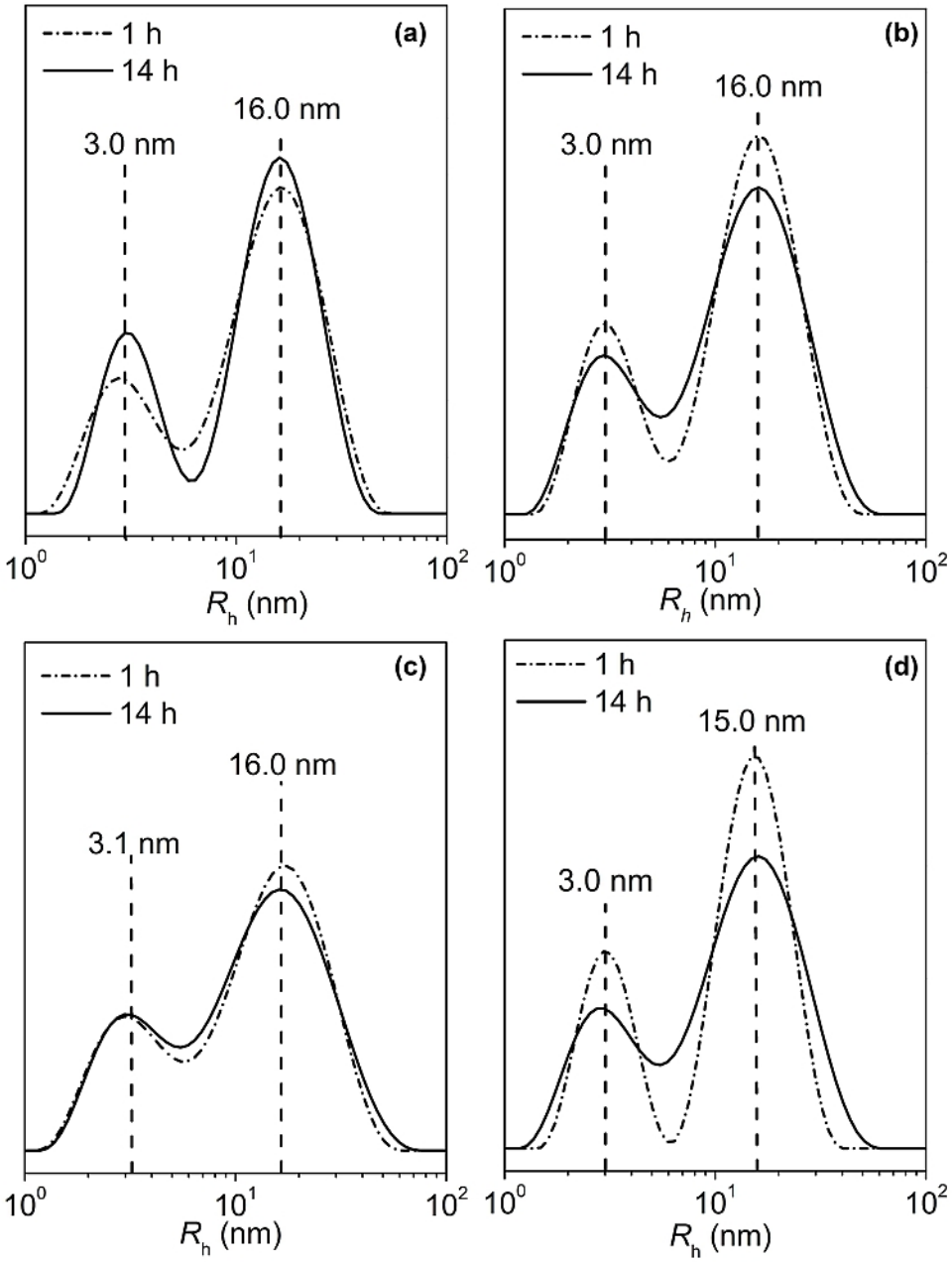

Figure 3.19 Apparent micelle size distributions of 1:5 (v/v) dilutions with 100% FBS of 0.75 wt % dispersions in water of (a) PG(3-24-0.16), (b) PA(3-21), and (c) PO(3-25), as well as (d) 100% FBS only. The measurement was carried out after the samples were mixed and kept at 25 °C for 1 h and 14 h, respectively.

The stability of the micelles with glucose-functionalized coronae after dilution with 100% FBS was further investigated by cryo-TEM. Figure 3.20 shows a representative cryo-TEM image of 100% FBS without polymeric micelles. Spherical particles with radii of 3 ± 1 nm were the predominant morphology, which corresponded to the suspended serum proteins such as globulins and albumin. On the other hand, no large particles with radii of ca. 18 nm were observed. This result was qualitatively consistent with our DLS analysis using Shibayama's multimodal treatment,[58] from which the weight fractions of the particles with R_h of 3 and 18 nm were determined to be 98.8 wt % and 1.2 wt %, respectively. After the micelle dispersions of PG(3-24-0.16) were diluted with 100% FBS, spherical micelles with radii of ca. 7 nm were observed as well as globular proteins with radii of ca. 3 nm (Figure 3.20b). The spherical micelles were well dispersed in the matrix, and no large aggregations were observed from all of the four grids examined. The combined DLS and cryo-TEM results led us to conclude that the micelles with glucose-functionalized coronae have excellent stability in 100% FBS. As an nonionic polymer, poly(DMA-*grad*-MAG) not only provides sufficient steric "stealth" effect to prevent the exposure of the extremely hydrophobic PEP cores, but also has minimal interactions with the serum proteins.

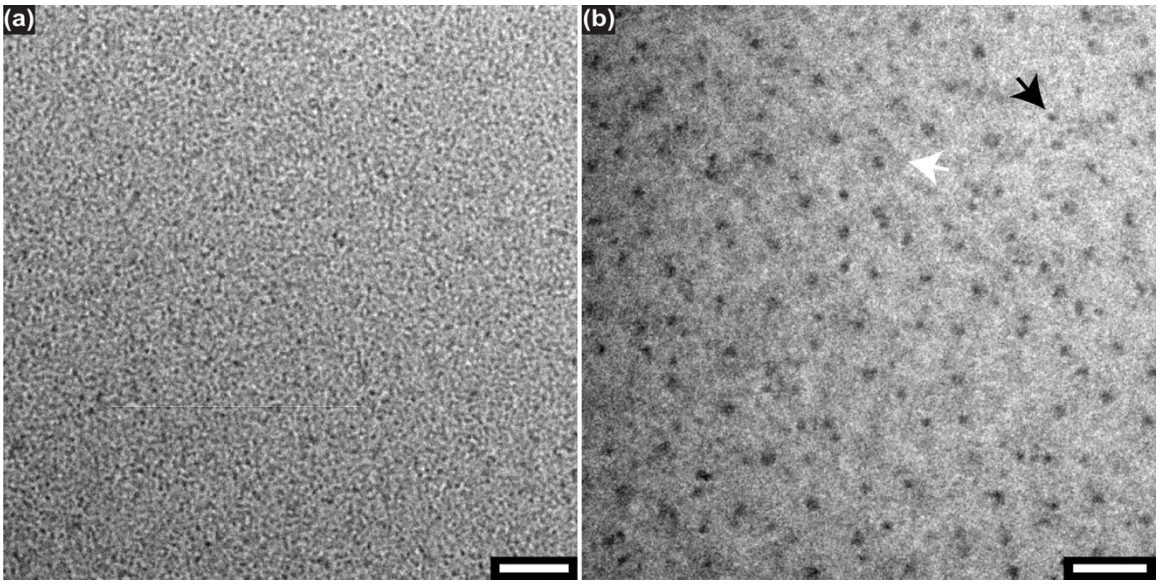

Figure 3.20 Representative cryo-TEM images of (a) 100% FBS only, and (b) a 0.75 wt % PG(3-24-0.16) dispersion in water after 1:5 (v/v) dilution in 100% FBS. The white arrow in (b) highlights the grey halo around a micelle core, indicating the micelle corona. The black arrow in (b) points to a globular protein particle. The scale bars indicate 100 and 50 nm in (a) and (b), respectively.

3.3 Conclusions

We have synthesized glucose-containing PEP–poly(DMA-*grad*-MAG) diblock terpolymers, investigated the resulting self-assembled micelles in water, and tested the stability of the micelles in four different biologically-relevant media. A combination of anionic and RAFT polymerizations afforded samples with precisely-defined structures, and the hydrophilic poly(meth)acrylamide blocks were inferred to be gradient copolymers based on the difference in reactivity ratios as determined in free-radical polymerizations. Incorporating glucose moieties greatly increased the polarity difference between the hydrophobic PEP and hydrophilic poly(meth)acrylamide components of the PG diblock terpolymers, which largely affected the processing method toward the self-assembled aggregates in water. For samples with relatively small MAG content (MAG mol % < 20% in the hydrophilic block), nanoprecipitation coupled with dialysis afforded micelle dispersions with monomodal size distributions and narrow dispersity. Spherical micelles with core radii of ca. 7 nm and overall hydrodynamic radii of ca. 15 nm were the predominant morphologies in all samples examined. On the other hand, a good solvent mixture was not able to be found for the sample with the highest MAG content (MAG mol % = 39% of the hydrophilic block), which necessitated the sample preparation by direct dissolution. The large particles in these samples as indicated by DLS were inter-micelle aggregates as revealed by cryo-TEM, and the formation was thought to be related with the high T_g of the hydrophilic block. Interestingly, the electron-dense MAG moieties greatly increased the native contrast of the micelle coronae, which were clearly viewed as grey halos around the micelle cores in cryo-TEM without any staining. Finally, the

stability of the glucose-installed micelles was tested in four different biologically relevant media by a combination of DLS and cryo-TEM, and micelle dispersions from a PG diblock terpolymer with 16 mol % of MAG in the hydrophilic block were stable in 100% FBS over at least 14 h, suggesting minimal interaction of sugar-functionalized coronae with serum proteins. Control experiments suggested that micelles composed of PDMA or PEO alone in the corona were also stable in 100% FBS. Therefore, these sugar-installed micelles have great potential as *in vivo* drug delivery vehicles with prolonged circulation time after intravenous injection.

3.4 Experimental Section

Materials. All chemicals were reagent grade and used as received unless otherwise noted. *sec*-Butyllithium (1.4 M in cyclohexane, Aldrich), oxalyl chloride (Aldrich, 99+%), 1,4-dioxane (Aldrich, anhydrous, 99.8%), methanol (Sigma-Aldrich, anhydrous, 99.8%), *n*-butyl amine (Sigma-Aldrich, 99.5%), tris(2-carboxyethyl)phosphine hydrochloride (TCEP, Aldrich, powder), Dulbecco's Phosphate-Buffered Saline (DPBS, Invitrogen), Opti-MEM Reduced Serum Medium (no phenol red, Invitrogen), Dulbecco's Modified Eagle Medium (DMEM, high glucose, no glutamine, no phenol red, Invitrogen), and 100% Fetal Bovine Serum (FBS, heat inactivated, Invitrogen) were used as received. 1,3-Isoprene (Aldrich, 99%) was degassed with three freeze-pump-thaw cycles followed by removing trace amounts of acidic impurities by multiple treatments with *n*-butyllithium (2.5 M in hexanes, Aldrich) for 1 h each. Ethylene oxide (Aldrich, 99.5+%) was degassed with three freeze-pump-thaw cycles followed by removing trace amounts of acidic impurities by multiple treatments with *n*-butylmagnesium chloride (2.0 M in diethyl ether, Aldrich) for 4 h each. 2,2'-Azobis(2-methylpropionitrile) (AIBN, Aldrich, 98%) was recrystallized from methanol twice and stored in a dark, –30 °C refrigerator before use. A radical addition-fragmentation transfer (RAFT) chain transfer agent (CTA) bearing carboxylic acid group, *S*-1-dodecyl-*S*'-(α,α'-dimethyl-α"-acetic acid)trithiocarbonate, was synthesized following reported procedure.[41] *N*,*N*-Dimethylacrylamide (DMA) (Aldrich, 99+%), 2-hydroxyethyl acrylate (HEA, Aldrich, 96%), and methyl acrylate (MA, Aldrich, 99%) were purified by passing through activated basic alumina columns to remove the trace amounts of inhibitors. Hydrochloric

acid (Sigma-Aldrich, 37%) was diluted with DI water to a concentration of 1.3 M before use. Cyclohexane (Sigma-Aldrich, 99+%), toluene (Sigma-Aldrich, HPLC grade, 99.9+%), and dichloromethane (Sigma-Aldrich, anhydrous, 99.8+%) were purified via a home-built solvent purification system equipped with two columns packed with activated alumina and a supported copper catalyst.[65] Tetrahydrofuran (THF, Sigma-Aldrich, HPLC grade, 99.9+%, inhibitor free) was purified by passing through two columns packed with activated alumina and molecular sieves.[65]

Synthesis of poly(ethylene-*alt*-propylene)–poly(DMA-*grad*-MAG) (PG) diblock terpolymers. Hydroxyl-terminated poly(ethylene-*alt*-propylene) (PEP-OH) was synthesized via anionic polymerization of isoprene followed by catalytic hydrogenation following established procedures.[66] Briefly, isoprene (35.4 g, 5.19×10^{-1} mol) was initiated by *sec*-butyllithium (9.10 mL of 1.30 M solution in cyclohexane, 1.18×10^{-2} mol) and anionically polymerized in 1.0 L of dry cyclohexane at 40 °C, after which ethylene oxide (24.2 g, 5.50×10^{-1} mol) was added to afford an ω-hydroxyl-terminated polyisoprene (PI-OH). The solvent and residual monomers were removed under vacuum. Conversion: 99%, M_n (^{1}H NMR, end-group analysis): 3.0 kg·mol^{-1}, 4,1-addition (^{1}H NMR): 91%, $Đ$ (SEC, chloroform, relative to PS standards): 1.05. Next, a solution of PI-OH in cyclohexane (ca. 10 wt %) was charged into a high-pressure reactor along with Pt/SiO_2 catalyst (ca. 1:10 PI-OH by mass), and reacted with 500 psi H_2 at 80 °C for 12 h. The catalyst was filtered off by passing the solution through a membrane with a pore size of 0.45 μm, and the solvent was removed under vacuum. Conversion (^{1}H NMR): > 99%, M_n (^{1}H NMR): 3.1 kg·mol^{-1}, $Đ$ (GPC, chloroform): 1.05. After removing the solvent,

PEP-OH (6.0 g, 1.9×10^{-3} mol) was dissolved in ca. 20 mL of dichloromethane and the flask was charged with a trithiocarbonate CTA[41] (2.09 g, 5.74×10^{-3} mol) that was pretreated with oxalyl chloride (1.70 mL, 1.95×10^{-2} mol). The reaction was carried out in a dry Argon atmosphere at 23 °C, and the product (PEP-CTA) was purified by precipitating five times from dichloromethane at 23 °C into methanol that was cooled by a dry ice/isopropanol bath. Conversion (^{1}H NMR): > 99%, M_n (^{1}H NMR): 3.6 kg·mol^{-1}, $Đ$ (GPC, chloroform): 1.08.

PG diblock terpolymers were made by RAFT copolymerizations of DMA and TMS-MAG with the PEP-CTA as the macromolecular chain transfer agent followed by acid-catalyzed hydrolysis, which was mostly done in the one-pot manner. The solvent in was a 1:1 (v/v) mixture of toluene and 1,4-dioxane, the temperature was 70 °C, and the radicals were supplied by AIBN. The total concentrations of the two monomers were 1.1–2.5 M, and the compositions of the monomers in the feed are listed in Table 3.1. Using PG(3-24-0.16) as an example, AIBN (0.46 mg, 2.8×10^{-6} mol), PEP-CTA (0.22 g, 6.1×10^{-5} mol), DMA (0.92 mL, 8.9×10^{-3} mol), and TMS-MAG (1.20 g, 2.25×10^{-3} mol) were dissolved in toluene/dioxane (1:1, v/v) to make a homogeneous solution with a total volume of 8.0 mL. The ratio of the reagent concentrations in the feed, $[AIBN]_0$:$[PEP\text{-}CTA]_0$:$[DMA]_0$:$[TMS\text{-}MAG]_0$, was 0.05:1:176.6:43.4, and the total concentration of DMA and TMS-MAG was 1.40 M. The mixture was then transferred into a 20-mL Shlenk tube, degassed via three freeze-pump-thaw cycles, and sealed under vacuum before being placed into a preheated oil bath at 70 °C. The mixture was allowed to react for 18 h before the reaction was quenched by placing the tube into liquid nitrogen

and opening to air. Conversion of DMA (^{1}H NMR): 91.9%, conversion of TMS-MAG (^{1}H NMR): 69.4%, M_n (^{1}H NMR): 35.4 kg·mol^{-1}, M_n (GPC): 24.7 kg·mol^{-1}, $Đ$ (GPC, chloroform): 1.29. After this, the solvent was removed and the mixture was redissolved in ca. 20 mL of dry THF/methanol (5:1, v/v), supplemented with 0.5 mL of 1.3 M HCl aqueous solution, and allowed to stir at 23 °C for 2 min. The solvent was then removed under vacuum and the solid product was washed with the same dry THF/Methanol (5:1, v/v) mixture twice more. PG(3-24-0.16) was isolated as light yellow powder by two precipitations from THF at 23 °C into pentane that was cooled by an acetone/dry ice bath. Hydrolysis (^{1}H NMR): > 99%. Total yield: 0.97 g, 68%.

The removal of the trithiocarbonate CTA fragment at the ω-terminus of PG diblock terpolymers was carried out via an aminolysis/Michael addition sequence following published procedures.[36] Using PG(3-24-0.16) as an example, PG(3-24-0.16) (0.91 g, 3.41×10^{-5} mol) was dissolved in a 6.0-mL mixture of chloroform/methanol (2:1, v/v) and degassed by Argon bubbling for 30 min. Then the flask was also charged with *n*-butyl amine (75 μL, 7.49×10^{-4} mol) and tris(2-carboxyethyl)phosphine hydrochloride (TCEP, 10.7 mg, 3.75×10^{-5} mol). The mixture was stirred at 23 °C for 24 h, after which the original bright yellow solution became almost colorless, but slightly pale yellow. Next, an α,β-unsaturated ester of 50-fold molar excess with respect to the trithiocarbonate moiety was added and the reaction mixture was stirred at 23 °C for another 24 h. MA was used for the modification of PG(3-39-0.21), and HEA was used for the rest of samples. The product of the reaction was isolated by precipitating three times

from THF into ice-cold mixtures of pentane/diethyl ether (1:1, v/v). Conversion (UV-vis): > 95%, and yield: 0.47 g, 52%.

PA(3-21) was synthesized in a very similar way to the PG diblock terpolymers except no TMS-MAG was included in the RAFT polymerization and thus no removal of TMS was needed.

The reactivity ratios of DMA and TMS-MAG in free-radical polymerizations. Thirteen free-radical polymerizations of DMA (as monomer 1) and TMS-MAG (as monomer 2) were carried out with the mole fraction of DMA in the feed in the range between 0.10 and 0.90, and the detailed information is as listed in Table 3.3. The temperature was 70 °C, the initiator was AIBN, and the solvent was a 1:1 (v/v) mixture of toluene and 1,4-dioxane, the same conditions as those in the RAFT synthesis of PG diblock terpolymers. Taking Run 6 as an example, a 2-mL ampule was charged with 0.12 mg of AIBN (7.5×10^{-7} mol), 38.5 μL of DMA (3.74×10^{-4} mol), 0.200 g of TMS-MAG (3.74×10^{-4} mol), and 0.50 mL of 1:1 (v/v) mixture of toluene and 1,4-dioxane along with a stir bar to form a homogeneous mixture. The ampule was then degassed by three freeze-pump-thaw cycles, sealed under vacuum, and placed into a preheated oil bath at 70 °C. The temperature was estimated to equilibrate over the ampule within less than 30 s. An aliquot of the starting solution was taken for ^{1}H NMR analysis to determine the mole fraction of DMA in the feed (f_1). After 15 min, the reaction was quenched as the ampule was placed into liquid nitrogen, warmed to 23 °C, and opened to air. An aliquot of the reaction mixture was taken for ^{1}H NMR analysis to determine the conversion of the two monomers. Calculations were made by comparing the integration

of two vinyl protons between δ = 6.6–6.3 ppm of DMA and that of three protons (H_1, H_8, and H_{10}, Figure 3.21) of TMS-MAG between 15 min and 0 min in reference to the TMS protons in TMS-MAG (36 H, H_{11}, Figure 3.21). The mole fraction of DMA in the copolymer (F_1) was calculated based on f_1 and the conversions of the two monomers. A nonlinear fit, using $F_1 = (r_1 f_1^2 + f_1 f_2)/(r_1 f_1^2 + 2 f_1 f_2 + r_2 f_2^2)$, was performed on the composition data, F_1 vs f_1. A linear treatment following Kelen-Tudos method[46] was carried out following published procedures.[67] The symmetry parameter, α, was 0.354 for the thirteen experimental runs as listed in Table 3.3.

Molecular characterization. ^{1}H NMR spectra were recorded on a Varian INOVA 500 or a Varian INOVA 300 spectrometer at 22 °C with $CDCl_3$ as the solvent unless otherwise specified. A mixture of THF-d_8 and methanol-d_4 was used for PG diblock terpolymers with MAG mol % higher than 10% of the poly(meth)acrylamide block. SEC measurement was carried out on a Hewlett-Packard 1100 series liquid chromatograph, which houses three Jordi polydivinylbenzene columns with pore sizes of 10000, 1000, and 500 Å, respectively. Chloroform was the mobile phase, which was run at a rate of 1.0 mL min^{-1} at 35 °C. The eluents were monitored by a Hewlett-Packard 1047A refractive index detector. A 10-point calibration curve was made using PS standards from Polymer Laboratories Inc.

The preparation of micelle dispersions. Direct dissolution (DD): dry diblock terpolymer samples were directly mixed with DI water at a concentration of 1.0 wt %, and allowed to stir in a closed vial at 60 °C for 2 weeks. Nanoprecipitation (NP): dry diblock copolymer or terpolymer samples were dissolved in THF or THF/methanol

mixtures at a concentration of 5.0 wt %, and methanol was added at 0.1 mL min^{-1} via a syringe pump to a final 1:3 (v/v) mixture of THF and methanol. Next, the sample was transferred into a dialysis bag with MWCO of 10 kg mol^{-1} and dialyzed against DI water (ca. 1:200, v/v), which was replaced for at least 4 times over 2 days. Micelles started to form PG(3-24-0.16) when the THF/methanol mixture reached a composition of ca. 15:4 (v/v) as revealed DLS.

Cryo-TEM imaging. Samples for cryo-TEM imaging were prepared using a Vitrobot Mark IV (FEI). An aliquot of the micelle dispersion (3.0 μL) was loaded onto a lacey support film coated with carbon (Ted Pella, Inc.), in which the size of the holes varied from ca. 0.25 μm to >10 μm. The grid was held by a pair of tweezers in a chamber with controlled water vapor saturation levels (95 or 100%) at 22 °C. Excess solution was blotted away using a piece of filter paper to form thin films (ca. 100–300 nm thick) spanning the holes, and then the grid was quickly plunged into liquid ethane (at ca. −183 °C) that was cooled by boiling liquid nitrogen. The vitrified sample was then stored in liquid nitrogen until being transferred into a Gatan 626 cryogenic sample holder for imaging. No staining was applied during sample preparation. The vitrified grids were imaged in a FEI Tecnai G^2 Spirit BioTWIN TEM at ca. −178 °C, and an accelerating voltage of 120 kV was applied onto a LaB_6 emitter. Images were acquired on an Eagle™ 2k CCD camera (up to 4 mega pixels), and analyzed with the FEI TEM Imaging and Analysis (TIA) software. Phase contrast was enhanced by imaging at 8–12 μm underfocus. The aqueous dispersion was vitrified ca. 1 h after the micelle dispersion of PG(3-24-0.16) was diluted with 100% FBS.

Dynamic light scattering (DLS). All samples were passed through syringe filters with a pore size of 0.20 μm before being loaded into dust-free glass tubes unless otherwise noted. The 1.0 wt % dispersion of PG(3-26-0.39) in water was centrifuged for 15 min under 3000×g to remove suspended particles larger than ca. 1 μm. Samples for serum-stability studies were prepared by diluting 0.15 mL of micelle dispersions in DI water (at a concentration of polymer in water of ca. 0.75 wt %) with 0.75 mL of the corresponding media and vigorously mixing on a Vortex-Genie 2 (Scientific Industries). The diluted samples were passed through syringe filters with a pore size of 0.20 μm, and then the measurement was carried out once per hour for 14 h without any further filtration. A decalin bath was used as the RI-matching matrix, and the temperature was controlled at 25.0 ± 0.3 °C. A Mini L-30 Laser (Brookhaven Instruments) provided the irradiating red laser source (λ = 637 nm), and the transient scattering intensity was detected by a BI-APD avalanche photo diode detector and processed with a BI-9000AT digital correlator. The optics was aligned on a BI-200SM goniometer. The second-order scattering intensity correlation functions, $g_2(t)$, were measured at 5–9 different scattering angles between 30° and 150°, and converted into the first-order correlation functions, $g_1(t)$, using the Siegert relation, $g_2(t) = 1 + |g_1(t)|^2$. The data treatment is similar to those of PE micelles as described in Chapter 2. Literature values of refractive index (n) and viscosity of the specific media at 25 °C were used for samples in the four biologically-relevant media, and the values are listed in Table 3.5.

Differential scanning calorimetry (DSC). Samples of known mass (ca. 5 mg) were encapsulated in hermetically-sealed Tzero aluminum pans and analyzed on a

Discovery DSC (TA Instruments). Temperature was ramped between 20 and 200 °C at a rate of 10 °C min^{-1}. The 2nd heating scans are reported. T_g values were determined using the TA TRIOS software version 2.2.

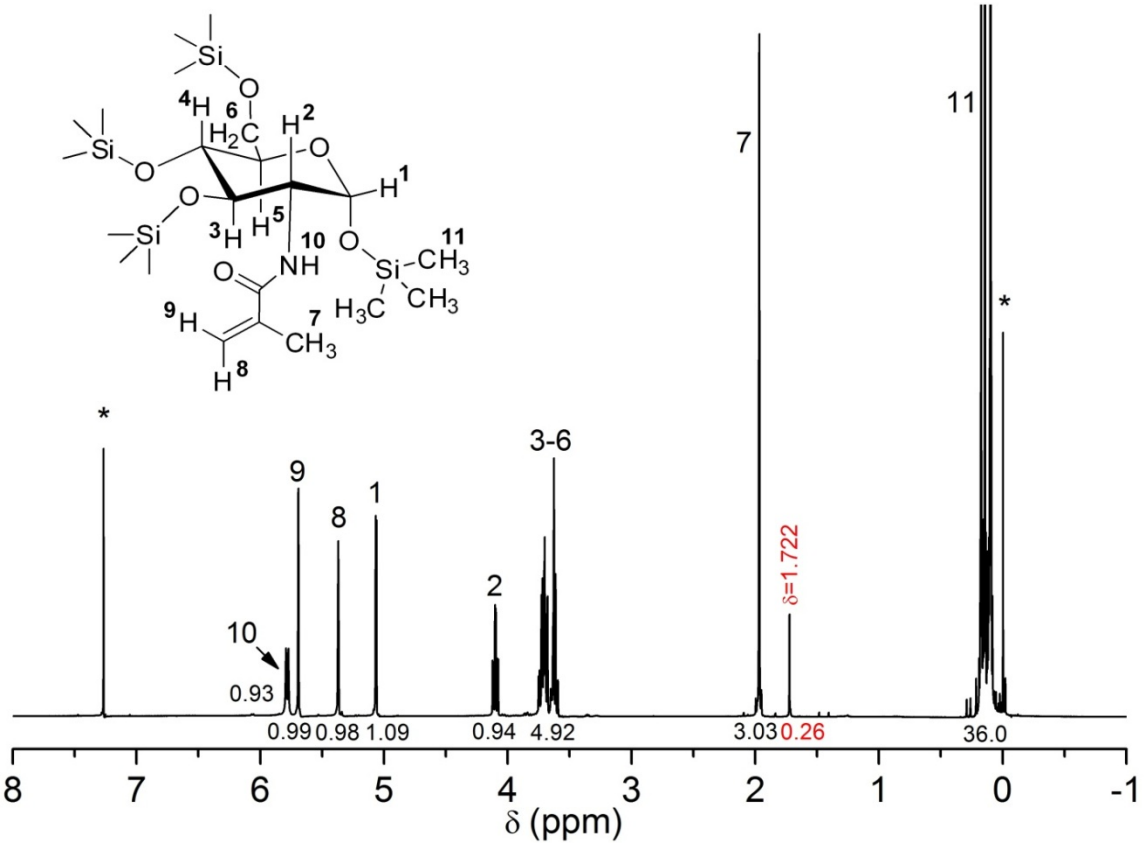

Figure 3.21 ^{1}H NMR spectrum of the TMS-MAG monomer in $CDCl_3$ at 23 °C. The values below each peak are the integration relative to the trimethylsilyl protons of 36H at 0.20–0.05 ppm. An unassigned peak at 1.722 ppm is highlighted in red. "*" signs denote the residual $CHCl_3$ peak at 7.26 ppm and tetramethylsilane standard at 0.00 ppm.

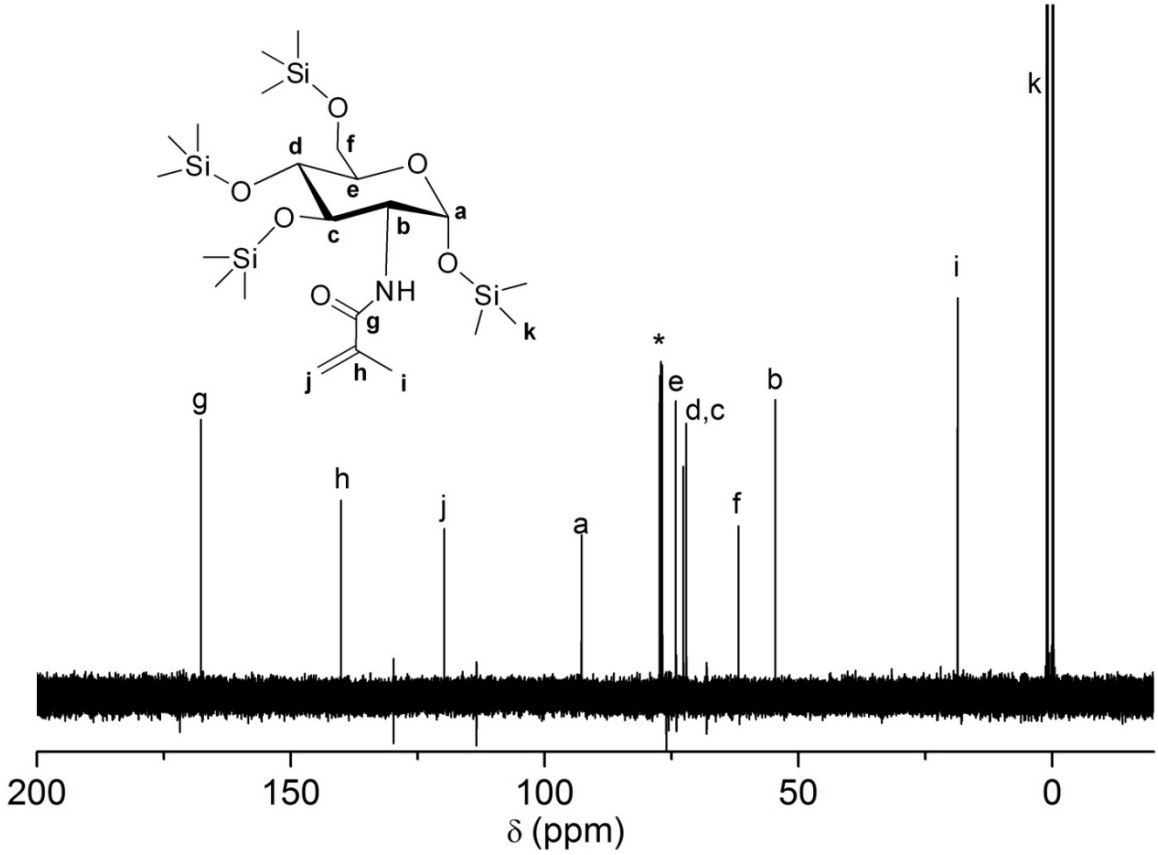

Figure 3.22 ^{13}C NMR spectrum of the TMS-MAG monomer in $CDCl_3$ at 22 °C. The "*" sign denotes the residual $CHCl_3$ peak at 77.07–77.01 ppm.

3.5 References

1. Duncan, R. *Nat. Rev. Drug Discovery* **2003,** 2, (5), 347-360.

2. Gaucher, G.; Dufresne, M. H.; Sant, V. P.; Kang, N.; Maysinger, D.; Leroux, J. C. *J. Controlled Release* **2005,** 109, (1-3), 169-188.

3. Tong, R.; Cheng, J. J. *Polym. Rev.* **2007,** 47, (3), 345-381.

4. Blanco, E.; Hsiao, A.; Mann, A. P.; Landry, M. G.; Meric-Bernstam, F.; Ferrari, M. *Cancer Science* **2011,** 102, (7), 1247-1252.

5. Moghimi, S. M.; Patel, H. M. *Adv. Drug Delivery Rev.* **1998,** 32, (1-2), 45-60.

6. Langer, R. *Nature* **1998,** 392, (6679), 5-10.

7. Knop, K.; Hoogenboom, R.; Fischer, D.; Schubert, U. S. *Angew. Chem., Int. Ed.* **2010,** 49, (36), 6288-6308.

8. Ishihara, T.; Maeda, T.; Sakamoto, H.; Takasaki, N.; Shigyo, M.; Ishida, T.; Kiwada, H.; Mizushima, Y.; Mizushima, T. *Biomacromolecules* **2010,** 11, (10), 2700-2706.

9. Cheng, J.; Teply, B. A.; Sherifi, I.; Sung, J.; Luther, G.; Gu, F. X.; Levy-Nissenbaum, E.; Radovic-Moreno, A. F.; Langer, R.; Farokhzad, O. C. *Biomaterials* **2007,** 28, (5), 869-876.

10. Petersen, M. A.; Yin, L.; Kokkoli, E.; Hillmyer, M. A. *Polym. Chem.* **2010,** 1, (8), 1281-1290.

11. Barz, M.; Luxenhofer, R.; Zentel, R.; Vicent, M. J. *Polym. Chem.* **2011,** 2, (9), 1900-1918.

12. Pearson, S.; Chen, G. J.; Stenzel, M., Synthesis of glycopolymers. In *Engineered carbohydrate-based materials for biomedical applications: polymers, surfaces, dendrimers, nanoparticles, and hydrogels*, Narain, R., Ed. John Wiley & Sons, Inc.: Hoboken, New Jersey, 2011; pp 1-118.

13. Okada, M. *Prog. Polym. Sci.* **2001,** 26, (1), 67-104.

14. Varma, A. J.; Kennedy, J. F.; Galgali, P. *Carbohydr. Polym.* **2004,** 56, (4), 429-445.

15. Ladmiral, V.; Melia, E.; Haddleton, D. M. *Eur. Polym. J.* **2004,** 40, (3), 431-449.

16. Ting, S. R. S.; Chen, G. J.; Stenzel, M. H. *Polym. Chem.* **2010,** 1, (9), 1392-1412.

17. Cairo, C. W.; Gestwicki, J. E.; Kanai, M.; Kiessling, L. L. *J. Am. Chem. Soc.* **2002,** 124, (8), 1615-1619.

18. Bernard, J.; Hao, X. J.; Davis, T. P.; Barner-Kowollik, C.; Stenzel, M. H. *Biomacromolecules* **2006,** 7, (1), 232-238.

19. Pearson, S.; Allen, N.; Stenzel, M. H. *J. Polym. Sci., Part A: Polym. Chem.* **2009,** 47, (6), 1706-1723.

20. Smith, A. E.; Sizovs, A.; Grandinetti, G.; Xue, L.; Reineke, T. M. *Biomacromolecules* **2011,** 12, (8), 3015-3022.

21. Ting, S. R. S.; Min, E. H.; Escale, P.; Save, M.; Billon, L.; Stenzel, M. H. *Macromolecules* **2009,** 42, (24), 9422-9434.

22. Ting, S. R. S.; Granville, A. M.; Quemener, D.; Davis, T. P.; Stenzel, M. H.; Barner-Kowollik, C. *Aust. J. Chem.* **2007,** 60, (6), 405-409.

23. Dong, C. M.; Chaikof, E. L. *Colloid. Polym. Sci.* **2005,** 283, (12), 1366-1370.

24. Dong, C. M.; Faucher, K. M.; Chaikof, E. L. *J. Polym. Sci., Part A: Polym. Chem.* **2004,** 42, (22), 5754-5765.

25. Dai, X. H.; Dong, C. M.; Yan, D. Y. *J. Phys. Chem. B* **2008,** 112, (12), 3644-3652.

26. Dai, X. H.; Dong, C. M. *J. Polym. Sci., Part A: Polym. Chem.* **2008,** 46, (3), 817-829.

27. Liu, L.; Zhang, J. C.; Lv, W. H.; Luo, Y.; Wang, X. J. *J. Polym. Sci., Part A: Polym. Chem.* **2010,** 48, (15), 3350-3361.

28. Munoz-Bonilla, A.; Heuts, J. P. A.; Fernandez-Garcia, M. *Soft Matter* **2011,** 7, (6), 2493-2499.

29. Suriano, F.; Coulembier, O.; Dubois, P. *J. Polym. Sci., Part A: Polym. Chem.* **2010,** 48, (15), 3271-3280.

30. Hetzer, M.; Chen, G. J.; Barner-Kowollik, C.; Stenzel, M. H. *Macromol. Biosci.* **2010,** 10, (2), 119-126.

31. Ohno, K.; Tsujii, Y.; Miyamoto, T.; Fukuda, T.; Goto, M.; Kobayashi, K.; Akaike, T. *Macromolecules* **1998,** 31, (4), 1064-1069.

32. Albertin, L.; Kohlert, C.; Stenzel, M.; Foster, L. J. R.; Davis, T. P. *Biomacromolecules* **2004,** 5, (2), 255-260.

33. Fraser, C.; Grubbs, R. H. *Macromolecules* **1995,** 28, (21), 7248-7255.

34. Chen, G. J.; Amajjahe, S.; Stenzel, M. H. *Chem. Commun.* **2009**, (10), 1198-1200.

35. Kumar, J.; Bousquet, A.; Stenzel, M. H. *Macromol. Rapid Commun.* **2011,** 32, (20), 1620-1626.

36. Qiu, X. P.; Winnik, F. M. *Macromol. Rapid Commun.* **2006,** 27, (19), 1648-1653.

37. Ruiz, C. C., *Sugar-based surfactants: fundamentals and applications*. CRC Press: Boca Raton, FL, 2009; Vol. 143.

38. Liu, J. B.; Zeng, F. Q.; Allen, C. *J. Controlled Release* **2005,** 103, (2), 481-497.

39. Liu, J. B.; Xiao, Y. H.; Allen, C. *J. Pharm. Sci.* **2004,** 93, (1), 132-143.

40. Yin, L.; Dalsin, M. C.; Sizovs, A.; Reineke, T. M.; Hillmyer, M. A. *Macromolecules* **2012,** 45, (10), 4322-4332.

41. Lai, J. T.; Filla, D.; Shea, R. *Macromolecules* **2002,** 35, (18), 6754-6756.

42. Moad, G.; Rizzardo, E.; Thang, S. H. *Aust. J. Chem.* **2005,** 58, (6), 379-410.

43. Zhou, C.; Hillmyer, M. A.; Lodge, T. P. *Macromolecules* **2011,** 44, (6), 1635-1641.

44. Chang, C. W.; Bays, E.; Tao, L.; Alconcel, S. N. S.; Maynard, H. D. *Chem. Commun.* **2009**, (24), 3580-3582.

45. Odian, G., *Principles of Polymerization*. 4th ed.; John Wiley & Sons, Inc.: Hoboken, New Jersey, 2004.

46. Kelen, T.; Tudos, F. *J. Macromol. Sci. Chem.* **1975,** A 9, (1), 1-27.

47. Zhang, L. F.; Eisenberg, A. *J. Am. Chem. Soc.* **1996,** 118, (13), 3168-3181.

48. Gohy, J.-F. *Adv. Polym. Sci.* **2005,** 190, (Block Copolymers II), 65-136.

49. Garnier, S.; Laschewsky, A. *Langmuir* **2006,** 22, (9), 4044-4053.

50. Hayward, R. C.; Pochan, D. J. *Macromolecules* **2010,** 43, (8), 3577-3584.

51. Nicolai, T.; Colombani, O.; Chassenieux, C. *Soft Matter* **2010,** 6, (14), 3111-3118.

52. Snyder, L. R.; Kirkland, J. J., Solvents. In *Introduction to modern liquid chromatography*, John Wiley & Sons: New York, 1979; pp 246-268.

53. Won, Y.-Y.; Brannan, A. K.; Davis, H. T.; Bates, F. S. *J. Phys. Chem. B* **2002,** 106, (13), 3354-3364.

54. Li, Z. B.; Kesselman, E.; Talmon, Y.; Hillmyer, M. A.; Lodge, T. P. *Science* **2004,** 306, (5693), 98-101.

55. Burkhardt, M.; Ruppel, M.; Tea, S.; Drechsler, M.; Schweins, R.; Pergushov, D. V.; Gradzielski, M.; Zezin, A. B.; Muller, A. H. E. *Langmuir* **2008,** 24, (5), 1769-1777.

56. Zana, R.; Kaler, E. W., *Giant Micelles: Properties and Applications*. 1st ed.; CRC Press: Boca Raton, FL, 2007.

57. Won, Y.-Y.; Davis, H. T.; Bates, F. S.; Agamalian, M.; Wignall, G. D. *J. Phys. Chem. B* **2000,** 104, (30), 7134-7143.

58. Shibayama, M.; Karino, T.; Okabe, S. *Polymer* **2006,** 47, (18), 6446-6456.

59. Devine, D. V.; Marjan, J. M. J. *Crit. Rev. Ther. Drug* **1997,** 14, (2), 105-131.

60. Hackley and Clogston, NIST - NCL Joint Assay Protocol PCC-1, 2007.

61. Hsu, C. Y. M.; Hendzel, M.; Uludag, H. *J. Gene Med.* **2011,** 13, (1), 46-59.

62. Rejman, J.; Tavernier, G.; Bavarsad, N.; Demeester, J.; De Smedt, S. C. *J. Controlled Release* **2010,** 147, (3), 385-391.

63. Kato, H.; Suzuki, M.; Fujita, K.; Horie, M.; Endoh, S.; Yoshida, Y.; Iwahashi, H.; Takahashi, K.; Nakamura, A.; Kinugasa, S. *Toxicol. in Vitro* **2009,** 23, (5), 927-934.

64. Reese, B. E.; Barnett, R. E.; Alaoui-Ismaili, M.; Habibi, E.; Mann, C. J. In *Quantitative analysis of living cells by digital holographic microscopy*, Biomedical Science & Engineering Conference, 2009. BSEC 2009. First Annual ORNL, 18-19 March, 2009; 2009; pp 1-4.

65. Pangborn, A. B.; Giardello, M. A.; Grubbs, R. H.; Rosen, R. K.; Timmers, F. J. *Organometallics* **1996,** 15, (5), 1518-20.

66. Hillmyer, M. A.; Bates, F. S. *Macromolecules* **1996,** 29, (22), 6994-7002.

67. Kress, A. O.; Mathias, L. J.; Cei, G. *Macromolecules* **1989,** 22, (2), 537-546.

4 Hydroxypropyl Methylcellulose Esters of Substituted Succinates as Matrices in Amorphous Solid Dispersions for Enhancing the *in vitro* Solubility of Phenytoin

4.1 Introduction

One of the biggest challenges in the pharmaceutical field is related with improving the aqueous solubility of active pharmaceutical ingredients (APIs). Currently, more than 40% of the drugs under development are estimated to suffer from insufficient solubility in water,[1] and the percentage has been continuously increasing.[2, 3] Such low aqueous solubility results in poor bioavailability of the drugs by oral administration, and thus a significant loss of therapeutic and economic opportunities. Efforts to address this problem include salt formation,[4] prodrugs,[5, 6] self-emulsifying drug delivery systems,[7-9] complexation with cyclodextrin,[10-12] nanosuspensions[13-15] and amorphous solid dispersions.[16-20] Among them, spray-dried dispersions (SDDs) have gained much interest as an effective and versatile form of amorphous solid dispersions.[21-23] Due to rapid drying, crystalline hydrophobic drugs are effectively rendered amorphous and further stabilized within the matrix of choice (often a polymer). Compared to the crystalline form, amorphous drugs have higher free energy and thus are more apt to dissolve in water. Besides, the drugs have extremely high surface area thus promoting rapid dissolution as they are molecularly dispersed within the matrices.[17] In addition, many

poorly water-soluble drugs are readily soluble in common organic solvents, and thus spray drying is suitable for drugs within a wide range of physicochemical properties.[20] Therefore, SDDs hold great promise in improving the aqueous solubility and oral bioavailability of crystalline hydrophobic drugs.

The matrix material of an SDD is critical in determining its bulk and solution performance. To date, numerous reports have shown that a cellulose ether ester, hydroxypropyl methylcellulose acetate succinate (HPMCAS), is more effective than many other candidates including synthetic homopolymers such as poly(ethylene glycol) (PEG) and poly(vinylpyrrolidone) (PVP) along with other cellulose derivatives such as hydroxypropyl methylcellulose (HPMC) and hydroxylpropyl methylcellulose phthalate (HPMCP).[20, 24-32] Specifically, SDDs with HPMCAS as matrices exhibit strong resistance against the moisture-induced crystallization of the dispersed amorphous drugs during storage, which favors extended shelf-life even under high relative humidity conditions.[20, 27] Moreover, HPMCAS is very effective at both achieving high levels of supersaturation and further inhibiting the recrystallization of dissolved drugs in solution, which can significantly enhance the delivery efficacy in gastrointestinal (GI) tract.[20, 24-26, 28-32]

The outstanding performance of HPMCAS as the matrices in SDDs is largely attributed to its multi-functional structure.[20, 26, 32] HPMCAS is a cellulose derivatives of two ethers, methoxy (MeO) and hydroxypropoxy (HPO), and two esters, acetate (Ac) and succinate (Su). The hydrophobic acetate groups are thought to facilitate the molecular dispersions of the hydrophobic drugs within the polymeric matrix in the bulk, and the small amount of unreacted hydrophilic hydroxyls allow sufficient hydration of the

resulting SDDs for drug release in solution. In addition, the carboxylic acids from the succinate groups are at least partially ionized at intestinal pH (~7). These negative charges provide excellent colloidal stability of polymer-drug nanostructures in solution, which are important in preventing the "desupersaturation" of the dissolved drugs.[20] On the other hand, the multifunctional nature also means many variables in defining the structure. Besides the factors in the cellulose backbone such as the molar mass and dispersity, each substituent adds an additional set of parameters in defining the structure including the identity of substituents, composition, and regiochemistry. While most of commercialized cellulosics have one or two substituents, HPMCAS has four. Therefore, efforts to understand and optimize HPMCAS are made difficult due to the low precision in the composition control and unclear definition of the molecular structure.

Modifying HPMC with a substituted succinic anhydride is a simple and effective method of synthesizing cellulose derivatives that simultaneously contain hydrophobic, hydrophilic, and pH-responsive functionalities. Such anhydrides allow reducing the number of derivatizing reagents while not sacrificing any functionality. Besides, the composition of the hydrophobic and pH-responsive moieties in the resulting materials is naturally fixed to be 1:1. Moreover, these two groups are precisely connected to each other through covalent linkages rather than being statistically distributed along the cellulose backbone, and thus result in better defined structures for HPMC esters of substituted succinates (HPMC-(R-SA)) than HPMCAS. A few examples of starch[33-38] and cellulose[39-45] derivatives of substituted succinates have been reported. In early patent literature, Caldwell and Wurzburg claimed the synthesis of polysaccharide derivatives of

substituted succinates, in which the substituent was an alkyl or aromatic group of C5–18.[33] Later, Kalbe et al. used non-aqueous systems to derivatize cellulose, which allowed cellulose esters with high degrees of substitution.[41] However, mostly long-chain alkenylsuccinic anhydrides such as 2-octen-1-ylsuccinic anhydride (C8) and 2-dodecen-1-ylsuccinic anhydride (C12) were employed in most cases.[33-45] Moreover, such modified polysaccharides were mainly targeting applications other than pharmaceutical formulations such as emulsifiers and viscosity modifiers,[33, 34, 36, 38, 39, 44] paper coating,[34, 41, 42] dialysis membranes,[40] biodegradable molded parts and films,[37, 41-43] and composites.[45]

In this chapter, the synthesis of HPMC esters using a variety of monosubstituted succinic anhydrides and their efficacy as the matrices of SDDs are demonstrated. Antiepileptic phenytoin was chosen as the model drug, which has a low aqueous solubility of 27.1 μg/mL.[46] The calculated logarithm of the partition coefficient between octanol and water (*c* log *P*), which measures the lipophilicity of a compound, is moderately high at 1.9.[46] Phenytoin has a high melting temperature (T_m) of 296 °C that indicates strong intermolecular interactions within crystals that can prevent the effective hydration of phenytoin in water.[47] SDDs with different matrices are comprehensively characterized in bulk and in aqueous media, and the structure–property relationships are established. Several of these new materials showed more effective *in vitro* supersaturation enhancement for phenytoin than HPMCAS.

4.2 Results

4.2.1 Synthesis and Molecular Characterization

Similar to the synthesis of HPMCAS, HPMC was the starting material, sodium acetate was the catalyst, and glacial acetic acid was the solvent towards synthesizing the HPMC esters of substituted succinates, or HPMC-(R-SA). Five monosubstituted succinic anhydrides were used to prepare HPMC esters, as shown in Scheme 4.1. Phenylsuccinic anhydride (Ph-SA) is commercially available, cyclohexylsuccinic anhydride (Cy-SA) was synthesized by dehydrating the dicarboxylic acid precursor (Scheme 4.2), and the three α-sulfur-substituted anhydrides (Cy-S-SA, Ph-S-SA, and Bn-S-SA) were synthesized using a one-step conjugate addition of a thiol to maliec anhydride (Scheme 4.3).[48]

Scheme 4.1 Synthesis of HPMC esters of substituted succinates, or HPMC-(R-SA). The structures of HPMC and HPMC-(R-SA) do not reflect the actual regiochemistry; the methyl, 2-hydroxypropyl, and substituted succinic groups are statistically distributed along the backbone.

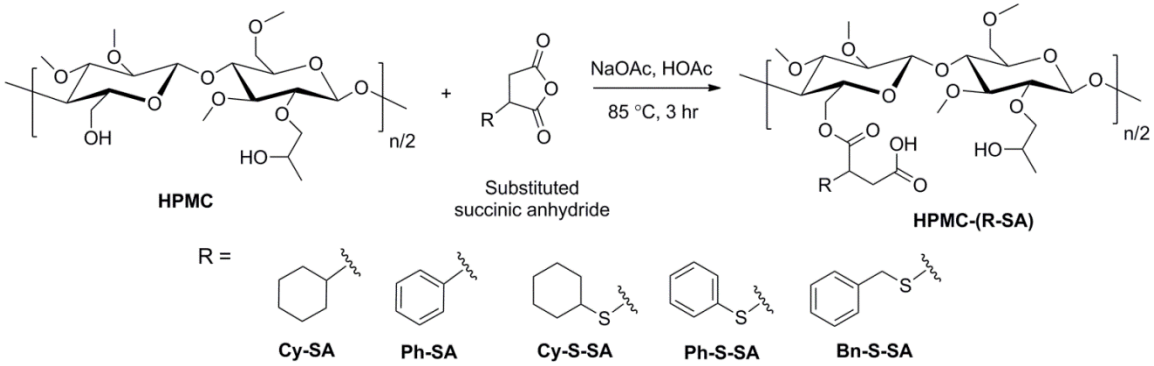

Scheme 4.2 Synthesis of cyclohexylsuccinic anhydride via dehydrating cyclohexyl-succinic acid.

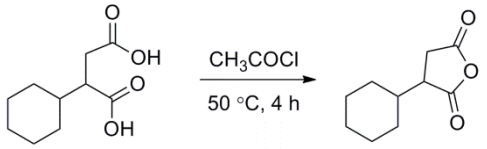

Scheme 4.3 Synthesis of substituted succinic anhydrides via thiol-ene chemistry.

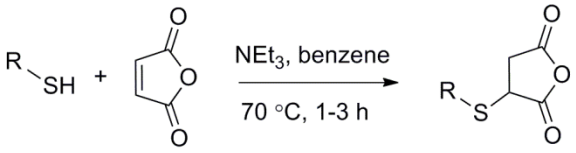

R: cyclohexyl, phenyl, and benzyl.

The anhydrides exhibited different levels of reactivity in the esterification with alcohols. As discussed by Zienty and coworkers, thiolated succinic anhydrides are more susceptible to hydrolysis than succinic and alkenylsuccinic anhydrides due to the electron-withdrawing effect of the thioether at the α-position.[48] To quantify the kinetics, model reactions of several anhydrides were examined with isopropyl alcohol, a secondary alcohol, as catalyzed by sodium acetate at 80 °C (Scheme 4.4). The concentrations of the anhydride and isopropyl alcohol in the feed were kept as 1:1, and the concentration of sodium acetate was kept constant in all reactions. Conversion was monitored by ^{1}H NMR spectroscopy. The apparent rate constants (k_{app}) were extracted as the slopes in Figure 4.1 based on Equations 4.1–4.3. The esterification of succinic anhydride with isopropyl alcohol was rather slow and characterized by a k_{app} of 1.5×10^{-2} M^{-1} min^{-1}. As an electron-withdrawing phenyl group existed at the α-position, Ph-SA showed ca. 4-fold enhancement as 7.1×10^{-2} M^{-1} min^{-1}. Thiolated succinic anhydrides were even more

reactive towards isopropyl alcohol, and k_{app} of Bn-S-SA and Ph-S-SA were ca. 40 (5.8×10^{-1} M^{-1} min^{-1}) and 60 times (9.4×10^{-1} M^{-1} min^{-1}) as large as that of succinic anhydride, respectively. Although the substituents in the α-position provided extra steric hindrance against the attacking of the electron-rich hydroxyls, these results suggest that the electron-withdrawing effect of aryl and arylthio groups prevailed and rendered the anhydrides more reactive in alcoholysis than the "bare" succinic anhydride. In addition, *S*-substituted succinic anhydrides showed higher reactivity than non-thiolated ones.

Scheme 4.4 Model reactions of substituted succinic anhydrides with isopropanol for determining the relative reactivity of anhydrides.

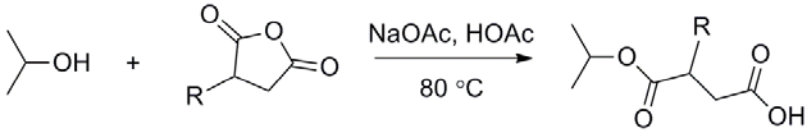

R = H: $[IPA]_0 = [anhydride]_0 = 0.2$ M, $[NaOAc] = 0.4$ M
R = phenyl, phenylthio, or benzylthio: $[IPA]_0 = [anhydride]_0 = 0.1$ M, $[NaOAc] = 0.4$ M

$$-\frac{d[anhydride]_t}{dt} = k \cdot [IPA]_t \cdot [anhydride]_t \cdot [NaOAc] \quad (4.1)$$

$$-\frac{d[anhydride]_t}{dt} = k_{app} \cdot [anhydride]_t^{\,2} \quad (4.2)$$

$$\frac{1}{[anhydride]_t} - \frac{1}{[anhydride]_0} = k_{app} \cdot t \quad (4.3)$$

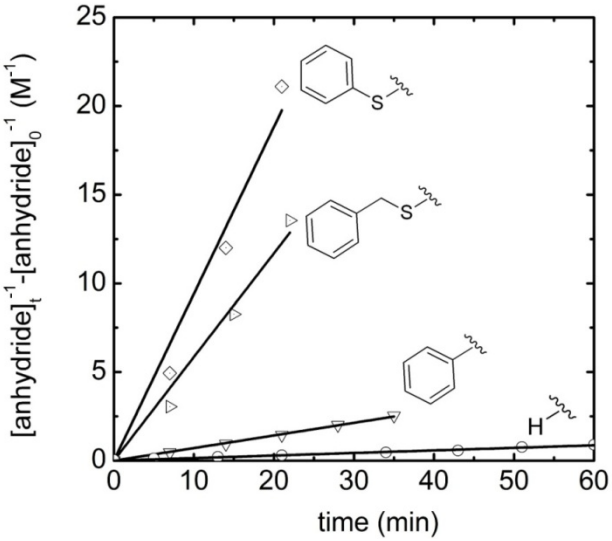

Figure 4.1 Kinetic plots for determining the apparent rate constants of the coupling reactions between isopropanol and succinic anhydride (SA), Ph-SA, Bn-S-SA, and Ph-S-SA at 80 °C.

From one HPMC,[49] five HPMC-(R-SA) were synthesized with different substituents but similar degrees of substitution (DS) of ~0.6. The ratio of the anhydride to hydroxyls in the feed was adjusted based on the reactivity of the anhydrides while the rest of the parameters (e.g., the concentration of hydroxyls, the amount of sodium acetate) were kept the same. Besides, three other HPMC cyclohexylthiosuccinates with varying DS in the range of 0.4–1.0 were also prepared to study the effect of DS. The molecular and thermal data of HPMC and the obtained HPMC-(R-SA) samples are summarized in Table 4.1. The mass-average molar mass (M_m) of the HPMC was 15.7 kg mol^{-1} and the dispersity ($Đ$) was 1.33 as revealed by an aqueous SEC equipped with light scattering (LS) and differential refractive index (dRI) detectors (Figure 4.2). HPMC with rather low molar masses were used to target HPMC esters with low viscosity in organic solvents, which were beneficial in controlling particle sizes during spray drying.[22] The DS of MeO

and HPO per anhydro glucopyranose unit (AGU) was 1.91 and 0.25, respectively. Correspondingly, the average number of hydroxyls per AGU available for subsequent esterification was 1.09, which included both unsubstituted backbone hydroxyls and those on HPO groups. The DS of the HPMC-(R-SA) was determined by ^{1}H NMR spectroscopy (Figure 4.3). The HPMC esters of substituted succinates are named as HPMC followed by the hydrophobic substituent of the anhydride and DS. For example, HPMC-CyS-0.57 stands for HPMC cyclohexylthiosuccinate with a DS of 0.57. These HPMC-(R-SA) showed monomodal elution curves by SEC in THF as exemplified by HPMC-Ph-0.63 and HPMC-CyS-0.57 (Figure 4.4), from which M_m were determined to be 25–33 kg mol^{-1} and $Đ$ were 1.4–1.6. In addition, an AFFINISOL™ (trademark of The Dow Chemical Company) HPMCAS 912 G was used as a reference material for comparison. The DS of MeO, HPO, Ac, and Su of the HPMCAS were 1.94, 0.25, 0.57, and 0.28, respectively. Correspondingly, the average number of the unreacted hydroxyls per AGU unit is 0.21. All of the HPMC esters (HPMC-(R-SA) and HPMCAS) showed apparent T_g of 94–124 °C and were soluble in acetone at a concentration of 2.0 wt %, and thus were well suited for normal spray-drying conditions.

Table 4.1 Molecular and thermal characteristics of HPMC and HPMC esters

Sample	Substituents[a]	$[-OH]_0$:$[Anhydride]_0$[b]	DS[c]	M_n NMR (kg/mol)[d]	M_n SEC (kg/mol)[e]	M_m SEC (kg/mol)[e]	$Đ$ [e]	dn/dc (mL/mg)[f]	T_g (°C) [g]
HPMC			0		11.8	15.7	1.33	0.146	132
HPMC-Cy-0.57	Cy	1:3	0.57	17.8	16.9	26.2	1.56	0.085	120
HPMC-Ph-0.63	Ph	1:2	0.63	18.2	17.2	26.2	1.52	0.098	124
HPMC-CyS-0.42	CyS	1:0.7	0.42	17.0	17.9	26.0	1.45	0.092	111
HPMC-CyS-0.57	CyS	1:1	0.57	18.9	19.8	28.3	1.43	0.089	100
HPMC-CyS-0.72	CyS	1:2	0.72	20.8	21.3	30.8	1.44	0.094	94
HPMC-CyS-0.99	CyS	1:5	0.99	24.1	23.5	33.3	1.42	0.099	94
HPMC-PhS-0.62	PhS	1:1	0.62	19.3	17.9	25.3	1.41	0.129	100
HPMC-BnS-0.57	BnS	1:1	0.57	19.2	19.5	28.5	1.46	0.106	96
HPMCAS	Succinate Acetate		S: 0.28 A: 0.57						121

[a] The kind of ester substituents in HPMC esters. All samples also contained two kinds of ether substituents, HPO and MeO. [b] The ratio of the initial concentration of hydroxyls on HPMC to that of anhydride in the feed. [c] DS of the ester substituents. [d] Number-average molar mass (M_n) calculated based on the M_n of HPMC by SEC and the DS of the HPMC-(R-SA) by ^{1}H NMR spectroscopy. The cellulose backbone was assumed to undergo no degradation or cross-linking during esterification. [e] Determined by a SEC that was equipped with a LS and a *d*RI detector. [f] Determined by the *d*RI signal assuming 100% mass recovery. [g] Apparent glass transition temperatures by DSC, which are likely to be underestimated due to a small amount of degraded product at temperatures of >60 °C.

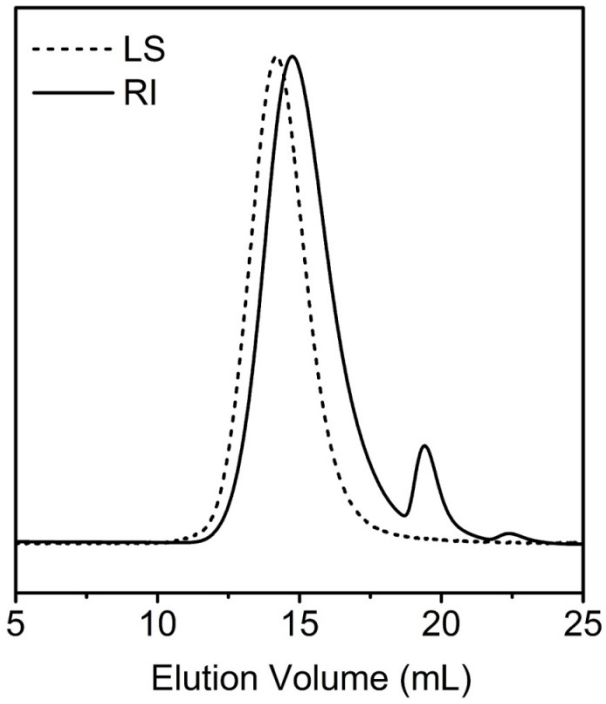

Figure 4.2 SEC traces of HPMC using a LS (at 90°) and a *d*RI detector. The mobile phase was 0.1 M Na_2SO_4 aqueous solution supplemented with 1% HOAc and the temperature was 25 °C.

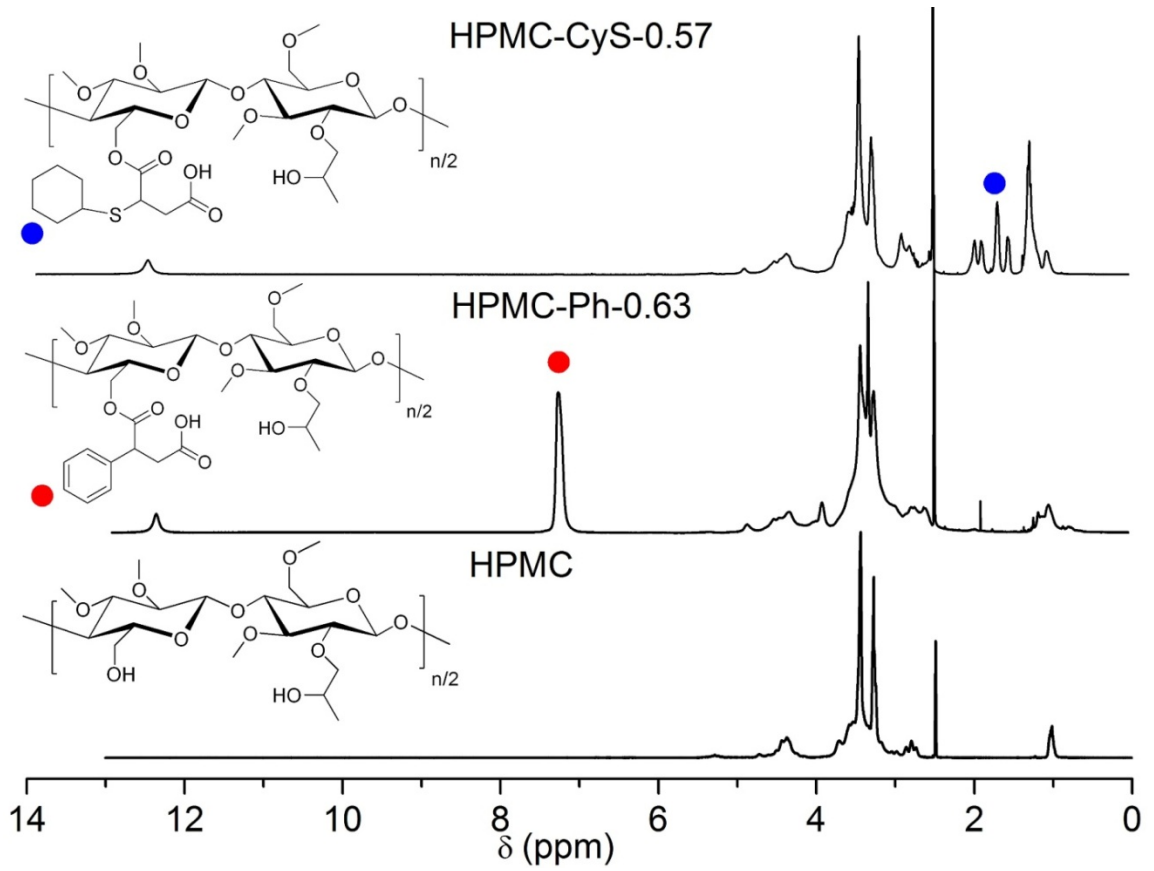

Figure 4.3 (From bottom to top) ^{1}H NMR spectra of HPMC, HPMC-Ph-0.63, and HPMC-CyS-0.57, respectively. The solvent was DMSO-d_6.

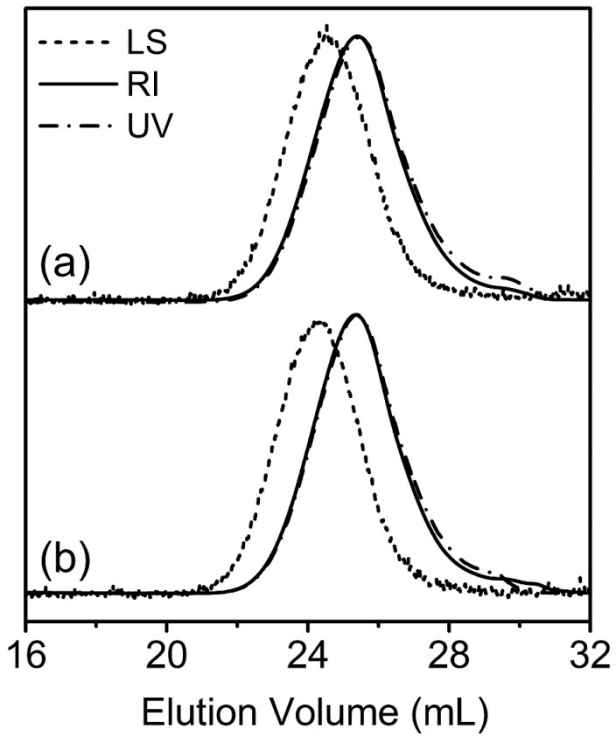

Figure 4.4 SEC traces of (a) HPMC-CyS-0.57 and (b) HPMC-Ph-0.63 using a UV-vis, a LS (at 90°), and a *d*RI detector. The mobile phase was THF and the temperature was 25 °C.

4.2.2 SDDs with Phenytoin and the Effect of Substituent

All samples were spray dried on a labscale spray dryer, and the drying parameters were kept the same to minimize the effect during processing. Initially we studied the effect of substituents and focused on HPMCAS and five HPMC-(R-SA) samples with a DS of ~ 0.6. The composition of an SDD is expressed as the weight fraction of a drug in the total solids. For example, 10 wt % drug loading corresponds to 1:9 of drug to polymer by weight in an SDD. At 10 wt % phenytoin loading, the SDDs with different polymeric matrices exhibited very similar bulk properties as revealed by scanning electron microscopy (SEM), powder X-ray diffraction (powder XRD), and differential scanning

calorimetry (DSC). The spray-dried particles looked similar to collapsed, grape-shaped particles in SEM (Figure 4.5). The size distribution was relatively broad—the largest dimension of the larger particles was ca. 1–10 μm and that of the smaller ones was ca. 20–100 nm. There were no apparent residual phenytoin crystals in the SDDs, which would exist as columnar particles with fine layered structures (Figure 4.6). Besides, the SDDs presented broad, featureless powder XRD patterns (Figure 4.7). The combined SEM and powder XRD evidence were consistent with amorphous solid dispersions containing insignificant content of crystalline phenytoin. The samples all showed a single T_g of ca. 70–85 °C during the first heating scans in DSC (Figure 4.8). The samples displayed homogeneous inner structures after the thermal treatment by SEM (Figure 4.9). These data suggested that the spray-dried particles with 10 wt % of phenytoin loading exhibited excellent thermal stability up to 180 °C without any apparent phase separation. Therefore, similar to HPMCAS, the SDDs with HPMC-(R-SA) samples provided the desired bulk properties in terms of sufficient drug loading and high T_g (i.e., 5–30 °C above common storage temperature, 40 °C[20]).

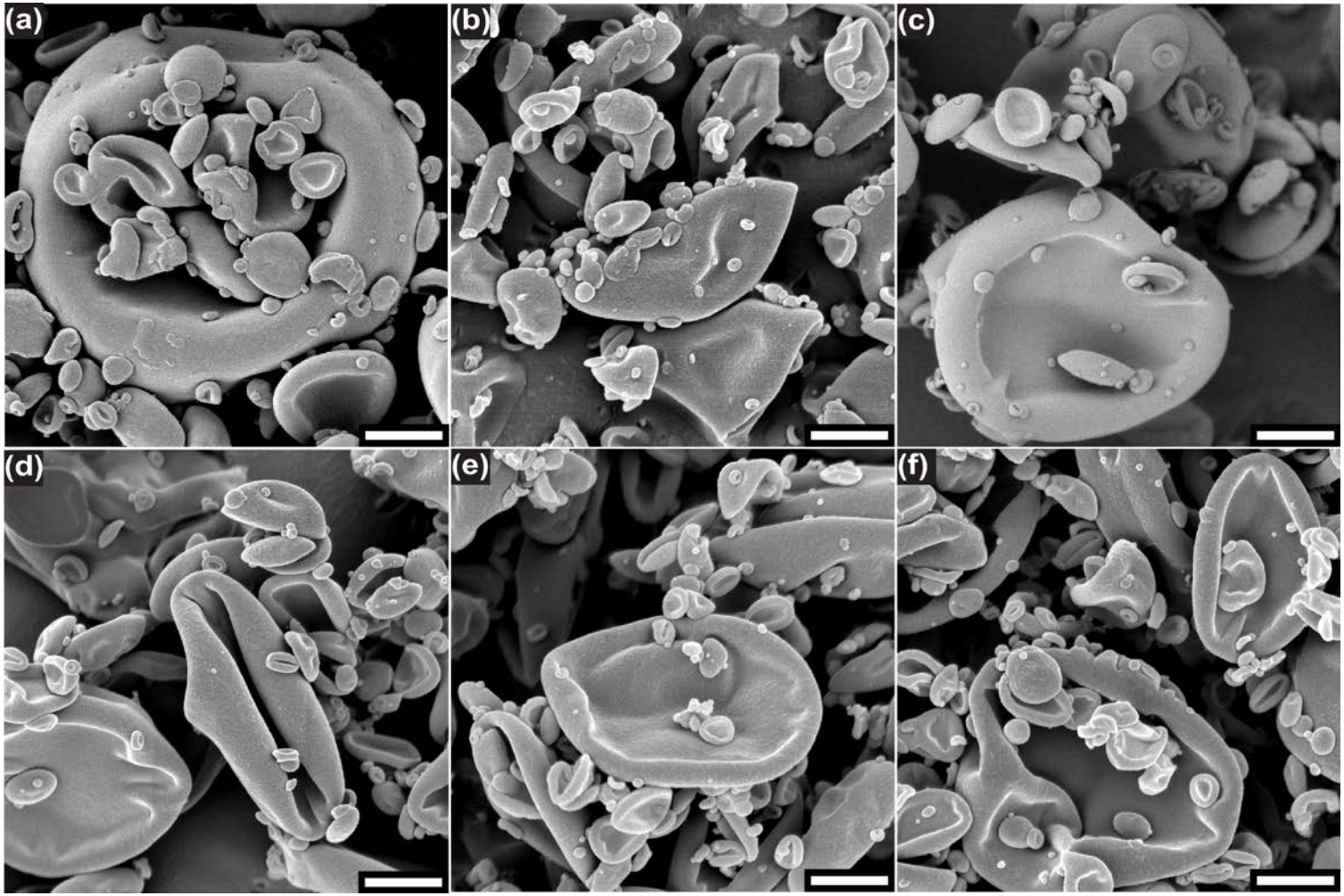

Figure 4.5 SEM pictures of SDDs of phenytoin with (a) HPMCAS, (b) HPMC-Cy-0.57, (c) HPMC-Ph-0.63, (d) HPMC-CyS-0.57, (e) HPMC-PhS-0.62, and (f) HPMC-BnS-0.57 as the matrices at 10 wt % loading. The scale bars indicate 800 nm.

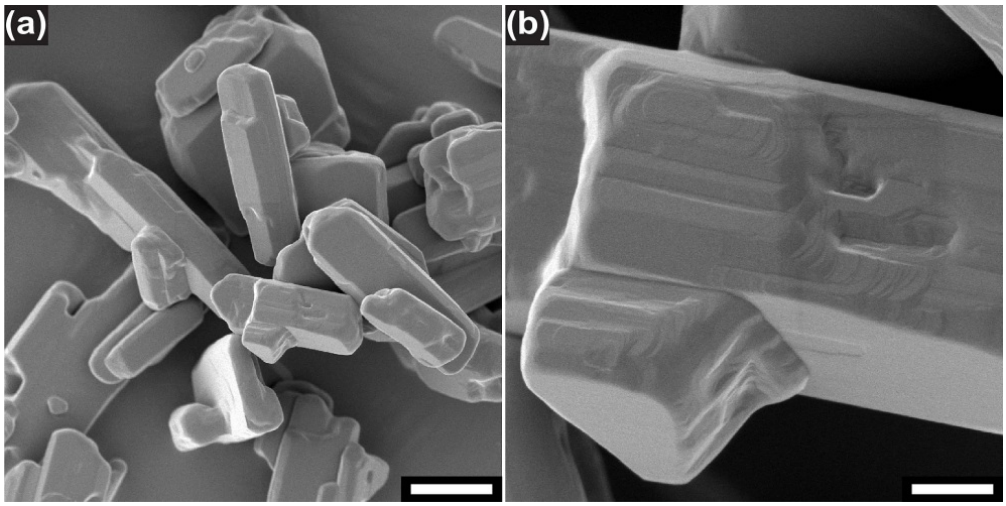

Figure 4.6 SEM pictures of crystalline phenytoin (as received). Scale bars indicate 5.0 and 1.0 μm in (a) and (b), respectively.

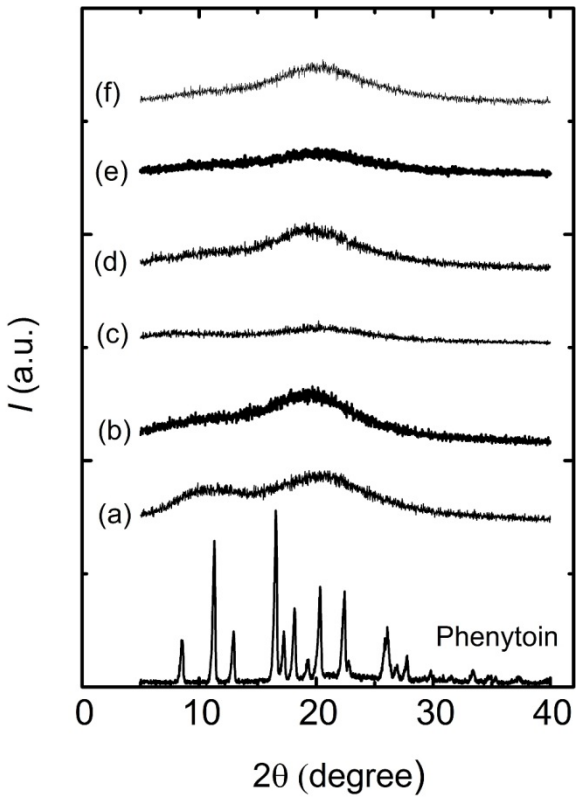

Figure 4.7 Powder XRD patterns of crystalline phenytoin and SDDs with (a) HPMCAS, (b) HPMC-Cy-0.57, (c) HPMC-Ph-0.63, (d) HPMC-CyS-0.57, (e) HPMC-PhS-0.62, and (f) HPMC-BnS-0.57 as the matrices at 10 wt % phenytoin loading.

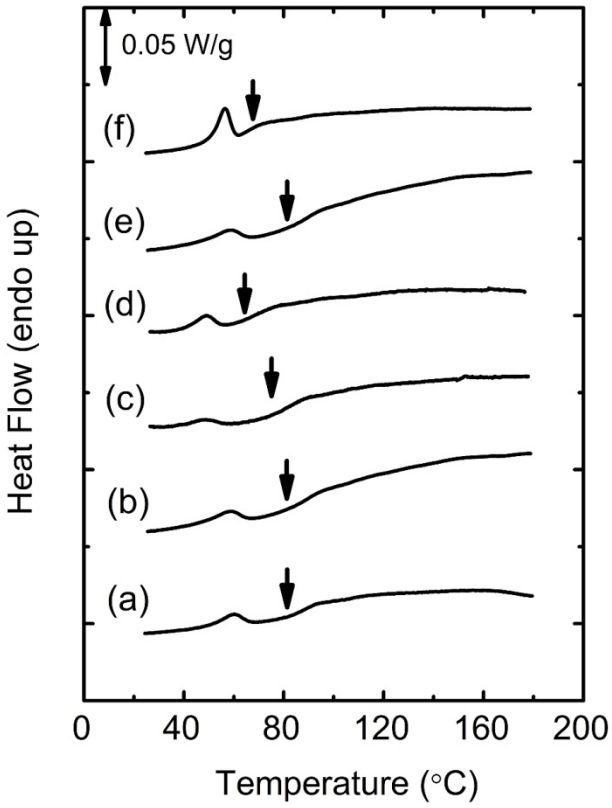

Figure 4.8 DSC curves of SDDs with (a) HPMCAS, (b) HPMC-Cy-0.57, (c) HPMC-Ph-0.63, (d) HPMC-CyS-0.57, (e) HPMC-PhS-0.62, and (f) HPMC-BnS-0.57 as the matrices at 10 wt % phenytoin loading. The temperature was increased from 22 to 180 °C at a rate of 2.5 °C min^{-1}. The arrows highlight glass transitions, and the T_gs are 82, 86, 81, 69, 75, and 68 °C for the SDDs with (a–f) as the matrices, respectively. The small endothermic peak around 55 °C in each run corresponded to evaporation residual acetone (~ 0.3 wt %) entrapped in the SDD.

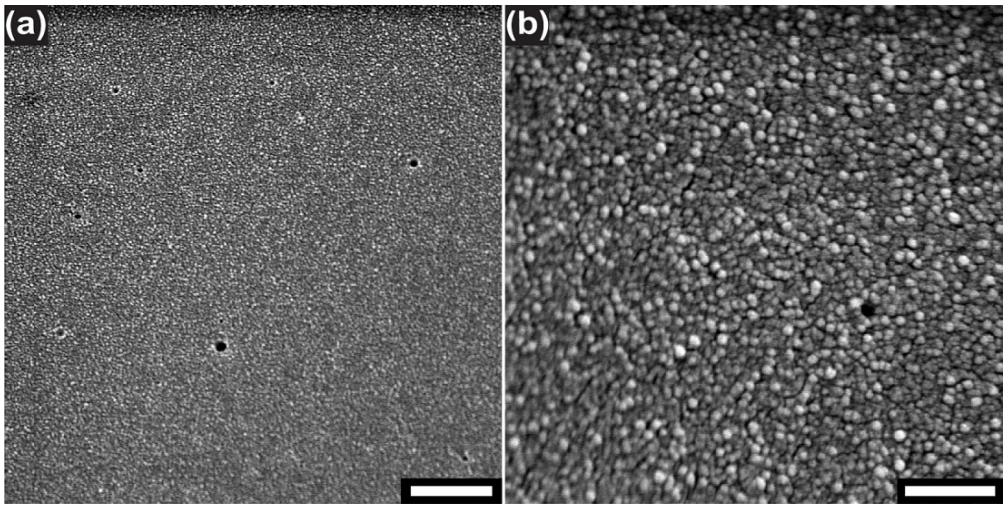

Figure 4.9 SEM pictures of SDDs of with HPMC-Ph-0.63 as the matrices at 10 wt % phenytoin loading after measurement on DSC. The sample was first heated from 22 to 180 °C, then cooled to 0 °C, and finally heated to 180 °C. The 1st heating scan was at a rate of 2.5 °C min^{-1}, and the 1st cooling and 2nd heating scans were at a rate of 10 °C min^{-1}. After this treatment, the white, powdery sample became an integrated, light yellow, transparent glassy piece, and shown are the inner sections as cut with a razor blade. The white dots of about 20 nm in diameter are likely due to surface roughness during sectioning (a 10 nm Au/Pd coating was applied to the surface). Scale bars indicate 1.5 μm and 200 nm in (a) and (b), respectively.

The performance of SDDs in solution, i.e., how well SDDs achieve and maintain the apparent supersaturation of phenytoin *in vitro*, reveals their potential to improve the bioavailability of phenytoin *in vivo*. In the dissolution tests, all undissolved phenytoin was separated from the solution using a microcentrifuge method, and the concentration of dissolved phenytoin was monitored as a function of time from 4 min to 6 h. From the dissolution profiles shown in Figure 4.10 and summarized Table 4.2, we observed three types of behavior from the SDDs:

(I) as exemplified by HPMCAS, the apparent concentration of dissolved phenytoin achieved maximum (c_{max}) initially, quickly decreased afterwards, and plateaued ($c_{360\ min}$)

at a value that was much smaller than c_{max}. In the case of HPMCAS, the c_{max} was 970 μg/mL at 4 min, which corresponded to the dissolution of almost 100% of the loaded phenytoin and a 20-fold improvement of the crystalline drug solubility alone in the aqueous buffer (48 μg/mL).[50] The total area under the concentration-vs-time curve during the 6-h test ($AUC_{360\ min}$) was 1.1×10^5 min μg/mL, which was 6.5 times as large as that of crystalline phenytoin. The SDDs with HPMC-Ph-0.63 and HPMC-PhS-0.62 as matrices exhibited similar behavior, but provided smaller c_{max}, $c_{360\ min}$, and $AUC_{360\ min}$ values than that with HPMCAS.

(II) as exemplified by HPMC-CyS-0.57, the concentration of phenytoin also achieved rather high levels of supersaturation at early time points, but it stayed constant for a significant amount of time (1.5 h) before slowly decreasing. In the case of HPMC-CyS-0.57, c_{max} was 740 μg/mL and smaller than that of HPMCAS as, but the $AUC_{360\ min}$ was 2.1×10^5 min μg/mL and two times as large as that with HPMCAS. Similar behavior was observed in the SDD with HPMC-BnS-0.57 as the matrix.

(III) as in HPMC-Cy-0.57, the concentration of phenytoin gradually increased over the course of 6 h, but the c_{max} was 250 μg/mL, 4 times as much as that of crystalline phenytoin in the aqueous buffer. Correspondingly, its $AUC_{360\ min}$ was 8.9×10^4 min μg/mL, which was smaller than the SDD with HPMCAS.

Among the three types of dissolution performance, Type I allowed attainment of high levels of initial phenytoin supersaturation, but was not very effective at maintaining it, and thus generated moderate enhancement of $AUC_{360\ min}$. Type II was very effective at not only achieving rather high levels of supersaturation, but also maintaining those

concentrations, and thus was very promising in improving the $AUC_{360\ min}$. Type III was not very promising as it did not achieve high levels of supersaturation over the course of 6 h, and thus exhibited slightly effective improvement of $AUC_{360\ min}$. Among the five HPMC-(R-SA) with similar DS but different substituents, the three sulfur-containing samples outperformed HPMCAS in terms of $AUC_{360\ min}$.

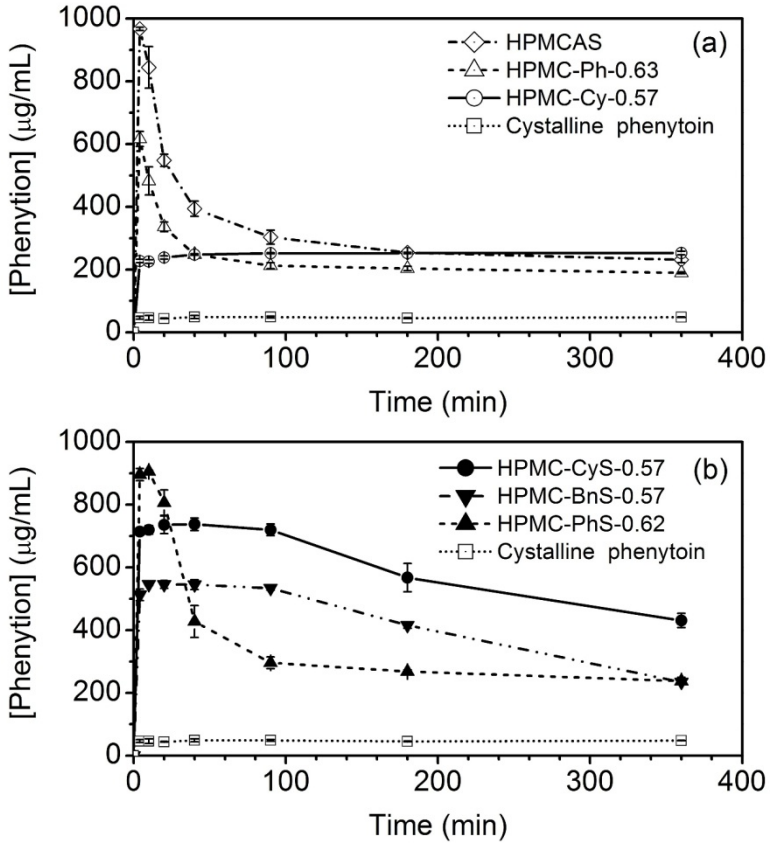

Figure 4.10 Dissolution profiles of SDDs at 10 wt % phenytoin loading. The polymeric matrices are HPMCAS and five HPMC-(R-SA) with a DS of ~0.6 but different substituted succinates. The dissolution profile of crystalline phenytoin was also included as a reference. The target concentration of phenytoin was 1000 μg/mL. The samples were run in triplicates, and the data shown are the mean ± standard deviations.

Table 4.2 Dissolution results of crystalline phenytoin and SDDs with nine polymeric matrices at 10 and 25 wt % phenytoin loadings.

Polymer	10 wt %				25 wt %			
	c_{max} (μg/mL)[a]	$c_{360\ min}$ (μg/mL)[b]	$AUC_{360\ min}$ (min μg/mL)[c]	EF[d]	c_{max} (μg/mL)[a]	$c_{360\ min}$ (μg/mL)[b]	$AUC_{360\ min}$ (min μg/mL)[c]	EF[d]
HPMCAS	970	230	1.1×10^5	6.5	460	190	7.9×10^4	4.7
HPMC-Cy-0.57	250	250	8.9×10^4	5.3	380	180	7.9×10^4	4.7
HPMC-Ph-0.63	620	190	8.0×10^4	4.8	370	130	5.8×10^4	3.5
HPMC-PhS-0.62	910	240	1.2×10^5	7.0	330	130	5.7×10^4	3.4
HPMC-BnS-0.57	550	230	1.5×10^5	8.9	450	190	8.3×10^4	5.0
HPMC-CyS-0.57	740	430	2.1×10^5	13	490	200	8.6×10^4	5.1
HPMC-CyS-0.42	890	210	1.2×10^5	7.0	620	190	8.6×10^4	5.1
HPMC-CyS-0.72	550	550	1.9×10^5	12	800	240	1.1×10^5	6.5
HPMC-CyS-0.99	410	410	1.4×10^4	8.5	700	290	1.3×10^5	7.7

[a] Maximum apparent concentration of phenytoin. [b] Apparent concentration of phenytoin at 360 min. [c] Total area under the curve during the 6-h dissolution test. [d] Enhancement factor defined as the ratio of $AUC_{360\ min}$ of a SDD to that of crystalline phenytoin. The c_{max}, $c_{360\ min}$, and $AUC_{360\ min}$ of crystalline phenytoin was 49 μg/mL, 48 μg/mL, and 1.7×10^4 min μg/mL, respectively.

4.2.3 The Effect of Degree of Substitution

HPMC cyclohexylthiosuccinates (HPMC-CyS) was further used as the model system to study the effect of DS. The DS of the four HPMC-CyS were 0.42, 0.57, 0.72, and 0.99, respectively. At 10 wt % phenytoin loading, the samples showed similar bulk properties as those described in Section 4.2.2 as revealed by SEM (Figure 4.11), powder XRD (Figure 4.12), and DSC (Figure 4.13). However, their dissolution performance exhibited significant dependence on DS (Figure 4.14 and Table 4.2). The SDD with HPMC-CyS-0.42 as the matrix showed Type I behavior, and was not effective at maintaining high levels of phenytoin supersaturation. As the DS increased to 0.72 and further 0.99, the resulting SDDs presented Type II behavior, but slightly different from HPMC-CyS-0.57, the concentrations of dissolved phenytoin remained constant over 6 h. Besides, c_{max} of these two samples were smaller than that of HPMC-CyS-0.57, which provided the highest $AUC_{360\ min}$ among the four samples with varying DS.

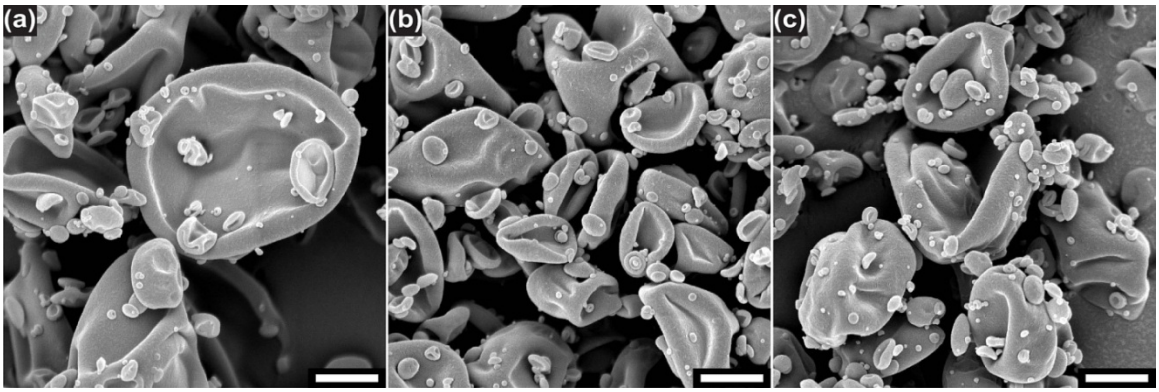

Figure 4.11 SEM pictures of SDDs of phenytoin with three HPMC-CyS as the matrices at 10 wt % loading: (a) HPMC-CyS-0.42, (b) HPMC-CyS-0.72, and (c) HPMC-CyS-0.99. The scale bars indicate 1.0 μm.

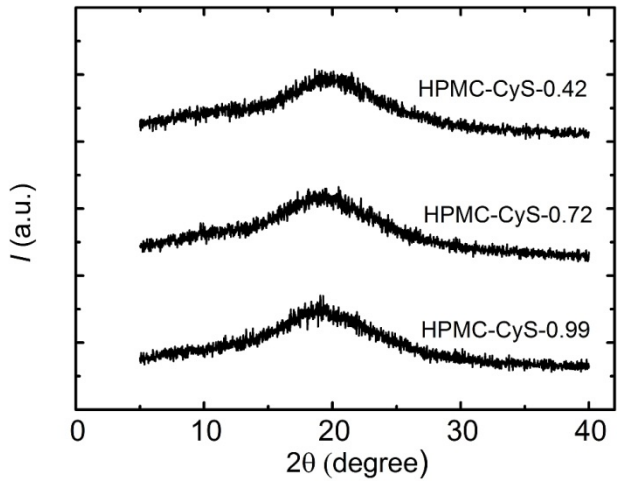

Figure 4.12 (From bottom to top) Powder XRD patterns of crystalline phenytoin and SDDs with HPMC-CyS-0.99, HPMC-CyS-0.72, and HPMC-CyS-0.42 as the matrices at 10 wt % phenytoin loading, respectively.

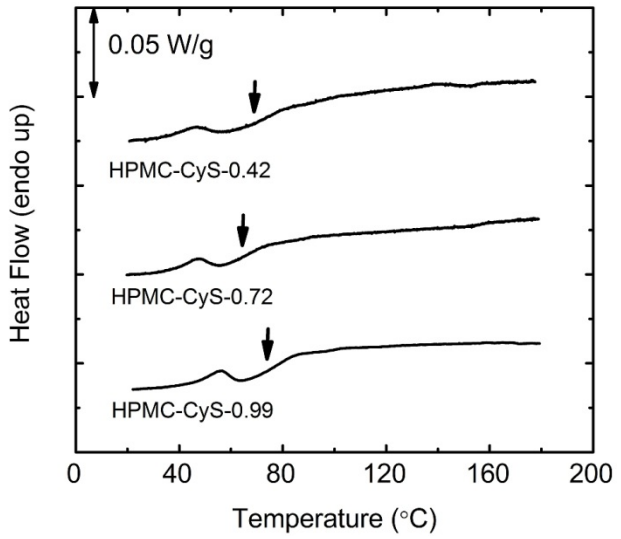

Figure 4.13 (From bottom to top) DSC curves of SDDs with HPMC-CyS-0.99, HPMC-CyS-0.72, and HPMC-CyS-0.42 as the matrices at 10 wt % phenytoin loading. The arrows highlight glass transitions, and the T_gs were 77, 69, and 73 °C for the SDDs with HPMC-CyS-0.99, HPMC-CyS-0.72, and HPMC-CyS-0.42 as the matrices, respectively.

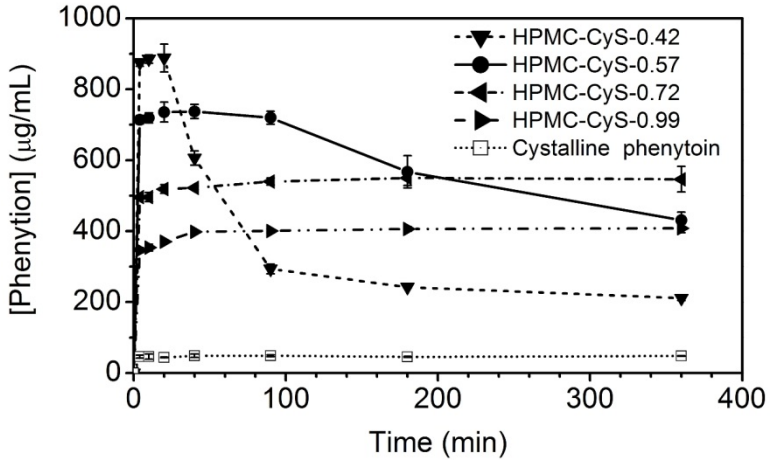

Figure 4.14 Dissolution profiles of the SDDs at 10 wt % phenytoin loading. The polymeric matrices are HPMC cyclohexylthiosuccinates with a DS of 0.42, 0.57, 0.72, and 0.99.

4.2.4 The Effect of Drug Loading.

SDDs at higher drug loading have economic significance, since less matrix material is incorporated for the same target drug concentration.[51] SDDs at 25 wt % phenytoin loading were also prepared with HPMCAS and the nine HPMC-(R-SA) as listed in Table 4.1 as the matrices. The SDDs were also likely to be amorphous solid dispersions as revealed by SEM (Figure 4.15) and powder XRD (Figure 4.16). But in DSC, besides the glass transitions at ca. 70 °C, the SDDs also showed exothermic peaks at 140–170 °C during the first heating scans (Figure 4.17). Besides, we observed columnar particles protruding from the surface of such thermally treated samples by SEM (Figure 4.18). These results led us to conclude that the phenytoin in SDDs at 25 wt % underwent cold crystallization and had reduced thermal stability compared to those at 10 wt % loading.

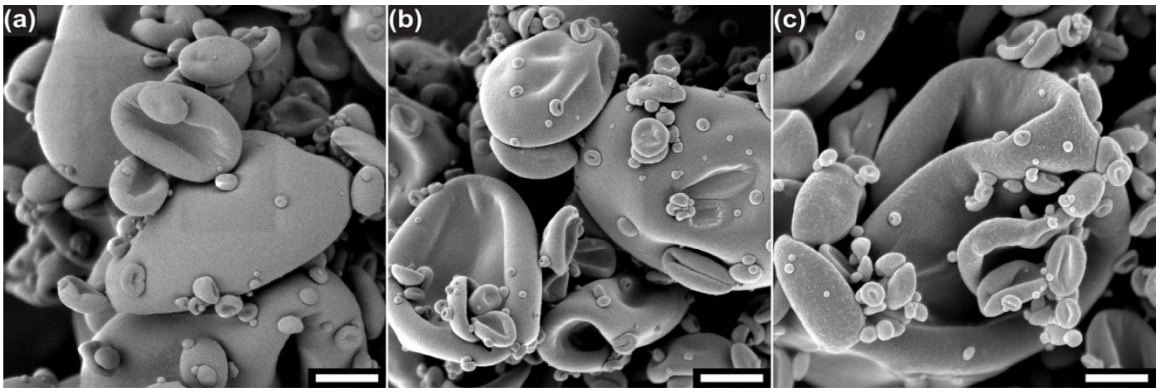

Figure 4.15 SEM pictures of SDDs of phenytoin with (a) HPMCAS (b) HPMC-Ph-0.63, and (c) HPMC-CyS-0.57 as the matrix materials at 25 wt % loading. The scale bars indicate 600 nm.

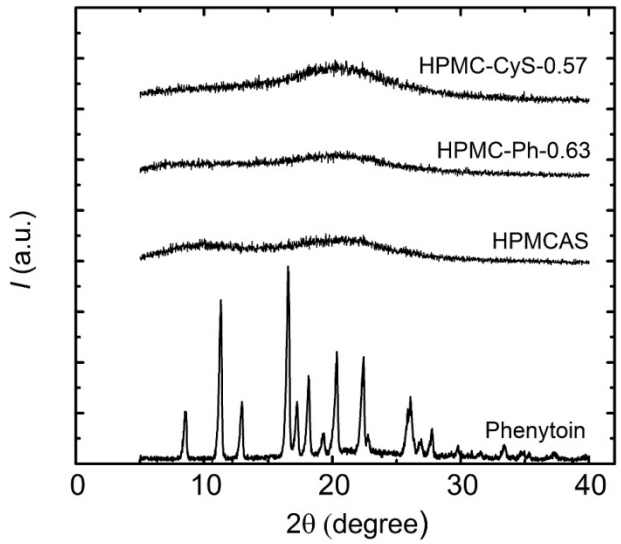

Figure 4.16 Powder XRD patterns of crystalline phenytoin and SDDs with HPMCAS, HPMC-Ph-0.63, and HPMC-CyS-0.57 as the matrices at 25 wt % phenytoin loading.

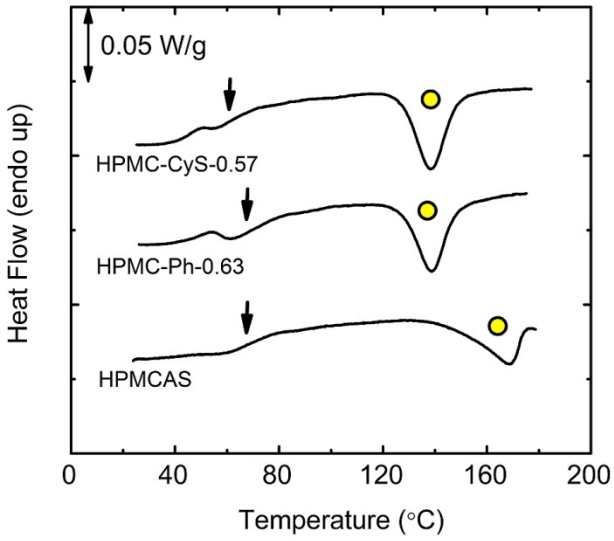

Figure 4.17 (From bottom to top) DSC curves of SDDs with HPMCAS, HPMC-Ph-0.63, and HPMC-CyS-0.57 as the matrices at 25 wt % phenytoin loading, respectively. The temperature was increased from 22 to 180 °C at a rate of 2.5 °C min^{-1}. The black arrows and yellow circles highlight the glass transitions of the SDD and the cold crystallization of phenytoin, respectively.

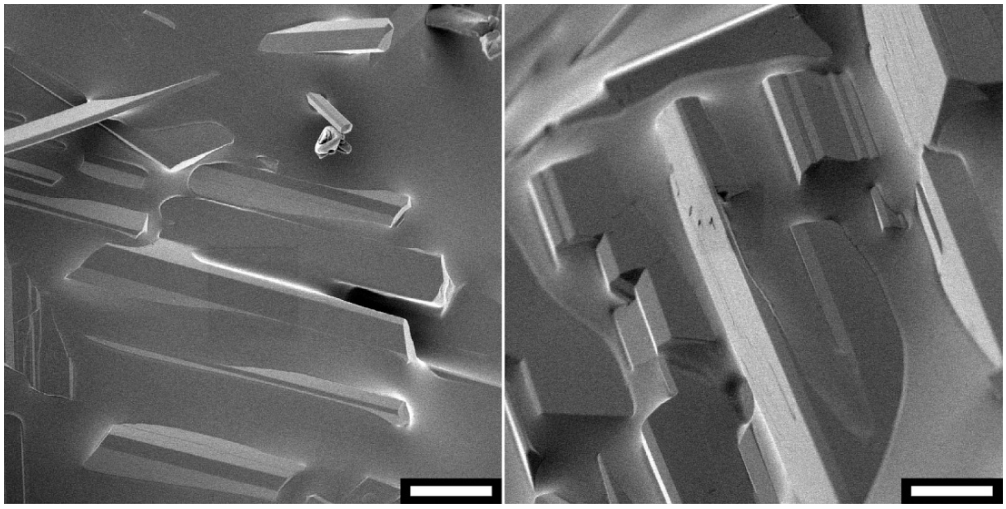

Figure 4.18 SEM pictures of SDDs of with HPMC-Ph-0.63 as the matrices at 25 wt % phenytoin loading after measurement on DSC. Shown are the outer surfaces. Scale bars indicate 3.0 and 1.0 μm in (a) and (b), respectively.

The SDDs with 25 wt % phenytoin loading also had reduced performance in solution compared to those at 10 wt % loading. As shown in Figure 4.19 and Table 4.2, all SDDs with 25 wt % phenytoin loading exhibited Type I behavior, and they were less effective at maintaining the high supersaturation levels of phenytoin achieved at 4 min than those with 10 wt % loading. For each polymeric matrix, $AUC_{360\ min}$ of the resulting SDD at 25 wt % loading was smaller than that at 10 wt % loading. Nevertheless, similar to the results obtained at 10 wt % loading, the HPMC-CyS-0.57 also provided the highest $AUC_{360\ min}$ among the five HPMC-(R-SA) with a DS of ~ 0.6 at 25 wt % phenytoin loading. On the other hand, $c_{360\ min}$ monotonously increased as the DS increased from 0.57 to 0.99 in HPMC-CyS samples. As a result, $AUC_{360\ min}$ gradually increased as DS increased from 0.57 to 0.99 in HPMC-CyS samples. The best performer, HPMC-CyS-0.99, provided a 65% increase of the $AUC_{360\ min}$ compared to HPMCAS at 25 wt % loading, which was also 20% higher than HPMCAS at 10 wt % phenytoin.

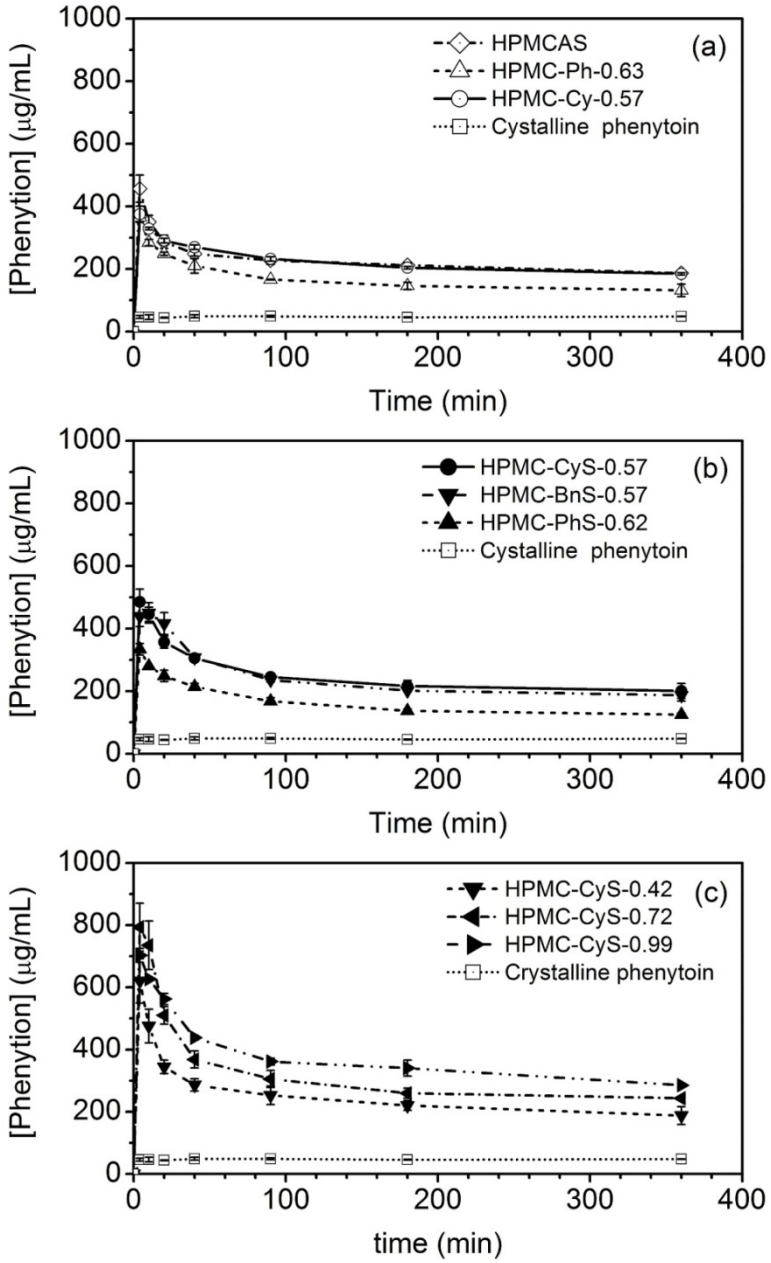

Figure 4.19 Dissolution profiles of SDDs with nine HPMC esters as matrices at 25 wt % phenytoin loading at 37 °C.

4.3 Discussion

Amorphous drugs have been well recognized to have markedly higher solubility than the crystalline counterparts.[46] As a result of enthalpic considerations, it is thermodynamically more favorable to solublize the amorphous form of a drug than the crystalline form. The theoretical solubility ratio of an amorphous drug to the crystalline counterpart is related with the difference in the free energy of the two forms, $\Delta G_{a\rightarrow c}$, as shown in Equation 4.4,[46]

$$G_{\text{amorphous}} - G_{\text{crystalline}} \equiv \Delta G_{a\rightarrow c} \approx RT \ln \frac{S_{\text{amorphous}}}{S_{\text{crystalline}}} \quad (4.4)$$

in which R is the gas constant, T is the temperature, and S is the solubility. Further, $\Delta G_{a\rightarrow c}$ can be estimated from T_m and the heat of fusion of the crystalline drug (ΔH_f) using Hoffman equation[52] as shown in Equation 4.5.

$$\Delta G_{a\rightarrow c} = \Delta H_f \frac{(T_m - T)T}{T_m^{\,2}} \quad (4.5)$$

Using a ΔH_f of 40.1 kJ mol^{-1},[47] we calculated $S_{\text{amorphous}}/S_{\text{crystalline}}$ of phenytoin to be 47.4 at 37 °C, which corresponded to the $S_{\text{amorphous}}$ of phenytoin of 1280 μg/mL. In other words, if the maximum solubility of amorphous phenytoin is achieved, the concentration of dissolved phenytoin would be 1280 μg/mL in DI water. However, dissolved phenytoin above the crystalline solubility limit is thermodynamically unstable, and has been well documented to "desupersaturate" through crystallization.[46] Among the nine samples investigated, three polymers (HPMCAS, HPMC-PhS-0.62, and HPMC-CyS-0.42) helped the resulting SDDs achieve the concentration of dissolved phenytoin that is close to 1000 μg/mL initially during the dissolution tests. More remarkably, the SDDs with four other

polymers (HPMC-CyS-0.57, HPMC-CyS-0.72, HPMC-CyS-0.99, and HPMC-BnS-0.57) as the matrices effectively inhibited the desupersaturation at concentrations that are 8–15 times of the solubility of crystalline phenytoin (although the c_{max} was 30–60% of the maximum solubility limit). Such supersaturation maintenance is critical in enhancing the $AUC_{360\ min}$, which is an indicator of the apparent *in vitro* bioavailability of phenytoin.

The ability of the SDDs to achieve high levels of supersaturation at 10 wt % phenytoin loading depends on the solubility of the polymeric matrix in the aqueous buffer. The diameter of the spray-dried particles is mostly 10 μm or less, which is much smaller than those produced industrially (50–100 μm). In designing the Mini-spray dryer, Bend Research (Bend, OR) attempted to mimic the industrial spray-drying process and mainly test the compatibility of a target drug with different matrix materials on the labscale. All of the properties of the SDD may not be the same as those produced on industrial spray dryers (e.g., the size of the spray-dried particles). Such small particles have sufficiently large specific surface area so that the releasing of the loaded drug from these SDDs is likely a dissolution-limited process, rather than a diffusion-limited process as usually observed in pressed tablets.[29] Indeed, all of the SDDs at 10 wt % phenytoin loading showed c_{max} within 20 min, most of which at the very first monitored time point, 4 min. Besides, c_{max} of a SDD was quantitatively consistent with the solubility of the matrix polymer in the aqueous buffer at 37 °C (Table 4.3). For example, the three SDDs that showed almost 100% dissolution of loaded phenytoin at 4 min were from polymers (HPMCAS, HPMC-PhS-0.62, and HPMC-CyS-0.42) that had a solubility of more than 9 mg/mL in the buffer. In the dissolution tests, all of added SDDs were dissolved and

formed clear solutions at 4 min (before centrifugation). In contrast, the solubility of HPMC-CyS-0.57 in PBS was ~ 7 mg/mL, lower than the administrated polymer concentration. As such, I observed some undissolved SDD powder in solution, and c_{max} was proportionally smaller. Besides, as the DS increased from 0.42 to 0.99, the solubility of HPMC-CyS and c_{max} of the corresponding SDDs decreased monotonously. The decreased solubility of HPMC-CyS was consistent with smaller hydrophilic hydroxyl content and larger hydrophobic cyclohexylthio and pH-responsive carboxylic acid at a higher DS. Unexpectedly, at a similar DS of ~ 0.6, HPMC esters of the five different succinates had vastly different solubility in the PBS buffer (e.g., ~ 7 fold difference in HPMC-Cy-0.57 and HPMC-CyS-0.57), and we are not clear about the exact reasons.

Table 4.3 Solubility of polymers in PBS (pH = 6.5) at 37 °C.

Polymer	Solubility (mg/mL)
HPMC-Cy-0.57	1
HPMC-CyS-0.42	> 9
HPMC-CyS-0.57	7
HPMC-CyS-0.72	3
HPMC-CyS-0.99	2
HPMC-PhS-0.62	> 9
HPMCAS	> 9

The ability of the prepared SDDs to maintain high levels of supersaturation does not come from the increased equilibrium solubility of crystalline phenytoin ($S_{crystalline}$) in the presentence of the cellulosic polymers. Increased $S_{crystalline}$ commonly occurs in

systems with surfactants[7-9] or cyclodextrin[10-12] as additives, in which some extra drug is thermodynamically stabilized in solution through either the hydrophobic interaction with the micelle cores or complexation. As such, the degree of supersaturation is decreased, and thus the thermodynamic force for crystallization is lowered. However, the measured solubility of phenytoin in the aqueous buffer in the presence of selected cellulosic polymers was roughly the same as that in the absence of any polymeric additive (Table 4.4), and thus argues against this mechanism. Instead, we believe that the crystallization (i.e., nucleation and growth) of phenytoin was effectively retarded through the formation of colloidally stable polymer–drug nanoaggregates in solution. Polymer–drug colloids of 20–300 nm,[20] whose detailed structure is not yet fully understood, have been well documented in supersaturated solutions from amorphous solid dispersions. Examples include HPMC with felodipine,[53] and HPMCAS with a variety of drugs including griseofulvin,[26, 30] danazol,[30] and progesterone.[54] Indeed, I observed a bluish tinge in the solutions that showed prolonged maintenance of the supersaturation of phenytoin (e.g., the SDDs with HPMC-CyS-0.72 at 10 wt % loading), which indicated the existence of colloidally stable nanostructures. Such bluish tinge persisted in the 6 h of dissolution tests. On the other hand, those solutions that showed rapid desupersaturation of phenytoin looked almost clear without apparent bluish tinge (e.g., the SDDS with HPMCAS at 10 wt % loading).

Table 4.4 Solubility of phenytoin in PBS (pH = 6.5) in the absence and presence of several cellulosic polymers at 37 °C.

Polymer	Solubility (μg/mL)
None	48 ± 1
HPMC-Cy-0.57	36 ± 1
HPMC-CyS-0.57	45 ± 1
HPMC-CyS-0.99	46 ± 3
HPMCAS	39 ± 2

We further recognize that inhibiting the nucleation of phenytoin is critical in preventing the desupersaturation of phenytoin in the dissolution media. At a target concentration of 1000 μg/mL, the SDDs with HPMC-CyS-0.72 and HPMC-CyS-0.99 as matrices at 10 wt % loading showed no concentration decrease for at least 6 h, corresponding to significantly prolonged induction time of the phenytoin nuclei. On the other hand, the induction time in the presence of HPMCAS was less than 4 min, after which the fast growth of phenytoin crystals led to rapidly-decreased concentration. As c_{max} were significantly different in these three SDDs, it may be difficult to directly compare the inhibition ability of the matrix polymers. Nevertheless, the dissolution tests at a lower target concentration, 500 μg/mL, gave consistent results (Figure 4.20 and Table 4.5). The c_{max} of the three SDDs were similar, corresponding to similar initial degrees of supersaturation. The induction time in the presence of HPMCAS increased to ~20 min, but still much shorter than those with HPMC-CyS-0.72 or HPMC-CyS-0.99, which were at least 6 h. Previous studies also suggest that while PVP does not affect the nucleation and only reduce the growth of bicalutamide,[55] cellulosics are effective at

inhibiting the nucleation of supersaturated drugs in solution rather than decelerating the growth process. As determined by Alonzo et al., the nucleation and growth rates of felodipine in the presence of HPMC were slowed by a factor of 1000 and 2 compared to those without any additives, respectively, which clearly suggested the importance of suppressing the nucleation in the system.[56] Further, Ilevbare et al. demonstrated that the growth of ritonavir by cellulose esters was effectively retarded at low supersaturation, but only marginally at supersaturations that are close to the maximum solubility limit of amorphous ritonavir.[57]

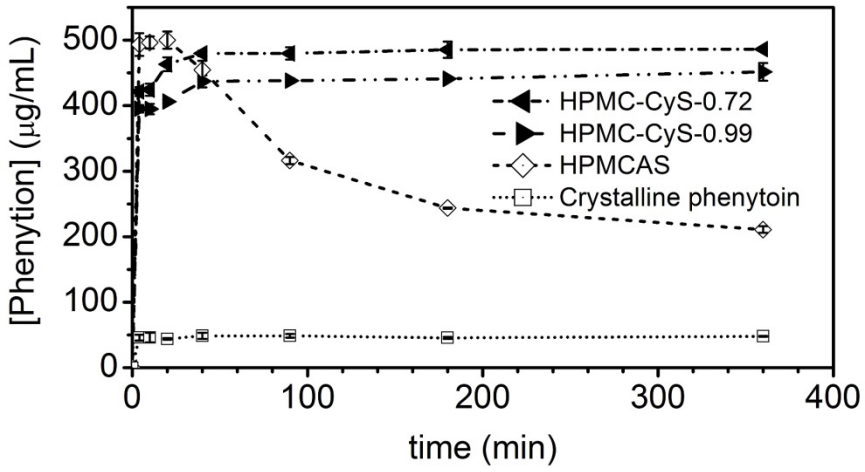

Figure 4.20 Dissolution profiles of SDDs with HPMCAS, HPMC-CyS-0.72, and HPMC-CyS-0.99 as matrices at 10 wt % phenytoin loading at 37 °C. The dissolution profile of crystalline phenytoin was also included as a reference. The target concentration of phenytoin was 500 μg mL^{-1}.

Table 4.5 Dissolution results of SDDs with three polymeric matrices at 10 wt % loading with a target concentration of 500 μg/mL.

Polymer	10 wt %			
	c_{max} (μg/mL)[a]	$c_{360\ min}$ (μg/mL)[b]	$AUC_{360\ min}$ (min μg/mL)[c]	EF[d]
HPMCAS	500	210	1.1×10^5	6.1
HPMC-CyS-0.72	490	490	1.7×10^5	10
HPMC-CyS-0.99	450	450	1.6×10^4	9.2

[a] Maximum apparent concentration of phenytoin. [b] Apparent concentration of phenytoin at 360 min. [c] Total area under the curve during the 6 h of dissolution test. [d] Enhancement factor defined as the ratio of $AUC_{360\ min}$ of a SDD to that of crystalline phenytoin. The c_{max}, $c_{360\ min}$, and $AUC_{360\ min}$ of crystalline phenytoin was 49 μg/mL, 48 μg/mL, and 1.7×10^4 min μg/mL, respectively.

Using only one anhydride allows us to decouple the effect of substituents and that of DS in the resulting HPMC esters, and further establish structure–property relationships

in a very straightforward manner. Among the five HPMC esters of monosubstituted succinates with a similar DS of ~0.6, only HPMC-CyS-0.57 and HPMC-BnS-0.57 maintained c_{max} for prolonged time (1.5 h) at a target concentration of 1000 μg/mL, and thus provided remarkable increase of $AUC_{360\ min}$ compared to HPMCAS. In contrast, those samples that do not contain sulfur (HPMC-Ph-0.63) or have an electron-withdrawing group connected with sulfur (HPMC-PhS-0.62) showed an induction time of less than 4 min. These results suggest that a combination of thioethers and weak electron-withdrawing groups is critical in the effective inhibition of nucleation. As discussed by Anwar et al., the nucleation event contains the formation of amorphous clusters of solute molecules followed by the reorganization into either single crystals or polycrystalline face-centered cubic structures.[58] Simulation results suggest that successful nucleation inhibitors have stronger affinity with the solute molecules than solvent as well as other inhibitor molecules. Our results indicate the much structural delicacy of promising nucleation-inhibiting substituents. Similarly, Ilevbare et al. studied the effect of polymer structures on the induction time of celecoxib, efavirenz, and ritonavir, and found that the most successful nucleation inhibitors have similar solubility parameters to the drug in question, a measure of the intermolecular cohesive interactions.[59] Further, a higher DS is more desired in reducing the crystallization of phenytoin as exemplified in the HPMC-CyS samples. At 10 wt % loading, the induction time increased from less than 4 min to more than 6 h as the DS increased from 0.42 to 0.72. At 25 wt % loading, all of HPMC-CyS samples showed an induction time of less than 4 min, suggesting the importance of sufficient concentrations of administrated polymers. Similar concentration effects have

been reported, and were ascribed to the less effective dispersion of phenytoin with the polymeric matrix in bulk as well as the less interaction of polymers to the solute clusters and thus the disruption of crystallization in solution.[25, 53, 60] Nevertheless, $c_{360\ min}$ and $AUC_{360\ min}$ monotonously increased as DS increased from 0.57 to 0.99. It is likely that a higher DS also allows more effective reduction of the growth of phenytoin crystals. Polymer additives are known to adsorb onto crystal surfaces via van der Waals forces and electrostatic forces, and this adsorption sterically prevents the diffusion of solute molecules onto the growing front.[32, 60, 61] At higher DS, higher cyclohexylthio content may allow larger coverage of phenytoin crystals, and the ionized carboxylic acids gave better colloidal stability of these nanoaggregates. Similarly, Miller et al. found that HPMCAS prepared from HPMC K-grade,[62] which had higher ester (acetate and succinate) substituent content than those from HPMC E-grade, were more effective at inhibiting the desupersaturation of phenytoin.[63] Ilevbare et al. also found that cellulose esters with higher DS of adipates rendered slower growth rates of ritonavir.[29] Furthermore, the reducing effect of cellulose adipates on both the nucleation[59] and the growth[57] showed significant dependence on the pH of the dissolution media, which indicated the importance of ionizable carboxylic acid groups.

4.4 Conclusions and Outlook

HPMC esters of substituted succinates are structurally analogous to HPMCAS as they also have cellulose skeleton and simultaneously contain hydrophobic, hydrophilic, and pH-responsive substituents. The structural multi-functionality grants great potential as the matrices of amorphous solid dispersions for enhancing the aqueous solubility of crystalline hydrophobic drugs. Importantly, using one anhydride allows examining the effect of substituents and that of DS in a completely orthogonal manner, which provides much simplicity in understanding and redesigning the resulting cellulose ether esters. Starting from one HPMC, five HPMC esters of monosubstituted succinates were synthesized with a similar DS of 0.6 along with HPMC cyclohexylthiosuccinates with varying DS of 0.4–1.0. In the formulated spray-dried dispersions with phenytoin, no significant difference was found in the bulk properties of samples with different matrices by SEM, powder XRD, and DSC. However, individual polymers at 10 wt % loading exhibited vastly different performance in enhancing the supersaturation of phenytoin in solution. Due to the rather small particle size, the releasing of loaded phenytoin from the SDDs depends on the solubility of polymers in the dissolution media. Moreover, since dissolved phenytoin has a strong crystallization tendency, the ability of maintaining supersaturation is crucial in improving the total area under the concentration-over-time curve in the dissolution tests, an indicator of bioavailability. HPMCAS was found to be effective at achieving high levels of supersaturation initially but not at maintaining such high supersaturation. Alternatively, several HPMC esters of monosubstituted succinates not only achieved rather high initial supersaturation, but also effectively maintained it for

prolonged time (varying from 1.5 h to more than 6 h). The most successful systems contain a sufficiently high DS and a combination of thioether and weak electron-withdrawing groups as the substituent. The maintenance was largely ascribed to the effective nucleation inhibition of phenytoin from the supersaturated solution. Further, such performance was not observed at 25 wt % loading and all SDDs showed an induction time of less than 4 min as the administrated concentration of polymer was significantly reduced. Nonetheless, HPMC cyclohexylthiosuccinates with a higher DS gave larger total area under the curve, which is likely to come from more effective retarding of crystal growth.

This chapter describes the finding of some HPMC-CyS materials, among other HPMC derivatives, as the matrices in spray-dried dispersions for the effective enhance of *in vitro* bioavailability of a crystalline hydrophobic drug, phenytoin. Many interesting and important questions are yet to be answered and thus call for further investigation. Immediate interests include the universality of the crystallization-inhibiting ability of these HPMC-CyS materials with different drugs. Other interesting candidates include griseofulvin,[64] danazol,[30] and intraconazole,[65] all of which are Class II drugs (low solubility, high permeability) in the Biopharmaceutics Classification System and the amorphous form shows strong crystallization tendency.

More important is to understand the behavior of HPMC-CyS vs HPMCAS on the colloidal level that results in the different performance in crystallization inhibition. The spray-drying process involved three phases—a starting solution of drug and polymer in an organic solvent (formulation), spray-dried dispersions in the solid state (storage), and

spray-dried dispersions in dissolution media (performance). Phenytoin is well soluble in acetone. The prepared HPMC-(R-SA) samples and the AFFINISOL™ HPMCAS from The Dow Chemical Company were mostly molecularly dissolved in acetone at 2.0 wt %. There are some implications of HPMCAS in acetone as indicated by the bluish tinge and the loss of materials via passing through 0.2-μm syringe filters. Causes include covalent intermolecular cross-linking and the physical association of not-fully-dissolved moieties (succinates). However, preliminary DLS data showed that the associated structures composed less than 1 wt % of the total administered HPMCAS in acetone. Besides, HPMC-(R-SA) samples resulted in clear solutions in acetone at 2.0 wt % and essentially no large aggregates as monitored by DLS. Therefore, it is tentatively assumed that no significant amount of associated structures existed in the starting solutions.

It is critical to track the differences in the latter two phases among samples with different polymeric matrices. Current results from SEM, DSC, and powder XRD provide information on the morphology, size, crystallinity, and thermal stability of SDDs in the solid state. In future, measuring the equilibrium solubility of phenytoin in these polymers would give useful guidance on the degree of mixing between phenytoin with the matrix materials (e.g., stable, meta-stable, or unstable in the phase diagram).[20] Complementary spectroscopy methods such as IR and Raman may reveal important functional groups that promote mixing. Moreover, the distribution of the drugs within the spray-dried particles may significantly affect the storage methods and the dissolution performance. Drugs are thought to be more populated toward the center of the spray-dried particles, since small molecules have much higher mobility than the polymers in the solution used for spray

drying. In other words, polymers crimp and form the outer skin layer during spray drying.[22] ATR-IR can determine the composition of polymer and drug on the surface (600–800 nm in depth) of the particles (40–60 μm in diameter, from industrial spray-drying apparatus).[20] Besides, TEM offers high resolution and will be extremely powerful in revealing the internal structures with appropriate sample preparation (controlling the thickness and contrast).

Studying the SDDs in the aqueous media would provide information directly related with the dissolution performance. Numerous reports have recognized the importance of polymer–drug aggregates in improving the apparent solubility of the easy-to-desupersaturate drugs.[20, 26, 30, 53] However, the nanosized suspenders are only supported by DLS data and no direct visualization using imaging methods have been published. Cryo-TEM is ideal for this purpose since it exerts little disturbance on the structures in solution while providing high resolution. On the other hand, the following points should be examined during image acquisition: (i) the contrast of polymer and drug against water, (ii) the number density of observable aggregates in the thin film due to the rather low concentration of polymer/drug content in the dissolution media, and (iii) the time sensitivity of SDDs in PBS.

The commercial potential of HPMC esters of substituted succinates is not fully examined without considering biocompatibility and cost. Interestingly, thiolated anhydrides (Cy-S-SA, Ph-S-SA, Bn-S-SA) are not yet commercially available, though the synthesis was patented more than 50 years ago.

4.5 Experimental Section

Reagents. All chemicals were reagent grade and used as received unless otherwise noted. Phenylsuccinic anhydride (Aldrich, 99%), cyclohexylsuccinic acid (Aldrich, 96%), maleic anhydride (Fluka, 99+%), cyclohexanethiol (Aldrich, 97%), thiophenynol (Aldrich, 99+%), benzyl mercaptan (Aldrich, 99%), triethylamine (Sigma-Aldrich, 99.0+%), sulfuric acid (BDH, 95.0-98.0% min), succinic anhydride (Aldrich, 99+%), acetyl chloride (Fluka, 99+%), benzene (Sigma-Aldrich, anhydrous, 99.8%), acetic acid (Sigma-Aldrich, 99.7+%), sodium acetate (Sigma-Aldrich, 99.0+%), isopropyl alcohol (Sigma-Aldrich, anhydrous, 99.5%), HPMC (E3 grade, The Dow Chemical Company), HPMCAS (AFFINISOL™ 912 G, The Dow Chemical Company), phenytoin (Sigma, 99+%), simulated intestinal fluid powder (Biorelevant), chloroform-*d* (Alrich, 99.96% atom D), acetic acid-d_4 (Cambridge Isotope Laborotaries, 99.5% D), and dimethyl sulfoxide-d_6 (Cambridge Isotope Laborotaries, 99.9% D) were used as received.

Molecular characterization. The DS of MeO, HPO, Ac, and Su in HPMCAS and the DS of MeO and HPO in HPMC were determined by The Dow Chemical Company following the monograph by United States Pharmacopeia and The National Formulary (USP–NF). ^{1}H and ^{13}C NMR spectra were recorded on either a Bruker AV-500, a Varian Inova 500, or a Varian Inova 300 spectrometer at 23 °C with DMSO-d_6 or $CDCl_3$ as the solvent unless otherwise specified. The SEC measurement of HPMC was carried out on an Agilent 1260 liquid chromatograph with 0.1 M Na_2SO_4 aqueous solution (supplemented with 1% acetic acid) as the mobile phase. The SEC houses a Eprogen (Downers Grove, IL) CATSEC guard column and three separating columns with

pore sizes of 1000, 300, and 100 Å, respectively. The detectors are an Agilent 1260 MWD UV-vis detector, a Wyatt Dawn Heleos II light-scattering detector, and a Wyatt Optilab T-rEX refractive-index detector. The SEC measurement of HPMC esters of substituted succinates was carried out on an Agilent 1260 liquid chromatograph with tetrahydrofuran (THF) as the mobile phase. The SEC houses a Waters Styragel guard column and three separating columns that cover an effective molecular weight range of 100–10,000,000 g mol^{-1}. The detectors are an Agilent 1260 VWD UV-vis detector, a Wyatt Dawn Heleos II light-scattering detector, and a Wyatt Optilab T-rEX refractive-index detector.

Synthesis of substituted succinic anhydrides. The synthesis of cyclohexyl-succinic anhydride (Cy-SA) was carried out following the published procedure toward cyclopentylsuccinic anhydride,[66] and the product was purified via vacuum distillation.[67]

The synthesis of phenylthiosuccinic anhydride (Ph-S-SA)[48, 68] and benzylthio-succinic anhydride (Bn-S-SA)[68] were carried out following published procedures except that the product were purified via column chromatography followed by vacuum distillation. Ph-S-SA: R_f = 0.54 in hexane/ethyl acetate = 8:2 (v/v), bp = 120 °C at 65 mTorr. Bn-S-SA: R_f = 0.75 in hexane/ethyl acetate = 8:2 (v/v), bp = 140 °C at 55 mTorr.

The detailed synthetic procedure of cyclohexylthiosuccinic anhydride (Cy-S-SA) is described as below. 11.3 mL of cyclohexanethiol (9.2×10^{-2} mol), 9.0 g of maleic anhydride (9.2×10^{-2} mol), and 256 μL of triethylamine (1.8×10^{-3} mol) were dissolved in 75 mL of benzene, and the reaction was allowed to proceed for 3.0 h at 70 °C. Then 200 μL of concentrated sulfuric acid was added into the mixture to quench the reaction. The

mixture was filtered and concentrated to afford dark red crude product. Further purifications with flash chromatography (R_f = 0.49 in hexane/ethyl acetate = 8:2, v/v) followed by fractional distillation (bp = 110 °C at 55 mTorr) gave nearly colorless, slightly yellow oil (conversion: 98% by ^{1}H NMR, yield: 11.8 g, 60%). ^{1}H NMR (in $CDCl_3$, 300 MHz, Figure 4.21): δ (ppm): 4.01 (dd, 1H, *J* = 4.07, 9.48 Hz), 3.40 (dd, 1H, *J* = 9.48, 19.19 Hz), 3.15-3.05 (m, 1H), 2.73 (dd, 1H, *J* = 4.07, 19.19 Hz), 2.15-2.00 (m, 1H), 2.00-1.80 (m, 1H), 1.80-1.65 (m, 2H), 1.65-1.50 (m, 1H), 1.50-1.20 (m, 5H). ^{13}C NMR (75 MHz, $CDCl_3$, Figure 4.22): 170.51, 168.72, 44.07, 37.81, 36.03, 33.00, 32.32, 25.60, 25.35, and 25.32 ppm. IR (melt, NaCl plate, Figure 4.23): $\nu_{C=O}$ = 1863, 1785 cm^{-1}.

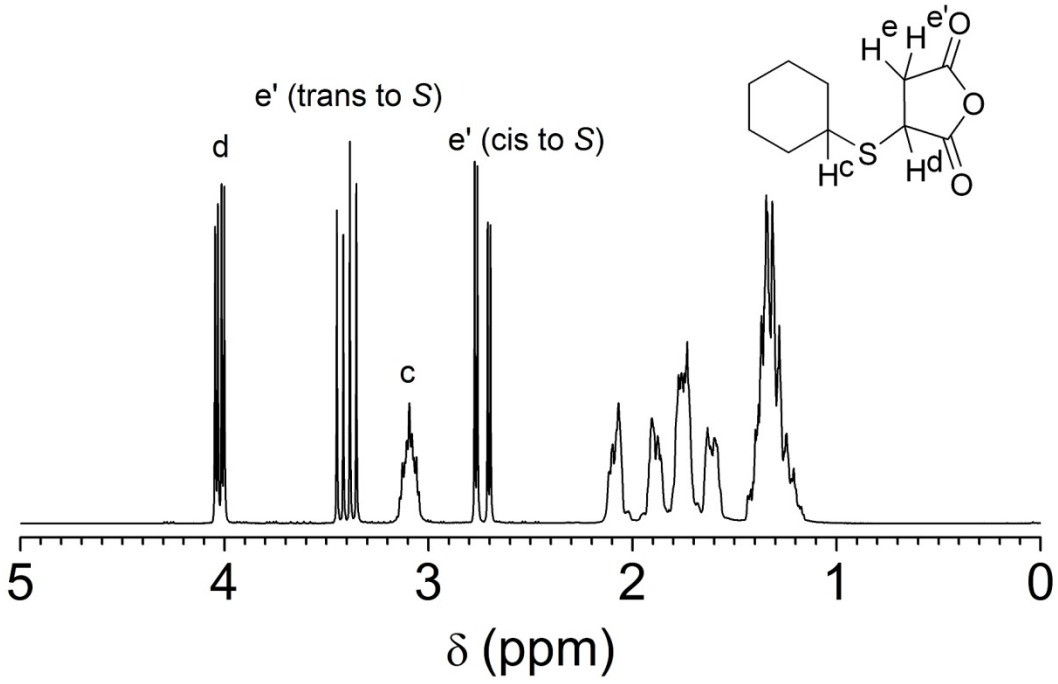

Figure 4.21 ^{1}H NMR spectrum of cyclohexylthiosuccinic anhydride (Cy-S-SA) in $CDCl_3$ at 23 °C.

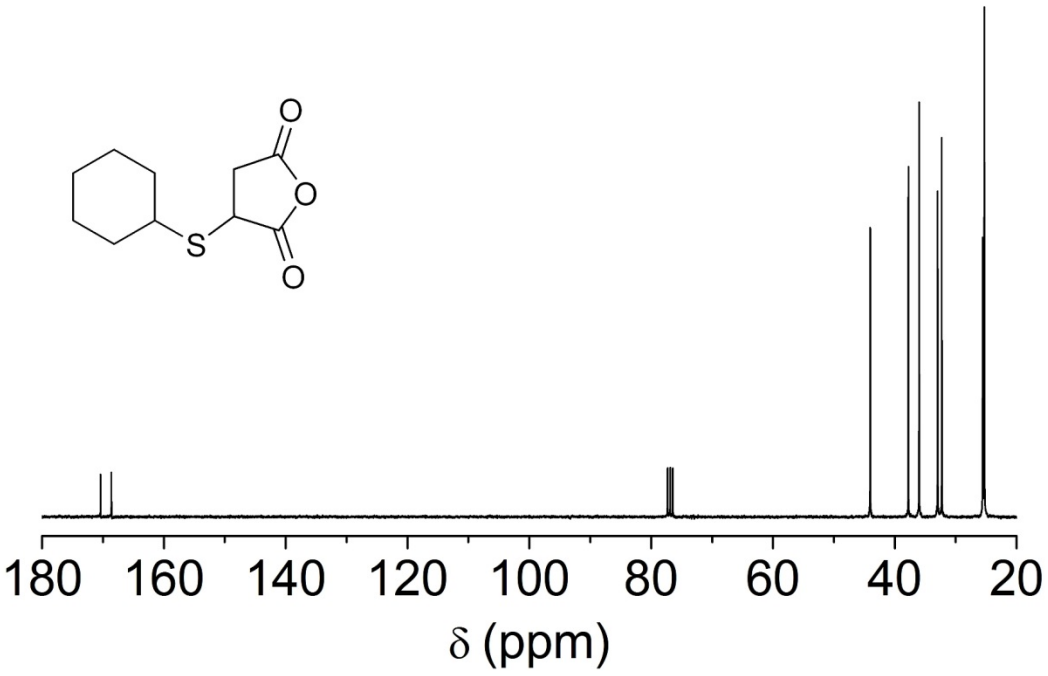

Figure 4.22 ^{13}C NMR spectrum of cyclohexylthiosuccinic anhydride (Cy-S-SA) in $CDCl_3$ at 23 °C.

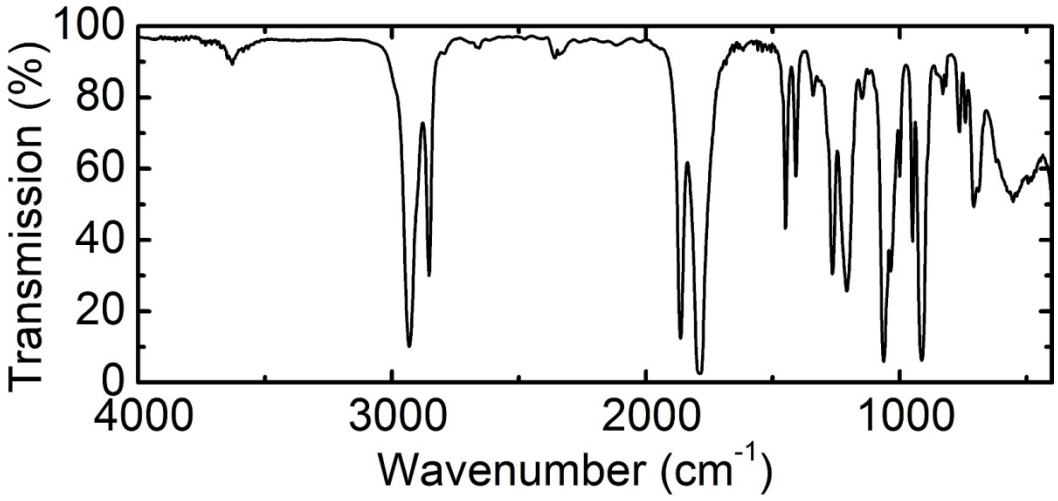

Figure 4.23 IR spectrum of cyclohexylthiosuccinic anhydride (Cy-S-SA) at 23 °C.

Synthesis of HPMC esters of substituted succinates. Generally speaking, the composition of HPMC, sodium acetate, and acetic acid in the feed was kept the same and a homogeneous mixture was first allowed to form at 85 °C ($[\text{-OH}]_0$:$[\text{NaOAc}]_0$ = 1:2, and $[\text{-OH}]_0 \approx 0.4$ M). Next, an appropriate amount of an anhydride was added to target a specific substituent and degree of substitution as listed in Table 4.1. The detailed procedure for synthesizing HPMC-CyS-0.72 is listed below as an example. 0.87 g of HPMC (pendent hydroxyl: 4.7×10^{-3} mol), 0.77 g of sodium acetate (9.4×10^{-3} mol), and 11.0 mL of glacial acetic acid were charged into a 50-mL round bottom flask, and allowed to form a homogeneous mixture at 85 °C with magnetic stirring. 2.0 g of Cy-S-SA (9.4×10^{-3} mol) was then added into the flask, and the reaction was allowed to proceed at 85 °C for 3.0 h. The reaction was quenched by adding 5 mL into the mixture. The mixture was precipitated into 1.0 L of water, redissolved in 20 mL of THF, precipitated into 1.0 L of water once more, and further dried under vacuum at 22 °C until constant mass was achieved. The product was white, slightly yellow powder. The conversion of the anhydride was 33% by ^{1}H NMR. Yield: 1.45 g, 95%.

Preparation of spray-dried dispersions (SDDs). SDDs were made at labscale, and the following procedure for HPMC-CyS-0.72 at 10 wt % phenytoin loading serves as an example. 225 mg of HPMC-CyS-0.72 and 25.0 mg of phenytoin were first mixed in 12.25 g of acetone (corresponding to the concentration of total solids as 2.0 wt %) to form a homogeneous solution with magnetic stirring. The solution was loaded in a 20-mL syringe on a syringe pump and SDDs were prepared with a Mini-sprayer (Bend Research, Bend, OR) at the following conditions: inlet temperature, 68 °C; N_2 flow rate, 12.8 L

min^{-1}; and solution flow rate, 0.65 mL min^{-1}. The outlet temperature was between 22 and 28 °C. The spray-dried powders were collected with the aid of an anti-static bar and further dried under vacuum (10 mTorr) for at least 12 h. SDDs with phenytoin were stored in a vacuum desiccator at 22 °C.

Scanning electron microscopy (SEM). Samples to be analyzed were spread with a spatula onto a carbon conductive tape (Ted Pella Inc), and then coated with 10 nm Au/Pd (60/40 by weight) in a 15 mTorr Argon atmosphere using a Denton DV-502A high vacuum deposition system. Samples were imaged using a secondary electron detector on a Hitachi S-900 field emission gun SEM. The accelerating voltage was 1.2 or 3.0 kV. The magnification was between 3,000 and 30,000.

Powder X-Ray diffraction (powder XRD). Powder samples (~ 50 mg) were packed in a 0.5 mm deep zero-background holder and analyzed on a Bruker-AXS D5005 diffractometer at 22 °C. The X-ray source (Cu, λ = 1.54 Å) was operated at a voltage of 45 kV and a current of 40 mA. Data were collected from 5 to 40° (2θ) with a step size of 0.02° and a scan rate of 1 second/step.

Differential scanning calorimetry (DSC). Samples of known mass (2–10 mg) were encapsulated in Tzero aluminum pans and analyzed on a Discovery DSC (TA Instruments). To determine the T_g of a neat polymer, standard pans were used and the temperature was ramped between 20 and 160 °C at a rate of 10 °C min^{-1}. T_g was determined using the 2nd heating scan. SDDs were put inside hermetically sealed pans, and the temperature was ramped from 22 °C to 180 °C at a rate of 2.5 °C min^{-1}. The 1st

heating scans are reported. All analyses were carried out using the TA TRIOS software version 2.2.

Dissolution tests. Samples (either spray dried dispersions or crystalline drug) were weighed into 1.5 mL conical microcentrifuge tubes in triplicates. An appropriate amount of phosphate buffer solution (PBS, 82 mM sodium chloride, 20 mM sodium phosphate dibasic, 47 mM potassium phosphate monobasic, 0.5 wt % simulated intestinal fluid powder, adjusted to pH 6.5 with NaOH) at 37 °C was added to produce a final concentration of drug of 1000 μg/mL if all material was fully dissolved unless otherwise noted (e.g. 18.0 mg of spray-dried dispersion consisting of 1.8 mg of drug and 16.2 mg of polymer was diluted with 1.8 mL of buffer solution). Samples were vortexed for 1 min and set in an isothermal aluminum sample holder at 37 °C. At each time point (4, 10, 20, 40, 90, 180, and 360 min), samples were centrifuged at 13,000 g for 1 min, and a 50-μL aliquot was removed and diluted with 250-μL ethanol. The samples were again vortexed for 30 s and held at 37 °C until the next time point. Drug concentration in each aliquot was determined by reverse phase HPLC. Samples were analyzed on an Agilent 1260 liquid chromatograph system with a multi-wavelength UV-vis detector, 1260 MWD. The HPLC housed an Agilent Poroshell 120 EC-C18 column of 4.6×50 mm. The pore size was 120 Å, and the particle size was 2.7 μm. The chromatogram was monitored at 254 nm. For phenytoin, the mobile phase was 45:55 (v/v) of MeCN/Water, the elution volume of phenytoin was 1.08 mL, and a calibration was made in the range of 10–1000 μg/mL.

The solubility of polymers in the PBS (w/o SIF powder) was tested by visually examining the clarity of the solution at 37 °C. The concentration of the solution was

sequentially diluted from 9.0, 7.0, 5.0, 3.0, 2.0, 1.5, to 1.0 mg/mL until a clear solution was formed. The dissolution was aided by 15 min of sonication followed by magnetic stirring for at least 2 h.

The solubility of phenytoin in the presence of polymers was tested by adding crystalline phenytoin into a PBS (w/i SIF powder) with pre-dissolved polymers. The concentration of preloaded polymers was 2.0 mg/mL, and the target concentration of phenytoin was 1.0 mg/mL. The mixture was allowed to equilibrate with magnetic stirring at 37 °C for 5 h. Undissolved phenytoin was removed by centrifuge at 13,000 g for 1 min, and aliquots were taken to determine the concentration of dissolved phenytoin by HPLC, similar to those in dissolution tests as described above.

4.6 References

1. Hauss, D. J. *Adv. Drug Delivery Rev.* **2007,** 59, (7), 667-676.

2. Lipinski, C. A. *J. Pharmacol. Toxicol. Methods* **2000,** 44, (1), 235-249.

3. Lipinski, C. A.; Lombardo, F.; Dominy, B. W.; Feeney, P. J. *Adv. Drug Delivery Rev.* **2001,** 46, (1-3), 3-26.

4. Serajuddin, A. T. M. *Adv. Drug Delivery Rev.* **2007,** 59, (7), 603-616.

5. Stella, V. J.; Nti-Addae, K. W. *Adv. Drug Delivery Rev.* **2007,** 59, (7), 677-694.

6. Rautio, J.; Kumpulainen, H.; Heimbach, T.; Oliyai, R.; Oh, D.; Jarvinen, T.; Savolainen, J. *Nat. Rev. Drug Discovery* **2008,** 7, (3), 255-270.

7. Gursoy, R. N.; Benita, S. *Biomed. Pharmacother.* **2004,** 58, (3), 173-182.

8. Gao, P.; Morozowich, W. *Expert Opin. Drug Delivery* **2006,** 3, (1), 97-110.

9. Kohli, K.; Chopra, S.; Dhar, D.; Arora, S.; Khar, R. K. *Drug Discovery Today* **2010,** 15, (21-22), 958-965.

10. Loftsson, T.; Brewster, M. E.; Masson, M. *Am. J. Drug Delivery* **2004,** 2, (4), 261-275.

11. Carrier, R. L.; Miller, L. A.; Ahmed, M. *J. Controlled Release* **2007,** 123, (2), 78-99.

12. Loftsson, T.; Brewster, M. E. *J. Pharm. Sci.* **2012,** 101, (9), 3019-3032.

13. Rabinow, B. E. *Nat. Rev. Drug Discovery* **2004,** 3, (9), 785-796.

14. Merisko-Liversidge, E. M.; Liversidge, G. G. *Toxicol. Pathol.* **2008,** 36, (1), 43-48.

15. Merisko-Liversidge, E.; Liversidge, G. G. *Adv. Drug Delivery Rev.* **2011,** 63, (6), 427-440.

16. Leuner, C.; Dressman, J. *Eur. J. Pharm. Biopharm.* **2000,** 50, (1), 47-60.

17. Vasconcelos, T.; Sarmento, B.; Costa, P. *Drug Discovery Today* **2007,** 12, (23&24), 1068-1075.

18. Crowley, M. M.; Zhang, F.; Repka, M. A.; Thumma, S.; Upadhye, S. B.; Battu, S. K.; McGinity, J. W.; Martin, C. *Drug Dev. Ind. Pharm.* **2007,** 33, (9), 909-926.

19. Repka, M. A.; Battu, S. K.; Upadhye, S. B.; Thumma, S.; Crowley, M. M.; Zhang, F.; Martin, C.; McGinity, J. W. *Drug Dev. Ind. Pharm.* **2007,** 33, (10), 1043-1057.

20. Friesen, D. T.; Shanker, R.; Crew, M.; Smithey, D. T.; Curatolo, W. J.; Nightingale, J. A. S. *Mol. Pharmaceutics* **2008,** 5, (6), 1003-1019.

21. Re, M. I. *Drying Technol.* **2006,** 24, (4), 433-446.

22. Vehring, R. *Pharm. Res.* **2008,** 25, (5), 999-1022.

23. Ormes, J. D.; Zhang, D.; Chen, A. M.; Hou, S.; Krueger, D.; Nelson, T.; Templeton, A. *Pharm. Dev. Technol.* **2013,** 18, (1), 121-129.

24. Tanno, F.; Nishiyama, Y.; Kokubo, H.; Obara, S. *Drug Dev. Ind. Pharm.* **2004,** 30, (1), 9-17.

25. Konno, H.; Handa, T.; Alonzo, D. E.; Taylor, L. S. *Eur. J. Pharm. Biopharm.* **2008,** 70, (2), 493-499.

26. Curatolo, W.; Nightingale, J. A.; Herbig, S. M. *Pharm. Res.* **2009,** 26, (6), 1419-1431.

27. Rumondor, A. C. F.; Stanford, L. A.; Taylor, L. S. *Pharm. Res.* **2009,** 26, (12), 2599-2606.

28. Alonzo, D. E.; Zhang, G. G. Z.; Zhou, D. L.; Gao, Y.; Taylor, L. S. *Pharm. Res.* **2010,** 27, (4), 608-618.

29. Tajarobi, F.; Larsson, A.; Matic, H.; Abrahmsen-Alami, S. *Eur. J. Pharm. Biopharm.* **2011,** 78, (1), 125-133.

30. Murdande, S. B.; Pikal, M. J.; Shanker, R. M.; Bogner, R. H. *J. Pharm. Sci.* **2011,** 100, (10), 4349-4356.

31. Qian, F.; Wang, J.; Hartley, R.; Tao, J.; Haddadin, R.; Mathias, N.; Hussain, M. *Pharm. Res.* **2012,** 29, (10), 2766-2776.

32. Ilevbare, G. A.; Liu, H. Y.; Edgar, K. J.; Taylor, L. S. *Cryst. Growth Des.* **2012,** 12, (6), 3133-3143.

33. Caldwell, C. G.; Wurzburg, O. B. Polysaccharide derivatives of substituted dicarboxylic acids. US2661349, 1953.

34. Billmers, R. L.; Mackewicz, V. L. Process for preparation of hydrophobic starch derivatives. EP761691A2, 1997.

35. Maliczyszyn, W.; Atkinson, J. G.; Tolchinsky, M. Preparation of hydrophobic starch derivatives by reaction with preemulsified anhydrides. US6037466A, 2000.

36. Cizova, A.; Koschella, A.; Heinze, T.; Ebringerova, A.; Srokova, I. *Starch/Staerke* **2007,** 59, (10), 482-492.

37. Wang, L.; Stogner, H. P.; Batson, B. C. Starch esters and method for their manufacture and moldings made from them. US20080146792A1, 2008.

38. Bai, Y.; Shi, Y.C. *Carbohydr. Polym.* **2011,** 83, (2), 520-527.

39. Peuscher, M.; Engelskirchen, K.; Gruenberger, E. Manufacture and use of water-soluble alkenyl- or alkylsuccinic acid ester-containing cellulose ethers. DE3620991A1, 1988.

40. Diamantoglou, M. Preparation of modified cellulose for biocompatible dialysis membranes. EP330106A1, 1989.

41. Kalbe, J.; Koch, R.; Muller, H. P.; Engelhardt, J.; Koch, W.; Muller, V. Thermoplastic and biodegradable polysaccharide esters / polysaccharide ether esters containing maleic acid addition product groups. US5717087, 1998.

42. Simon, J.; Mueller, H.-P.; Koch, R.; Dijkstra, D. J.; Engelhardt, J.; Mueller, V. Manufacture of compostable, water-insoluble thermoplastic cellulose ether esters with 2-hydroxycarboxylic acid and other acids. DE19618826A1, 1997.

43. Takihara, T.; Yoshida, Y.; Isogai, A. *Cellulose* **2007,** 14, (4), 357-366.

44. Gardner, J. B.; Fevola, M. J.; Sun, F. C.; Walters, R. M. Superhydrophilic amphiphilic copolymers and processes for making the same. WO2011042379A1, 2011.

45. Salminen, A. Method for production of hydrophobic microfibrillated cellulose. WO2012089929A1, 2012.

46. Mithani, S. D.; Bakatselou, V.; TenHoor, C. N.; Dressman, J. B. *Pharm. Res.* **1996,** 13, (1), 163-7.

47. Wassvik, C. M.; Holmen, A. G.; Draheim, R.; Artursson, P.; Bergstrom, C. A. S. *J. Med. Chem.* **2008,** 51, (10), 3035-3039.

48. Zienty, F. B.; Vineyard, B. D.; Schleppnik, A. A. *J. Org. Chem.* **1962,** 27, (9), 3140-3146.

49. E3 grade under the trademark of METHOCEL from The Dow Chemical Company (Midland, MI). This grade is also the starting material for several commercial HPMCAS by The Dow Chemical Company.

50. The measured concentration of crystalline phenytoin in the aqueous buffer at 37 °C is larger than the literature value of its equilibrium solubility in water, 27.1 μg/mL. The increase is largely caused by the stabilization of extra phenytoin in the lipids as 0.5 wt % of simulated intestinal fluid (SIF) powder was added in the solution.

51. For the target concentration of 1000 μg/mL in the dissolution tests, the concentrations of added polymers are 9000 and 3000 μg/mL for SDDs with 10 and 25 wt % drug loadings, respectively.

52. Hoffman, J. D. *J. Chem. Phys.* **1958,** 29, 1192-3.

53. Alonzo, D. E.; Gao, Y.; Zhou, D. L.; Mo, H. P.; Zhang, G. G. Z.; Taylor, L. S. *J. Pharm. Sci.* **2011,** 100, (8), 3316-3331.

54. Miller, J. M.; Beig, A.; Carr, R. A.; Spence, J. K.; Dahan, A. *Mol. Pharmaceutics* **2012,** 9, (7), 2009-2016.

55. Lindfors, L.; Forssen, S.; Westergren, J.; Olsson, U. *J. Colloid Interface Sci.* **2008,** 325, (2), 404-413.

56. Alonzo, D. E.; Raina, S.; Zhou, D.; Gao, Y.; Zhang, G. G. Z.; Taylor, L. S. *Cryst. Growth Des.* **2012,** 12, (3), 1538-1547.

57. Ilevbare, G. A.; Liu, H.; Edgar, K. J.; Taylor, L. S. *CrystEngComm* **2012,** 14, (20), 6503-6514.

58. Anwar, J.; Boateng, P. K.; Tamaki, R.; Odedra, S. *Angew. Chem., Int. Ed.* **2009,** 48, (9), 1596-1600.

59. Ilevbare, G. A.; Liu, H.; Edgar, K. J.; Taylor, L. S. *Cryst. Growth Des.*, Ahead of Print.

60. Raghavan, S. L.; Trividic, A.; Davis, A. F.; Hadgraft, J. *Int. J. Pharm.* **2001,** 212, (2), 213-221.

61. Hasegawa, A.; Taguchi, M.; Suzuki, R.; Miyata, T.; Nakagawa, H.; Sugimoto, I. *Chem. Pharm. Bull.* **1988,** 36, (12), 4941-50.

62. Commercially available under the trademark of METHOCEL from the Dow Chemical Company (Midland, MI). The DS of methoxy in HPMC of K grade is 1.15–1.50, and thus allows a total DS of acetate and succinate of 1.50–1.85 in the resulting HPMCAS. In comparison, the DS of methoxy in HPMC of E grade is 1.80–1.95, which allows a maximum total DS of acetate and succinate of 1.05–1.20.

63. Miller, W. K.; Lyon, D. K.; Friesen, D. T.; Caldwell, W. B.; Vodak, D. T.; Dobry, D. E. Hydroxypropyl methyl cellulose acetate succinate with enhanced acetate and succinate substitution. WO2011159626A1, 2011.

64. Al-Obaidi, H.; Buckton, G. *Aaps Pharmscitech* **2009,** 10, (4), 1172-1177.

65. Prasad, R. S.; Yandrapu, S. K.; Manavalan, R. *Int. J. ChemTech Res.* **2010,** 2, (1), 133-142.

66. Bergmeier, S. C.; Ismail, K. A. *Synthesis-Stuttgart* **2000**, (10), 1369-1371.

67. Rowley, J. M.; Lobkovsky, E. B.; Coates, G. W. *J. Am. Chem. Soc.* **2007,** 129, (16), 4948-4960.

68. Kaydos, J. A.; Smith, D. L. *J. Org. Chem.* **1983,** 48, (7), 1096-1099.

Bibliography

Abbas, S.; Li, Z.; Hassan; Lodge, T. P. *Macromolecules* **2007,** 40, (11), 4048-4052.

Agrawal, S. K.; Sanabria-DeLong, N.; Tew, G. N.; Bhatia, S. R. *Macromolecules* **2008,** 41, (5), 1774-1784.

Ahmed, F.; Discher, D. E. *J. Controlled Release* **2004,** 96, (1), 37-53.

Albertin, L.; Kohlert, C.; Stenzel, M.; Foster, L. J. R.; Davis, T. P. *Biomacromolecules* **2004,** 5, (2), 255-260.

Alexandridis, P.; Lindman, B., *Amphiphilic Block Copolymers: Self-Assembly and Applications*. 1st ed.; Elsevier: Amsterdam, 2000.

Alonzo, D. E.; Gao, Y.; Zhou, D. L.; Mo, H. P.; Zhang, G. G. Z.; Taylor, L. S. *J. Pharm. Sci.* **2011,** 100, (8), 3316-3331.

Alonzo, D. E.; Raina, S.; Zhou, D.; Gao, Y.; Zhang, G. G. Z.; Taylor, L. S. *Cryst. Growth Des.* **2012,** 12, (3), 1538-1547.

Alonzo, D. E.; Zhang, G. G. Z.; Zhou, D. L.; Gao, Y.; Taylor, L. S. *Pharm. Res.* **2010,** 27, (4), 608-618.

Anderson, K. S.; Lim, S. H.; Hillmyer, M. A. *J. Appl. Polym. Sci.* **2003,** 89, (14), 3757-3768.

Anwar, J.; Boateng, P. K.; Tamaki, R.; Odedra, S. *Angew. Chem., Int. Ed.* **2009,** 48, (9), 1596-1600.

Azzam, T.; Eisenberg, A. *Angew. Chem., Int. Ed.* **2006,** 45, (44), 7443-7447.

Bai, Y.; Shi, Y.-C. *Carbohydr. Polym.* **2011,** 83, (2), 520-527.

Baird, J. A.; Taylor, L. S. *Adv. Drug Delivery Rev.* **2012,** 64, (5), 396-421.

Bang, J.; Jain, S.; Li, Z.; Lodge, T. P.; Pedersen, J. S.; Kesselman, E.; Talmon, Y. *Macromolecules* **2006,** 39, (3), 1199-1208.

Barz, M.; Luxenhofer, R.; Zentel, R.; Vicent, M. J. *Polym. Chem.* **2011,** 2, (9), 1900-1918.

Baskaran, D.; Mueller, A. H. E. *Prog. Polym. Sci.* **2007,** 32, (2), 173-219.

Bates, F. S.; Fredrickson, G. H. *Annu. Rev. Phys. Chem.* **1990,** 41, 525-557.

Bates, F. S.; Fredrickson, G. H. *Phys. Today* **1999,** 52, (2), 32-38.

Bellare, J. R.; Davis, H. T.; Scriven, L. E.; Talmon, Y. *J. Electron Micr. Tech.* **1988,** 10, (1), 87-111.

Bergmeier, S. C.; Ismail, K. A. *Synthesis-Stuttgart* **2000**, (10), 1369-1371.

Bergstrom, C. A. S.; Wassvik, C. M.; Johansson, K.; Hubatsch, I. *J. Med. Chem.* **2007,** 50, (23), 5858-5862.

Bernard, J.; Hao, X. J.; Davis, T. P.; Barner-Kowollik, C.; Stenzel, M. H. *Biomacromolecules* **2006,** 7, (1), 232-238.

Bhargava, P.; Zheng, J. X.; Li, P.; Quirk, R. P.; Harris, F. W.; Cheng, S. Z. D. *Macromolecules* **2006,** 39, (14), 4880-4888.

Billmers, R. L.; Mackewicz, V. L. Process for preparation of hydrophobic starch derivatives. EP761691A2, 1997.

Blanazs, A.; Madsen, J.; Battaglia, G.; Ryan, A. J.; Armes, S. P. *J. Am. Chem. Soc.* **2011,** 133, (41), 16581-16587.

Blanco, E.; Hsiao, A.; Mann, A. P.; Landry, M. G.; Meric-Bernstam, F.; Ferrari, M. *Cancer Science* **2011,** 102, (7), 1247-1252.

Burkhardt, M.; Ruppel, M.; Tea, S.; Drechsler, M.; Schweins, R.; Pergushov, D. V.; Gradzielski, M.; Zezin, A. B.; Muller, A. H. E. *Langmuir* **2008,** 24, (5), 1769-1777.

Cairo, C. W.; Gestwicki, J. E.; Kanai, M.; Kiessling, L. L. *J. Am. Chem. Soc.* **2002,** 124, (8), 1615-1619.

Caldwell, C. G.; Wurzburg, O. B. Polysaccharide derivatives of substituted dicarboxylic acids. US2661349, 1953.

Carrier, R. L.; Miller, L. A.; Ahmed, M. *J. Controlled Release* **2007,** 123, (2), 78-99.

Castillo, R. V.; Arnal, M. L.; Muller, A. J.; Hamley, I. W.; Castelletto, V.; Schmalz, H.; Abetz, V. *Macromolecules* **2008,** 41, (3), 879-889.

Chang, C. W.; Bays, E.; Tao, L.; Alconcel, S. N. S.; Maynard, H. D. *Chem. Commun.* **2009**, (24), 3580-3582.

Chen, C. K.; Lin, S. C.; Ho, R. M.; Chiang, Y. W.; Lotz, B. *Macromolecules* **2010,** 43, (18), 7752-7758.

Chen, G. J.; Amajjahe, S.; Stenzel, M. H. *Chem. Commun.* **2009**, (10), 1198-1200.

Chen, L.; Shen, H.; Eisenberg, A. *J. Phys. Chem. B* **1999,** 103, (44), 9488-9497.

Chen, Q.; Zhao, H.; Ming, T.; Wang, J.; Wu, C. *J. Am. Chem. Soc.* **2009,** 131, (46), 16650-16651.

Chen, W. R.; Butler, P. D.; Magid, L. J. *Langmuir* **2006,** 22, (15), 6539-6548.

Chen, W. Y.; Li, C. Y.; Zheng, J. X.; Huang, P.; Zhu, L.; Ge, Q.; Quirk, R. P.; Lotz, B.; Deng, L. F.; Wu, C.; Thomas, E. L.; Cheng, S. Z. D. *Macromolecules* **2004,** 37, (14), 5292-5299.

Cheng, J.; Teply, B. A.; Sherifi, I.; Sung, J.; Luther, G.; Gu, F. X.; Levy-Nissenbaum, E.; Radovic-Moreno, A. F.; Langer, R.; Farokhzad, O. C. *Biomaterials* **2007,** 28, (5), 869-876.

Choi, S. H.; Bates, F. S.; Lodge, T. P. *Macromolecules* **2011,** 44, (9), 3594-3604.

Choi, S. H.; Lee, S.; Soto, H. E.; Lodge, T. P.; Bates, F. S. *J. Am. Chem. Soc.* **2011,** 133, (6), 1722-1725.

Choi, S.-H.; Bates, F. S.; Lodge, T. P. *J. Phys. Chem. B* **2009,** 113, (42), 13840-13848.

Choi, S.-H.; Lodge, T. P.; Bates, F. S. *Phys. Rev. Lett.* **2010,** 104, (4), 047802.

Chu, B., *Laser Light Scattering: Basic Principles and Practice*. 2nd ed.; Academic Press: Boston, 1991.

Cizova, A.; Koschella, A.; Heinze, T.; Ebringerova, A.; Srokova, I. *Starch/Staerke* **2007,** 59, (10), 482-492.

Cochran, E. W.; Garcia-Cervera, C. J.; Fredrickson, G. H. *Macromolecules* **2006,** 39, (7), 2449-2451.

Crowley, M. M.; Zhang, F.; Repka, M. A.; Thumma, S.; Upadhye, S. B.; Battu, S. K.; McGinity, J. W.; Martin, C. *Drug Dev. Ind. Pharm.* **2007,** 33, (9), 909-926.

Cui, H.; Chen, Z.; Zhong, S.; Wooley, K. L.; Pochan, D. J. *Science* **2007,** 317, (5838), 647-650.

Cui, H.; Hodgdon, T. K.; Kaler, E. W.; Abezgauz, L.; Danino, D.; Lubovsky, M.; Talmon, Y.; Pochan, D. J. *Soft Matter* **2007,** 3, (8), 945-955.

Curatolo, W.; Nightingale, J. A.; Herbig, S. M. *Pharm. Res.* **2009,** 26, (6), 1419-1431.

Dai, X. H.; Dong, C. M. *J. Polym. Sci., Part A: Polym. Chem.* **2008,** 46, (3), 817-829.

Dai, X. H.; Dong, C. M.; Yan, D. Y. *J. Phys. Chem. B* **2008,** 112, (12), 3644-3652.

de Gennes, P.-G., *Scaling Concepts in Polymer Physics*. 1st ed.; Cornell University Press: Ithaca, NY, 1979.

Degennes, P. G. *Macromolecules* **1980,** 13, (5), 1069-1075.

Devine, D. V.; Marjan, J. M. J. *Crit. Rev. Ther. Drug* **1997,** 14, (2), 105-131.

Diamantoglou, M. Preparation of modified cellulose for biocompatible dialysis membranes. EP330106A1, 1989.

Dong, C. M.; Chaikof, E. L. *Colloid. Polym. Sci.* **2005,** 283, (12), 1366-1370.

Dong, C. M.; Faucher, K. M.; Chaikof, E. L. *J. Polym. Sci., Part A: Polym. Chem.* **2004,** 42, (22), 5754-5765.

Dove, A. P. *Chem. Commun.* **2008**, (48), 6446-6470.

Du, Z. X.; Xu, J. T.; Fan, Z. Q. *Macromolecules* **2007,** 40, (21), 7633-7637.

Du, Z.-X.; Xu, J.-T.; Fan, Z.-Q. *Macromol. Rapid Commun.* **2008,** 29, (6), 467-471.

Duncan, R. *Nat. Rev. Drug Discovery* **2003,** 2, (5), 347-360.

Edmonds, W. F.; Li, Z.; Hillmyer, M. A.; Lodge, T. P. *Macromolecules* **2006,** 39, (13), 4526-4530.

Erhardt, R.; Böker, A.; Zettl, H.; Kaya, H.; Pyckhout-Hintzen, W.; Krausch, G.; Abetz, V.; Müller, A. H. E. *Macromolecules* **2001,** 34, (4), 1069-1075.

Erhardt, R.; Zhang, M.; Boker, A.; Zettl, H.; Abetz, C.; Frederik, P.; Krausch, G.; Abetz, V.; Muller, A. H. E. *J. Am. Chem. Soc.* **2003,** 125, (11), 3260-3267.

Fetters, L. J.; Lohse, D. J.; Richter, D.; Witten, T. A.; Zirkel, A. *Macromolecules* **1994,** 27, (17), 4639-4647.

Forster, S.; Zisenis, M.; Wenz, E.; Antonietti, M. *J. Chem. Phys.* **1996,** 104, (24), 9956-9970.

Fraser, C.; Grubbs, R. H. *Macromolecules* **1995,** 28, (21), 7248-7255.

Friesen, D. T.; Shanker, R.; Crew, M.; Smithey, D. T.; Curatolo, W. J.; Nightingale, J. A. S. *Mol. Pharmaceutics* **2008,** 5, (6), 1003-1019.

Fu, J.; Luan, B.; Yu, X.; Cong, Y.; Li, J.; Pan, C. Y.; Han, Y. C.; Yang, Y. M.; Li, B. Y. *Macromolecules* **2004,** 37, (3), 976-986.

Gadt, T.; Ieong, N. S.; Cambridge, G.; Winnik, M. A.; Manners, I. *Nat. Mater.* **2009,** 8, (2), 144-150.

Gao, P.; Morozowich, W. *Expert Opin. Drug Delivery* **2006,** 3, (1), 97-110.

Gardner, J. B.; Fevola, M. J.; Sun, F. C.; Walters, R. M. Superhydrophilic amphiphilic copolymers and processes for making the same. WO2011042379A1, 2011.

Garnier, S.; Laschewsky, A. *Langmuir* **2006,** 22, (9), 4044-4053.

Gaucher, G.; Dufresne, M. H.; Sant, V. P.; Kang, N.; Maysinger, D.; Leroux, J. C. *J. Controlled Release* **2005,** 109, (1-3), 169-188.

Gehlsen, M. D. Catalytic Hydrogenation of Polymer: Synthesis and Characterization of Model Polyolefins. Ph.D. Thesis, University of Minnesota, 1993.

Gerber, J. J.; Caira, M. R.; Lotter, A. P. *J. Cryst. Spectrosc.* **1993,** 23, (11), 863-869.

Ghoroghchian, P. P.; Li, G. Z.; Levine, D. H.; Davis, K. P.; Bates, F. S.; Hammer, D. A.; Therien, M. J. *Macromolecules* **2006,** 39, (5), 1673-1675.

Gilroy, J. B.; Lunn, D. J.; Patra, S. K.; Whittell, G. R.; Winnik, M. A.; Manners, I. *Macromolecules* **2012,** 45, (14), 5806-5815.

Gohy, J.-F. *Adv. Polym. Sci.* **2005,** 190, (Block Copolymers II), 65-136.

Gore, T.; Dori, Y.; Talmon, Y.; Tirrell, M.; Bianco-Peled, H. *Langmuir* **2001,** 17, (17), 5352-5360.

Gursoy, R. N.; Benita, S. *Biomed. Pharmacother.* **2004,** 58, (3), 173-182.

Ha, J. M.; Hamilton, B. D.; Hillmyer, M. A.; Ward, M. D. *Cryst. Growth Des.* **2009,** 9, (11), 4766-4777.

Halperin, A. *Macromolecules* **1987,** 20, (11), 2943-2946.

Halperin, A.; Tirrell, M.; Lodge, T., Tethered chains in polymer microstructures. In *Macromolecules: Synthesis, Order and Advanced Properties*, Springer: Berlin / Heidelberg, 1992; pp 31-71.

Hamley, I. W.; O'Driscoll, B. M. D.; Lotze, G.; Moulton, C.; Allgaier, J.; Frielinghaus, H. *Macromol. Rapid Commun.* **2009,** 30, (24), 2141-2146.

Hasegawa, A.; Taguchi, M.; Suzuki, R.; Miyata, T.; Nakagawa, H.; Sugimoto, I. *Chem. Pharm. Bull.* **1988,** 36, (12), 4941-50.

Hauss, D. J. *Adv. Drug Delivery Rev.* **2007,** 59, (7), 667-676.

Hawker, C. J.; Bosman, A. W.; Harth, E. *Chem. Rev.* **2001,** 101, (12), 3661-3688.

Hayward, R. C.; Pochan, D. J. *Macromolecules* **2010,** 43, (8), 3577-3584.

He, W. N.; Xu, J. T. *Prog. Polym. Sci.* **2012,** 37, (10), 1350-1400.

He, W. N.; Xu, J. T.; Du, B. Y.; Fan, Z. Q.; Sun, F. L. *Macromol. Chem. Phys.* **2012,** 213, (9), 952-964.

He, Y. Y.; Li, Z. B.; Simone, P.; Lodge, T. P. *J. Am. Chem. Soc.* **2006,** 128, (8), 2745-2750.

Heidman, J. L.; Tsonopoulos, C.; Brady, C. J.; Wilson, G. M. *Aiche Journal* **1985,** 31, (3), 376-384.

Helfand, E.; Wasserman, Z. R. *Macromolecules* **1976,** 9, (6), 879-888.

Helfand, E.; Wasserman, Z. R. *Macromolecules* **1978,** 11, (5), 960-966.

Helfand, E.; Wasserman, Z. R. *Macromolecules* **1980,** 13, (4), 994-998.

Hetzer, M.; Chen, G. J.; Barner-Kowollik, C.; Stenzel, M. H. *Macromol. Biosci.* **2010,** 10, (2), 119-126.

Hiemenz, P. C.; Rajagopalan, R., *Principles of Colloid and Surface Chemistry*. 3rd ed.; CRC Press, Taylor & Francis Group, LLC: Boca Raton, FL, 1997.

Hillmyer, M. A.; Bates, F. S. *Macromolecules* **1996,** 29, (22), 6994-7002.

Hoffman, J. D. *J. Chem. Phys.* **1958,** 29, 1192-3.

Hsu, C. Y. M.; Hendzel, M.; Uludag, H. *J. Gene Med.* **2011,** 13, (1), 46-59.

Hucul, D. A.; Hahn, S. F. *Adv. Mater.* **2000,** 12, (23), 1855-1858.

Ilevbare, G. A.; Liu, H.; Edgar, K. J.; Taylor, L. S. *Cryst. Growth Des.* Ahead of Print.

Ilevbare, G. A.; Liu, H.; Edgar, K. J.; Taylor, L. S. *CrystEngComm* **2012,** 14, (20), 6503-6514.

Ilevbare, G. A.; Liu, H. Y.; Edgar, K. J.; Taylor, L. S. *Cryst. Growth Des.* **2012,** 12, (6), 3133-3143.

Ishihara, T.; Maeda, T.; Sakamoto, H.; Takasaki, N.; Shigyo, M.; Ishida, T.; Kiwada, H.; Mizushima, Y.; Mizushima, T. *Biomacromolecules* **2010,** 11, (10), 2700-2706.

Jain, S.; Bates, F. S. *Science* **2003,** 300, 460-464.

Jain, S.; Bates, F. S. *Macromolecules* **2004,** 37, (4), 1511-1523.

Jakes, J. *Collect. Czech. Chem. Commun.* **1995,** 60, (11), 1781-1797.

Jintao, Z.; Ryan C., H. *Angew. Chem. Int. Ed.* **2008,** 47, (11), 2113-2116.

Johnsson, M.; Edwards, K. *Biophys. J.* **2003,** 85, (6), 3839-3847.

Kalbe, J.; Koch, R.; Muller, H. P.; Engelhardt, J.; Koch, W.; Muller, V. Thermoplastic and biodegradable polysaccharide esters / polysaccharide ether esters containing maleic acid addition product groups. US5717087, 1998.

Kato, H.; Suzuki, M.; Fujita, K.; Horie, M.; Endoh, S.; Yoshida, Y.; Iwahashi, H.; Takahashi, K.; Nakamura, A.; Kinugasa, S. *Toxicol. in Vitro* **2009,** 23, (5), 927-934.

Kaydos, J. A.; Smith, D. L. *J. Org. Chem.* **1983,** 48, (7), 1096-1099.

Kelen, T.; Tudos, F. *J. Macromol. Sci. Chem.* **1975,** A 9, (1), 1-27.

Kelkar, S. S.; Reineke, T. M. *Bioconjugate Chem.* **2011,** 22, (10), 1879-1903.

Kline, S. R. *J. Appl. Crystallogr.* **2006,** 39, 895-900.

Knop, K.; Hoogenboom, R.; Fischer, D.; Schubert, U. S. *Angew. Chem., Int. Ed.* **2010,** 49, (36), 6288-6308.

Kohli, K.; Chopra, S.; Dhar, D.; Arora, S.; Khar, R. K. *Drug Discovery Today* **2010,** 15, (21-22), 958-965.

Konno, H.; Handa, T.; Alonzo, D. E.; Taylor, L. S. *Eur. J. Pharm. Biopharm.* **2008,** 70, (2), 493-499.

Korczagin, I.; Hempenius, M. A.; Fokkink, R. G.; Stuart, M. A. C.; Al-Hussein, M.; Bomans, P. H. H.; Frederik, P. M.; Vancso, G. J. *Macromolecules* **2006,** 39, (6), 2306-2315.

Krause, S.; Gormley, J. J.; Roman, N.; Shetter, J. A.; Watanabe, W. H. *J. Polym. Sci., Part A: General Papers* **1965,** 3, (10), 3573-3586.

Kress, A. O.; Mathias, L. J.; Cei, G. *Macromolecules* **1989,** 22, (2), 537-546.

Kryuchkov, V. A.; Daigle, J. C.; Skupov, K. M.; Claverie, J. P.; Winnik, F. M. *J. Am. Chem. Soc.* **2010,** 132, (44), 15573-15579.

Kumar, J.; Bousquet, A.; Stenzel, M. H. *Macromol. Rapid Commun.* **2011,** 32, (20), 1620-1626.

Ladmiral, V.; Melia, E.; Haddleton, D. M. *Eur. Polym. J.* **2004,** 40, (3), 431-449.

Lai, J. T.; Filla, D.; Shea, R. *Macromolecules* **2002,** 35, (18), 6754-6756.

Langer, R. *Nature* **1998,** 392, (6679), 5-10.

Lazzari, M.; Lopez-Quintela, M. A. *Macromol. Rapid Commun.* **2009,** 30, (21), 1785-1791.

Lazzari, M.; Scalarone, D.; Hoppe, C. E.; Vazquez-Vazquez, C.; Lopez-Quintela, M. A. *Chem. Mater.* **2007,** 19, (24), 5818-5820.

Lazzari, M.; Scalarone, D.; Vazquez-Vazquez, C.; Lopez-Quintela, M. A. *Macromol. Rapid Commun.* **2008,** 29, (4), 352-357.

Leermakers, F. A. M.; Scheutjens, J. *J. Chem. Phys.* **1988,** 89, (5), 3264-3274.

Leibler, L.; Orland, H.; Wheeler, J. C. *J. Chem. Phys.* **1983,** 79, (7), 3550-3557.

Leube, W.; Monkenbusch, M.; Schneiders, D.; Richter, D.; Adamson, D.; Fetters, L.; Dounis, P.; Lovegrove, R. *Energy & Fuels* **2000,** 14, (2), 419-430.

Leuner, C.; Dressman, J. *Eur. J. Pharm. Biopharm.* **2000,** 50, (1), 47-60.

Li, T.; Wang, W. J.; Liu, R.; Liang, W. H.; Zhao, G. F.; Li, Z.; Wu, Q.; Zhu, F. M. *Macromolecules* **2009,** 42, (11), 3804-3810.

Li, Z. B.; Kesselman, E.; Talmon, Y.; Hillmyer, M. A.; Lodge, T. P. *Science* **2004,** 306, (5693), 98-101.

Lin, E. K.; Gast, A. P. *Macromolecules* **1996,** 29, (12), 4432-4441.

Lindfors, L.; Forssen, S.; Westergren, J.; Olsson, U. *J. Colloid Interface Sci.* **2008,** 325, (2), 404-413.

Lipinski, C. A. *J. Pharmacol. Toxicol. Methods* **2000,** 44, (1), 235-249.

Lipinski, C. A.; Lombardo, F.; Dominy, B. W.; Feeney, P. J. *Adv. Drug Delivery Rev.* **2001,** 46, (1-3), 3-26.

Liu, G. *Adv. Mater.* **1997,** 9, (5), 437-439.

Liu, H. Y.; Zhu, X. X. *Polymer* **1999,** 40, (25), 6985-6990.

Liu, J. B.; Xiao, Y. H.; Allen, C. *J. Pharm. Sci.* **2004,** 93, (1), 132-143.

Liu, J. B.; Zeng, F. Q.; Allen, C. *J. Controlled Release* **2005,** 103, (2), 481-497.

Liu, L.; Zhang, J. C.; Lv, W. H.; Luo, Y.; Wang, X. J. *J. Polym. Sci., Part A: Polym. Chem.* **2010,** 48, (15), 3350-3361.

Lodge, T. P.; Bang, J. A.; Li, Z. B.; Hillmyer, M. A.; Talmon, Y. *Faraday Discuss.* **2005,** 128, 1-12.

Loftsson, T.; Brewster, M. E. *J. Pharm. Sci.* **2012,** 101, (9), 3019-3032.

Loftsson, T.; Brewster, M. E.; Masson, M. *Am. J. Drug Delivery* **2004,** 2, (4), 261-275.

Lu, J.; Choi, S.; Bates, F. S.; Lodge, T. P. *Acs Macro Letters* **2012,** 1, (8), 982-985.

Lund, R.; Willner, L.; Pipich, V.; Grillo, I.; Lindner, P.; Colmenero, J.; Richter, D. *Macromolecules* **2011,** 44, (15), 6145-6154.

Lund, R.; Willner, L.; Richter, D.; Dormidontova, E. E. *Macromolecules* **2006,** 39, (13), 4566-4575.

Lund, R.; Willner, L.; Richter, D.; Iatrou, H.; Hadjichristidis, N.; Lindner, P. *J. Appl. Crystallogr.* **2007,** 40, S327-S331.

Lund, R.; Willner, L.; Stellbrink, J.; Lindner, P.; Richter, D. *Phys. Rev. Lett.* **2006,** 96, (6).

Maliczyszyn, W.; Atkinson, J. G.; Tolchinsky, M. Preparation of hydrophobic starch derivatives by reaction with preemulsified anhydrides. US6037466A, 2000.

Massey, J. A.; Temple, K.; Cao, L.; Rharbi, Y.; Raez, J.; Winnik, M. A.; Manners, I. *J. Am. Chem. Soc.* **2000,** 122, (47), 11577-11584.

Matsen, M. W.; Bates, F. S. *J. Polym. Sci., Part B: Polym. Phys.* **1997,** 35, (6), 945-952.

Matyjaszewski, K.; Xia, J. *Chem. Rev.* **2001,** 101, (9), 2921-2990.

Meier, D. J. *J. Polym. Sci., Part A: Polym. Symp.* **1969,** 26, (1), 81-98.

Meli, L.; Santiago, J. M.; Lodge, T. P. *Macromolecules* **2010,** 43, (4), 2018-2027.

Merisko-Liversidge, E.; Liversidge, G. G. *Adv. Drug Delivery Rev.* **2011,** 63, (6), 427-440.

Merisko-Liversidge, E. M.; Liversidge, G. G. *Toxicol. Pathol.* **2008,** 36, (1), 43-48.

Mihut, A. M.; Chiche, A.; Drechsler, M.; Schmalz, H.; Di Cola, E.; Krausch, G.; Ballauff, M. *Soft Matter* **2009,** 5, (1), 208-213.

Mihut, A. M.; Crassous, J. J.; Schmalz, H.; Drechsler, M.; Ballauff, M. *Soft Matter* **2012,** 8, (11), 3163-3173.

Miller, J. M.; Beig, A.; Carr, R. A.; Spence, J. K.; Dahan, A. *Mol. Pharmaceutics* **2012,** 9, (7), 2009-2016.

Miller, W. K.; Lyon, D. K.; Friesen, D. T.; Caldwell, W. B.; Vodak, D. T.; Dobry, D. E. Hydroxypropyl methyl cellulose acetate succinate with enhanced acetate and succinate substitution. WO2011159626A1, 2011.

Mithani, S. D.; Bakatselou, V.; TenHoor, C. N.; Dressman, J. B. *Pharm. Res.* **1996,** 13, (1), 163-7.

Moad, G.; Rizzardo, E.; Thang, S. H. *Aust. J. Chem.* **2005,** 58, (6), 379-410.

Moghimi, S. M.; Patel, H. M. *Adv. Drug Delivery Rev.* **1998,** 32, (1-2), 45-60.

Munoz-Bonilla, A.; Heuts, J. P. A.; Fernandez-Garcia, M. *Soft Matter* **2011,** 7, (6), 2493-2499.

Murdande, S. B.; Pikal, M. J.; Shanker, R. M.; Bogner, R. H. *J. Pharm. Sci.* **2011,** 100, (10), 4349-4356.

Nakano, M.; Matsumoto, K.; Matsuoka, H.; Yamaoka, H. *Macromolecules* **1999,** 32, (12), 4023-4029.

Nicolai, T.; Colombani, O.; Chassenieux, C. *Soft Matter* **2010,** 6, (14), 3111-3118.

Noolandi, J.; Hong, K. M. *Macromolecules* **1983,** 16, (9), 1443-1448.

Odian, G., *Principles of Polymerization*. 4th ed.; John Wiley & Sons, Inc.: Hoboken, New Jersey, 2004.

Ohno, K.; Tsujii, Y.; Miyamoto, T.; Fukuda, T.; Goto, M.; Kobayashi, K.; Akaike, T. *Macromolecules* **1998,** 31, (4), 1064-1069.

Okada, M. *Prog. Polym. Sci.* **2001,** 26, (1), 67-104.

Ormes, J. D.; Zhang, D.; Chen, A. M.; Hou, S.; Krueger, D.; Nelson, T.; Templeton, A. *Pharm. Dev. Technol.* **2013,** 18, (1), 121-129.

Pangborn, A. B.; Giardello, M. A.; Grubbs, R. H.; Rosen, R. K.; Timmers, F. J. *Organometallics* **1996,** 15, (5), 1518-20.

Patra, S. K.; Ahmed, R.; Whittell, G. R.; Lunn, D. J.; Dunphy, E. L.; Winnik, M. A.; Manners, I. *J. Am. Chem. Soc.* **2011,** 133, (23), 8842-8845.

Paudel, A.; Worku, Z. A.; Meeus, J.; Guns, S.; Van, d. M. G. *Int. J. Pharm.* **2012**.

Peacock, A. J., *Handbook of Polyethylene: Structures: Properties, and Applications.* Marcel Dekker: New York, 2000.

Pearson, S.; Allen, N.; Stenzel, M. H. *J. Polym. Sci., Part A: Polym. Chem.* **2009,** 47, (6), 1706-1723.

Pearson, S.; Chen, G. J.; Stenzel, M., Synthesis of glycopolymers. In *Engineered carbohydrate-based materials for biomedical applications: polymers, surfaces, dendrimers, nanoparticles, and hydrogels*, Narain, R., Ed. John Wiley & Sons, Inc.: Hoboken, New Jersey, 2011; pp 1-118.

Pedersen, J. S.; Schurtenberger, P. *Macromolecules* **1996,** 29, (23), 7602-7612.

Pedersen, J. S.; Svaneborg, C.; Almdal, K.; Hamley, I. W.; Young, R. N. *Macromolecules* **2003,** 36, (2), 416-433.

Percec, V.; Wilson, D. A.; Leowanawat, P.; Wilson, C. J.; Hughes, A. D.; Kaucher, M. S.; Hammer, D. A.; Levine, D. H.; Kim, A. J.; Bates, F. S.; Davis, K. P.; Lodge, T. P.; Klein, M. L.; De Vane, R. H.; Aqad, E.; Rosen, B. M.; Argintaru, A. O.; Sienkowska, M. J.; Rissanen, K.; Nummelin, S.; Ropponen, J. *Science* **2010,** 328, (5981), 1009-1014.

Petersen, M. A.; Yin, L.; Kokkoli, E.; Hillmyer, M. A. *Polym. Chem.* **2010,** 1, (8), 1281-1290.

Petzetakis, N.; Dove, A. P.; O'Reilly, R. K. *Chem. Sci.* **2011,** 2, (5), 955-960.

Petzetakis, N.; Walker, D.; Dove, A. P.; O'Reilly, R. K. *Soft Matter* **2012,** 8, (28), 3408-3414.

Peuscher, M.; Engelskirchen, K.; Gruenberger, E. Manufacture and use of water-soluble alkenyl- or alkylsuccinic acid ester-containing cellulose ethers. DE3620991A1, 1988.

Portinha, D.; Belleney, J.; Bouteiller, L.; Pensec, S.; Spassky, N.; Chassenieux, C. *Macromolecules* **2002,** 35, (5), 1484-1486.

Portinha, D.; Boue, F.; Bouteiller, L.; Carrot, G.; Chassenieux, C.; Pensec, S.; Reiter, G. *Macromolecules* **2007,** 40, (11), 4037-4042.

Qi, F.; Guerin, G.; Cambridge, G.; Xu, W. G.; Manners, I.; Winnik, M. A. *Macromolecules* **2011,** 44, (15), 6136-6144.

Qian, F.; Wang, J.; Hartley, R.; Tao, J.; Haddadin, R.; Mathias, N.; Hussain, M. *Pharm. Res.* **2012,** 29, (10), 2766-2776.

Qiu, X. P.; Winnik, F. M. *Macromol. Rapid Commun.* **2006,** 27, (19), 1648-1653.

Rabinow, B. E. *Nat. Rev. Drug Discovery* **2004,** 3, (9), 785-796.

Radulescu, A.; Mathers, R. T.; Coates, G. W.; Richter, D.; Fetters, L. J. *Macromolecules* **2004,** 37, (18), 6962-6971.

Raghavan, S. L.; Trividic, A.; Davis, A. F.; Hadgraft, J. *Int. J. Pharm.* **2001,** 212, (2), 213-221.

Rajagopal, K.; Mahmud, A.; Christian, D. A.; Pajerowski, J. D.; Brown, A. E. X.; Loverde, S. M.; Discher, D. E. *Macromolecules* **2010,** 43, (23), 9736-9746.

Rautio, J.; Kumpulainen, H.; Heimbach, T.; Oliyai, R.; Oh, D.; Jarvinen, T.; Savolainen, J. *Nat. Rev. Drug Discovery* **2008,** 7, (3), 255-270.

Re, M. I. *Drying Technol.* **2006,** 24, (4), 433-446.

Reese, B. E.; Barnett, R. E.; Alaoui-Ismaili, M.; Habibi, E.; Mann, C. J. In *Quantitative analysis of living cells by digital holographic microscopy*, Biomedical Science & Engineering Conference, 2009. BSEC 2009. First Annual ORNL, 18-19 March, 2009; 2009; pp 1-4.

Rejman, J.; Tavernier, G.; Bavarsad, N.; Demeester, J.; De Smedt, S. C. *J. Controlled Release* **2010,** 147, (3), 385-391.

Repka, M. A.; Battu, S. K.; Upadhye, S. B.; Thumma, S.; Crowley, M. M.; Zhang, F.; Martin, C.; McGinity, J. W. *Drug Dev. Ind. Pharm.* **2007,** 33, (10), 1043-1057.

Richter, D.; Schneiders, D.; Monkenbusch, M.; Willner, L.; Fetters, L. J.; Huang, J. S.; Lin, M.; Mortensen, K.; Farago, B. *Macromolecules* **1997,** 30, (4), 1053-1068.

Riess, G. *Prog. Polym. Sci.* **2003,** 28, (7), 1107-1170.

Roe, R.-J., *Methods of X-ray and neutron scattering in polymer science*. Oxford University Press: New York, NY, 2000.

Rowley, J. M.; Lobkovsky, E. B.; Coates, G. W. *J. Am. Chem. Soc.* **2007,** 129, (16), 4948-4960.

Ruiz, C. C., *Sugar-based surfactants: fundamentals and applications*. CRC Press: Boca Raton, FL, 2009; Vol. 143.

Rumondor, A. C. F.; Stanford, L. A.; Taylor, L. S. *Pharm. Res.* **2009,** 26, (12), 2599-2606.

Saito, N.; Liu, C.; Lodge, T. P.; Hillmyer, M. A. *Macromolecules* **2008,** 41, (22), 8815-8822.

Salminen, A. Method for production of hydrophobic microfibrillated cellulose. WO2012089929A1, 2012.

Sandström, M. C.; Johansson, E.; Edwards, K. *Biophys. Chem.* **2008,** 132, (2-3), 97-103.

Schmalz, H.; Schmelz, J.; Drechsler, M.; Yuan, J.; Walther, A.; Schweimer, K.; Mihut, A. M. *Macromolecules* **2008,** 41, (9), 3235-3242.

Schmelz, J.; Karg, M.; Hellweg, T.; Schmalz, H. *ACS Nano* **2011,** 5, (12), 9523-9534.

Schwahn, D.; Richter, D.; Wright, P. J.; Symon, C.; Fetters, L. J.; Lin, M. *Macromolecules* **2002,** 35, (3), 861-870.

Semenov, A. N. *Sov. Phys. JETP* **1985,** 61, 733.

Serajuddin, A. T. M. *Adv. Drug Delivery Rev.* **2007,** 59, (7), 603-616.

Shen, H.; Zhang, L.; Eisenberg, A. *J. Am. Chem. Soc.* **1999,** 121, (12), 2728-2740.

Shen, L.; Wang, H.; Guerin, G.; Wu, C.; Manners, I.; Winnik, M. A. *Macromolecules* **2008,** 41, (12), 4380-4389.

Shibayama, M.; Karino, T.; Okabe, S. *Polymer* **2006,** 47, (18), 6446-6456.

Simon, J.; Mueller, H.-P.; Koch, R.; Dijkstra, D. J.; Engelhardt, J.; Mueller, V. Manufacture of compostable, water-insoluble thermoplastic cellulose ether esters with 2-hydroxycarboxylic acid and other acids. DE19618826A1, 1997.

Simone, P. M.; Lodge, T. P. *Macromol. Chem. Phys.* **2007,** 208, (4), 339-348.

Smith, A. E.; Sizovs, A.; Grandinetti, G.; Xue, L.; Reineke, T. M. *Biomacromolecules* **2011,** 12, (8), 3015-3022.

Soto, A. P.; Gilroy, J. B.; Winnik, M. A.; Manners, I. *Angew. Chem., Int. Ed.* **2010,** 49, (44), 8220-8223.

Stella, V. J.; Nti-Addae, K. W. *Adv. Drug Delivery Rev.* **2007,** 59, (7), 677-694.

Suriano, F.; Coulembier, O.; Dubois, P. *J. Polym. Sci., Part A: Polym. Chem.* **2010,** 48, (15), 3271-3280.

Tajarobi, F.; Larsson, A.; Matic, H.; Abrahmsen-Alami, S. *Eur. J. Pharm. Biopharm.* **2011,** 78, (1), 125-133.

Takihara, T.; Yoshida, Y.; Isogai, A. *Cellulose* **2007,** 14, (4), 357-366.

Tanno, F.; Nishiyama, Y.; Kokubo, H.; Obara, S. *Drug Dev. Ind. Pharm.* **2004,** 30, (1), 9-17.

Thybo, P.; Pedersen, B. L.; Hovgaard, L.; Holm, R.; Mullertz, A. *Pharm. Dev. Technol.* **2008,** 13, (5), 375-386.

Ting, S. R. S.; Chen, G. J.; Stenzel, M. H. *Polym. Chem.* **2010,** 1, (9), 1392-1412.

Ting, S. R. S.; Granville, A. M.; Quemener, D.; Davis, T. P.; Stenzel, M. H.; Barner-Kowollik, C. *Aust. J. Chem.* **2007,** 60, (6), 405-409.

Ting, S. R. S.; Min, E. H.; Escale, P.; Save, M.; Billon, L.; Stenzel, M. H. *Macromolecules* **2009,** 42, (24), 9422-9434.

Tong, Q.; Krumova, M.; Gottker-Schnetmann, I.; Mecking, S. *Langmuir* **2008,** 24, (6), 2341-2347.

Tong, R.; Cheng, J. J. *Polym. Rev.* **2007,** 47, (3), 345-381.

Trossarelli, L.; Meirone, M. *J. Polym. Sci.* **1962,** 57, 445-52.

Tuzar, Z.; Kratochvil, P. *Surf. Colloid Sci.* **1993,** 15, 1-83.

Varma, A. J.; Kennedy, J. F.; Galgali, P. *Carbohydr. Polym.* **2004,** 56, (4), 429-445.

Vasconcelos, T.; Sarmento, B.; Costa, P. *Drug Discovery Today* **2007,** 12, (23&24), 1068-1075.

Vehring, R. *Pharm. Res.* **2008,** 25, (5), 999-1022.

Vernizzi, G.; Sknepnek, R.; de la Cruz, M. O. *PNAS* **2011,** 108, (11), 4292-4296.

Vilgis, T.; Halperin, A. *Macromolecules* **1991,** 24, (8), 2090-2095.

Voets, I. K.; Keizer, A. d.; Waard, P. d.; Frederik, P. M.; Bomans, P. H. H.; Schmalz, H.; Walther, A.; King, S. M.; Leermakers, F. A. M.; Stuart, M. A. C. *Angew. Chem. Int. Ed.* **2006,** 45, (40), 6673-6676.

Walther, A.; André, X.; Drechsler, M.; Abetz, V.; Müller, A. H. E. *J. Am. Chem. Soc.* **2007,** 129, (19), 6187-6198.

Walther, A.; Yuan, J.; Abetz, V.; Muller, A. H. E. *Nano Lett.* **2009,** 9, (5), 2026-2030.

Wang, L.; Stogner, H. P.; Batson, B. C. Starch esters and method for their manufacture and moldings made from them. US20080146792A1, 2008.

Wang, W. J.; Liu, R.; Li, Z. Y.; Meng, C. F.; Wu, Q.; Zhu, F. M. *Macromol. Chem. Phys.* **2010,** 211, (13), 1452-1459.

Wang, X.; Guerin, G.; Wang, H.; Wang, Y.; Manners, I.; Winnik, M. A. *Science* **2007,** 317, (5838), 644-647.

Wang, X. S.; Liu, K.; Arsenault, A. C.; Rider, D. A.; Ozin, G. A.; Winnik, M. A.; Manners, I. *J. Am. Chem. Soc.* **2007,** 129, (17), 5630-5639.

Wang, Y.; Hillmyer, M. A. *Macromolecules* **2000,** 33, (20), 7395-7403.

Wassvik, C. M.; Holmen, A. G.; Draheim, R.; Artursson, P.; Bergstrom, C. A. S. *J. Med. Chem.* **2008,** 51, (10), 3035-3039.

Weber, C. H. M.; Chiche, A.; Krausch, G.; Rosenfeldt, S.; Ballauff, M.; Harnau, L.; Goettker-Schnetmann, I.; Tong, Q.; Mecking, S. *Nano Lett.* **2007,** 7, (7), 2024-2029.

Weimann, P. A.; Hajduk, D. A.; Chu, C.; Chaffin, K. A.; Brodil, J. C.; Bates, F. S. *J. Polym. Sci., Part B: Polym. Phys.* **1999,** 37, (16), 2053-2068.

Willner, L.; Poppe, A.; Allgaieri, J.; Monkenbusch, M.; Lindner, P.; Richter, D. *Europhys. Lett.* **2000,** 51, (6), 628-634.

Won, Y.-Y.; Brannan, A. K.; Davis, H. T.; Bates, F. S. *J. Phys. Chem. B* **2002,** 106, (13), 3354-3364.

Won, Y.-Y.; Davis, H. T.; Bates, F. S. *Science* **1999,** 283, (5404), 960-963.

Won, Y.-Y.; Davis, H. T.; Bates, F. S. *Macromolecules* **2003,** 36, (3), 953-955.

Won, Y.-Y.; Davis, H. T.; Bates, F. S.; Agamalian, M.; Wignall, G. D. *J. Phys. Chem. B* **2000,** 104, (30), 7134-7143.

Wu, J.; Pearce, E. M.; Kwei, T. K.; Lefebvre, A. A.; Balsara, N. P. *Macromolecules* **2002,** 35, (5), 1791-1796.

Xu, J. T.; Fairclough, J. P. A.; Mai, S. M.; Ryan, A. J. *J. Mater. Chem.* **2003,** 13, (11), 2740-2748.

Yin, L.; Dalsin, M. C.; Sizovs, A.; Reineke, T. M.; Hillmyer, M. A. *Macromolecules* **2012,** 45, (10), 4322-4332.

Yu, K.; Eisenberg, A. *Macromolecules* **1996,** 29, (19), 6359-6361.

Yu, S. M.; Mecking, S. *Macromolecules* **2009,** 42, (11), 3669-3673.

Yu, Y.; Zhang, L.; Eisenberg, A. *Langmuir* **1997,** 13, (9), 2578-2581.

Zana, R.; Kaler, E. W., *Giant Micelles: Properties and Applications.* 1st ed.; CRC Press: Boca Raton, FL, 2007.

Zhang, H.; Lin, W. R.; Liu, A. H.; Yu, Z. N.; Wan, X. H.; Liang, D. H.; Zhou, Q. F. *Langmuir* **2008,** 24, (8), 3780-3786.

Zhang, J.; Wang, L. Q.; Wang, H. J.; Tu, K. H. *Biomacromolecules* **2006,** 7, (9), 2492-2500.

Zhang, L.; Barlow, R. J.; Eisenberg, A. *Macromolecules* **1995,** 28, (18), 6055-6066.

Zhang, L. F.; Eisenberg, A. *Science* **1995,** 268, (5218), 1728-1731.

Zhang, L. F.; Eisenberg, A. *J. Am. Chem. Soc.* **1996,** 118, (13), 3168-3181.

Zhao, Y.; Shi, X. B.; Gao, H. Y.; Zhang, L.; Zhu, F. M.; Wu, Q. *J. Mater. Chem.* **2012,** 22, (12), 5737-5745.

Zheng, J. X.; Xiong, H. M.; Chen, W. Y.; Lee, K. M.; Van Horn, R. M.; Quirk, R. P.; Lotz, B.; Thomas, E. L.; Shi, A. C.; Cheng, S. Z. D. *Macromolecules* **2006,** 39, (2), 641-650.

Zhou, C.; Hillmyer, M. A.; Lodge, T. P. *Macromolecules* **2011,** 44, (6), 1635-1641.

Zhu, J.; Ferrer, N.; Hayward, R. C. *Soft Matter* **2009,** 5, (12), 2471-2478.

Zhu, J.; Hayward, R. C. *J. Am. Chem. Soc.* **2008,** 130, (23), 7496-7502.

Zhulina, E. B.; Adam, M.; LaRue, I.; Sheiko, S. S.; Rubinstein, M. *Macromolecules* **2005,** 38, (12), 5330-5351.

Zhulina, E. B.; Borisov, O. V. *Macromolecules* **2012,** 45, (11), 4429-4440.

Zienty, F. B.; Vineyard, B. D.; Schleppnik, A. A. *J. Org. Chem.* **1962,** 27, (9), 3140-3146.

Zinn, T.; Willner, L.; Lund, R.; Pipich, V.; Richter, D. *Soft Matter* **2012,** 8, (3), 623-626.

Zupancich, J. A.; Bates, F. S.; Hillmyer, M. A. *Macromolecules* **2006,** 39, (13), 4286-4288.

A. Spray-dried Dispersions of Hydroxypropyl Methylcellulose (HPMC) Substituted Succinates with Probucol

A.1 Results and Discussion

Besides phenytoin as described in Chapter 4, hydroxypropyl methyl cellulose substituted succinates (HPMC-(R-SA)) was also formulated with another drug to test their efficacy as the matrices in spray-dried dispersions (SDDs). Probucol, an anti-hyperlipidemic drug, is also categorized as Class II compounds (low solubility and high permeability) in the Biopharmaceutics Classification System (Figure A.1). The aqueous solubility of probucol at pH = 7 is extremely low as 0.041 μg/mL.[1] Such low solubility is thought not to come from the same reason as phenytoin; the melting point (T_m) of probucol is 125 °C (Form I),[2] which indicates the relatively weak crystallization tendency of amorphous probucol.[3] Indeed, only a glass transition at 21 °C and no crystallization were observed as the temperature was ramped to –20 °C during the 1st cooling ramp in DSC (Figure A.2). Instead, the *c* log *P* value (calculated logarithm of the partition coefficient between octanol and water) at 25 °C is very high as 8.9, which reflects the very lipophilic nature of probucol. Therefore, probucol may be viewed as "grease balls" rather than "brick dusts" such as phenytoin.[4] The crystalline probucol particles had irregular morphologies and looked similar to potatoes, and the particles size varied between 1 and 100 μm (Figure A.3).

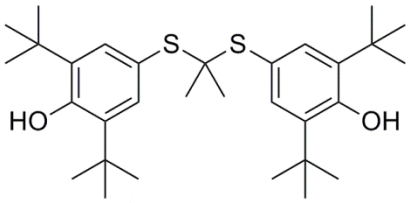

Figure A.1 Chemical structure of probucol.

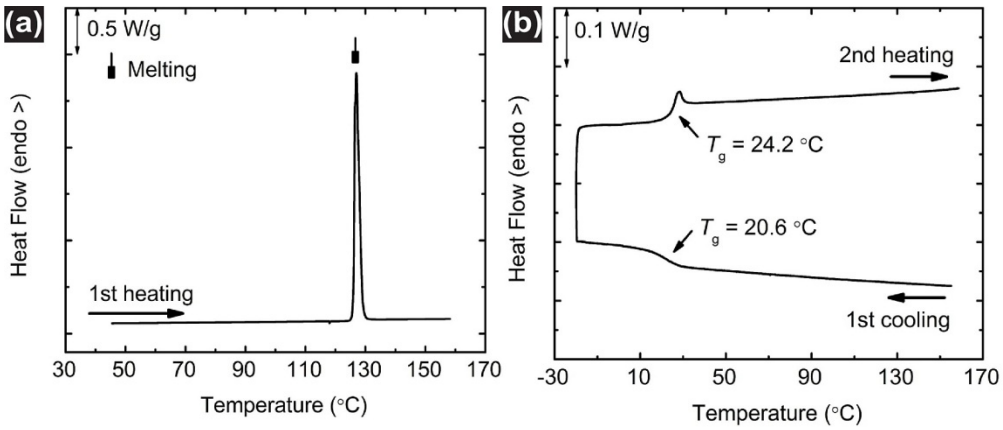

Figure A.2 DSC curves of probucol (as received). The melting peak during the 1st heating scan was at 127 °C and the heat of fusion (ΔH_m) was 69.0 J g^{-1}. The temperature was ramped at a rate of 5.0 °C min^{-1}.

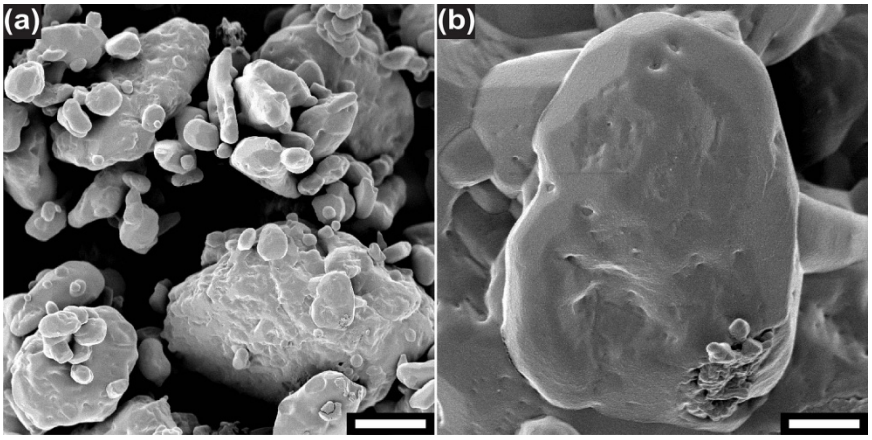

Figure A.3 SEM pictures of crystalline probucol (as received). The crystals are potato-like particles with irregular surfaces. The particles are mostly 1–100 μm in the largest dimension. Scale bars: (a) 10.0 μm and (b) 1.5 μm.

The molecular parameters of HPMC-(R-SA)s that were used to formulate with probucol are listed in Table A.1. HPMCAS, HPMC-Ph-0.63, and HPMC-CyS-0.57 have been described in Chapter 4. In addition, two samples, HPMC-Ph-0.24 and HPMC-Ph-0.44, were synthesized to study the effect of DS. HPMC-Ph-0.44 showed a monomodal elution curve in SEC with a moderate $Đ$ of 1.48, and the calculated M_n from ^{1}H NMR was consistent with that determined from LS-SEC within experimental error (Figure A.4 and Table A.1). However, HPMC-Ph-0.24 exhibited a bimodal elution curve, and there existed a second peak with the larger apparent molar mass. Correspondingly, the M_m and $Đ$ determined by LS-SEC were much larger than the rest HPMC-(R-SA)s shown in Table A.1. The peak with low elution volume indicated that there may be some intermolecular covalent linkages or HPMC-Ph-0.24 was not fully soluble in THF due to the physical association of lyophobic groups (e.g., hydroxyls and succinates). Possible future experiments include studying the dependence of the physical association on concentration and SEC characterization of samples after full acetylation of pendent carboxylic acids. In addition, T_g of HPMCAS and the four HPMC-(R-SA)s were 120 °C or above and thus well suitable for normal spray-drying conditions.

A. Spray-dried Dispersions with Probucol

Table A.1 Molecular and thermal characteristics of HPMC esters.

Sample	Substituents[a]	$[\text{-OH}]_0$:$[\text{Anhydride}]_0$[b]	DS[c]	M_n NMR (kg/mol)[d]	M_n SEC (kg/mol)[e]	M_m SEC (kg/mol)[e]	$Đ$ [e]	dn/dc (mL/mg)[f]	T_g (°C) [g]
HPMC-CyS-0.57	CyS	1:1	0.57	17.8	16.9	26.2	1.56	0.085	120
HPMC-Ph-0.24	Ph	1:0.5	0.24	14.3	24.6	83.3	3.38	0.092	140
HPMC-Ph-0.44	Ph	1:1	0.44	16.3	15.6	23.1	1.48	0.106	132
HPMC-Ph-0.63	Ph	1:2	0.63	18.2	17.2	26.2	1.52	0.098	124
HPMCAS	Succinate Acetate		S: 0.28 A: 0.57						121

[a] The kind of ester substituents in HPMC esters. All samples also contain two kinds of ether substituents, hydroxypropoxy (HPO) and methoxy (MeO). [b] The ratio of the initial concentration of hydroxyls on HPMC to that of anhydride in the feed. [c] DS of the ester substituents. [d] Number-average molar mass (M_n) calculated based on the M_n of HPMC by SEC and the DS of the HPMC-(R-SA) by ^{1}H NMR spectroscopy. The cellulose backbone was assumed to undergo no degradation or cross-linking during esterification. [e] Determined by a SEC that was equipped with a LS and a *d*RI detector. The mobile phase was an aqueous buffer for HPMC, and THF for HPMC esters. [f] Determined by the *d*RI signal assuming 100% mass recovery. [g] Apparent glass transition temperatures (T_gs) by DSC.

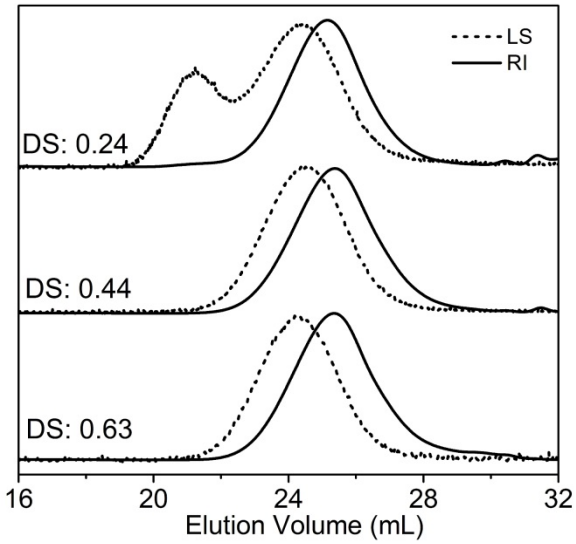

Figure A.4 (from top to bottom) SEC traces of HPMC phenylsuccinates with a DS of 0.24, 0.44, and 0.63, respectively. The mobile phase was THF at 25 °C.

SDDs of probucol with HPMCAS and four HPMC-(R-SA)s were prepared using a labscale Mini-spray dryer (Bend Research, OR). All samples were dried from acetone solutions except HPMC-Ph-0.24, which was not soluble in acetone at a concentration of 2.0 wt % and was dried from THF instead. At 10 wt % probucol loading, SDDs with different polymeric matrices had very similar morphologies and all looked like collapsed spheres, raisin-shape particles. The size distribution of the SDDs was relatively broad—the larger particles were ca. 1–10 μm and the smaller one were ca. 20–100 nm in the largest dimension (Figure A.5). The particles were less folded as the probucol loading increased from 10 to 50 wt % (Figure A.6). Importantly, these SEM pictures suggested that there were no apparent residual probucol crystals in the SDDs, which was also supported by powder XRD (Figure A.7).

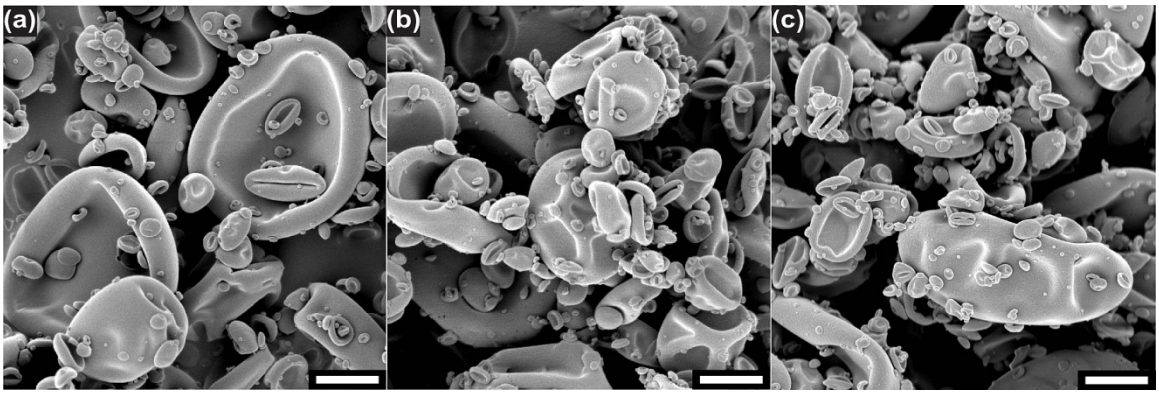

Figure A.5 SEM pictures of SDDs at 10 wt % probucol loadings with (a) HPMCAS, (b) HPMC-Ph-0.63, and (c) HPMC-CyS-0.57 as the matrices, respectively. The scale bars indicate 1.5 μm.

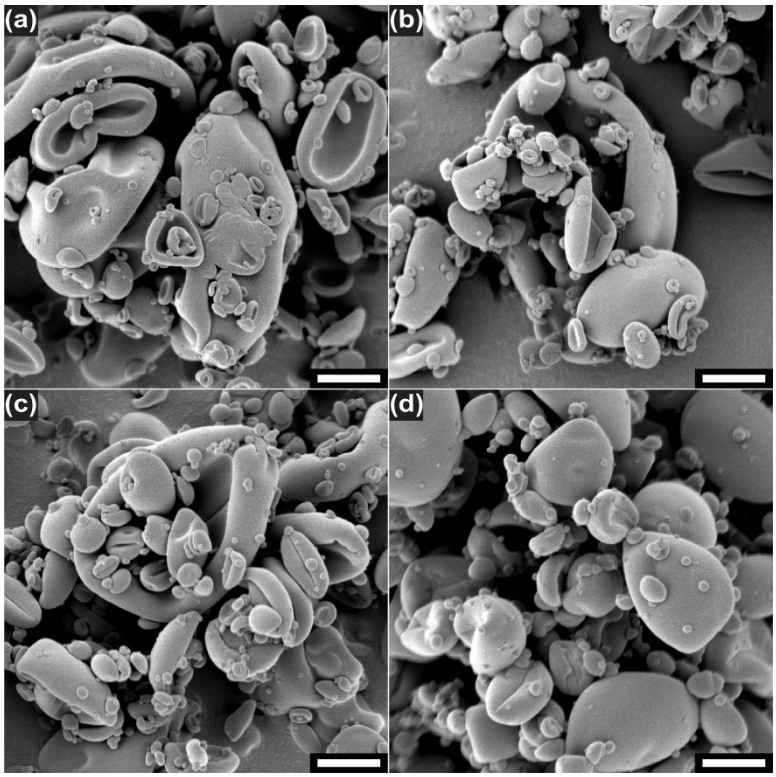

Figure A.6 SEM pictures of SDDs with HPMC-Ph-0.63 as the matrix at (a) 10, (b) 25, (c) 33, and (d) 50 wt % probucol loadings. The scale bars indicate 1.0 μm.

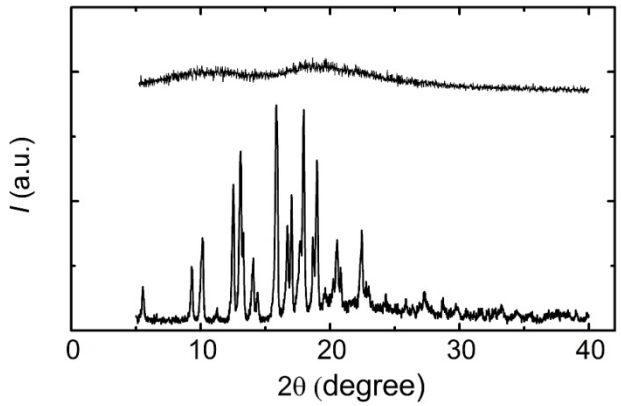

Figure A.7 Powder XRD patterns of (bottom) crystalline probucol as received and (top) the SDD with HPMCAS as the matrix at 33 wt % probucol loading. In contrast with the sharp characteristic diffraction peaks from crystalline probucol (Form I), the SDD showed broad featureless patterns, indicating minimal amount of detectable probucol crystals in the sample.

The thermal properties of the SDDs were characterized using DSC. As T_m of probucol is rather low (125 and 116 °C for Form I and Form II of the polymorphs, respectively[2]), increasing temperature to 180 °C can quantitatively reveal the amount of residual probucol crystals in the SDDs. At relatively low probucol loadings (10 and 25 wt %), the SDDs with three different polymeric matrices looked very similar. There were no apparent exothermic or endothermic transitions during the 1st heating scan (Figure A.8), suggesting that the initial SDDs contained minimal amount of detectable probucol crystals. At 33 wt % loading, the SDDs with HPMCAS and HPMC-CyS-0.57 as matrices first showed exothermic transitions starting at ca. 82 °C, which corresponded to the cold crystallization of amorphous probucol from the polymeric matrices. The produced probucol crystals were mainly Form II, as revealed by the following endothermic melting transition with a peak at ca. 116 °C. The released heat during crystallization was equal to the absorbed heat during melting within experimental error, suggesting that there were

also essentially no residual probucol crystals in the starting SDDs (Table A.2). In comparison, the SDD with HPMC-Ph-0.63 as the matrix at 33 wt % loading did not exhibit any significant transitions except a small endothermic peak of the Form II polymorph. Comparison of the measured heat of fusion to literature values revealed that 98 wt % of probucol in the starting SDD was amorphous. Therefore, the SDD with HPMC-Ph-0.63 as the matrix was also an amorphous solid dispersion, and more stable against cold crystallization than those with HPMCAS and HPMC-CyS-0.57 as matrices at elevated temperatures. We hypothesize that the enhanced thermal stability came from the extra π–π interactions between the phenyl groups in HPMC-Ph-0.63 and probucol. At 50 wt % loading, all three SDDs showed cold crystallization followed by melting of mainly Form-II probucol during the 1st heating scans. Quantitative analysis indicated that the starting SDDs contained 4–10 wt % of crystalline probucol. SEM imaging of the cross sections of the SDDs with HPMCAS as the matrix after thermal treatment suggested that the one with 10 wt % probucol loading was a homogeneous mixture, while the other two with 25 and 50 wt % loadings contained microsized spherical droplets of probucol within the matrix (Figure A.9). Therefore, although there were no significant transitions during the 1st heating scan as detected by DSC, the SDDs at 25 wt % loading reached the solubility limit of probucol in the polymeric matrices and underwent amorphous–amorphous demixing.[5]

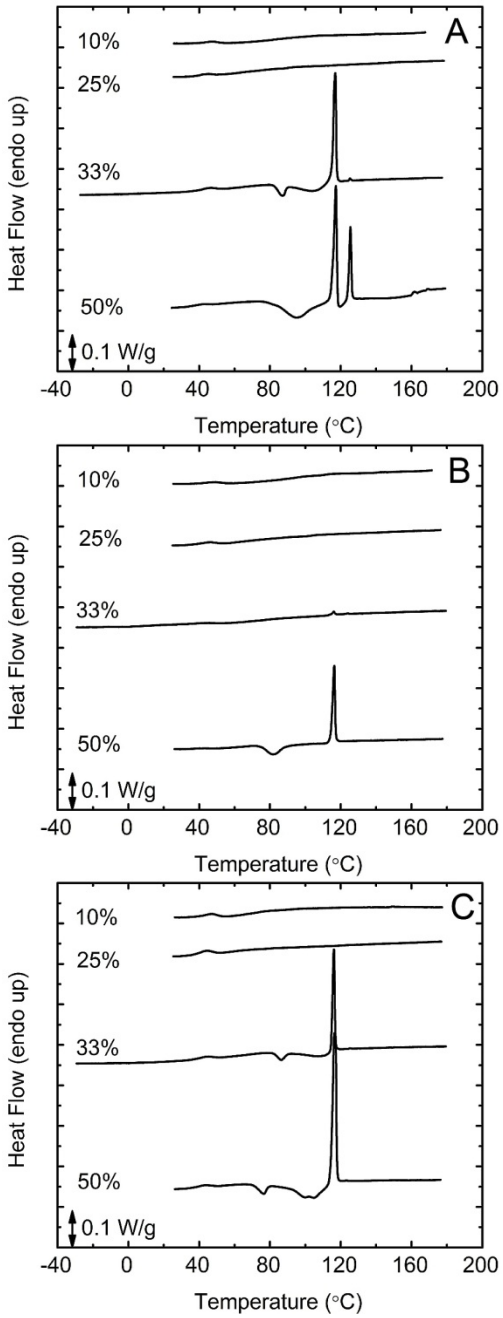

Figure A.8 DSC curves of SDDs of probucol with (A) HPMCAS, (B) HPMC-Ph-0.63, and (C) HPMC-CyS-0.57 as the matrices. The loadings were 10, 25, 33, and 50 wt %. The heating rate was 2.5 °C min^{-1}, and shown here are the 1st heating scans. Each sample was run in triplicates, and one representative run is shown.

A. Spray-dried Dispersions with Probucol

Table A.2 Thermal characteristics of SDDs with HPMCAS, HPMC-Ph-0.63, and HPMC-CyS-0.57 as the matrices at 33 and 50 wt % probucol loadings.

Polymer	Loading	T_c[a] (onset, °C)	T_c[a] (peak, °C)	ΔH[a] (J g^{-1})	T_m[b] (peak, °C)	ΔH[b] (J g^{-1})	T_m[c] (peak, °C)	ΔH[c] (J g^{-1})
HPMCAS	33 wt %	82.8 ± 0.2	87.2 ± 0.1	10.3 ± 0.7	116.9 ± 0.1	11.6 ± 0.8	125.3 ± 0.1	0.11 ± 0.05
HPMC-Ph-0.63	33 wt %	*d*	*d*	*d*	116.2 ± 0.1	0.46 ± 0.09	123.6 ± 0.6	0.12 ± 0.08
HPMC-CyS-0.57	33 wt %	82.0 ± 0.1	86.3 ± 0.4	7.9 ± 0.6	115.3 ± 1.0	8.4 ± 0.6	125.2 ± 0.1	0.05 ± 0.01
HPMCAS	50 wt %	73.0 ± 1	78.8 ± 0.9	25.9 ± 0.8	117.1 ± 0.3	26.2 ± 0.3	125.0 ± 0.1	1.2 ± 0.3
HPMC-Ph-0.63	50 wt %	74.1 ± 0.8	80.4 ± 1.2	5.2 ± 0.4	116.3 ± 0.1	8.6 ± 0.6	*d*	*d*
HPMC-CyS-0.57	50 wt %	70.3 ± 0.4	101 ± 3	21.3 ± 1.0	116.8 ± 0.4	22.7 ± 1.3	*d*	*d*

[a] The onset temperatures, peak temperatures, and released heat of cold crystallization during the 1st heating scan. [b] The peak temperatures and absorbed heat corresponding to the melting of probucol (From II) during the 1st heating scan. [c] The peak temperature and absorbed heat corresponding to the melting of probucol (From I) during the first heating scan. Using literature values, polymorph I of probucol: ΔH: 64 J g^{-1}, T_m: 125 °C; polymorph II: ΔH: 68 J g^{-1}, T_m: 116 °C.[2] [d] Not observed. Each sample was run in triplicates, and shown are the average value ± one standard deviation.

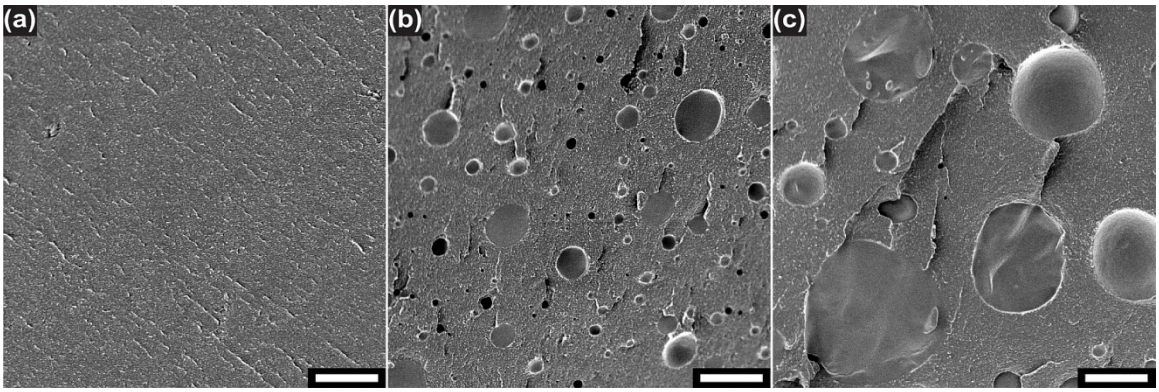

Figure A.9 SEM pictures of SDDs of with HPMC-Ph-0.63 as the matrices at (a) 10, (b) 25, and (c) 50 wt % probucol loadings after measurement on DSC. The sample was first heated from 22 to 180 °C, then cooled to −40 °C, and finally heated to 180 °C. The 1st heating scan was at a rate of 2.5 °C min^{-1}, and the 1st cooling and 2nd heating scans were at a rate of 10 °C min^{-1}. After this treatment, the white, powdery sample became an integrated, light yellow, and transparent glassy piece, and shown are the inner sections as cut with a razor blade. Scale bars indicate 2.5 μm.

The dissolution performance of the SDDs in PBS was further investigated. As shown in Figure A.10, the SDDs with HPMCAS, HPMC-Ph-0.63, and HPMC-CyS-0.57 as matrices at 33 wt % loading all reached c_{max} within 20 min, and more than 90% of the loaded probucol was dissolved. The apparent concentration was 2.2×10^4 times as large as the solubility of crystalline probucol in water. More importantly, such supersaturation was well maintained without any decreasing over the 3-h dissolution tests. The effective maintenance was largely due to the weak crystallization tendency of amorphous probucol as indicated by its not very high T_m. Therefore, achieving initial high levels of supersaturation is critical in maximizing the total area under the curve for SDDs of probucol in the dissolution tests. Besides, the dissolution performance of the three SDDs with different HPMC esters as the matrices exhibited weak dependence on the ester substituents as they showed very similar dissolution performance. Previous studies

showed that c_{max} of SDDs with polyvinylpyrrolidone (PVP) K-30 as the matrices were highly dependent on the drug loading, and less than 5% of the applied probucol was dissolved for a SDD at 33 wt % loading.[6] Therefore, these cellulose derivatives are more effective than PVP at increasing the *in vitro* bioavailability of probucol as the matrices in SDDs. In addition, the dissolution performance of the SDDs showed significant dependence on the DS as exemplified by HPMC phenylsuccinates (Figure A.11). At 10 wt % probucol loading, the SDDs with matrices of HPMC phenylsuccinates of three different DS exhibited similar performance. However, as the probucol loading increased to 25 wt %, c_{max} monotonously decreased as DS decreased from 0.63 to 0.44 and finally 0.24. Similar variations were also observed in SDDs at 33 and 50 wt % of probucol loading.

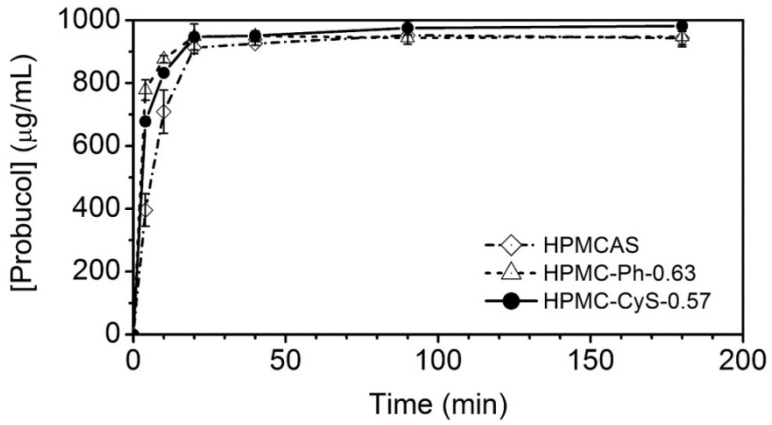

Figure A.10 Dissolution profiles of SDDs with HPMCAS, HPMC-Ph-0.63, and HPMC-CyS-0.57 as matrices at 33 wt % probucol loadings. The solubility of crystalline probucol was < 1 μg/mL. The target concentration of probucol was 1000 μg mL^{-1}. The samples were run in triplicates, and the data shown are the mean value ± one standard deviation.

A. Spray-dried Dispersions with Probucol

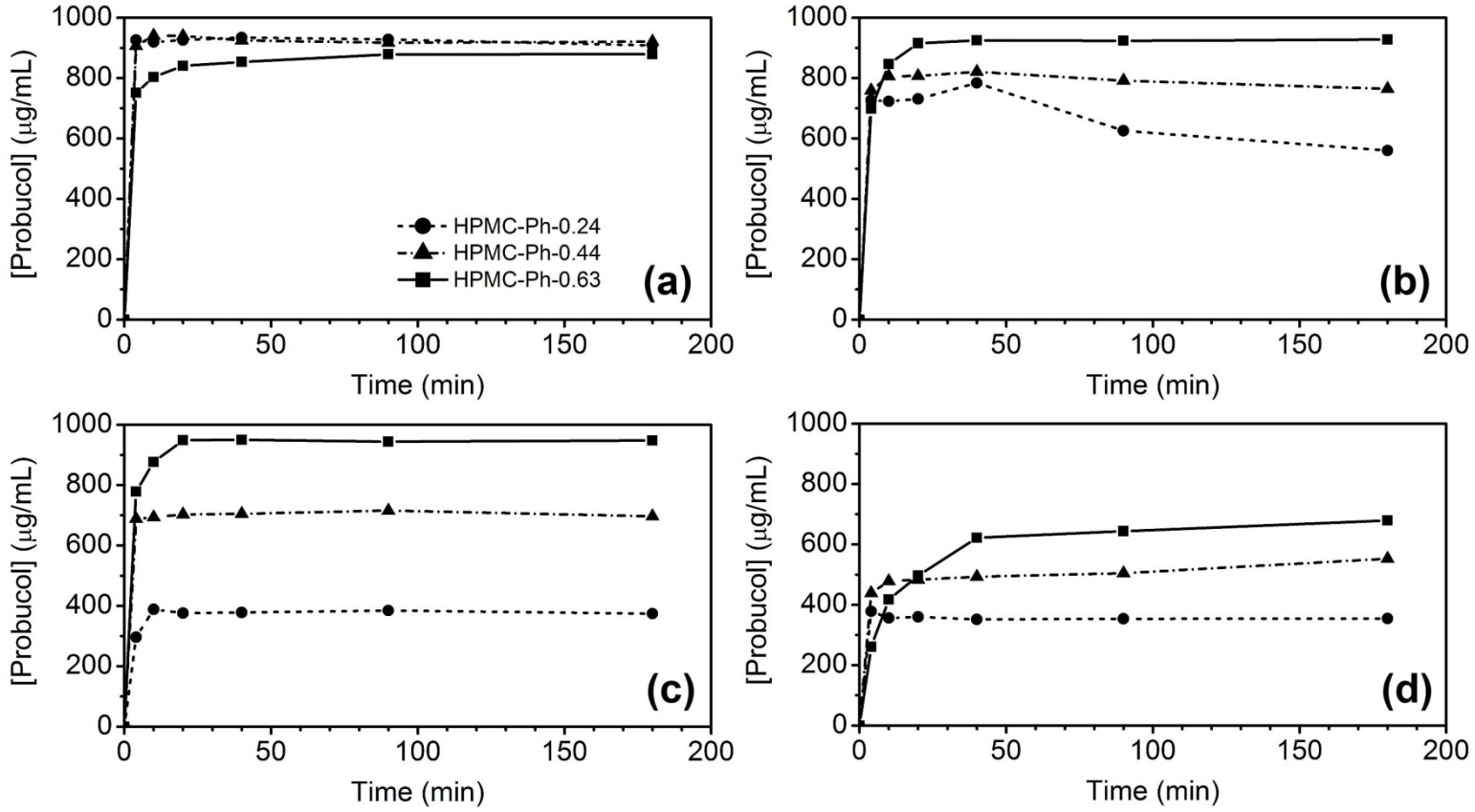

Figure A.11 Dissolution profiles of SDDs with HPMC-Ph-0.24, HPMC-Ph-0.44, and HPMC-Ph-0.6357 as matrices at (a) 10, (b) 25, (c) 33, and (d) 50 wt % probucol loadings. The target concentration of probucol was 1000 μg mL^{-1}.

A.2 Experimental Section

The spray-drying conditions, SEM, DSC, powder XRD, and dissolution tests of the SDDs of probucol were very similar to those of phenytoin as described in Chapter 4. The synthesis of HPMC phenylsuccinates and HPLC conditions are presented below.

Synthesis of HPMC phenylsuccinates. Generally speaking, the composition of HPMC, sodium acetate, and acetic acid in the feed was kept the same ($[\text{-OH}]_0$:$[\text{NaOAc}]_0$ = 1:2, and $[\text{-OH}]_0 \approx 0.4$ M) and a homogeneous mixture was first allowed to form at 85 °C. Next, an appropriate amount of an anhydride was added to target a specific substituent and degree of substitution (Table A.1). The synthesis of HPMC-Ph-0.63 is described below as an example. 3.40 g of HPMC (E3 grade from The Dow Chemical Company, pendent hydroxyl: 1.8×10^{-2} mol), 3.01 g of sodium acetate (3.7×10^{-2} mol), and 35 mL of glacial acetic acid were charged into a 100-mL round bottom flask, and the mixture was allowed to form a homogeneous solution at 85 °C with magnetic stirring. After that, 6.5 g of phenylsuccinc anhydride (Ph-SA, 3.7×10^{-2} mol) was added into the flask. The reaction was allowed to proceed at 85 °C for 3.0 h. The reaction was quenched by adding 10 mL of DI water into the mixture. The product was isolated by precipitating into 1.0 L of water three times, and then dried under vacuum at 22 °C until constant mass was achieved. Conversion of Ph-SA: 31% by ^{1}H NMR.

HPLC. The apparent concentration of probucol in the aqueous buffer (PBS, pH=6.5, supplemented with 0.5 wt % of simulated intestinal fluid powder) was determined by analyzing the aliquots on a reverse-phase HPLC. The Agilent 1260 liquid chromatograph system housed a Poroshell 120 EC-C18 column of 4.6 × 50 mm from

Agilent. The pore size was 120 Å, and the size of the silica particles was 2.7 μm. The chromatogram was monitored using a multi-wavelength UV-vis detector, 1260 MWD, at 254 nm. The mobile phase was 96:4 (v/v) of MeCN/Water, and the elution volume of probucol was 2.90 mL. The concentration of probucol was quantified by referring to a calibration in the range of 10–2000 μg/mL.

A.3 References

1. Calculated using Advanced Chemistry Development (ACD/Labs) Software V11.02 (© 1994-2011 ACD/Labs)

2. Gerber, J. J.; Caira, M. R.; Lotter, A. P. *J. Cryst. Spectrosc.* **1993,** 23, (11), 863-869.

3. The T_m of probucol of the other polymorph (Form II) is 116 °C and the heat of fusion is 69.0 J g^{-1}.

4. Bergstrom, C. A. S.; Wassvik, C. M.; Johansson, K.; Hubatsch, I. *J. Med. Chem.* **2007,** 50, (23), 5858-5862.

5. Baird, J. A.; Taylor, L. S. *Adv. Drug Delivery Rev.* **2012,** 64, (5), 396-421.

6. Thybo, P.; Pedersen, B. L.; Hovgaard, L.; Holm, R.; Mullertz, A. *Pharm. Dev. Technol.* **2008,** 13, (5), 375-386.

B. Graft Copolymers of Hydroxypropyl Methylcellulose (HPMC) with Poly(ethylene oxide) (PEO)

B.1 Results

Grafting cellulose with other polymers holds great promise in systematically improving the properties of cellulosics. This section describes my efforts on synthesizing PEO-grafted HPMC, which may be used as drug carriers in amorphous solid dispersions. Due to the excellent biocompatibility and large commercial availability, PEO homopolymers have long been used as matrices of solid dispersions for poorly water-soluble drugs.[1] In particular, PEO is hydrophilic and thus PEO-modified cellulosics may exhibit fast dissolution kinetics of the loaded drugs in the gastrointestinal (GI) tract. PEO-grafted HPMC was prepared using the anhydride chemistry—the pendent hydroxyls on HPMC were esterified with an ω-succinic-anhydride-terminated PEO (PEO-SA).

An ω-thiol-terminated PEO (PEO-SH) was synthesized following literature procedures (Scheme B.1).[2] The starting material was an α-methyl-ω-hydroxyl-functionalized PEO (PEO-OH) with a M_n of 2.0 kg mol^{-1} as determined by ^{1}H NMR spectroscopy. In each of the following steps, the peak corresponding to the methylene protons at the ω-terminus of the reactant PEO completely disappeared and shifted to a new position in ^{1}H NMR spectra (Figure B.1), indicating very high conversions. Besides, the ratios of the integration of the characteristic protons at the ω-terminus (including the methylene protons and those on the end groups) to that of the methyl protons at the α-end were 0.98, 0.95, and 0.96 in the product PEO-Ts, PEO-SAc, and PEO-SH, respectively.

In other words, the end groups of PEO were effectively transformed and more than 95% of the overall functionality was attained in the PEO-SH product. PEO-SH presented a monomodal elution curve with a $Đ$ of 1.14 in SEC, indicating minimal amount of the coupling byproduct (via disulfide). The PEO-SH exhibited a melting peak at 54 °C during the 2nd heating scan at a rate of 10 °C min^{-1} in DSC. The heat of fusion was 167 J g^{-1}, which corresponded to a crystallinity of 84%.

Scheme B.1 Synthesis of PEO-SH.

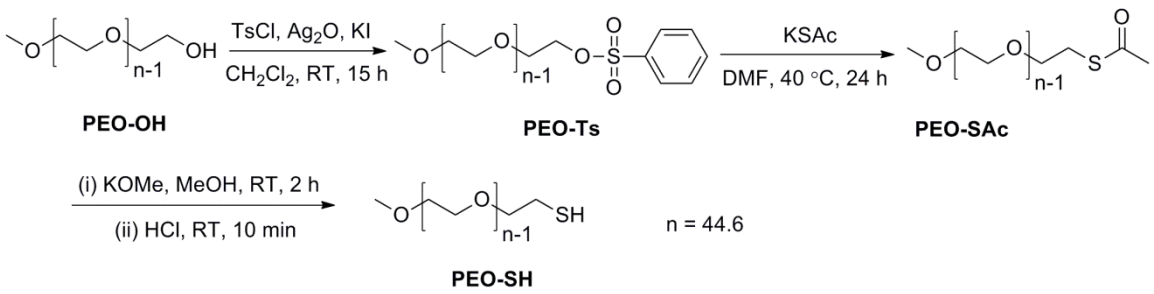

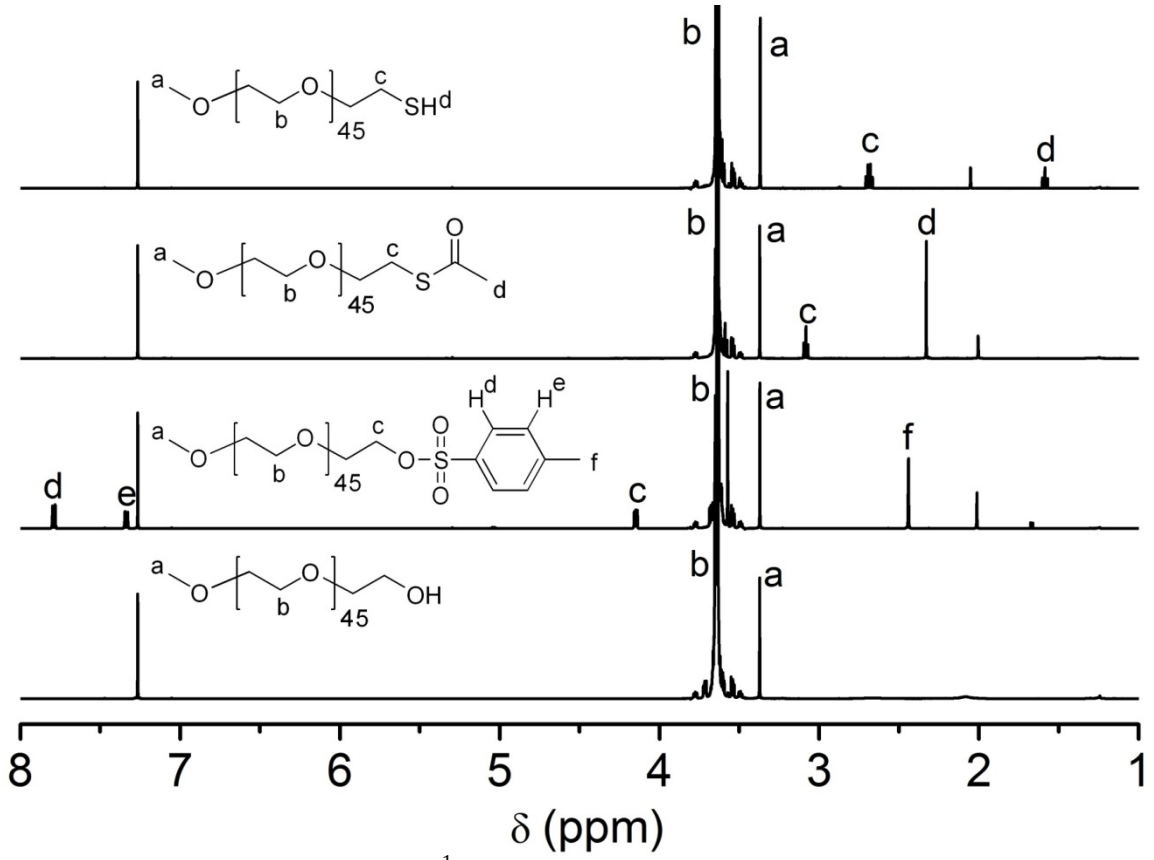

Figure B.1 (from bottom to top) ^{1}H NMR spectra of PEO-OH, PEO-Ts, PEO-SAc, and PEO-SH, respectively.

Next, a PEO-SA was synthesized via the conjugate addition of PEO-SH to maleic anhydride (Scheme B.2). As monitored by ^{1}H NMR spectroscopy (Figure B.2), the peak (a doublet of a triplet) corresponding to methylene protons neighboring the thiols at 2.7 ppm in PEO-SH disappeared, and two new peaks (a doublet of a doublet of a doublet) showed up at 3.2 and 2.7 ppm, respectively, indicating complete conversion. The ratio of the integration of the methylene protons at the ω-terminus to that of the methyl protons at the α-end in the PEO-SA product was 0.83. This result means 14% of the PEO chains lost the end-group functionality during this one-step transformation. The loss may be caused

by some side reactions, which have been reported in the synthesis of small-molecule alkylthiosuccinic anhydrides[3] but the nature is yet to be explored in detail.

Scheme B.2 Synthesis of PEO-SA.

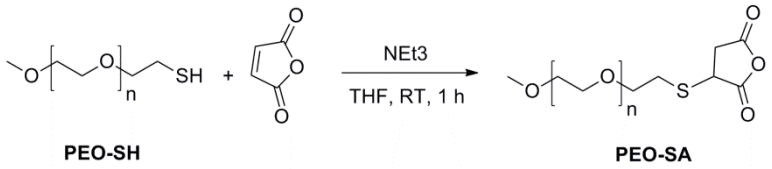

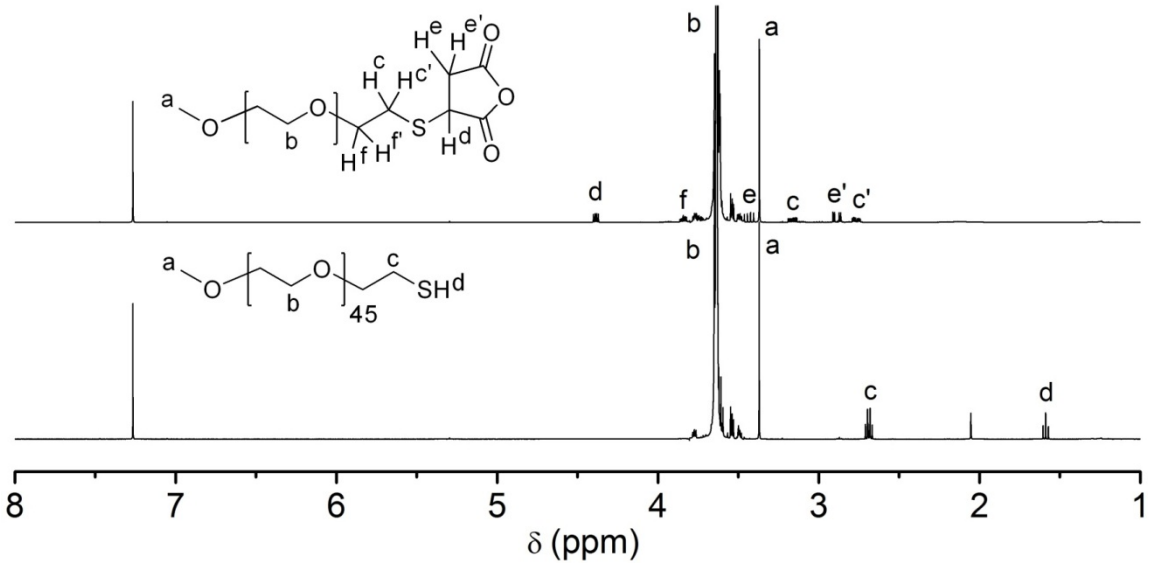

Figure B.2 ^{1}H NMR spectra of (bottom) PEO-SH and (top) PEO-SA.

One attempt was further made to synthesize PEO-grafted HPMC (HPMC-*graft*-PEO) following Scheme B.3. The HPMC sample had a mass-average molar mass (M_m) of 15.7 kg mol^{-1} and a $Đ$ of 1.33 as determined by LS-SEC. The average number of hydroxyls available for further esterification per anhydro glucopyranose unit was 1.09. More details of this HPMC are described in Chapter 4. In the esterification, the

concentration of the hydroxyls on HPMC was 0.29 M, and the ratio of the concentration of the hydroxyls to that of PEO-SA to that of the catalyst sodium acetate was 12:1:24. In other words, the hydroxyls were 12-fold excessive to the succinic anhydrides. The reaction was allowed to proceed at 85 °C for 5 h. The crude product was purified by dialysis against water using a membrane with a molar-mass cut-off value of 3.5 kg mol^{-1} followed by freeze-drying. As such, the unreacted PEO-SA should have been removed and the isolated product only contained HPMC-*graft*-PEO and unreacted HPMC (if any). LS-SEC characterization of the isolated product gave M_m = 17.8 kg mol^{-1} and $Đ$ = 1.24. Correspondingly, the conversion of the PEO-SA was 20%. Such low conversion is tentatively ascribed to the low efficiency of this anhydride chemistry and the "grafting-to" strategy.

Scheme B.3 Synthesis of HPMC-*graft*-PEO.

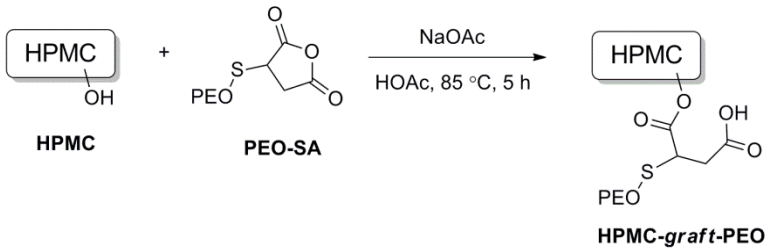

B.2 Experimental Section

The synthesis of PEO-SH from PEO-OH (M_n = 2.0 kg mol^{-1}, Fluka) was carried out following published procedures.[2] The overall yield was 73% after the three steps as shown in Scheme B.1.

Synthesis of PEO-SA. 1.00 g of PEO-SH (5.0×10^{-4} mol), 13.9 μL of triethylamine (NEt_3, 1.0×10^{-5} mol), and 5.0 mL of THF were charged to a 50-mL round-bottomed flask at room temperature and allowed to form a clear solution with magnetic stirring. Next, a 5-mL THF solution that contained 49.0 mg of maleic anhydride (5.0×10^{-4} mol) was added into the flask dropwise over 2 h. The reaction was allowed to proceed for another 30 min. The product was then isolated by precipitating the reaction mixture into 500 mL of diethyl ether that was cooled by a dry ice/acetone bath. Yield: 0.65 g (62%). ^{1}H NMR ($CDCl_3$, 500 MHz): 4.4 ppm (dd, 1H, J = 5.17, 9.75 Hz), 3.8–3.5 ppm (br, 178H), 3.4 ppm (dd, 1H, J = 9.76, 19.18 Hz), 3.1 ppm (s, 3H), 3.2 ppm (ddd, 1H, J = 3.88, 8.06, 14.79 Hz), 2.9 ppm (dd, 1H, J = 5.17, 19.19 Hz), 2.7 ppm (ddd, 1H, J = 3.70, 5.81, 14.76 Hz).

Synthesis of HPMC-*graft*-PEO. 0.54 g of HPMC (pendent hydroxyl: 2.9×10^{-3} mol), 0.48 g of sodium acetate (5.8×10^{-3} mol), and 5.0 mL of glacial acetic acid were charged into a 50-mL round-bottomed flask and allowed to form a homogeneous solution at 85 °C with magnetic stirring. A 5.0-mL acetic-acid solution that contained 0.50 g of PEO-SA (2.5×10^{-4} mol) was added into the flask dropwise over 3.0 h. The reaction was allowed to proceed at 85 °C for another 2.0 h and thus the total reaction time was 5.0 h. The reaction was quenched by adding a small amount of DI water into the mixture. The

product was isolated by dialysis against DI water using a membrane with MWCO of 3.5 kg mol^{-1} followed by lyophilization. Yield: 0.64 g (62%).

B.3 References

1. Paudel, A.; Worku, Z. A.; Meeus, J.; Guns, S.; Van, d. M. G. *Int. J. Pharm.* **2012**.

2. Petersen, M. A.; Yin, L.; Kokkoli, E.; Hillmyer, M. A. *Polym. Chem.* **2010,** 1, (8), 1281-1290.

3. Zienty, F. B.; Vineyard, B. D.; Schleppnik, A. A. *J. Org. Chem.* **1962,** 27, (9), 3140-3146.